2010

Feasibility Study of Solar Driven Underground Cooling System

Michel E. Shafik
University of Nebraska at Lincoln, misho.emil@gmail.com

FEASIBILITY STUDY OF SOLAR DRIVEN

UNDERGROUND COOLING SYSTEM

By

Michel E. Shafik

A THESIS

Presented to the Faculty of

The Graduate College at the University of Nebraska

In Partial Fulfillment of Requirements

For the Degree of Master of Science

Major: Architectural Engineering

Under the Supervision of Professor Haorong Li

Lincoln, Nebraska

July, 2010

FEASIBILITY STUDY OF SOLAR DRIVEN UNDERGROUND COOLING SYSTEM

Michel E. Shafik, M.S.

University of Nebraska, 2010

Adviser: Haorong Li

In the United States the peak electrical use occurs during the summer. In addition, the building sector consumes a major portion of the annual electrical energy consumption. One of the main energy consuming components in the building sector is the Heating, Ventilation, and Air-Conditioning (HVAC) systems. This research studies the feasibility of implementing a solar driven underground cooling system that could contribute to reducing building cooling loads. The developed system consists of an Earth-to-Air Heat Exchanger (EAHE) coupled with a solar chimney that provides a natural cool draft to the test facility building at the Solar Energy Research Test Facility in Omaha, Nebraska. Two sets of tests have been conducted: a natural passively driven airflow test and a forced fan assisted airflow test. The resulting data of the tests has been analyzed to study the thermal performance of the implemented system. Results show that: The underground soil proved to be a good heat sink at a depth of 9.5ft, where its temperature fluctuates yearly in the range of (46.5°F-58.2°F). Furthermore, the coupled system during the natural airflow modes can provide good thermal comfort conditions that comply with ASHRAE standard 55-2004. It provided 0.63 tons of cooling, which almost covered the building design cooling load (0.8 tons, extreme condition). On the other hand, although the coupled system during the forced airflow mode could not comply with ASHRAE standard 55-2004, it provided 1.27 tons of cooling which is even more than the building load requirements. Moreover, the underground soil experienced thermal saturation during the forced airflow mode due to the oversized fan, which extracted much more airflow than the EAHE ability for heat dissipation and the underground soil for heat absorption. In conclusion, the coupled system proved to be a feasible cooling system, which could be further improved with a few design recommendations.

DEDICATION

I dedicate this thesis first to the glory of Jesus Christ, my Lord and Savior, whose resurrection power gives me everything I need to live a joyful and purposeful life. He is the one who has given me the ability and strength to accomplish this lifelong goal.

And to the ones who loved, taught, guided and helped me without saying a word, my lovely parents, my dad Emil Shafik and my mom Evon Fahmy. I love you both so much. Lastly, to all of my family, especially my aunt and grandmother, for their love, support and prayers; and to my friends for always encouraging me to reach for new horizons in my life.

إهداء

إهدي هذه الرسالة أولآ لمجد يسوع المسيح، سيدي و مخلصى، الذي بقوة قيامته أعطاني كل شئ أحتاج إليه لأحي حياة هادفه و سعيدة. هو وحده الذي أعطانى القوة و القدرة لإنجاز هذا العمل الذي طالما حلمت به طوال حياتي.

و إلي من أحبانى، أرشدانى و سعادانى بدون كلمة واحده، أبي و أمي الأعزاء، إميل شفيق و إيڤون فهمي. أحبكما كثيرآ جدآ. و أخيرآ و ليس أخرآ لكل عائلتى، و على الأخص عمتي و جدتي، لمحبتهم، تعضيدهم و صلواتهم؛ و لكل أصدقائى الذين طالما شجعونى للوصول إلي أفاق جديدة في حياتي.

شكرآ

AUTHER'S ACKNOWLEDGEMENTS

I would like to gratefully acknowledge my committee members Dr. Bing Chen, Dr. Haorong Li, and Dr. Siu-Kit Lau. Dr. Chen, I owe my deepest gratitude to you for your generous and sincere help, kindness and patience. Dr. Li, thank you for your commitment and support in helping me to reach this goal. Dr. Lau, thank you for your encouragement and support. Without all of you, my thesis would not have been possible.

It is my pleasure to give a special thank you to Dr. Gang Wang, who assisted me a great deal on my data analysis during the summer seasons, and Dr. Long Ni, for his academic help on my thesis, reviews and recommendations, as well as for his kindness and patience. Also, with grateful thanks, to Joerg Henkel for his technical expertise and James Devaney for his hard labor and work on the facility during the hot summer months. And finally, a special thanks to Dr. Maher Tadros, for his concerned guidance.

In addition to the above professors, advisors, and colleagues, I also thank Charity Stahl for her amazing help, support, kindness and understanding. Thank you to Videgla Sekpe and Nader El-Alaraj for their friendship, support and help as well. And finally, to my parents and aunt for their love, understanding and kind support.

TABLE OF CONTENTS

LIST OF TABLES

LIST OF FIGURES

NOMENCLATURE

ASHRAE	American Society of Heating, Refrigerating and Air-Conditioning Engineers
Btu	British Thermal Units
°C	Degree Calicoes
$C_{P_{air}}$	Constant-Pressure Specific Heat of Air, Btu/(lbm-°F) [J/(kg-K)]
CFM	Cubic Feet per Minute
$\mathrm{CFM_{EAHE}}$	EAHE Supply Air Mass Flow Rate, ft^3/min
EAHE	Earth-to-Air Heat Exchanger
e	Error
$e_{instrument}$	Uncertainty of a Specific Measuring Instrument
e_n	Uncertainty Interval in the n^{th} Variable
e_R	Uncertainty Interval in the Results
e_{ref}	Precision Error of the Reference Measuring Instrument
e_{stab}	Stable Bias Error Between the Reference and Measuring Instrument
e_{TC}	Thermocouple Average Measurement Error
e_{AF}	Airflow Transmitter Average Measurement Error
$e_{S,cooling}$	Uncertainty of the Calculated Sensible Cooling Capacity
°F	Degree Fahrenheit
ft	Feet
ft^3	Cubic Feet
HVAC	Heating, Ventilation and Air-Conditioning

h_{fg}	Enthalpy of Vaporization, Btu/lbm (J/kg)
hr	Hour
h_{OA}	Outdoor Air Enthalpy, Btu/lbm (J/kg)
h_{RA}	Room/Indoor Air Enthalpy, Btu/lbm (J/kg)
h_{SA}	Supply Air Enthalpy, Btu/lbm (J/kg)
in.H_2O	Inch Water
J	Joule
K	Degree Kelvin
kg	Kilogram
kJ	Kilo Joule
lbm	Pound-Mass
Max.	Maximum
Min	Minimum
m^3	Cubic Meter
mAmps.	Milliampere
min	Minute
$\dot{m}_{air}$	Mass Flow Rate of Airflow, lbm/hr (kg/s)
$\dot{m}_w$	Mass Flow Rate of Water Condensation/Vaporization, lbm/hr (kg/s)
OAT	Outdoor Air Temperature, °F (°C)
Q_{air}	Volume Flow Rate of Airflow, ft^3/hr (m^3/s)
$\dot{Q}_{l,cooling}$	Rate of Latent Cooling Heat Transfer, Btu/hr (W)
$\dot{Q}_{s,cooling}$	Rate of Sensible Cooling Heat Transfer, Btu/hr (W)

$\dot{Q}_{total,coolir}$	Rate of Total Cooling Heat Transfer, Btu/hr (W)
R	Calculated Results
RAT	Room/Indoor Air Temperature, °F (°C)
Ref.	Reference
RH%	Relative Humidity Percentage
s	Second
SAT	Supply Air Temperature, °F (°C)
T	Temperature, °F (°C)
T_{OAT}	Outdoor Air Temperature, °F (°C)
T_{RAT}	Average Room/Indoor Air Temperature, °F (°C)
T_{SAT}	EAHE Supply Air Temperature, °F (°C)
UUS	Undisturbed Underground Soil
W	Watt
ρ_{air}	Specific Density of Air, lbm/ft^3 (kg/m^3)
v_{air}	Specific Volume of Air, ft^3/lbm (m^3/kg)
ω_{OA-HR}	Outdoor Air Humidity Ratio
ω_{RA-HR}	Room/Indoor Air Humidity Ratio
ω_{SA-HR}	EAHE Supply Air Humidity Ratio
Δh	Enthalpy Difference, Btu/lbm (J/kg)
ΔT	Temperature Difference, °F (K)
$\Delta\omega$	Humidity Ratio Difference

Chapter, 1

INTRODUCTION

The energy crisis in the early 70's increased the whole worlds' awareness of the possible depletion of non-renewable energy sources (i.e. fossil fuels) and the inevitability of finding other alternatives. In the mean time it has been found that using fossil fuels has a huge impact on the environment, and the human health and well being.

One of those environmental impacts is the emission of greenhouse gases (GHG) (e.g. carbon dioxide CO_2) which is responsible for many other serious environmental issues (e.g. climate change, global warming, and water and air pollution). These emissions are consequently affecting human health and the ecosystems.

According to the U.S. Environmental Protection Agency (EPA), fossil fuel burning is responsible for 64% of the increased amounts of carbon dioxide (CO_2) in the atmosphere since 1850. It is worth mentioning that in the United States carbon dioxide CO_2 emissions represents 82.7% of the total greenhouse gases (GHG) emissions. According to the U.S. Energy Information Administration's (EIA[1], 2008) annual energy review report for/of (2008), North America produces almost 24% of the world's annual carbon dioxide (CO_2) emissions while the Unites States alone produces 20.2%.

In addition to the fact that the fossil fuels will be depleted in the near future and have negative environmental effects, its prices have been increasing lately. The U.S. Department of Energy - EIA annual energy review report for (2008) show that the fossil fuel and the electricity prices have been increasing since 1999.

[1] The U.S. Energy Information Administration (EIA) is a section of the U.S. Department of Energy (DOE).

All of these reasons; non-renewable energy sources depletion, the environmental impact of fossil fuels, and the increase in energy prices with the current global economical recession that started in the late 2000's, have stimulated countries around the world to increase their energy savings by reducing their energy consumption and utilizing renewable energy sources with a belief that the "renewable energy can play an important role in meeting the ultimate goal of replacing large parts of fossil fuels (Chel and Tiwari, 2009).

Accordingly, researchers around the world started to investigate the possible alternative solutions. In doing so, the major energy consuming sectors have been investigated and it was found that the building sector consumes about 70% of the annual electrical energy consumption and 41% of the annual primary energy usage. It has also been found that electricity represents 40% of the total energy consumed by households. It is worth mentioning that the United States is the number one country in the world in terms of energy production, while it consumes 33.8% more than what it actually produces (DOE/EIA annual energy review for 2008).

On the other hand statistics show that renewable energy contributes only by 7% in the total annual primary energy production in the United States and only by 1.5% of the annual primary energy production in the whole world. It is also found that only 7% of the total energy consumed by the building sector comes from renewable energy sources (DOE/EIA annual energy review for 2008).

It is very clear from the above statistics that the building sector is one of the biggest non-renewable energy consuming sectors that are not utilizing much of the renewable energy available in the United States. Accordingly, research is being

conducted on the building sector to find ways of saving non-renewable energy and utilizing renewable energy sources.

It should be mentioned that one of the main building sector components that consumes most of its energy is the conventional Heating Ventilation and Air-Conditioning (HVAC) systems. The conventional HVAC system consists of a cooling coil that receives its cooling capacity from a mechanical chiller, and an electrical fan which drives the air through the system and consequently to the end user. Both the mechanical chiller and the electrical fan are non-renewable energy consumers as they are both electrically driven.

For this reason, the research presented in this thesis focuses on utilizing two means of renewable energy sources (namely geothermal and passive solar energy) to provide a natural, feasible, alternative for the cooling and ventilation of residential and commercial buildings. This alternative will help reduce the non-renewable energy consumption. The developed solar driven underground cooling system aims to eliminate the electricity usage by replacing the cooling coil with an earth-to-air heat exchanger (EAHE) and replacing the fan by a solar chimney, thus, reducing the peak summer loads in buildings using an environmentally friendly system that utilizes renewable energy.

A full scale experimental setup was installed in the early 90's at the Solar Energy Research Test Facility utilizing an earth-to-air heat exchanger which was later coupled to a solar chimney by a long buried 188 foot (57 m) EAHE to create a cool draft into the test facility. The test results show that the coupled system can provide acceptable indoor thermal environmental comfort conditions during the natural airflow test, complying with the American Society of Heating, Refrigerating, and Air-Conditioning Engineers

(ASHRAE) standard 55-2004 for thermal comfort. Moreover, it provided 0.63 tons of cooling, which almost covered the building design cooling load (0.8 tons, extreme condition). On the other hand, although the coupled system during the forced airflow mode could not comply with ASHRAE standard 55-2004, it provided 1.27 tons of cooling which is even more than the building load requirements. The underground soil proved to be a good heat sink at a depth of 9.5ft, where its temperature fluctuates in the range of (46.5°F-58.2°F), although it experienced thermal saturation during the forced airflow mode due to the oversized fan. The fan extracted much more airflow than the EAHE ability for heat dissipation and the underground soil for heat absorption. In conclusion, the coupled system proved to be a feasible cooling system, which could be further improved with a few design recommendations.

Chapter, 2

LITERATURE REVIEW

2.1 Introduction

The probability of fossil fuels depletion in the near future, as well as increasing prices during the last decade and negative environmental impacts, created a big trend among the scientists and researchers to study ways to reduce the usage of the non-renewable energy sources (i.e. fossil fuels). Therefore, much effort has been put into investigating the possibility of utilizing the renewable energy sources, which are believed to play an important potential role in meeting the ultimate goal of replacing large parts of fossil fuel (Chel and Tiwari, 2009).

Accordingly, much research has been conducted, especially on the building sector, as it is one of the biggest energy consuming sectors in the United States, to investigate the capability of utilizing different low cost and environmentally friendly renewable energy sources to substitute for fossil fuels.

In this research, two of these renewable energy sources have been further investigated. The first renewable energy source to be investigated in the current research is the geothermal energy. According to the American Society of Heating, Refrigerating and Air-Conditioning Engineers (ASHRAE), the geothermal energy is defined as "the thermal energy within the earth's crust – the thermal energy in rock and fluid (water, steam or water containing large amounts of dissolved solids) that fills the pores and fractures within the rock, and sand and gravel" (ASHRAE, 1999).

This renewable energy source (i.e. geothermal energy) has been a point of attraction for different generations in different eras. There have been many attempts since ancient times to utilize the geothermal energy for different purposes. Many ancient peoples including the Romans, Chinese, and Native Americans, used hot mineral springs for bathing, cooking and heating. Today, water from hot springs is used worldwide in spas, for heating buildings, and for agricultural and industrial uses (BOEMRE, 2004).

One of the main reasons that attracted the researchers today to investigate the possibility of utilizing the geothermal energy is the relatively stable temperature of the ground (i.e. soil) at the depth of about 13ft (4m) (Ghosal, et al., 2004; Shukla, et al., 2006; Zhang and Haghighat, 2009). This relatively stable underground temperature is related to the high thermal inertia of the underground soil that dampens the temperature fluctuations at the ground surface exposed to the external climate, deeper in the ground (De Paepe and Janssens, 2003).

In order to utilize such a renewable energy source with the underground high thermal inertia, many techniques have been developed in the last few decades such as Ground Source Heat Pumps (GSHP), Earth-to-Air Heat Exchangers (EAHE), etc.

One of the main goals of this research is studying the performance of an EAHE for the purpose of cooling residential and commercial buildings.

In order to understand what is an EAHE and how this technique utilizes the geothermal energy to cool residential buildings, the EAHE system will be illustrated.

The EAHE is simply a pipe that is buried at a certain depth underground (Bojic, et al., 1997) in which hot ambient air during summer time is drawn through one end of

the pipe (inlet) and migrates to the other end (outlet) which is connected to the building to be cooled. While the hot air migrates from the inlet side to the outlet side of the EAHE, heat is dissipated from the air to the earth due to the low earth temperature (Bansal, et al., 2009a). It is worth mentioning that the capability of using the EAHE for heating of buildings during the winter time has been investigated by different researchers as well (Mihalakakou, et al., 1996a; Mihalakakou, et al., 1996b; Mihalakakou, 2003; Bansal, et al., 2009b).

Showing a desire to further understand the EAHE system, the contemporary research work on EAHE will be discussed on the "Earth-to-Air Heat Exchanger" section of this chapter with more details on the different levels of study (e.g. mathematical modeling, experimental validation and Performance analysis) that have been conducted in the last few decades.

The other renewable energy source to be investigated in the current research is passive solar energy. According to the United States Environmental Protection Agency (EPA) the solar energy is defined as "Energy from the sun, also known as solar radiation and short-wave radiation. Solar energy includes ultra-violet radiation, visible radiation, and infra-red radiation". Utilizing the solar energy requires a collector to collect the solar energy, a medium (e.g. air or water) to distributer or transfer the energy from the collector to the end users. It is worth mentioning that some systems require converters to convert the solar energy to another form of energy (e.g. Photovoltaic (PV) that converts the solar energy to electrical energy) and storage system (e.g. charging batteries or thermal mass walls).

There are two main strategies in utilizing the solar energy for heating and cooling of buildings called "Active Solar Systems" and "Passive Solar Systems". According to ASHRAE an active solar system is one that uses either liquid or air as the collector fluid and has constant access to non-renewable energy, generally in the form of electricity, to operate pumps and fans (ASHRAE, 1999). A passive solar system is defined as a system that works without the use of fans, pumps, or complex collectors to collect, store, and redistribute solar energy (Lechner, 2001). In other words, it is a system that functions with little, if any, nonrenewable energy (ASHRAE, 1999). Many civilizations have attempted to use the solar energy in different ways and for various purposes. The ancient Greeks used the sun to heat their homes, while the Romans used glass in their windows sometime around 50 A.D. to make a heat trap for the solar energy to increase the efficiency of heating their homes and baths. The seventeenth century in Northern Europe saw a revival for solar heating while the eighteenth century became known as the "Age of greenhouses[2]". Aside from these early examples, utilizing the sun for heating of homes was slowly progressing until the 1930s when the potential of solar energy started to be explored by a number of different American architects especially in designing what is called "solar homes" (Lenchener, 2001). In the recent days, different techniques have been developed to utilize the active/passive solar energy (e.g. the Photovoltaic (PV) and solar chimney).

Another goal of this research is studying the performance of a solar chimney as another technique that utilizes a different renewable energy source (i.e. passive solar

[2] A greenhouse is a building with glass walls and roof; for the cultivation and exhibition of plants under controlled conditions. (http://wordnetweb.princeton.edu)

energy) for the purpose of reducing the temperature inside the buildings as well as providing natural ventilation.

In order to understand what is a solar chimney and how this technique utilizes the passive solar energy to cool and ventilate residential buildings, the solar chimney system will be illustrated.

The solar chimney is a vertical or inclined air channel where its bottom end is connected to the building to be cooled and ventilated. This air channel generates air movement by buoyancy forces and stack ventilation[3], drawing cooler air through the building in a continuous cycle in which hot air rises and exits from the top of the chimney (Bacharoudis, et al., 2007). In other words, a solar chimney is a natural draft device which utilizes energy produced by solar radiation to build up stack pressure, consequently, driving airflow through the chimney (Chen, et al., 2003).

To further understand the solar chimney system; a literature review on the contemporary research work that have been conducted in the last few decades on the solar chimney will be discussed on the "Solar Chimney" section of this chapter.

These two techniques (i.e. EAHE and solar chimney) are further investigated in this research to study the capability of developing an environmentally friendly and energy saving system that could provide cooling for residential buildings during hot summer days to reduce the current summer electrical peak loads in the United States. The following three sections of this chapter provide a literature review for the Earth-to-Air Heat Exchanger (EAHE) system, the Solar Chimney system as well as the

[3] Stack ventilation is cause by stack pressure or buoyancy at an opening due to variation in air density as a result of temperature difference across the opening (Nugroho, et al., 2006).

Coupled system (i.e. EAHE coupled with Solar Chimney). They are followed by two sections providing a summary for the literature review as well as the main objective of this research and how it contributes to the science and the literature.

2.2 Earth-to-Air Heat Exchanger

Many researchers have studied the EAHE from different points of view, some focused on developing mathematical models to predict the performance on an EAHE, and others conducted different types of experiments to evaluate the heating/cooling potential of an EAHE, as well as understanding the main parameters that affects its design. These different views of studying the EAHE are presented in the following sub-sections.

2.2.1 Mathematical Modeling

Different mathematical models have been developed to describe the performance of an EAHE; some of these models are analytical where the differential equations that describe the system can be solved directly. Other models are numerical where they use some sort of numerical time-stepping procedure to obtain the models behavior over time and provide an approximate solutions for the equations (SERC, 2010). In this section, the different types of models that have been developed in the last few decades are presented.

2.2.1.1 Analytical Models

One of the early models presented treated the EAHE as a cylindrical two dimensional heat transfer problem. In doing so, a single cylindrical tube has been simulated in this model taking into account different parameters such as

ambient air temperature, air velocity inside the tube, the tube radius and the air traveled distance along the length of the tube. Though this model is considered a very good beginning for EAHE modeling, it only considered the sensible heat transfer of air to the soil without taking into account the latent heat transfer (Chen et al., 1983b; Newman, 1983).

Another model treated the inlet air temperature (i.e. ambient temperature) to the EAHE as a harmonic periodic sinusoidal input. In this model, a cylindrical EAHE with adiabatic/isothermal boundary conditions submitted to constant airflow with harmonic temperature signal has been simulated. Based on that model it has been shown that depending on its thickness, the soil layer could induce either an amplitude-dampening or phase-shifting regimes. It is shown that during the summer time for a thin soil layer that submitted to an adiabatic boundary condition, it is possible to completely phase-shift the periodic input while barely dampening its amplitude (Hollmuller, 2003).

Though this model is considered a precise analytical model that took into consideration both the steady state as well as the periodic state heat transfer in the EAHE, it did not take into consideration the latent heat transfer and the natural airflow (buoyancy or wind).

A different model that aimed to simplify the EAHE problem and bringing it out of the academic world to make it easy to use by designers considered the EAHE problem as a mere heat exchanger. In doing so, some of the model inputs parameters are considered as known designed requirements (i.e. air mass flow rate inside the tube and the outlet temperature of the tube $T_{air, out}$)

while other input parameters are considered as given climatic conditions (i.e. the tube inlet temperature $T_{air, in}$ and the ground temperature). In this way, the EAHE problem is reduced to determining the size of the tube (i.e. Tube length L and diameter D) once the number of tubes to be used is known. Now the EAHE model became a simple one-dimensional analytical model instead of the two-/three-dimensional models previously presented by other researchers. This model can help in evaluating the thermo-hydraulic performance of the EAHE through using the Number of Transfer Units (NTU) and the heat exchanger effectiveness method (De Paepe and Janssens, 2003).

In his model, Al-Ajmi (2006) separated the soil temperature model from the EAHE model. Where the first is used to mathematically model the annual sub-surface soil temperature based on heat conduction theory applied to a semi-infinite homogenous solid, the second model uses the subsoil temperature (predicted from the first model) as a boundary condition input to model a circular ground cooling pipe (i.e. EAHE) as a cross–flow heat exchanger with one fluid unmixed (i.e. air) in order to predict the EAHE outlet temperature as well as its cooling potential. Using these models several new parameters have been taken into consideration (e.g. the soil annual temperature fluctuations) (Al-Ajmi, et al., 2006).

This model is considered as a simple practical model to be used by designers though it only considered the forced air flow without taking into consideration the natural airflow (buoyancy or wind).

In addition to the above mentioned methods used by different researchers to develop an analytical model to describe the EAHE system, the energy balance equations have been also used as a way of modeling an EAHE coupled with a greenhouse. First, the energy balance equations were used to determine the stored energy within the ground, thereby the earth's surface and subsurface temperatures. Here, the solar energy absorbed at the soil surface is balanced with the heat losses by the outgoing long wave radiations and the convective heat exchange with the ambient air mass. Second, another set of energy balance equations were used to predict (determine) the heating and cooling potential of the EAHE, thereby finding the temperature inside the greenhouse. In doing so, the energy conducted and radiated from greenhouse walls, floor and EAHE is balanced with the heat gained/lost from/to the air inside the greenhouse and the ambient air. Using this detailed analytical model the heating and cooling potential of an EAHE coupled with a green house was evaluated. Moreover, studies of the effect of the different EAHE parameters on the system performance have been conducted. The model has been validated against experimental data. And the proximity of the measured and predicted data was verified using the coefficient of correlation (c_r) and root mean square percent deviation (e_r), which showed fair agreement (Ghosal and Tiwari, 2006).

In another study, a more detailed analytical model that utilizes the energy balance equations for describing the EAHE system has been used. In this model, more parameters have been taken into consideration. For example, the

annual soil temperature variations due depth and time, the soil convective heat transfer, the solar radiation absorbed by the ground, the long wave radiation emitted from the ground surface, and finally the latent heat loss due to evaporation. The energy balance among these parameters was implemented on an analytical model to determine the soil temperature profile as a function of time and depth. In the mean time a two dimensional heat transfer equations were used to describe the heat transfer between ambient air, soil, EAHE and air inside the pipe. An overall heat transfer coefficient using the thermal resistance concept was used to facilitate driving the equations of the EAHE model. Using these two models, investigations on the effect of some parameter (e.g. EAHE length, radius, depth and airflow) on the EAHE have been conducted (Lee and Strand, 2006). Though the model has taken into considerations many parameters, it should be noted, however, that it would have been better if the model has been validated against experimental data and included latent heat exchange within the air inside the pipe (Thevenard, 2007).

2.2.1.2 Numerical Models

Since numerical models are easier to be programmed and sometimes more powerful than analytical models, many researchers preferred to develop numerical models to describe the performance of the EAHE system, though they only provide an approximate solution for the problem.

Different numerical models utilized different numerical methods (e.g. Finite Difference and Computation Fluid Dynamics (CFD) to simulate an EAHE system.

Some of these models utilized the finite difference method to simulate the performance of an EAHE. One of the early models that used the finite difference method to simulate the EAHE considered the system as a transient axi-symmetric system. This model presents an accurate transient model based on coupled and simultaneous transfer of heat and mass into the soil and circulating air. In this model, the humidity variations of the circulating air, the natural thermal stratification of the ground, latent and sensible heat transfer and ground surface conditions have been taken into consideration. The model has been validated against experimental data and showed that it could accurately predict the tube extracted temperature variations along the length with an error range of (±1.6%) (Kumar, et al., 2003).

Another model that utilized the finite difference method to solve the EAHE modeling equations treated the heat transfer inside the EAHE system as fully three-dimensional heat diffusion in soil with a flexible border conditions. This model has accounted for sensible as well as for latent heat exchanges (Hollmuller and Lachal, 2005). Though the predicted data showed a very good agreement with the analytical model (previously presented by: Hollmuller, 2003), its agreement with the experimental results were not as good.

In this model a new idea has been presented in which the EAHE has been divided into “n” sections perpendicular to the exchanger pipe where the heat conduction problem of each section has been solved using the response factor method in order to reduce the computational time. Each response factor is

calculated using a finite element program that solves 2D conduction problem (Tittelein, et al., 2009). Though this model would save the computational time when simulating a single pipe EAHE system, it has been found to be time consuming when simulating a multi-pipe EAHE system. It could have been better if it took into consideration the axial conduction transfers in the ground as well as the probability of the presence of a building near the pipe that could influence the ground temperature. Moreover, the model has been only validated against analytical models not against real experimental data.

As some researchers have used the finite difference technique in simulating the EAHE performance, other has used the Computational Fluid Dynamics (CFD) technique as well. One of the reasons behind using the CFD method is that it is well known to be a powerful tool in studying heat and mass transfer for many years. It is also worth mentioning that CFD codes are structured around the numerical algorithms that can tackle fluid flow problems. This provides numerical solutions for partial differential equations governing airflow and heat transfer in discretized form (Bansal, et al., 2009a). Accordingly, a transient and implicit numerical model, which is based on the CFD to predict the thermal performance and cooling/heating capacity of an EAHE, has been developed. The model has been validated against experimental data and showed good agreement though it considered air as an incompressible fluid. (Bansal, et al., 2009a; Bansal, et al., 2009b).

Another model that utilized the CFD in simulating the performance of an EAHE, considered a square section heat exchanger. In that model, a two layer

turbulent method has been used to investigate the airflow and the thermal behavior in large ducts. Using this model, it has been claimed that large cross-section area EAHE have been found to be more efficient than conventional small ones (Zhang and Haghighat, 2009).

As the Artificial Neural Network (ANN) systems have been shown to present the capacity of modeling complex non-linear processes to arbitrary degrees of accuracy, newly developed intelligent numerical techniques (i.e. Artificial Neural Networks and Genetic Algorithms) have been also used to simulate the EAHE system.

ANNs imitate the learning process of a biological brain. Through the learning (training) process, the neural network understands the underlying functional relationships in the loaded data. The date is stored as inter-neuron connection strengths or synoptic weights (Kumar, et al., 2006). These computing systems attempt to simulate the structure and function of biological neurons. The structure of the network is determined by how the inter-neuron connections are arranged and the nature of the connections (cited after: Mihalakakou, 2003). The intelligent techniques do not require as many input parameters as the ordinary numerical models. A neural network approach was used for estimating the thermal performance of the system in heating of the city of Athens. In this model, a back-propagation algorithm has been used to train the Artificial Neural Network (ANN) model developed. Though the ANN model showed a convenient agreement with the deterministic numerical model, this agreement is not considered a sufficient validation as the ANN

model and has not been validated against experimental data. Moreover, the model has only considered the heating performance (cited after: Mihalakakou, 2003).

As a way of simplifying the EAHE problem to help the designer to evaluate any aspect of EAHE and behavior of final configuration, another model that is based on the ANNs approach has been developed. As it is believed that neural network models are not programmed but are trained. Consequently, a deterministic model has been developed first, where the EAHE modeled as a transient axi-symmetric system and finite difference technique is used to determine temperature at subsequent nodes. This deterministic model accounts for humidity variations of circulating air, natural thermal stratification of the ground, latent and sensible heat transfer, and ground surface conditions, etc. Second, a neural network model based on a back-propagation algorithm has been developed to estimate the temperature at the buried pipe exit. This data driven model used ground temperatures, air temperature, relative humidity, ground temperature at burial depth, air mass flow rate, and pipe (tunnel) length as inputs. When the two models (i.e. deterministic and neural network) were compared, it was found that the ANN model predicted the outlet air temperature with and accuracy of ±2.6% while the deterministic model showed an error of ±5.3%. The data show that the ANN model could be helpful in evaluating the aspects related to the passive heating or cooling of buildings as well as investigating the energy potential of

heating and cooling of EAHE system even though the model was mode trained the outlet air temperature of an EAHE (Kumar, et al., 2006).

The genetic algorithms (GAs) are another intelligent technique that has been introduced to numerically model an EAHE system. It is considered to be a powerful technique in analyzing natural problems like EAHE and subsequently the thermal performance of non air-conditioned buildings. Two models were employed to determine the heating and cooling potential of an EAHE system, namely deterministic and intelligent (i.e. GA model). The intelligent model incorporated more accuracy than the deterministic model. It has been shown that the GA model could be utilized in sizing of an EAHE in a non air-conditioned residential building as well as calculating the outlet air temperature and therefore the heating and cooling potential of the EAHE system (Kumar, et al., 2008). Though, GA models are claimed to be used to simplify the design problem of an EAHE, it should be noted, however, that they did not find a wide acceptance among scientists and researchers as they are believed to have computation complexity (Deb, et al. 2000).

Few other researchers used other numerical techniques to simulate the EAHE system, evaluate its heating/cooling performance as well as to aid designers in the design and sizing aspects of the system. For example, one of the numerical techniques utilized by one of the researchers is using the fourth order “Runge-Kutta” numerical method which is employed to solve the energy balance equations that have been used to describe the EAHE system (Chel and Tiwari, 2009).

Another numerical technique called "the time marching methodology[4]" has been developed at Kragujevac University in Kragujevac, Yugoslavia for the numerical modeling of an EAHE system. With this technique, the soil has been numerically divided into elementary layers where the governing relations for all layers form a set of linear equations that has been solved numerically using such a technique. Using this technique and model the technical (i.e. heating and cooling) performance of an EAHE coupled with a building that uses 100% fresh air as heating or cooling medium during winter and summer has been evaluated. It has been shown that the EAHE system covers a portion of the daily building-energy needs, especially during the summer time (Bojic, et al., 1997).

Different numerical software packages haven been also utilized to numerically solve the energy balance equations of an EAHE system. For example, an explicit numerical model which is adapted to TRNSYS[5] has been developed to simulate the EAHE system. This model simultaneously accounts for both latent and sensible heat exchanges, as well as for frictional losses and water infiltration and flow along the EAHE tube (Hollmuller and Lachal, 2001).

[4] A building simulation program developed at Kragujevac University in Kragujevac, Yugoslavia.
[5] TRNSYS is a modular energy system simulation environment, developed by the University of Wisconsin. (http://sel.me.wisc.edu/trnsys/).

The Energy-Plus[6] building performance modeling code program has been also used to analytically simulate the EAHE system. Using this program a detailed model that took into account different parameters (e.g. solar radiation) has been developed. Utilizing the developed model, a study of the effect of the EAHE system parameters on its performance have been conducted. Where it was found that the system performance is enhanced by increasing the pipe length and depth and decreasing the pipe diameter and air flow. It has been claimed that even though the EAHE could reduce the cooling loads to a certain degree, it cannot be used as a stand-alone system as it does not maintain thermally comfortable conditions under hot ambient conditions (Lee and Strand, 2006). This claim could have been considered as enough evidence for the poor performance of the system only if the model has been validated against experimental data.

In summary, various researchers have used different mathematical models (e.g. analytical and numerical) that utilize distinct techniques (e.g. energy balance, Finite difference or ANN) to describe the performance of an EAHE system to help in the design aspects of an EAHE as well as in evaluating the system performance.

[6] Energy-Plus is a building energy simulation program developed by the Energy Efficiency & Renewable Energy (EERE) a section of U.S. Department of Energy (DOE).

2.2.2 Experimental Investigations

Not only were the researchers concerned about the mathematical modeling and simulation of the EAHE system but also about the experimental study of the system. Accordingly, different experiments on the EAHE system, with various materials, sizes, types, functions, locations, experimental setups and scientific research objectives have been conducted around the globe. The common major objective of all the experiments is to further understand the EAHE system, through investigating its potential for heating and cooling, understanding the main parameters that affects its performance, and the capability of evaluating its performance using different techniques (e.g. Mathematical models).

One of the early experiments was conducted on a four open loop EAHEs at the University of Nebraska, with different diameters, lengths, air velocities and burial depths to determine the main design parameters that affect the performance of the system. For this set of experiments results showed that the maximum effect for an EAHE is heavily dependent on temperature difference between the ambient air and soil surrounding the tube (i.e. EAHE). It has also been found that for a constant flow rate, the wider the tube the better the performance, which has been attributed to the increase of the surface area exposed to the soil. Furthermore, the thermal performance of the system has been enhanced by increasing the burial depth and length of the EAHE as well as reducing the airflow rate, which allows for a better heat transfer (Chen, et al., 1983a). This kind of experimental study is usually called “Parametric Study” or “Sensitivity Analysis”; more attention will be given to this type of experiments on the section “Performance Analysis” of this chapter.

Other sets of experiments have been conducted through applying different airflows on a two identical open loop EAHEs coupled with a residential building. One of the pipes were made of mild steel while the other of PVC. The main objective of these experiments was to understand the effect of different pipe materials on the performance of an EAHE system during the summer and winter seasons. In these studies, it has been concluded that the thermal performance of the EAHE system is not affected by the different materials, thereby, the system installation costs could be reduced (Bansal, et al., 2009a; Bansal, et al., 2009b).

In conducting the different experiments, some of the researchers built a full-scale experimental setup to achieve a certain scientific goal as well as to help the future generations in conducting further research. For example, the Passive Solar Research Testing Facility located in Omaha, Nebraska, includes a single open loop EAHE integrated with a testing building. This full-scale experimental setup has been used by different researchers for different scientific goals. One of these goals was to analyze and evaluate the performance of the EAHE when forced airflow is drawn through the pipe. The thermal performance has been investigated through applying various air flows at several ground saturation levels for a single open loop EAHE system. Experimental results demonstrated that the system is able to provide up to 1.5 tons of cooling (18,000 Btu) at a flow rate of 1600 CFM during hot summer days. It is worth mentioning, that the cooling performance of the system did not drop even though soil thermal saturation was noticed around the tube over the test period (Henkel, et al., 2004).

Experiments have not been only limited to an experimental setup in research facilities. In fact, some experiments have been conducted on actual occupied buildings. As an example, an experimental study of three different EAHEs systems integrated with three different office building located at Hamm, Freiburg and Weilheim[7] in Germany was conducted to characterize the efficiency of each system as well as to provide a standardized method of evaluating the performance of an EAHE system. In this study, it has been concluded that designing and evaluating the performance of the EAHE is a multilayered process that involves a wide range of criteria and ventilation demands. Therefore, evaluating the efficiency of the EAHE should be based on project-specific criteria. In addition, the thermal performance (i.e. temperature performance and energy efficiency) should be evaluated using different techniques (e.g. COP, energy gain, etc.). Moreover, the thermal efficiency of the EAHE should be taken into consideration at design decisions, as well as other design parameters (e.g. EAHE length, diameter, etc.). For example, the surface area for heat transfer of the system will be different base on whether the EAHE is aimed at a higher specific energy performance or at a higher temperature ratio at the design phase. Accordingly, a standardized method for evaluating the thermal performance of the EAHE based on (R_T, h_{mean}, Θ, and COP) has been developed. (Pfafferott, 2003).

Another example is the multi-pipe EAHE systems coupled with the "Caroubier" multifamily and commercial building standing in the city of Geneva and the "Schwerzenbacherhof" commercial and administrative building located near Zurich, Switzerland. These two systems (i.e. experimental setups) have been utilized as

[7] Hamm, Freiburg and Weilheim are three different cities in Germany.

existing experimental setups for the validation of one of the numerical models developed to describe the EAHE system performance, as well as to examine the fundamental difference between winter pre-heating and summer cooling potential of buried pipe (i.e. EAHE) systems under Central European climate, where both the sensible and latent heat exchanges have been considered. The multi-pipe EAHE systems integrated with these two buildings is different from the conventional (i.e. single pipe) EAHE systems. They use more than 40 parallel pipes (i.e. multi-pipes) connected together in the form of a serpentine, with one end (inlet) of the serpentine subjected the fresh outdoor air while the other end (outlet) connected to an air blower which in turn is connected to the building to be conditioned. The mere reason for using a multi-pipe EAHE system instead of a single straight pipe EAHE is to increase the heat exchanger exposed surface area to improve the system performance. The above mentioned systems were used for both summer preheating in conjunction with a heat recovery system, as well as for summer cooling (with slightly enhanced air flow), in conjunction with direct night ventilation. The experimental results demonstrated that the system is not as effective for the winter preheating as it is for the summer cooling. Furthermore, it was found that the summer cooling potential could dampen the indoor air temperatures below the comfort threshold. This allows the EAHE system to compete with conventional air conditioning systems, especially because it could provide simultaneous savings on electricity, capital cost, and CFC[8] gases. These results were used to validate a numerical model. Comparing the

[8] **CFC** (a fluorocarbon with chlorine; formerly used as a refrigerant and as a propellant in aerosol cans) *"the chlorine in CFCs causes depletion of atmospheric ozone"*.
http://wordnetweb.princeton.edu/perl/webwn?s=cfc

experimentally measured test data model's with predicted data showed very good agreement (Hollmuller and Lachal, 2001; Hollmuller and Lachal, 2005).

Some of the experiments were focused on the experimental validation of a pre-developed mathematical model, parametric study of the EAHE system, or the heating and cooling potential of the system. Others were focused on studying new ideas of utilizing the EAHE system as well as new applications.

One of these ideas is to study the performance of a single pipe EAHE coupled with a mechanical air-conditioning system that uses 100% fresh air as heating or cooling medium during winter and summer. The potential of the EAHE to pre-heat and pre-cool the fresh air entering to the mechanical air-conditioning system as well as its economical performance have been evaluated. It is found that the EAHE covers a portion of the daily cooling demand. Furthermore, the system is found to be more energy and cost efficient during summer than winter (Bojic, et al., 1997).

Another idea was to evaluate the performance as well as to study the annual energy saving potential of a closed loop EAHE system integrated with an adobe house building with a vault or inverted U-shape and dome shape roof structures located in New Delhi, India. The closed loop EAHE integrated with the adobe house consists of an air blower and PVC pipes of 6 cm diameter buried at a depth of 1.5 m underground. Both the inlet and outlet of the EAHE pipe are connected to the adobe building to be conditioned. Operating the air blower sucks the room air into the air duct through a filter and then air is circulated through the underground EAHE system. The outlet air pipe (i.e. delivery pipe) is fed inside the room which supplies hot/cool air during winter/summer month respectively. In that sense, the closed loop EAHE is

different from the open loop EAHE in order to provide natural thermal comfort. The experimental results have been used to validate a numerical model. Simulations illustrated that annual energy savings of 10321 kWh/year as well as CO_2 mitigation of about 16 tons/year could be achieved (Chel and Tiwari, 2009).

The EAHE applications are not limited to the heating and cooling of residential buildings but it also includes various different applications for example, stabilizing the temperature inside a greenhouses. Where the relatively stable temperature of ground at certain depths is utilized to overcome the large temperature variations between day and night hours both in summer and winter that affects the quality and quantity of crops being cultivated in greenhouses. A multi-pipe closed loop EAHE system integrated with the greenhouse located in India Institute of Technology (IIT) Delhi, India was built for different research purposes on the EAHE coupled with a green house.

One of the early research goals conducted on that system was to investigate the heating and cooling potential of EAHE buried under bare soil for real climatic conditions at IIT Delhi. Moreover, the thermal capacity of such system has been simulated and compared with the potential of the same system, buried under glazed surface (greenhouse covered earth) soil with an aim to improve and to study its performance by using different soil surface conditions. Consequently, the experiments conducted on the system have been used to experimentally validate an analytical model, where comparison showed a fair agreement. Results showed that the system could rise the greenhouse temperature by 6-7°C during winter and lower it

by 3-4°C during summer. Contradicting the previous experiments conducted on residential buildings, it was found that the EAHE is more effective in winter than in summer especially under the glazed surface conditions (Ghosal, et al., 2004).

Another goal was to compare the potential of using the stored thermal energy of ground for space heating using this system (i.e. EAHE) and a ground air collector (GAC) system coupled with a greenhouse. Experiments proved that the GAC system arrangement provides better heating performance than the EAHE for the greenhouse (Ghosal, et al., 2005).

One of the recent research goals conducted on this greenhouse-EAHE experimental setup was to validate the thermal model developed previously by Ghoshal and Tiwari (2004) by round the year experimental work at IIT Delhi. The thermal model has been evaluated using the correlation coefficient (C_r) and root-mean-square percentage deviation (e_r) methods, while the performance of the system has been assessed in terms of thermal potential, coefficient of performance (COP) and thermal load leveling (TLL) for each month of the year. In contrast with other papers written on the experimental validation for mathematical models, more details on the experimental validation process have been presented rather than focusing on the mathematical modeling equations. Though more details on the experimental setup have been presented in this paper, it would have been better if the instrumentation calibration process as well as sensors installations were presented. Contradicting the results by (Ghosal, et al., 2004), in this study, it has been concluded that EHAE is

more effective in summer than in winter because of the more steady temperatures inside the greenhouse during summer time (Tiwari, et al., 2006).

It is worth mentioning that the EAHE system integrated with greenhouses are different from that integrated with residential buildings. Integrated systems with greenhouses are usually composed of a multi-pipe system buried at a depth of only 1m underground as the heating/cooling load in greenhouses are much less than that of residential buildings. Another difference is that greenhouses are always a closed loop systems with an air blower connected to them, as the main purpose of the system is to reduce the temperature fluctuations between day and night hours both in summer and winter, or in other words to stabilize the greenhouse temperature in order to improve the quality and quantity of crop cultivated. This is in contrast to residential buildings where EAHEs are used to introduce fresh air as well as providing thermal comfort for the occupants.

In summary, different experiments with diverse experimental setups have been conducted to further understand the EAHE systems. Accordingly, some experiments focused on the parametric study of the system, while others focused on the heating/cooling potential of the system coupled with residential building or greenhouses. A number of experiments aimed to evaluate/compare the performance of the system with other systems (e.g. ground air collector (GAC) system), while others were designed for the experimental validation of mathematical models (analytical or numerical) so it could be reliably used to either design (i.e. size) or evaluate the performance of an EAHE.

It could be better that most of the research papers written on such experimental goals were focused on not only the results of the research but also presenting the experimental setup and the process used to reach such results. As one of the reasons, full-scale experimental setup with all the experimental details (e.g. sensor installation and instrumentation calibration) is presented in the current study on chapter 3 and 4.

2.2.3 Performance Analysis

Understanding the performance of the EAHE system leads to improving its efficiency, and consequently, satisfying its design purposes. Numerous experiments have been conducted on different levels to analyze and understand this topic of improved efficiency.

One of the attempts to understand the performance of the EAHE system was to conduct a parametric study in order to understand the main parameters that affect the performance of the system. Some of these parametric studies focused on the design parameters of the system (e.g. the EAHE pipe length and diameter) while others focused on the surrounding environmental parameters (e.g. soil cover and temperature). In this next section, a literature review on all the performance aspects of EAHE systems will be presented.

In pursuing a parametric study on an EAHE system coupled with a residential building, an experiment was conducted using four distinct types of EAHEs. Each had a different size ranging from 1 - 1.5ft (0.3 - 0.46m), buried at various depths underground ranging from 4.9 - 5.5ft (1.5 – 1.7m), with several airflow rates and experimental periods. Temperature and airflow data has been collected at numerous positions along the lengths of each EAHE on a quarter hour basis. Results showed

that the parameters that were necessary to find cooling performance were: ambient and soil temperature characteristics, tube material, tube length, tube radius, thermal conductivity of soil, air, and tube material, heat transfer of air and tube material and air flow rates (Newman, 1983; Chen, et al., 1983a).

On further parametric studies conducted on EAHE systems, researchers narrowed down the design parameters affecting the system thermal performance to four main parameters namely; pipe length (L), pipe diameter (D), burial depth (d) and air velocity inside the pipe (υ). Where it has been found that the thermal performance (i.e. heating and cooling) of the system improves with increasing pipe length (L), decreasing pipe diameter (D), increasing the depth of the buried pipe under the earth surface (d), and decreasing air velocity inside the tube (υ). These experimental parametrical results were found to be the same for the various experiments conducted on EAHEs coupled with either residential buildings or green houses for heating and cooling purposes (Santamouris, et al., 1995; Mihalakakou, et al., 1996; Ghosal and Tiwari, 2006).

Based on the experimental parametric studies of the EAHE system some researchers developed parametrical models for the prediction of the thermal performance of the system. The above mentioned four variables (i.e. L, D, d and υ) influencing the thermal performance of the system were taken into account in the models. The models developed are suitable for the calculation of the exit air temperature and therefore the cooling/heating potential of the system. A theoretical parametrical study has been conducted on one of the models to validate the effect of

the previous mentioned parameters on the thermal performance of the system (Mihalakakou, et al., 1995; Lee and Strand, 2006).

It is worth mentioning that a special parametric study was conducted on a two identical open loop EAHEs, except that one was made of PVC, while the other was made of mild steel. The two pipes were connected to a common intake and outlet manifold for air passage. Global valves were fitted for each pipe assembly for flow control of air. The whole system was coupled with a residential building where the common intake pipe was connected with an air blower with a variable speed drive. Through applying different airflows to the two pipes and collecting airflow and temperature data for both pipe during summer and winter, it has been shown that different EAHE material did not affect the performance of the system (Bansal, et al., 2009a; Bansal, et al., 2009b).

As mentioned earlier, some of the parametrical studies were focused on studying the main design parameters affecting the thermal performance of the EAHE system, while others were focused on studying the effect of the surrounding environmental parameters. For example, one of the studies used ten years hourly data of air and ground temperatures at different depths below bare and short grass soil at Dublin Airport. The data was used to investigate the influence of diverse ground surface boundary conditions on the efficiency of a single and multi-pipe parallel EAHE system. The heating potential of the two systems buried under bare soil were evaluated and compared with that of the same systems buried under short-grass-covered soil. The main goal behind this research was to study the affect of different ground covers on the thermal performance of EAHE system. Results showed that the

bare soil surface could increase the system's heating capacity (Mihalakakou, et al., 1996a).

Another parametrical study on the effect of the surrounding environmental parameter on the thermal performance of the EAHE system was held in New Delhi, India. In this study the effect of different treatments of bare soil surfaces namely blackened, wetted, blackened and glazed were examined. Consequently, a quasi-steady state mathematical model was developed to predict the outlet air temperature and monthly heating and cooling potentials of an EAHE system under the all three conditions. Results showed that the blackened, wetted, and blackened and glazed surfaces could sharply increase the heating potential of the system due to the high absorptive property of the surface during winter. The cooling potential can also be increased due to the wetted surface in summer conditions and to the evaporation of absorbed thermal energy (Shukla, et al., 2006).

After understanding the main parametrical factors that affected EAHE system performance, the thermal performance (i.e. heating and/or cooling potentials) was evaluated for different researchers. Various techniques have been used for the thermal performance evaluation of the system. Collecting temperature data along the length of the EAHE and calculating the thermal capacity in (kWh) over a certain period of time was one of the techniques used (Henkel, et al., 2004). It was found that the performance varied based on the different design and environmental parameter, location, application and time of the year. In one of the researches it was claimed that the system daily average cooling potential was about 456 kWh while the heating potential was about 296 kWh (Kumar, et al., 2003). Another research claimed that the

system summer cooling potential was 19.6 MWh while the winter preheating potential was 25.7 MWh (Hollmuller and Lachal, 2001).

Other techniques like the coefficient of performance (COP) which gives an idea of how efficient the system is and the thermal load leveling (TLL) which indicates the fluctuation of temperature inside the greenhouse, were also used to evaluate the EAHE thermal performance (Ghosal, et al., 2005). Calculating the monthly variations in COP, it was found that the COP was higher in summer (ranging 0.96-1.41), medium in winter (ranging 0.63-0.78), and lower during monsoon season (0.46-0.095) for an EAHE system coupled with a greenhouse. It was also found that the TLL values were lower for the greenhouse with an EAHE than a greenhouse without an EAHE, proving the effectiveness of the system (Tiwari, et al., 2006).

In another study that aimed to compare three different EAHE systems, it has been claimed that in order to characterize the efficiency of the system, three levels of study should be pursued. First, the temperature behavior was described by plots over time and characteristic lines and compared by standardized duration curves. Second, the energy gain was illustrated by standardized graphs. Third, a parametric model was used to provide general efficiency criteria. Accordingly, the thermal performance (temperature performance and energy efficiency) of EAHEs was assessed using four different approaches (R_T, h_{mean}, Θ and COP) (Pfafferott, 2003).

A number of attempts were pursued to understand the performance of the EAHE system not only from the technical performance perspective but also from other various perspectives (e.g. economical performance). Reducing current peak electrical energy loads and finding an environmentally friendly air-conditioning system were

some of the factors that enhanced the utilization of the EAHE system. It was important to evaluate the system performance from both economical as well as the environmental perspectives. For this reason one of the studies determined the annual energy savings potential of adobe house for three conditions: (i) before renovation, (ii) after renovation and (iii) with EAHE were calculated to be 4182 kWh/year, 4946 kWh/year and 10321 kWh/year respectively. The life cycle cost (LCC) analysis showed that the payback period was less than 2 years for the investment on an EAHE system. It was also found that the system's average seasonal energy efficiency ratio (SEER)[9] for heating and cooling was determined as 1.8 and 2.9 respectively. From the environmental perspective the CO_2 emissions mitigation was calculated for the same above three conditions and it was found to be nearly equal 7 tons/year, 8 tons/year and 16 tons/year, accordingly, the carbon credits that can be earned by the adobe house with EAHE is about € 320/year (Chel and Tiwari, 2009).

In another research study, the economical and environmental aspects of a closed loop EAHE system coupled with a 2.32 kW photovoltaic power system that powers an electric air blower (integrated with the system) has been studied. It was found that the annual heating and cooling energy conservation potential due to the EAHE for three rooms (each $63m^3$) was determined as 3327 kWh/year and 2667 kWh/year respectively. This led to mitigation of CO_2 emissions 9.4 tons/year which was

[9] SEER is a measure of equipment energy efficiency over the cooling season. It represents the total cooling of a central air conditioner or heat pump (in Btu) during the normal cooling season as compared to the total electric energy input (in watt-hours) consumed during the same period. SEER is based on tests performed in accordance with AHRI 210/240 (formerly ARI Standard 210/240). (http://www.energystar.gov/index.cfm?c=airsrc_heat.pr_crit_as_heat_pumps)

equivalent to carbon credit of €188. Hence, use of EHAE for heating/cooling of an adobe house was found to be a promising and environmentally friendly option in New Delhi, India (Chel and Tiwari, 2010).

In summary, understanding the performance of the EAHE is one of the main concerns for researchers and scientists. For that reason, many studies were conducted to understand the different aspects that affect the performance of the system. Several of these studies focused on understanding the main EAHE design parameters (e.g. length and diameter), while others focused on the surrounding environmental parameters (e.g. ground surface cover) that affects the system. The thermal performance as well as the economical and environmental performance was the main aspects that researchers tackled to evaluate the efficiency as well as the effectiveness and applicability of the system. Studies showed that the EAHE could be a feasible alternative for the mechanical air-conditioning systems, as it was proved to be thermally efficient, environmentally friendly and cost effective.

2.3 Solar Chimney

The other technique utilizing a non-renewable energy source that the current study focuses on is the solar chimney. As with the EAHE, the solar chimney has undergone a number of different research experiments and investigations to understand its performance. Mathematical models as well as performance analysis methods have been developed to evaluate its efficiency and practicality. Accordingly, a literature review on the various aspects for studying the solar chimney is presented in the following sub-sections.

2.3.1 Mathematical Modeling

As the solar chimney problem involves both fluid movement as well as heat transfer, it was found that the computation fluid dynamics (CFD) is a good tool to describe the system numerically (Nugroho, et al., 2006; Ming, et al., 2008). The CFD has been used as a tool to simulate the airflow and heat transfer in the solar chimney in order to predict the mass flow rate per unit length in the chimney. Accordingly, some of the CFD models were used to evaluate the performance of a glazed solar chimney for heat recovery in naturally ventilated buildings (Gan and Riffat, 1998). Other models were used to study the thermal behavior and efficiency of a four wall solar chimney used for cooling of buildings. In doing so, a simulation of six turbulence models was conducted using the commercial, well-known, general-purpose CFD code, Fluent®. Using these six different models the thermo-fluid phenomena inside the wall solar chimneys were investigated and where the buoyancy-driven flow field and heat transfer inside them were also studied. The governing elliptic equations of the chimneys were solved in two-dimensional domain using a control volume method. It was found that the k-ε model provides superior performance when compared with experimental data (Bacharoudis, et al., 2007).

A CFD model was used to study the fluid flow and heat transfer patterns (profiles) of the solar chimney; while, an engineering mathematical model was developed to determine the tilt that maximizes the natural air flow inside the chimney. The monthly average daily value of total irradiance and the ambient

temperature along with some design information (i.e. dimensions and construction material properties) for the different chimney components (i.e. absorber, glazing, installation) were used as inputs for the model. Processing these inputs, the hourly absorbed solar irradiation components (i.e. direct, diffuse, ground-reflected) by the solar chimney were calculated at various chimney heights and tilts at a given time (Day of year, hour) and location (latitude). Thereafter, the chimney glazing transmittance and absorbance were computed for the different solar irradiation components and various tilts. Accordingly, the temperature and air velocity inside the chimney as well as the temperatures of the glazing and black painted absorber were predicted (outputted), as functions of tilt and height. This engineering model has been validated against the CFD and experimental data. Results showed that the predicted data is in a reasonable agreement with the CFD and experimental data. Accordingly, the use of the model as a technique for evaluating design parameters was encouraged (Sakonidou, et al., 2008).

Other techniques have also been used beside the CFD to simulate the solar chimney systems. One of these techniques was used to study a system that is mainly used for heating and ventilation of dwellings. A conjugate heat transfer study by natural convection, conduction, and radiation was carried out to determine the importance (effect) of each heat transfer mode on the performance of the system. A two dimensional conservation equations for mass, momentum and energy were used to describe the system. The conservation equations were then solved by finite difference-control volume numerical method. It was found that the radiation heat transfer could not be neglected in the solar chimney

systems, mainly because the surface radiation modified the flow and temperature fields (Nouanégué and Bilgen, 2009).

Solar chimneys have a number of different applications such as ventilation, passive solar heating and cooling of buildings, solar energy drying and power generation (Chen, et al., 2003). The numerical simulation was not limited to the mere solar chimney system but it has also extended to cover some complementary applications coupled with the system. As an example, one of the numerical models was established to analyze the characteristics of heat transfer and air flow in the solar chimney power plant (SCPP) system with an energy storage layer. Where the model covered the four major components of the solar chimney power plant system: collector, chimney, wind turbine, and energy storage layer (Ming, et al., 2008).

2.3.2 Experimental Investigations

Many experimental investigations were carried out to evaluate the performance and the potential of the solar chimney systems. While, some investigations emphasized on evaluating the thermal performance of the system, others, emphasized the experimental validation of mathematical models.

One of the thermal performance experimental investigations was carried out on an experimental solar chimney model with internal dimensions of 1.5m high, 0.62m wide and a variable chimney gap from 100 to 600 mm. Various uniform heat fluxes were applied to one of the chimney walls, at different chimney gaps and inclination angles. The goal of these experiments was to investigate the effect of varying the heat flux and changing the chimney gap and

inclination on the airflow and temperature distribution inside the solar chimney. Contradicting to previous experimental investigations, it was shown that by changing the chimney gap while maintaining other conditions, the airflow increased continuously with increasing chimney gap. Results also showed that the airflow reached a maximum at a chimney inclination angle of around 45° for a 200 mm gap and 1.5m high chimney, which was about 45% higher than that for a vertical chimney under otherwise identical conditions (Chen, et al., 2003).

A different experimental investigation conducted on a chimney duct that has the shape of narrow parallelepiped, mantled on a mechanism that allows the chimney to lie at different tilt positions. It was found that there were two things that have opposite directions with respect to the air flow occur: the more the inclination the more the chimney exposed to solar irradiance, hence higher airflow and buoyancy forces occurs; on the other hand, increasing the inclination reduces the effective pressure head of the chimney and diminishes the air flow. From this opposite action came the idea of optimum tilt. Accordingly, a numerical model was developed to determine the tilt that maximized natural airflow inside a solar chimney. Results for various chimney lengths (1-12m) and tilts (30-90°) delineated the usefulness of the model but also marked its limitations (Sakonidou, et al., 2008).

The smart idea of coupling the solar chimney system with the EAHE system was experimentally investigated. The solar chimney was designed to drag airflow through the EAHE system instead of using an electrical fan. The pressure

balance and airflow balance equations where used to theoretically model the airflow through the system. The theoretical design principles of the solar chimney and solar collector where also presented. The thermal performance of the coupled system was investigated through installing thermocouples along the collector and the chimney as well as an airflow meter at the pipe outlet. Results showed that increasing the chimney height, diameter and solar collector size significantly improves the airflow inside the chimney. It is worth mentioning that at sizing the chimney special care should be given to the chimney structure strength, stability, installation space, material and construction cost (Wang, et al., 2004).

2.3.3 Performance Analysis

In the recent years, a number of experimental, numerical and theoretical investigations have contributed to the current understanding of solar chimneys (Chen, et al., 2003). Through the different investigations, it has been found that thermal performance of the solar chimney is affected by either design parameters (e.g. height, width, glazing etc.) or environmental parameters (e.g. solar irradiance, wind speed etc.). In this section, the parametric and thermal (experimental and theoretical) investigations on the solar chimney system will be further discussed.

Some of these investigations indicated that the thermal performance of the solar chimney is greatly impacted by the chimney "gap" (width). In an experimental study on a solar chimney of 2 m height and variable gap width (ranging 0.1-1m), it was found that when the chimney gap is small (0.2m) the flow is upward. However, when the gap is large (0.5m), air flows upwards near

the heated walls due to the buoyancy effect but near the center of the chimney air flows downwards. Another words the mass flow rate inside the chimney increases as the chimney gap increase to a certain level (about one-tenth of the chimney height) then decreases as the gap further increases (Bouchair, 1994).

This phenomenon was also observed in a numerical study showing that there is an optimum chimney width at which a maximum ventilation flow rate can be achieved. This phenomenon was attributed to the occurrence of back flow at the outlet of the chimney (Gan and Riffat, 1998). A number of experimental and theoretical investigations have been conducted for the determination of the size of a solar chimney, showing that the velocity of airflow and temperature of different parts are functions of the chimney gap, ambient air temperature, and the elevation of air exit above the inlet duct (Cited after: Bacharoudis, et al., 2007). These studies have also showed that there are noticeably different flow patterns among various chimney gaps and that the chimney gap-to-height ratio affects the air flow rate (Cited after: Sakonidou, et al., 2008).

All of the above-mentioned investigations confirmed the existence of the optimum chimney gap-to-height ratio. In a different experimental investigation, solar chimneys with uniform heat flux on one wall were investigated for various gaps, inclinations, and heat flux inputs. These investigations covered a gap-to-height ratio from 1:15 to 2:5. It was found that by changing the chimney gap while maintaining all the other conditions, the airflow rate increase continuously with increasing the gap, even up to the gap-to-height ratio of 2:5 – no optimum gap has been found. It was concluded that this might be caused by a decrease in

the inlet pressure loss due to the simultaneous increase of the chimney inlet by extending the chimney gap (Chen, et al., 2003).

One of the other design parameters that showed to have an impact on the solar chimney performance is the chimney tilt. The idea of optimum chimney tilt came from an experimental investigation. As mentioned before in the solar chimney "experimental investigations" section, the inclination of the chimney oppositely affects the air flow and effective pressure head of the chimney. It is apparent there must be an optimum tilt that leads to the highest flow rate. For this studies, results show that the maximum chimney airflow occurs when the chimney tilt varies in a narrow range between 65° and 76° (Sakonidou, et al., 2008). The existence of an optimum chimney tilt was also illustrated in a different experimental investigation; where, the results show that the maximum airflow rate was reached at a chimney inclination angle of around 45° for a 200mm gap and 1.5 m high chimney (Z.D. Chen, et al., 2003).

In a more detailed parametric study, it was concluded that the optimum design parameters of solar chimney are height, width, length and material. Where it was found that the air mass flow rate increase with the increase of the chimney height and length. The idea of optimum gap-to-height ratio as well as different materials affecting the chimney performance has also been emphasized in this study (Nugroho, et al., 2006).

The effects of other chimney aspects (e.g. inlet size, glazing etc.) on its thermal performance have also been investigated. For example, it was found that

for a given chimney gap, the flow rate increase with inlet height due to decreasing entry flow resistance (Gan and Riffat, 1998). A different study showed that increasing the solar collector surface area and the chimney height and diameter could generate more chimney available draft (Wang, et al., 2004). Further investigations on a special type of solar chimneys called "Trombe Wall", in which the sun-facing wall of a chimney is glazed, have been conducted (Chen, et al., 2003). In addition, the effects of different glazing levels and solar irradiance on the system performance have been investigated. It was found that the effect of glazing on the predicted ventilation rate depends on the total solar irradiance. Accordingly, it was concluded that using single or even double glazing is inadequate for solar chimneys due to the possible condensation and downdraught in cold winter, while triple glazing can reduce both risks of condensation and downdraught as well as increasing the ventilation rate (Gan and Riffat, 1998).

In summary, solar chimneys have been investigated by a number of researchers for several applications including passive solar heating and cooling of buildings, ventilation, power generation, etc. The performance of solar chimneys (mainly used to enhance cooling and air movement in naturally ventilated buildings) has been further discussed. It was found that the thermal performance of solar chimneys is affected by design parameters (i.e. height, gap, length or diameter, inlet size, collector surface area, wall temperature, glazing level and chimney tilt) as well as environmental parameters (i.e. solar irradiation and wind speed). Consequently, a good thermal performance of the solar can be achieved by a careful selection among the above-mentioned parameters.

2.4 Coupled System

Few researchers have thought of coupling the EAHE system with the solar chimney system to achieve the maximum possible passive cooling and ventilation strategy for buildings. In such a coupled system, the solar chimney is designed to drag airflow through the EAHE system. In fact the historical heating system called "Roman hypocaust" which dated back to the ancient Roman times, utilized the same concept as the coupled system (i.e. EAHE and solar chimney). In the hypocaust, the combustion gases (resulting from burning wood in a furnace) were drawn through underground channels to heating chambers which were built under the room/apartment to be heated. These hot gases migrated through a piping system, which surrounded the walls of the room to be heated, by means of a chimney (Bansal and Shail, 1998). It is clear that the major difference between the two systems (i.e. hypocaust and coupled system) is that the hypocaust used combustion gases for heating of buildings; while the coupled system uses fresh ambient air for heating/cooling and ventilation of buildings. The same concept was utilized again in the 16^{th} century in what is called the "sicrocco rooms". In which underground corridors and water features were used in conjunction with solar chimneys to provide cooling and ventilation for buildings (cited after: Chen, et al. 2003).

Recently, few attempts were made to study coupled systems. Some of these attempts focused on the numerical study of the coupled system integrated with different buildings (e.g. office building and auditorium). Accordingly, a numerical model consisting of three sub-models was developed. The first sub-model was used

to describe the behavior of the solar chimney through predicting its outlet air temperature. The second sub-model was used to describe the behavior of the EAHE system by predicting its inlet air temperature, while the third was used to predict the overall natural ventilation rate. Using this model a parametric study on the effect of the different parameters of the EAHE and the solar chimney has been conducted. In the parametric study, the cooling degree hours and the heating potential (measured in kWh) were used to evaluate the coupled system. Moreover, the thermal comfort of occupants in different settings has been discussed. It was found that the system can reach a minimum of 360 cooling degree hours for and auditorium (Correia-da-Silva, 2004) and 278 cooling degree hours for an office building (Correia-da-Silva, 2006). It was also found that for winter heating the system could achieve a heating potential of 12500 kWh (Correia-da-Silva, 2007).

One of the innovative attempts was to study the performance of a hybrid systems in which a conventional HVAC system was used in conjunction with a coupled system. Here, the cylindrical shape of the building served as a solar chimney. A CFD model was used to describe the system performance. It was found that the coupled system could provide cooling as well as ventilation for the occupied building without the need to run the chillers (Athienitis, et al., 2005).

In another experimental investigation of the coupled system (Wang, et al., 2004) studied the thermal performance of the system with more focus given to the solar chimney performance. The pressure balance and airflow balance equations were used to theoretically model the airflow through the system. The theoretical design principles of the solar chimney and solar collector were also presented. The thermal

performance of the coupled system was investigated through installing thermocouples along the collector and the chimney along with an airflow meter at the pipe outlet. Results showed that increasing the chimney height, diameter and solar collector size significantly improves the airflow inside the chimney. It is worth mentioning that at sizing the chimney special care should be given to the chimney structure strength, stability, installation space, material and construction cost (Wang, et al., 2004).

2.5 Literature Review Summary

Through the literature review of the earth-to-air heat exchanger (EAHE), the solar chimney, and the resultant coupled system, some preliminary conclusions can be derived:

(1) The EAHE and solar chimney or "coupled system" utilizing the geothermal and passive solar energy respectively reduces the energy consumption of building sector have aroused great interest in many countries.

(2) There are many numerical, analytical and experimental investigations which have been carried out for both systems. This has contributed to the current understanding of the coupled system. It can be concluded that both sub-systems have good potential to be practically implemented in buildings for the purposes of cooling and ventilation during the summer time, leading to a significant reduction in summer electrical peak loads.

(3) The experimental investigations on the EAHE system indicate that the system performance could be enhanced by increasing the EAHE length and burial depth while decreasing the diameter and air velocity inside the tube. It has also been

illustrated that the EAHE material does not affect the system thermal performance, therefore, the less expensive the better. Other investigations have shown that the ground surface cover above the EAHE has an impact on its thermal performance.

(4) For EAHEs coupled with greenhouses, experiments show that EAHEs can increase the air temperature during winter and decrease it during summer for greenhouses. This would help to stabilize the temperature inside greenhouses and improve the crop production.

(5) For the solar chimney system, it has been found that the CFD is one of the best tools to simulate the chimney performance. The system performance was found to be affected by design parameters, such as chimney gap, length, inclination, and glazing, as well as environmental parameters such as solar irradiation and wind speeds.

However, according to the current state of art, very few preliminary studies have connected EAHE with a solar chimney to form a coupled system. The coupled system, which "couples" the EAHE with solar chimney to utilize the geothermal and passive solar energy simultaneously, can achieve great energy savings within the building sector and reduce the peak electrical demand in the summer. It is necessary to conduct further investigations on the coupled system performance and to compare between the natural and forced airflow modes of the coupled system.

2.6 Thesis Main Work

The coupled system, which couples the EAHE with solar chimney to utilize the geothermal and passive solar energy simultaneously, can achieve great energy saving of building sector and reduce the electrical peak demand in summer. However, according to the current state of art, only few preliminary studies have connected EAHE with a solar chimney to compose a coupled system. It is necessary to conduct further investigations on the coupled system performance and to compare between the coupled system and the EAHE.

Current research starts with a detailed illustration of the experimental design, construction and installation in chapter 3. Thereafter, the instrumentation calibration and uncertainty analysis will be discussed in chapter 4. Moreover, analysis of the undisturbed ground performance for a whole year testing is presented, followed by a thermal analysis of the performance of the solar driven EAHE as well as the fan assisted coupled system. Furthermore, an analysis of the ground thermal saturation period is presented on chapter 5 of the current research. Our conclusions on the findings of the current experimental research with a discussion on future work and further improvements are included in chapter 6.

Chapter, 3

EXPERIMENTAL DESIGN AND CONSTRUCTION

3.1 Objectives

The main objective of the current research is to develop an optimal performing full scale demonstration of an all passive cooling and ventilation system coupled at the Solar Energy Research Test Facility at the University of Nebraska. The all passive system employs two techniques namely EAHE and solar chimney. This full scale demonstration is then used to evaluate the performance of the coupled system (i.e. EAHA coupled with solar chimney) for two cases, first: natural driven air flow, second: forced driven air flow. The system performance is evaluated through assessing the maximum air flow rate (CFM) and cooling (in tons) that the system can provide to the building during hot summer time for each case study.

Another objective is to study the practicality of the coupled system technology through assessing various issues concerning the system. For example, the undisturbed ground annual temperature profile, the ground thermal saturation, indoor thermal comfort, and economical aspects. Moreover, a comparison of the coupled system with a conventional air-conditioning system is presented to ascertain the effectiveness and practicality of the system as well as to evaluate the cost pay back and lifetime energy savings. In order to achieve these objectives, specific goals have been established. These goals are:

(1) Presenting a detailed illustration of the experiment design and construction as well as sensors locations and installation.

(2) Discussing the instrumentation calibration and uncertainty analysis.

(3) Analyzing the undisturbed ground temperature profile over the course of a year.

(4) Analyzing the thermal performance of the coupled system under two conditions: naturally driven air flow and forced air flow, through evaluating the maximum tons of cooling and air flow rate that can be provided in each case.

(5) Evaluating the level of indoor thermal comfort that the system can provide in each case.

(6) Analyzing the effect of the coupled system and the cooling performance on the ground thermal saturation for the soil surrounding the EAHE during the forced airflow test of the coupled system.

(7) Discussing how to improve the system performance on the future (e.g. delay the onset of ground thermal saturation, and eliminating building negative pressure as well as infiltration rate).

The pursuit of these goals aims to provide an answer to two important questions: first, can an all passive cooling system function successfully over the course of a summer to provide cooling to the testing facility building which has been fine tuned to maximize cooling; second, can a forced air flow (fan assisted) coupled system sustain a maximum cooling rate without saturating the soil surrounding the EAHE?

3.2 The Principle of the Experiment System

In this section, the main principle and theory of the experiments is illustrated, while, in sections 3.3 – 3.6 the design and construction of the different parts of the experiments is discussed.

According to Wang, et. al. (2004) an experimental facility for the coupled system was built in 1990 on "Allwine Prairie Preserve" owned by the University of Nebraska. The experimental facility is located in northwestern Omaha, Nebraska at latitude 41°20'18.00" N, and longitude 96°08'53.63" W, with an elevation of 1172 ft. It mainly consists of four components the testing facility building where the cooling, ventilation and heating experiments take place, the EAHE, the solar collector and the solar chimney. Figure 3-1 shows a photographic picture for the test facility.

Fig. 3-1 – A photographic picture of the Solar Energy Research Test Facility-Four components

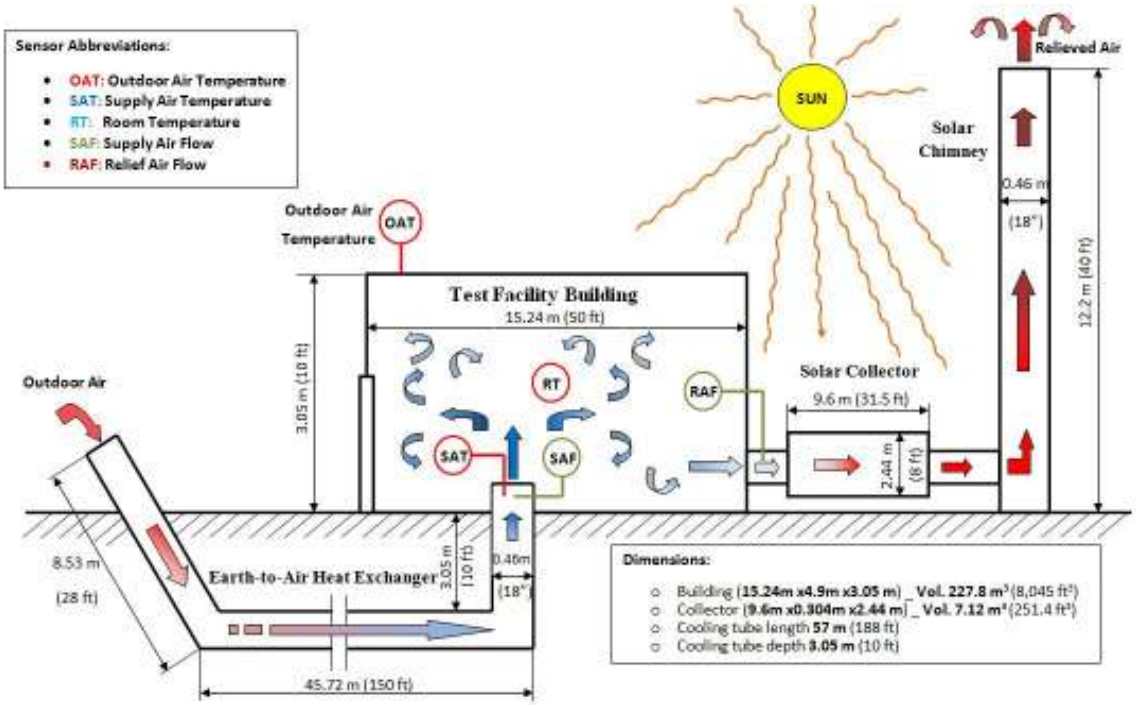

Fig. 3-2 – Schematic diagram of the cooling process by the coupled system

Figure 3-2 shows the schematic diagram of the coupled system. As shown in Figure 3-2 an EAHE is coupled with a solar chimney and solar collector to provide cooling and ventilation for the Solar Energy Research Test Facility. The cooling and ventilation process can be illustrated as follows: the air inside the solar collector is heated up as the solar radiation strikes the solar collector; hence, the hot air migrates from the solar collector to chimney bottom and rises to the top of the chimney. As the system components are tightly connected, this hot air migration draws the ambient air through the EAHE; as the warm ambient air travels through the length of the EAHE tube it cools down due to the heat exchange process that occurs with the underground soil, providing a fresh nice cool air draft to the test facility building. The Solar

Energy Research Test Facility is sealed and has low air leakage. In this way a low cost and environmentally friendly passive cooling and ventilation is achieved.

3.3 Measurement of the Weather

Two sets of measurements have been taken at various locations of the experimental setup at two different testing periods to study the thermal performance of the system. A customized program have been created using the National Instruments LabVIEW software package (version 6), to read, log, average and store the measured data on the computer system hard drive which is hocked to the measuring sensors. For the two testing periods and for all the different measurements, the data is read every minute and averaged over a 15 minute span and then this average is stored as a single measurement on the computer system every 15 minute time interval.

The first testing period lasted for 18 days starting from August 14th, 2008 and ending on August 31st, 2008. The main measurements were: time and date, wind speed (mph), wind direction (° degrees), barometric pressure (in. Hg.), the indoor relative humidity (%), outdoor relative humidity (%), supply air relative humidity (%), supply air flow rate (CFM), solar collector air flow rate (CFM), air temperature inside the EAHE at 20 different locations, ground temperatures 12 different locations, indoor air temperature at 13 different locations, the control room air temperature, the air temperature inside the collector at 11 different locations, the solar chimney air temperatures at 5 different locations, and the ambient air temperature.

The second testing period lasted for 43 days starting from July 24th, 2009 and ending on September 4th, 2009. The main measurements that took place on that period are the same as that of the first testing period plus the soil moisture content that has been measure at 20 different locations above and next to the EAHE. It should be mentioned that all the thermocouples used for ground temperature measurements were replaced with new ones before the second testing period. Moreover, new ground temperature thermocouples were added at different locations, more information about the two testing period ground temperature and moisture sensor locations is given in the "Earth-to-Air Heat Exchanger" section of this chapter. Furthermore, schematic diagrams as well as discussion on the distribution and locations of the measuring instruments are given in the following sections. In addition, a discussion on the measuring instruments, their calibration, and sensitivity analysis will be presented in chapter 4 of the current study.

3.4 Earth-to-Air Heat Exchanger

Since on 1990, when the EAHE was installed at the University of Nebraska's Solar Energy Research Test Facility, there were just few scientific papers published on the design methods and criteria of the EAHE system, it was designed based on the parametric research made by Chen, et al. (1983). Accordingly, the main design parameters of the EAHE (i.e. Length, diameter, burial depth, and air velocity inside the pipe) were selected based on the common sense to provide a reasonable cooling to the testing facility building.

Consequently, according to Henkel, et al. (2004) a 188 ft (57 m) culvert steel EAHE, with 18 inch (0.45 m) diameter, and buried at a depth of about 10 ft (3 m) underground was installed at the PSER testing facility of the University of Nebraska. The EAHE tube runs southeast to northwest. It starts with a slanted inlet of 28 ft (8.53 m) (as shown in Figure 3-2), then penetrates the ground for 10 ft (3 m) and curves to a horizontal portion of about 150 ft (45.7 m), finally bends upwards for 12 ft (3.65 m) at a right angle to enter the PSER facility through its concrete slab near the south side of the building.

While the inlet of the EAHE is covered with a net mesh screen to prevent insects and small animals (e.g. rabbits) from entering the tube as shown in figure 3-3. Its outlet, which is 2 ft above the ground inside the testing facility building, is equipped with a manual damper (as shown in figure 3-4) in case the airflow needs to be regulated or the system needs to be shut down during the un-working seasons.

Moreover, the outlet has fixtures to mount an electric fan (as shown in figure 3-4) in case a forced airflow is required.

Fig. 3-3 – EAHE slanted inlet covered with mesh screen

Fig. 3-4 – EAHE outlet equipped with a manual damper and fixtures to mount a fan

It should be noted that the main horizontal portion of the EAHE is perforated from the bottom to allow for moisture drainage if condensation occurs during the cooling process. Furthermore, the entire horizontal portion of the EAHE was laid over a sand bed gravel to prevent moisture build-up underneath the tube as shown in Figure 3-5. Moreover, a horizontal perforated PVC pipe of 0.5 inch (1.27 cm) diameter which could be connected to a water source (e.g. water faucet) was installed next to the horizontal portion of the EAHE (as shown in Figures 3-5 and 3-6) in order to increase the water content of the soil surrounding the tube if required by the various research purposes.

Fig. 3-5 – Perforated PVC water pipe – for moisturizing the soil surrounding the EAHE

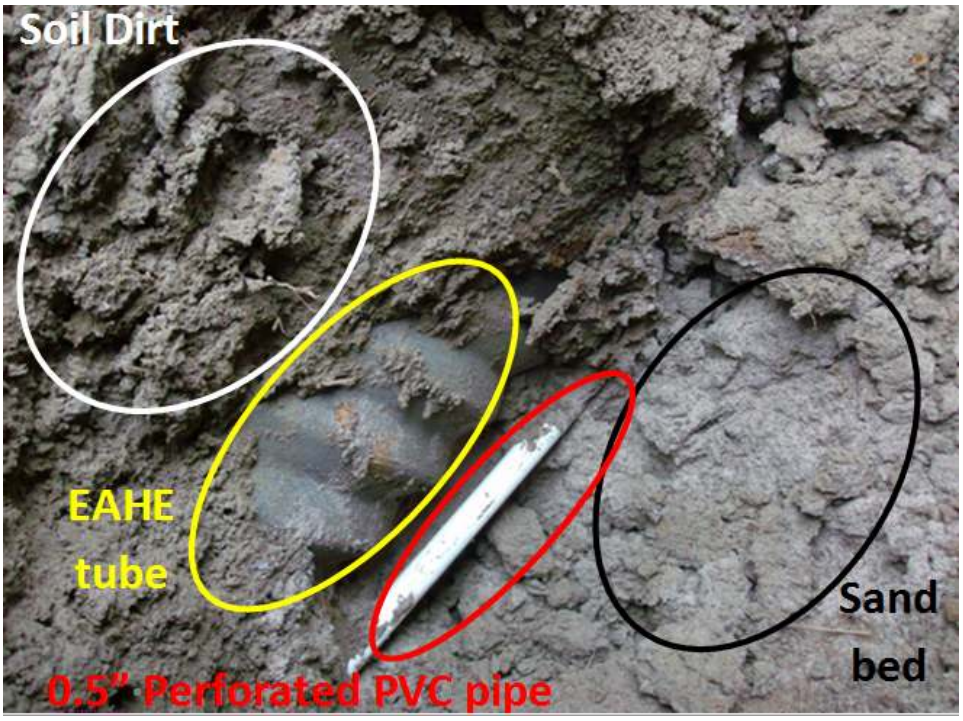

Fig. 3-6 – EAHE sand bed, dirt cover, and perforated PVC water pipe

A number of different sensors have been installed inside and outside the EAHE for monitoring the air temperatures inside the tube as well as the temperature and moisture content of the soil surrounding the tube. Figure 3-7 shows the names and locations of the thermocouple sensors installed inside the EAHE. Moreover, it shows the horizontal distance of the locations of the sensors installed above the EAHE, from the testing facility building (e.g. 90' sensors location, etc.). Figure 3-8 and figure 3-9 show the cross sectional view of the EAHE at the "30' sensors location" with the upward longitudinal distance of the thermocouples and moisture sensors from the EAHE tube installed during the 2008 and 2009 testing periods respectively. It should be mentioned that the other sensor sets installed at the different locations along the length of the EAHE have the same sensor arrangements as the 30' sensors location.

EAHE Side Profile

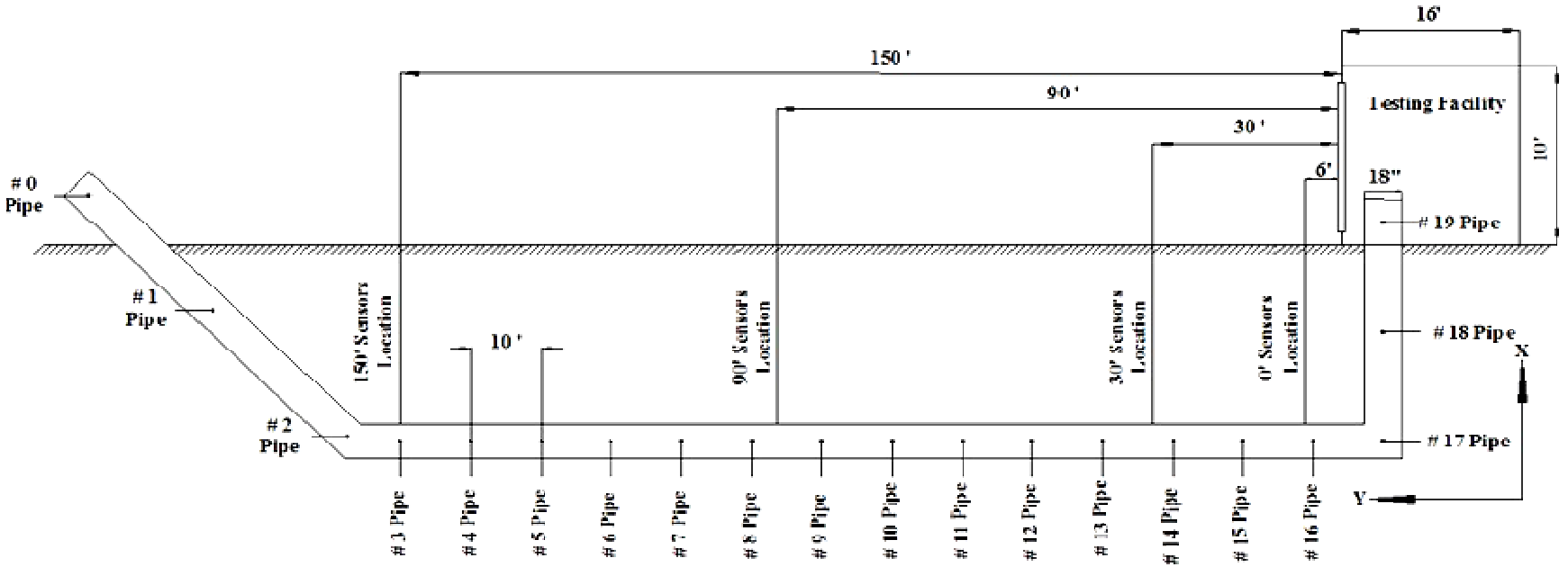

Fig. 3-7 – Sensor locations inside and outside the EAHE

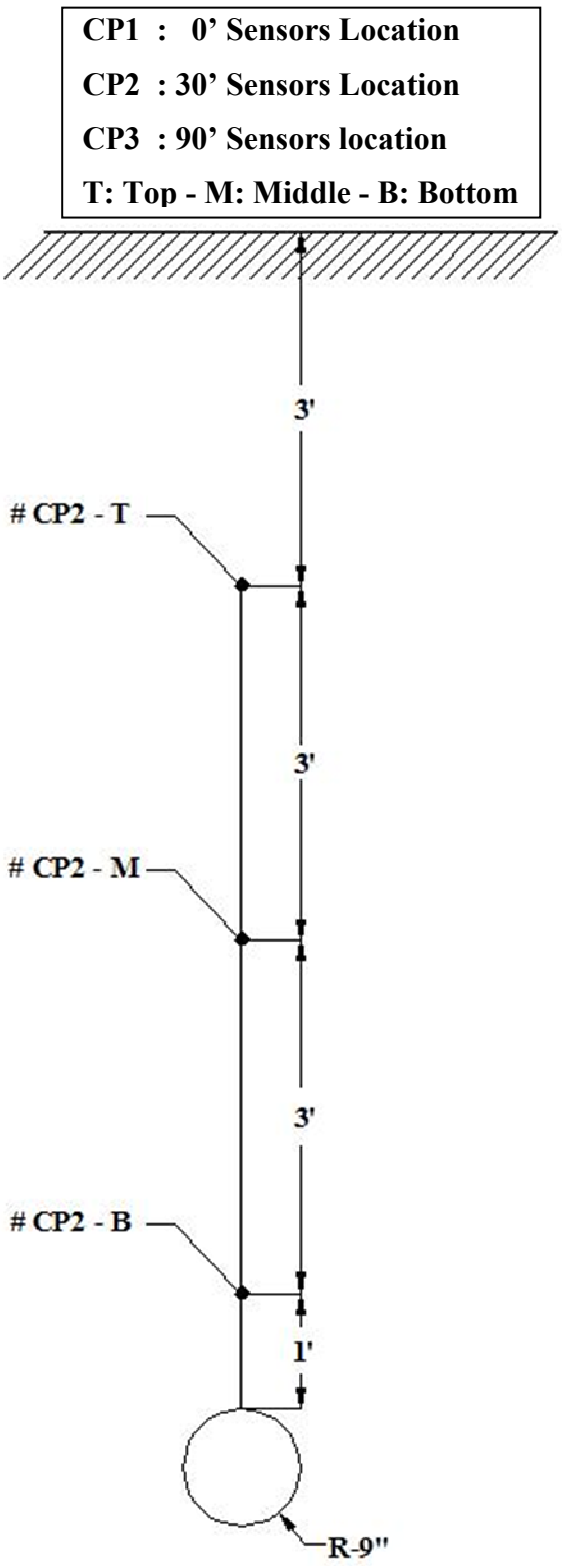

Fig. 3-8 – EAHE cross section at 30' sensors location – 2008 testing period

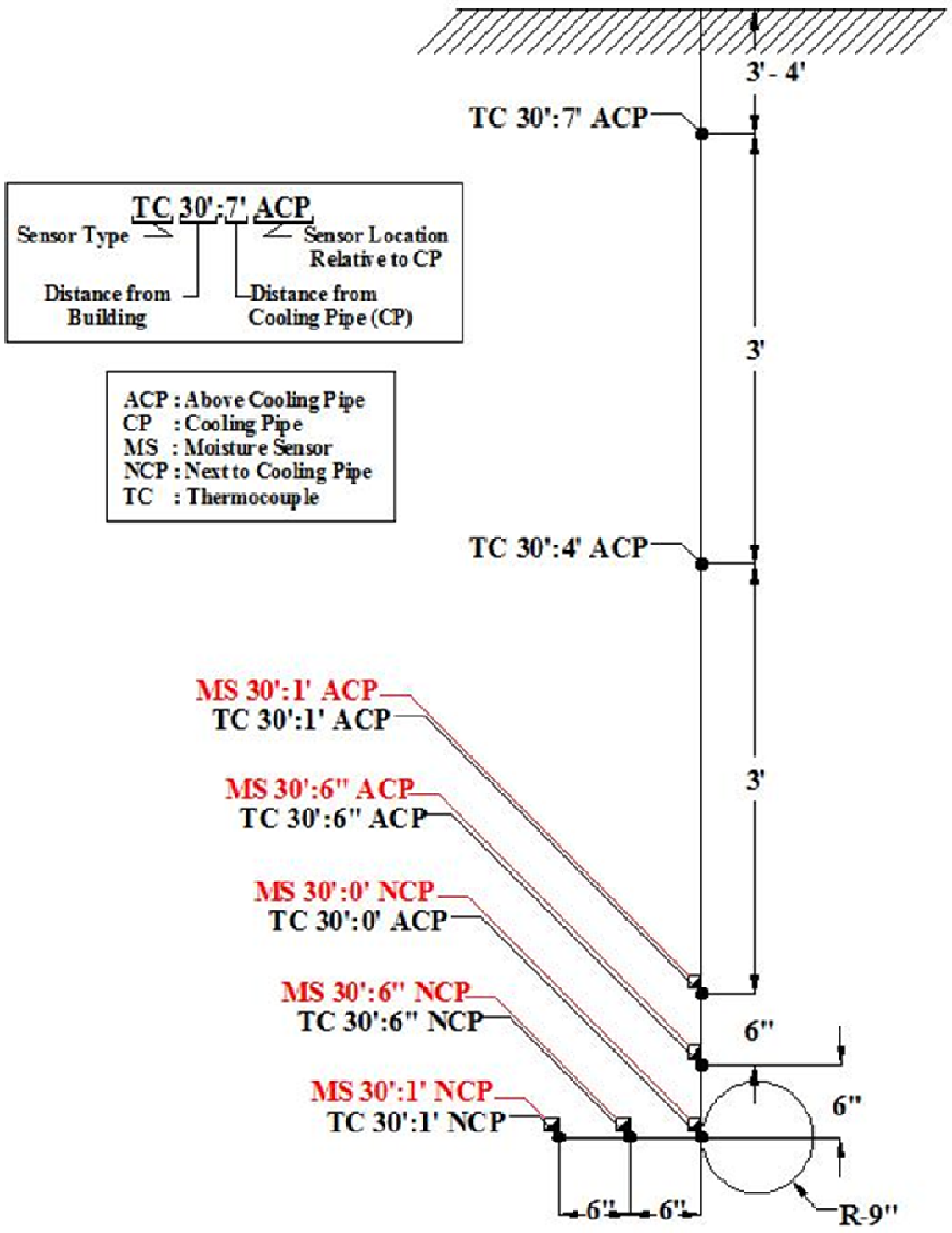

Fig. 3-9 – EAHE cross section at 30' sensors location – 2009 testing

3.5 Solar Energy Research Test Facility

As mentioned before the test facility building was built on 1990. It is a one-story building with external dimensions of 63'8" length, 16' width, and 10' height, setting on a concrete slab. It includes a testing room - where the experiments took place – a computer room (i.e. control room) for data logging and monitoring, and a bathroom. The main test room dimensions are 49'10.5" length, 14'10" width, and 7'9" height. It has 10 south facing windows each of them is 6' in length and 45" in width. The concrete slab with the 10 windows creates a huge cooling load during the summer time. Figure 3-10 shows the floor plan of the testing facility building with more detailed dimensions and information. For example, it provides information about the locations of the solar collector and solar chimney compared to the building as well as the names of the different sensors that have been used during the testing periods (i.e. thermocouples, wind speed, wind directions, solar pyronometer, airflow, and humidity sensors) and their exact locations inside/outside the building.

The computer room is equipped with a computer system and various types of data-loggers for monitoring the performance of the whole system. It should be mentioned that all the different sensor types except the soil moisture sensors are integrated with the National Instruments modular data-loggers which in turn are connected to the computer system. The National Instruments LabVIEW software package (version 6) was used to create a customized program that helps in calibrating, controlling and monitoring the sensors. On the other hand, the soil moisture sensors were integrated with independent data-loggers (Watermark data loggers which come

with the soil moisture sensors) that are synchronized to log the data at the same time with the same time interval as the National Instruments data loggers integrated with the computer system.

For the temperature measurements of the indoor air inside the building, four sets of type T thermocouples were used. Each set has been installed in one of the testing room corners (i.e. Northwest, Northeast, Southwest, and Southeast), where each set consists of three sensors located at 1 ft, 4 ft and 7 ft above the ground level to study the thermal distribution of air inside the building as shown in Figure 3-10.

Airflow measurements have been taken in two different locations with three air velocity transmitters. The first location is at the EAHE outlet inside the testing facility building at the ground level (where two velocity transmitters were installed) and the second location is at the connection pipe between the test facility building and the solar collector as shown in Figure 3-10.

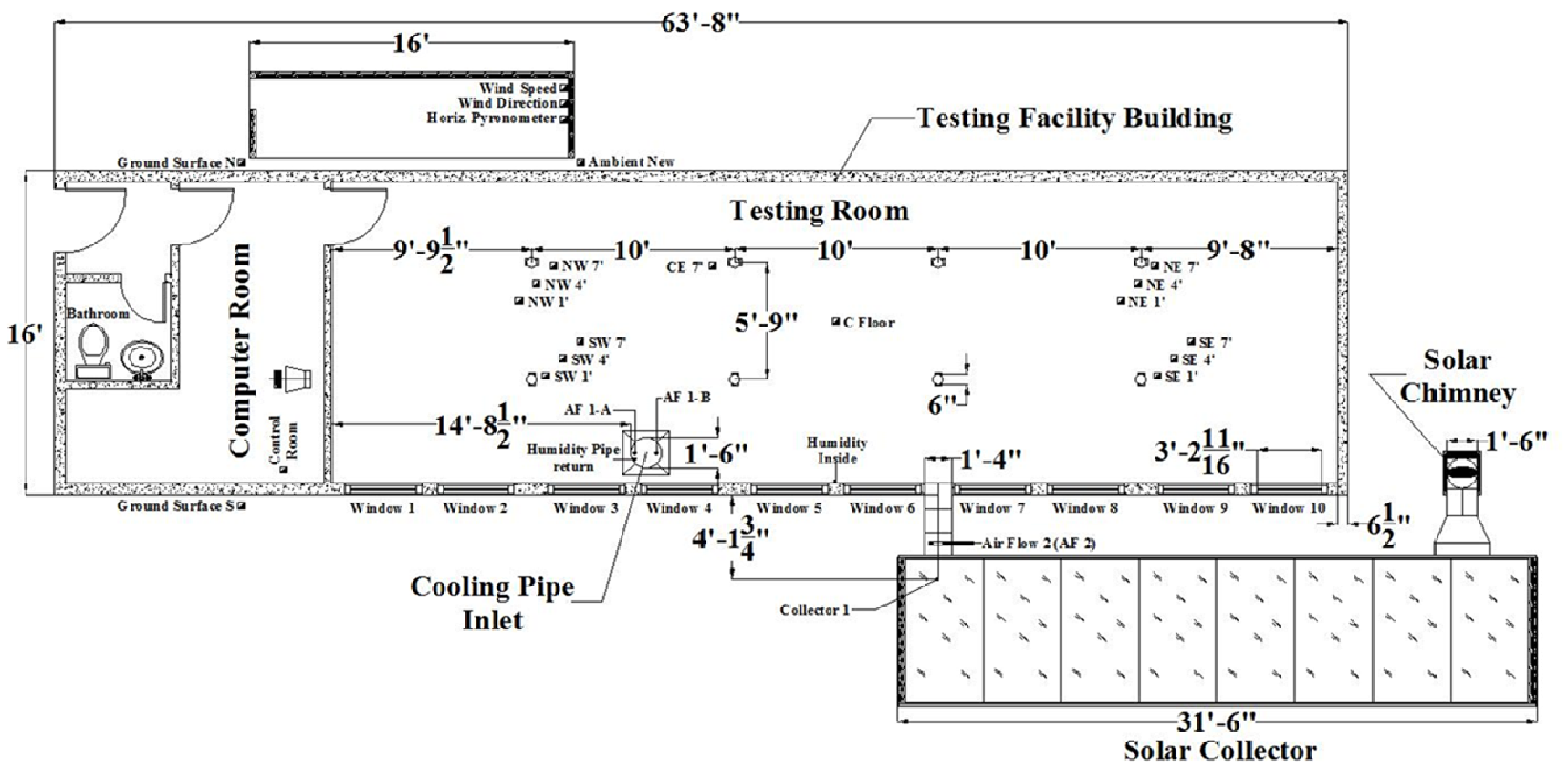

Fig. 3-10 – The Solar Energy Research Test Facility building floor plan – (Including various sensor locations)

Figure 3-11 shows two different snapshots taken for the testing facility building at two seasons from different angles. The left snapshot shows the insulated windows during the summer testing periods, while the right snapshot shows the location of EAHE inlet and the outdoor humidity sensor compared to the testing facility building location.

Fig. 3-11 – Two snapshots of the testing facility building at different seasons

3.6 Solar Collector

According to Wang, et al. (2004), the solar collector is the vital key part of the system as the size of the solar collector beside the chimney height and diameter specify the chimney available draft. In other words, the solar collector size indirectly specifies the amount of air flowing through the EAHE. Since increasing the solar collector size and its absorption surface area can improve the solar chimney available draft, the solar collector was designed with an absorbing surface area of 215 ft^2 (20 m^2) considering that the solar irradiation is 126 Btu/(h•ft^2) (400 W/m^2) with a heat loss coefficient of 1/3 Btu/(h•°F•.ft^2) (8.5 W/(°C•m^2)) and an absorptivity of 0.8.

According to Wang, et al. (2004), designing the solar collector did not only include the absorption surface area but also the angle of tilt and location. The angle of inclination of the solar collector was chosen based on the solar altitude angle during the hottest month in Omaha, Nebraska. It was found that the solar altitude is 64° in August in Omaha, Nebraska, consequently, the solar collector inclination angle was chosen to be 26° with the horizontal level. In addition, it was placed on the south side of the building in order to be oriented to the sun for the maximum absorption of the solar radiation.

The solar collector was constructed by wood and a special type of solar glass that traps the solar irradiation inside the collector. In 2008 when the current research started, the solar collector was renovated and all the rotten plywood skin and wooden skeleton has been replaced. All of its corners and angles have been sealed with black tar, and a layer of (R-5) insulation has been added to the bottom side of the collector. Then it was covered with a layer of plywood which in turn was painted in black to prevent any solar irradiation losses from the sides of the collector. Figure 3-12 shows a cross sectional view of the solar collector with detailed dimensions and some sensor information, while Figures 3-13 a, b, c, and d show some snapshots for the solar collector at different re-construction phases.

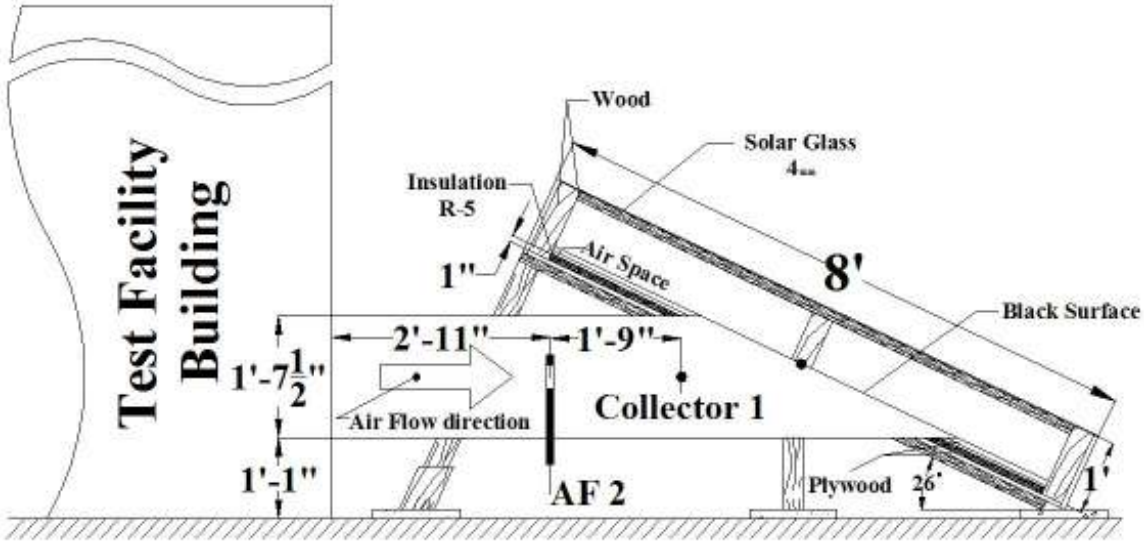

Fig. 3-12 – A cross section view of the solar collector and the Solar Energy Research Test Facility-solar collector connection pipe

Fig. 3-13 (a) – Solar collector re-construction (replacing the rotten wood and adding R-5 Insulation to the bottom side

Fig. 3-13 (b) – Solar collector re-construction (sealing the corners and separations with black tar and painting the inner sides in black

Fig. 3-13 (c) – Solar collector re-construction (black painted interior)

Fig. 3-13 (d) – Solar collector (After renovation)

Eleven type T thermocouples have been installed inside the solar collector at different positions to study the heat transfer process. The first thermocouple is installed in the connection pipe between the testing facility building and the collector; while, the eleventh thermocouple is installed in the connection pipe between the collector and the solar chimney. Figure 3-14 shows the names and locations of the thermocouples installed inside the solar collector.

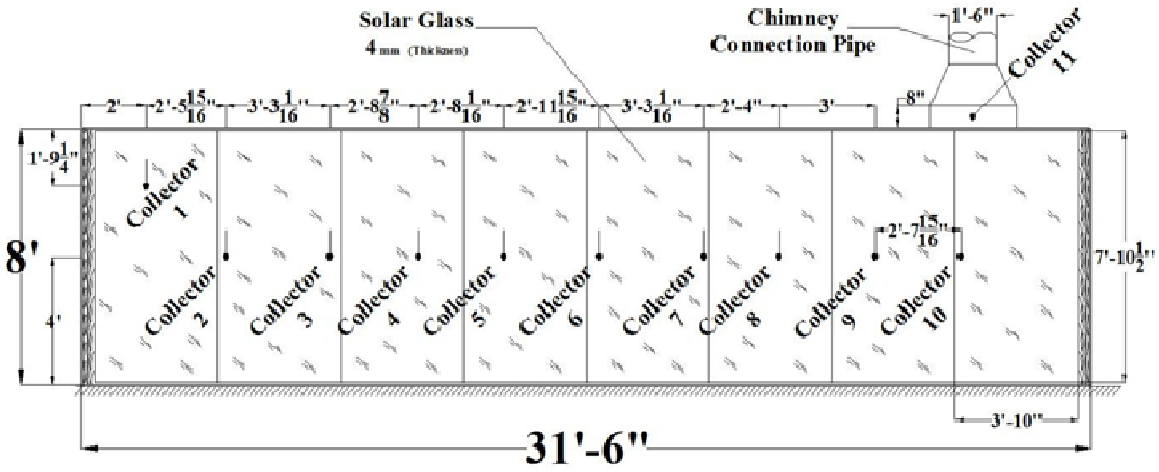

Fig. 3-14 – A schematic diagram of the solar collector – including the thermocouple sensors locations

3.7 Solar Chimney

According to Wang, et al. (2004), the solar chimney was designed so that its available draft overcomes the EAHE pressure losses as well as the negative thermal gravity effect of the air column inside the solar chimney, under the design ventilation airflow rate. Accordingly, the solar chimney height and diameter were selected as 40 ft (12.2 m) and 18 inches (0.457 m) respectively to provide an available draft of more than 0.02 inches of water (5 Pa) at a temperature of 135 °F (57° C). The chimney was built of four steel spiral pipes; each pipe is 10 ft (3.048 m) in length, stacked over each other. The chimney is placed over a 5 ft (1.5 m) steel stand which in turn is bolted to a concrete foundation of 3 ft in depth. The chimney is strengthened by nine steel wires; every three wires are attached to the chimney at three different heights on the same vertical line then stretched out and bolted into the ground away from the chimney to increase its stability and resistance against the wind. The three sets of wires form a Y shape in which the point of intersection of all the Y shape (i.e. 3 sets) is concentric with the chimney cylinder. Five type T thermocouples have been installed inside the chimney to study its thermal performance. Three were installed in the middle, one at each connection point between every two pipes, and one at the bottom of the chimney, while the last was installed at the very top of the chimney. Figure 3-15 shows a schematic diagram of the solar chimney with the names and locations of the thermocouples inside the chimney as well as its dimensions, and base. Figure 3-16 (a) and (b) show snapshots of the chimney, strengthening wires and holding base.

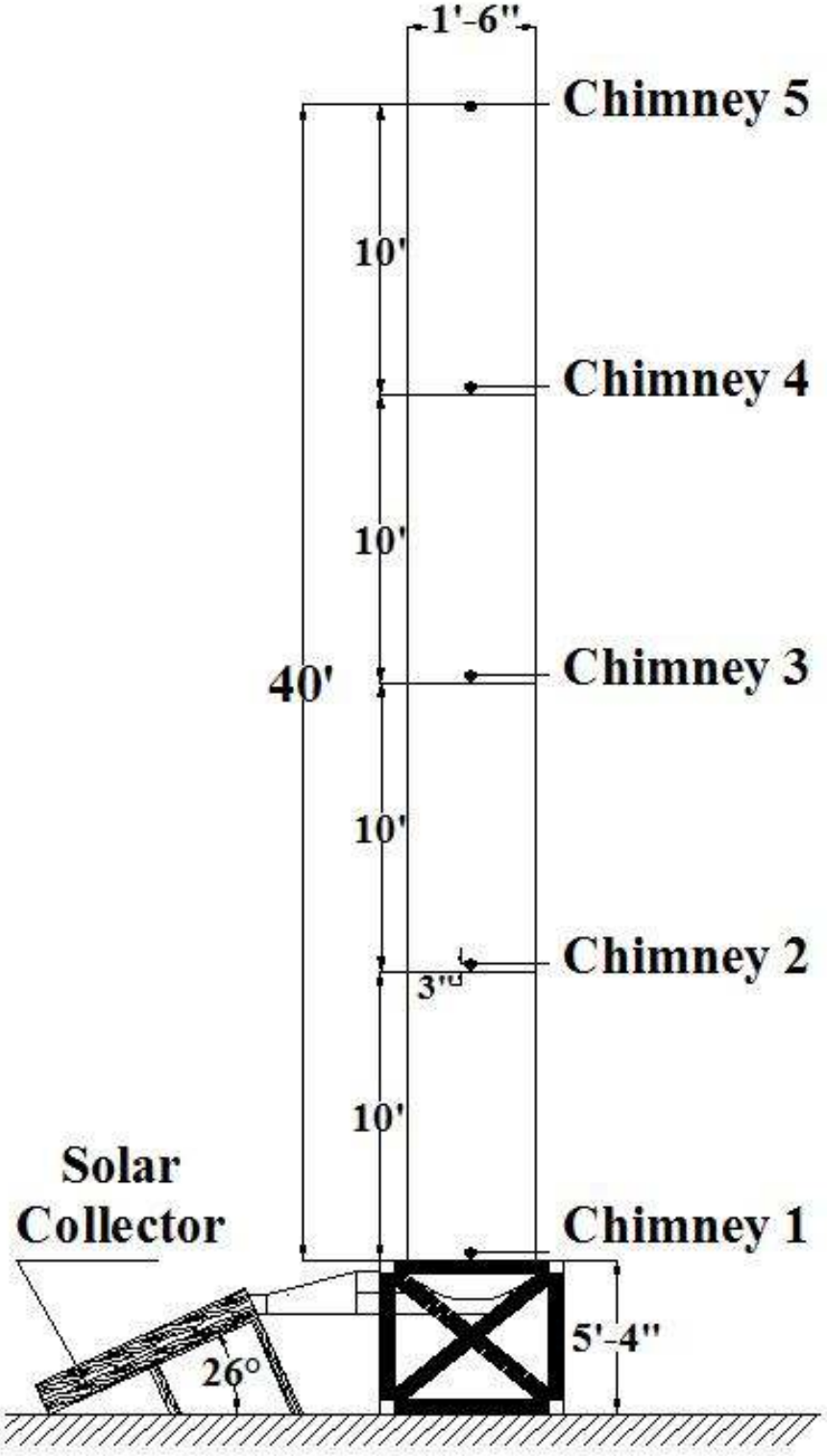

Fig. 3-15 – A schematic diagram of the solar chimney – including the thermocouple sensors names and locations

Fig. 3-16 (a) – Solar chimney snapshot (strengthening wires)

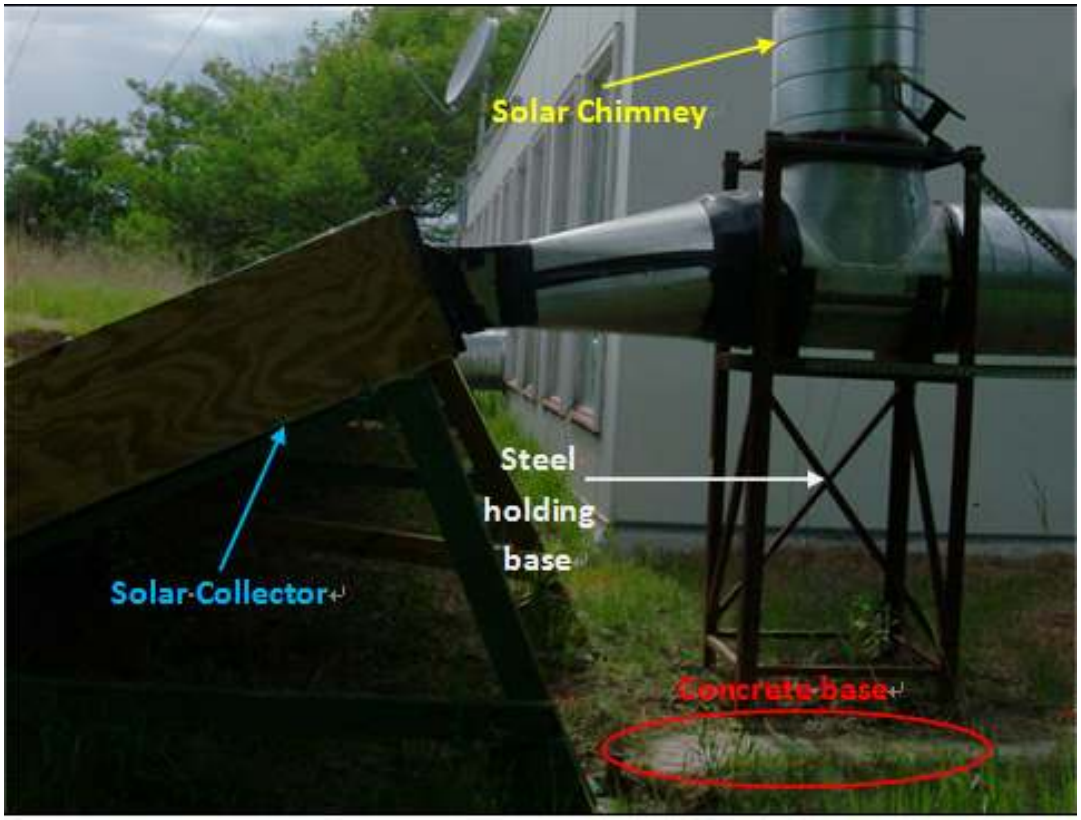

Fig. 3-16 (b) – Solar chimney snapshot (holding base)

3.8 Summary

In this chapter, the main principle behind the research has been illustrated and the measurements that have been carried out in the testing periods have been mentioned. Furthermore, an illustration of the design and sensor installation of each section of the experiment has been presented.

Chapter, 4

INSTRUMENTATION CALIBRATION AND UNCERTAINTY ANALYSIS

4.1 Measuring Instruments

As previously mentioned in chapter 3, different weather measurements (e.g. wind speed, temperatures, wind direction, barometric pressure, humidity, etc.) have been carried out during the two sets of experiments held on 2008 and 2009 respectively. These measurements have been carried out using various measuring instruments; this section will focus on the weather measurement instruments that have been used in the current research. The weather instruments include: temperature measurement instruments, the airflow measurement instruments, the soil moisture measurement instruments, and the relative humidity measurement instruments. Moreover, a sample of the main data that has been collected using these measuring instruments during the 2008 and 2009 testing periods is presented in Appendix A.

4.1.1 Temperature Measurement

For all the temperature measurements (e.g. air temperature, underground soil temperature, etc.) held during the 2008 and 2009 testing periods, Type "T" thermocouples (TC) were used. The thermocouples have a maximum temperature reading of 212 °F (100°C) with a perfluoroalkoxy (PFA) coating as shown in Figure 4-1. Appendix B includes the thermocouple wire data sheet. The type T thermocouple consists of a positive Copper wire (the white wire) and negative

Constantan wire (the red wire). For temperature measurements using the thermocouple wire, the wire is cut to the desired length, and then the positive and negative wires of one end are soldered together, while those of the other end are connected to the National Instruments Module for data logging. Before using the thermocouple wire for measurements it has to be calibrated. More information about the thermocouple wire calibration is given in the "Calibration of Experimental Devices" section of this chapter.

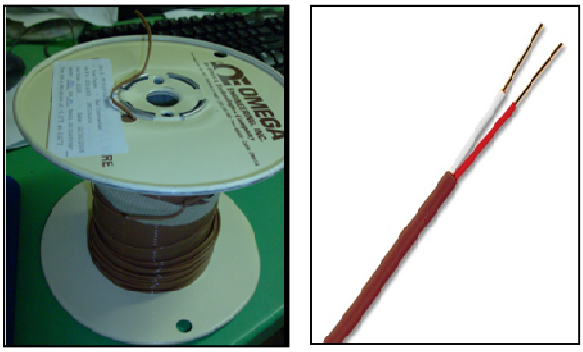

Fig. 4-1 - Type T thermocouple wire

4.1.2 Airflow Measurement

For airflow measurements, Dwyer (series 641RM) air velocity transmitters (as shown in Fig. 4-2) have been used. These transmitters use a heated mass flow sensor, which allows for precise velocity measurements at various flow rates and temperatures. The maximum air velocity measurement range of each transmitter is 15,000 FPM, with an output signal range of 4-20 mA proportional to the velocity range. Appendix B includes the Dwyer (series 641RM) air velocity transmitter data sheet for more information.

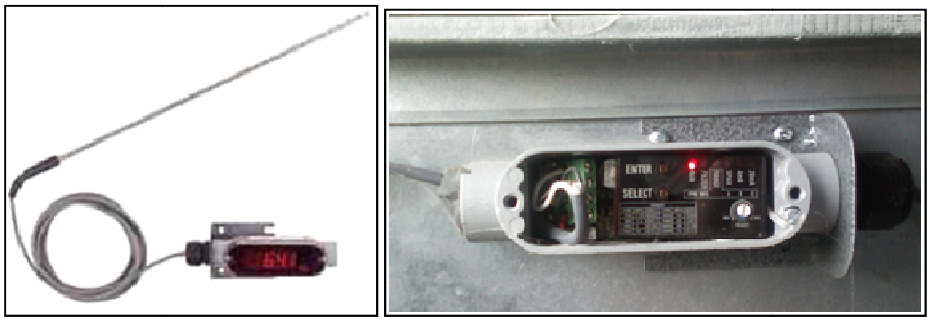

Fig. 4-2 – Air velocity transmitters

Three air velocity transmitters have been used for airflow measurements during the 2008 and 2009 testing periods at two different locations. The first location is the EAHE outlet inside the house, where two transmitters (AF1-A and AF1-B) are used, while, the second location is at the solar collector inlet, inside the connection pipe between the testing facility building and the solar collector, where one transmitter (AF2) is used. The three transmitters are connected to the National Instruments modules and consequently to the computer system for data logging. While the air flows through the probe of the transmitter, the air velocity measurements are taken and a proportional current signal is sent to the National Instruments module where the current signal is converted to a voltage signal. Thereafter, the computer receives the voltage signal and converts it to an airflow measurement (in CFM) using the LabVIEW software customized program whereby the airflow measurements are logged and stored in a note pad sheet over a 15 minute span. More information about the airflow measurement instrument calibration and the conversion from air velocity measurement to airflow measurement is given on the "Calibration of Experimental Devices" section of this chapter.

4.1.3 Soil Moisture Measurement

For soil moisture content measurements, watermark sensors along with watermark data loggers have been used. The watermark sensors are electrical resistance type, soil moisture sensors that are used to measure the soil water tension (i.e. soil water potential). The soil water potential is then converted to the soil water content which gives an indication of the amount of water present in the soil profile. It should be mentioned that the soil water potential sometimes referred as the "matric potential". The watermark soil moisture sensors cover a matric potential reading range from 0 to 200 kPa (Irmak, et al., 2006). Unlike the other measurement instruments, the soil moisture sensors are not connected to the National instruments data loggers; instead, they are connected to the watermark data loggers which in turn are synchronized to read average and store data over a 15 minute interval the same as the National Instruments data logger system. Figure 4-3 shows the watermark soil moisture sensor as well as the data logger.

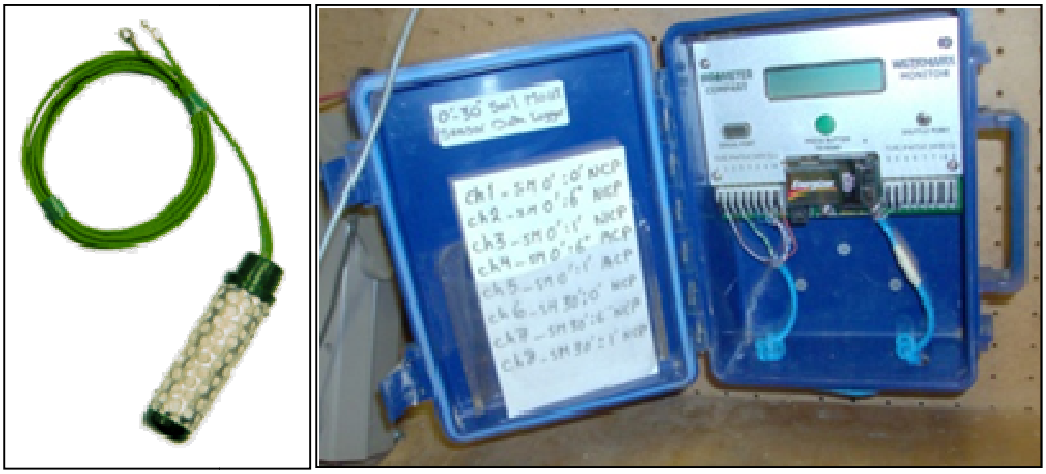

Fig. 4-3 – Left: Soil moisture sensor and Right: Moisture sensors data logger

4.1.4 Relative Humidity

Different humidity sensors are used for the air humidity measurements at various points in the testing facility.

Outdoor humidity measurement is taken near the EAHE tube inlet as shown in Figure 4-4, indoor humidity measurement is taken at a spot in between the EAHE outlet and the solar collector inlet, while supply air humidity measurement is taken at the EAHE outlet.

Fig. 4-4 – Outdoor and indoor humidity sensors

4.2 Calibration of Experimental Devices

Calibration for the different measurement instruments has been carried out before the actual use of the instruments to ensure its accuracy and reliability. In this section the calibration of the type T thermocouples used for temperature measurements as well as the air velocity transmitters used for airflow measurements are described. It should be mentioned that the relative humidity sensors and the soil moisture sensors have not undergone any calibration procedure for lack of high precision. Moreover, the uncertainty analysis for the type T thermocouples as well as the air velocity transmitters will be presented on the “Experimental Uncertainty Analysis” section of

this chapter to ensure the accuracy and precision of the Instruments used in the current research.

4.2.1 Type T Thermocouple Calibration

The thermocouple calibration was carried out through measuring the freezing and boiling points of water. These two temperature points (i.e. the freezing and boiling points of water) have been chosen because they are previously known temperatures, where the freezing point of water is 32°F (0°C) while the boiling point of water is 212°F (100°C). First, every thermocouple has been inserted in a boiling water pot (as shown in Figure 4-5 a) for several minutes until the temperature stabilizes then its boiling point temperature measurements is recorded every 20 milliseconds over a 1 minute span, then these temperature measurements are averaged to be the thermocouple water boiling point measurement value. Thereafter, it has been inserted in an ice water tank (as shown in Figure 4-5 b) for few minutes till the temperature stabilize and then its freezing point temperature measurements is recorded every 20 milliseconds over a 1 minute span, then these temperature measurements are averaged to be the thermocouple water freezing point measurement value. In order to determine the governing relationship between the thermocouple temperature measurements and the actual water boiling and freezing points temperatures, the measured data is compared with the actual temperatures and a curve fitting (as shown in Figure 4-6) is then applied. Consequently, the thermocouple calibration curve equation is created in the form of a linear relationship as follows:

$$f(x) = ax + b \qquad (4.1)$$

where: $f(x)$ = the calibrated temperature reading of the thermocouple.

x= the pre-calibrated thermocouple reading.

a =the the thermocouple offset from the actual temperature.

b = the slope of the thermocouple temperature calibration curve.

Fig. 4-5 (a) – Thermocouple calibration – water boiling point measurement

Fig. 4-5 (b) – Thermocouple calibration – water freezing point measurement

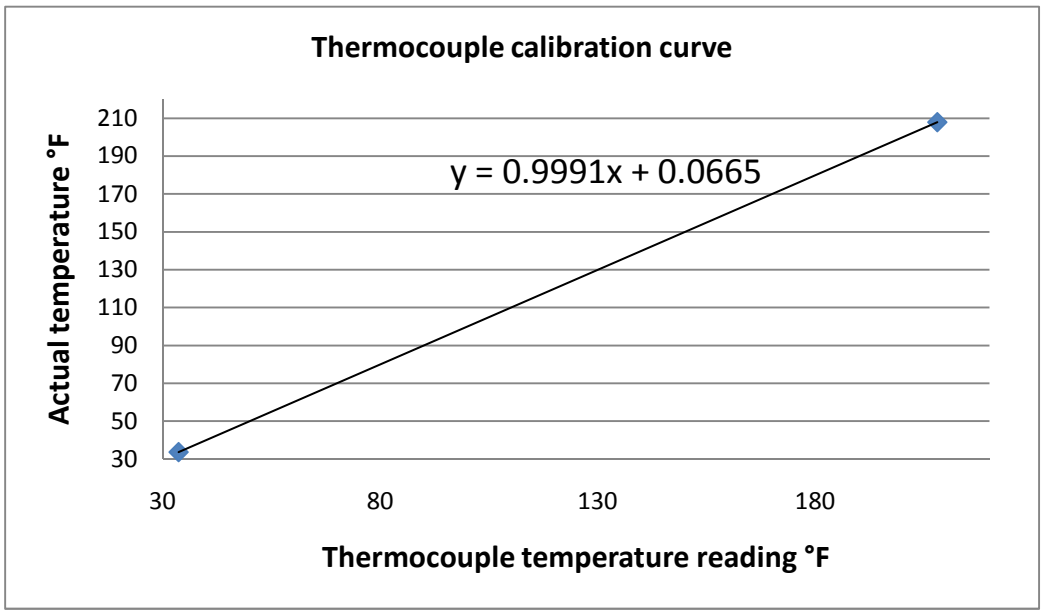

Fig. 4-6 – The computer room thermocouple calibration curve

Every equation for each thermocouple is then programmed into the LabVIEW customized program so that thermocouples give the accurate temperature measurements. Moreover, for a second check on the thermocouples accuracy the outdoor air temperature (OAT), supply air temperature (SAT), and room air temperature (RAT) have been collected by a different temperature logging system called "HOBO data loggers" (HDL) (Appendix B includes the data sheet for the HOBO data loggers). These data loggers have been set to log the above mentioned temperatures every 15 minute span; they have been synchronized with the National Instrument and computer logging system. Thereafter, the thermocouple temperatures are compared with the corresponding HOBO data loggers temperatures (as shown in Figures 4-7 a, b 4-8 a, b 4-9 a and b). The comparison shows that the average temperature error is about 0.26°F (with an average error range ±0.44).

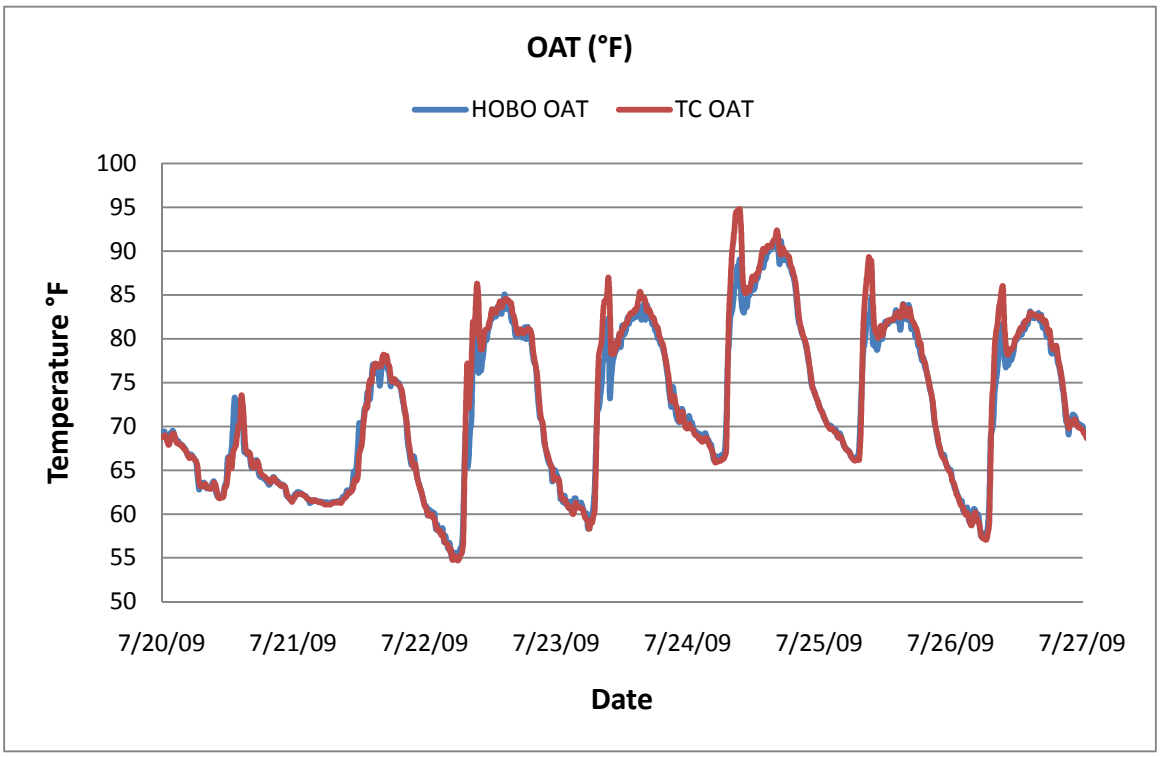

Fig. 4-7 (a) – Time series comparison between the TC and HDL OA-Temperatures

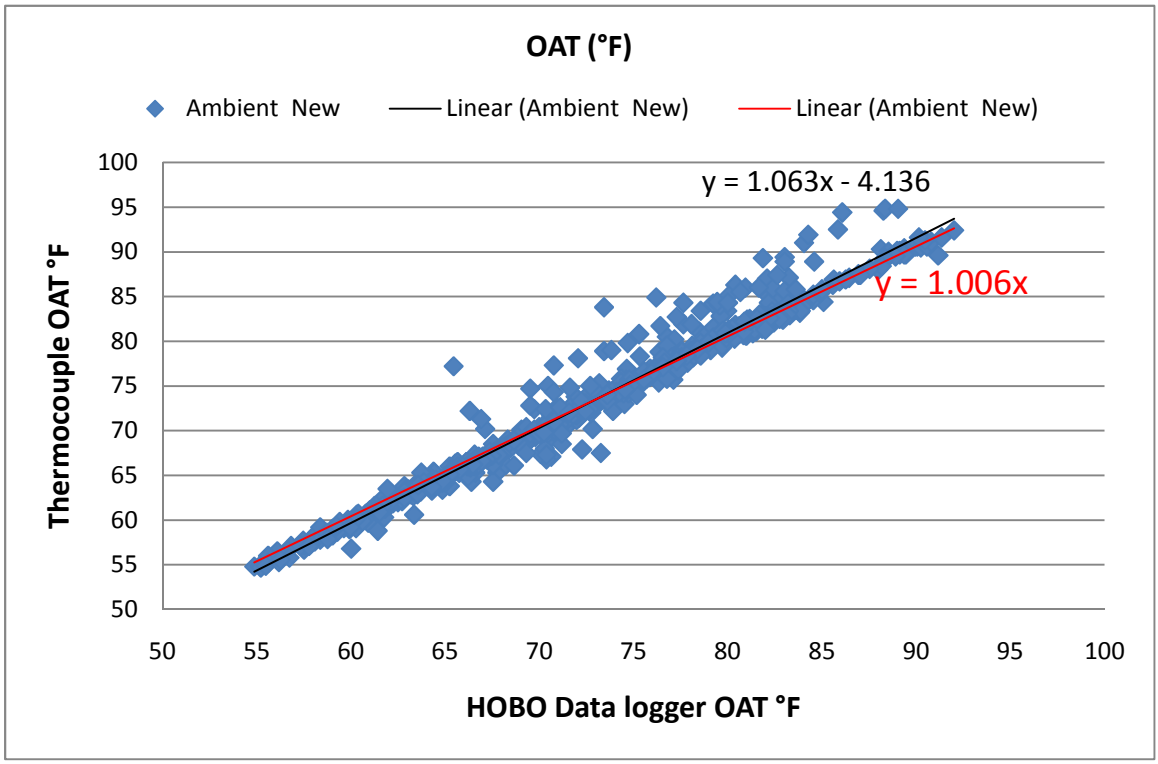

Fig. 4-7 (b) – Direct comparison between the TC and HDL OA-Temperatures

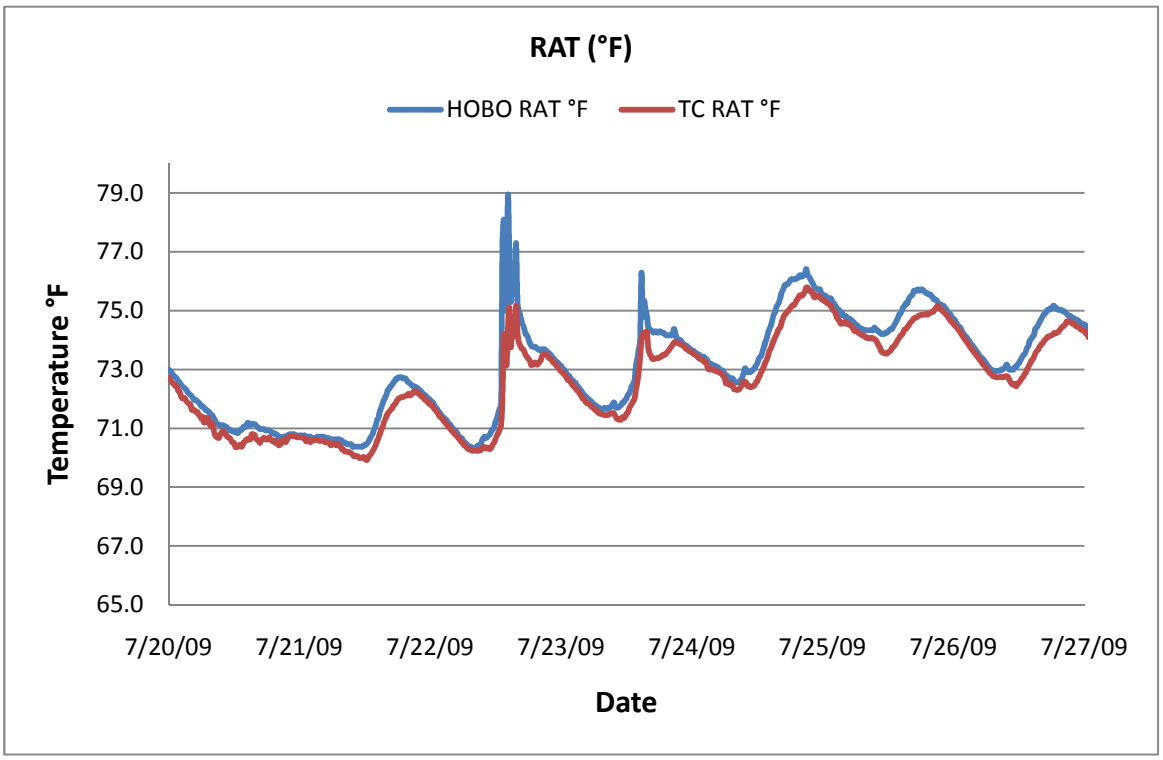

Fig. 4-8 (a) – Time series comparison between the TC and HDL RA-Temperatures

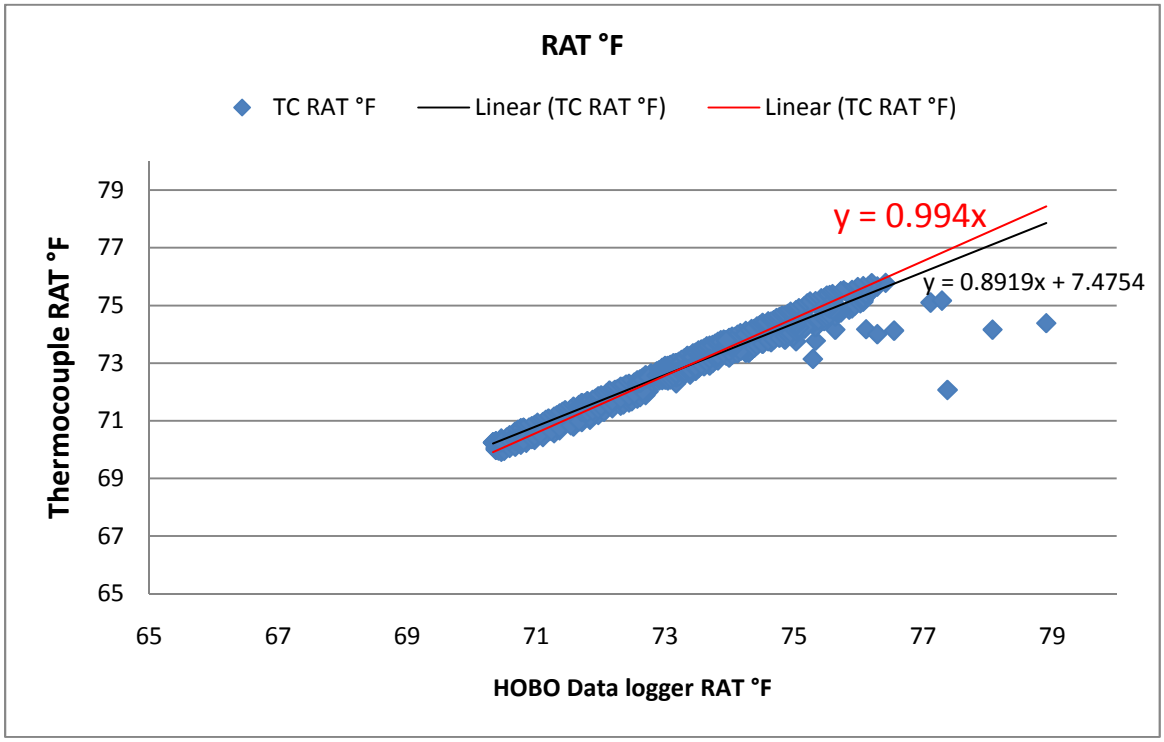

Fig. 4-8 (b) – Direct comparison between the TC and HDL RA-Temperatures

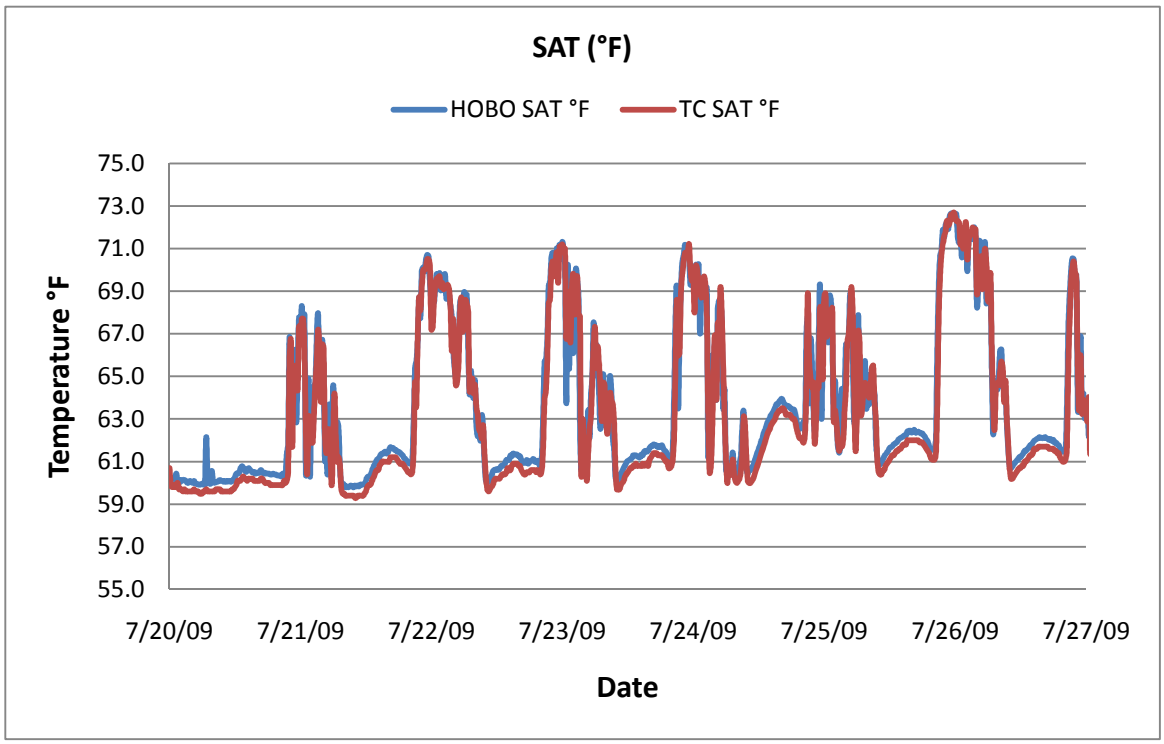

Fig. 4-9 (a) – Time series comparison between the TC and HDL SA-Temperatures

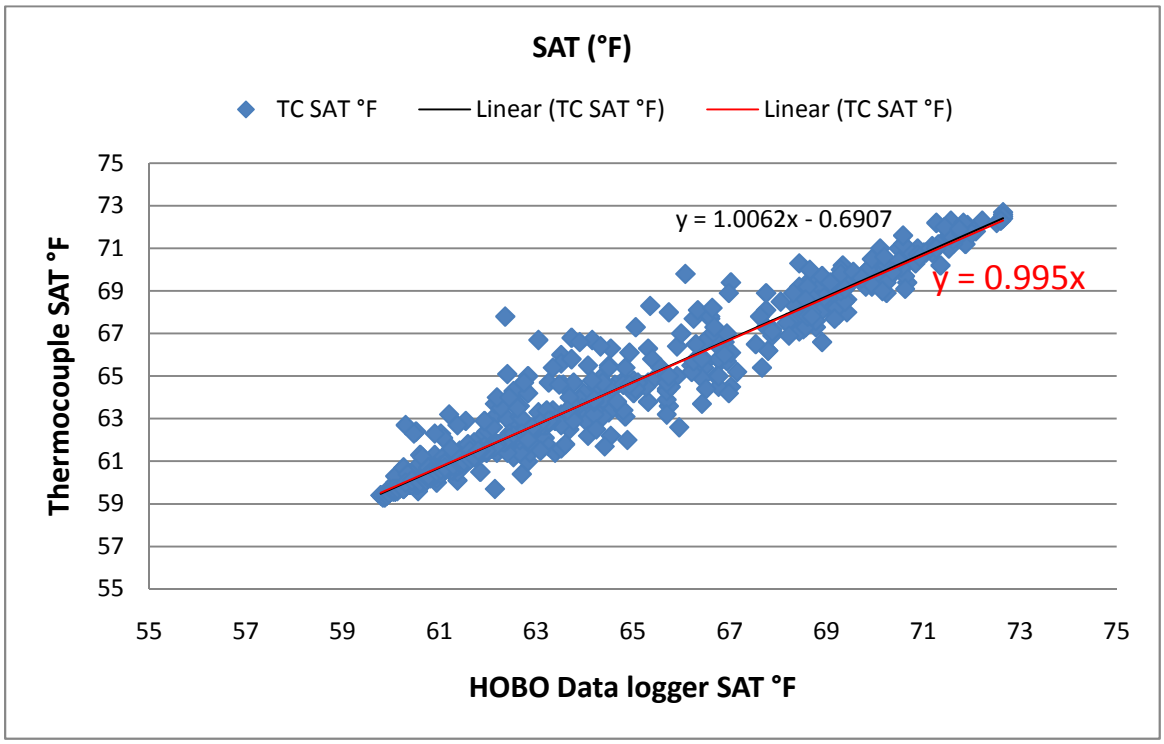

Fig. 4-9 (b) – Direct comparison between the TC and HDL SA-Temperatures

4.2.2 Air Velocity Transmitters Calibration

Unlike thermocouple calibration, where two thermocouple temperature readings are compared against two previously known temperatures, the air velocity transmitters' calibration is done against the readings of an accurate precision airflow meter known as the "FlowHood" (model CFM-88L). In this calibration process, the damper, installed at the EAHE outlet inside the testing facility building, is set to four different positions (i.e. 100% open, 75% open, 50% open, and 25% open). At each damper position, ten airflow measurements are recorded using the air FlowHood, while concurrently the corresponding ten air velocity measurements are recorded using the air velocity transmitters. It should be mentioned that the air velocity measurements have been taken in the form of a proportional current signal in milliamperes.

In order to obtain the airflow calibration curve and to drive the relationships between the airflow and the DC-current signal of the air velocity transmitters, the airflow data obtained by the FlowHood is plotted against the DC-current signal data from the air velocity transmitters and linear curve fit is applied as shown in Figures 4-10 a, b, and c. Using this calibration method over a large range of airflows (10 CFM - 2000 CFM), which covers all the possible airflows through the EAHE, allows for the direct estimation of the airflow rate from the DC-current signal of the air velocity sensor.

These linear relationships (i.e. equations) are then programmed and implemented into the customized LabVIEW program, so that the calibrated airflow measurements are recorded and logged directly. For a more accurate

reading of the supply airflow, two air velocity transmitters are installed at the EAHE outlet where two readings, one with each transmitter, are taken at the same moment and their average is recorded as one airflow measurement. Moreover, the precision and accuracy of the airflow measurements are tested by conducting an uncertainty analysis on each of the air velocity transmitters, more information about the uncertainty analysis and the air velocity transmitters' precision is given on the "Experimental Uncertainty Analysis" section of this chapter.

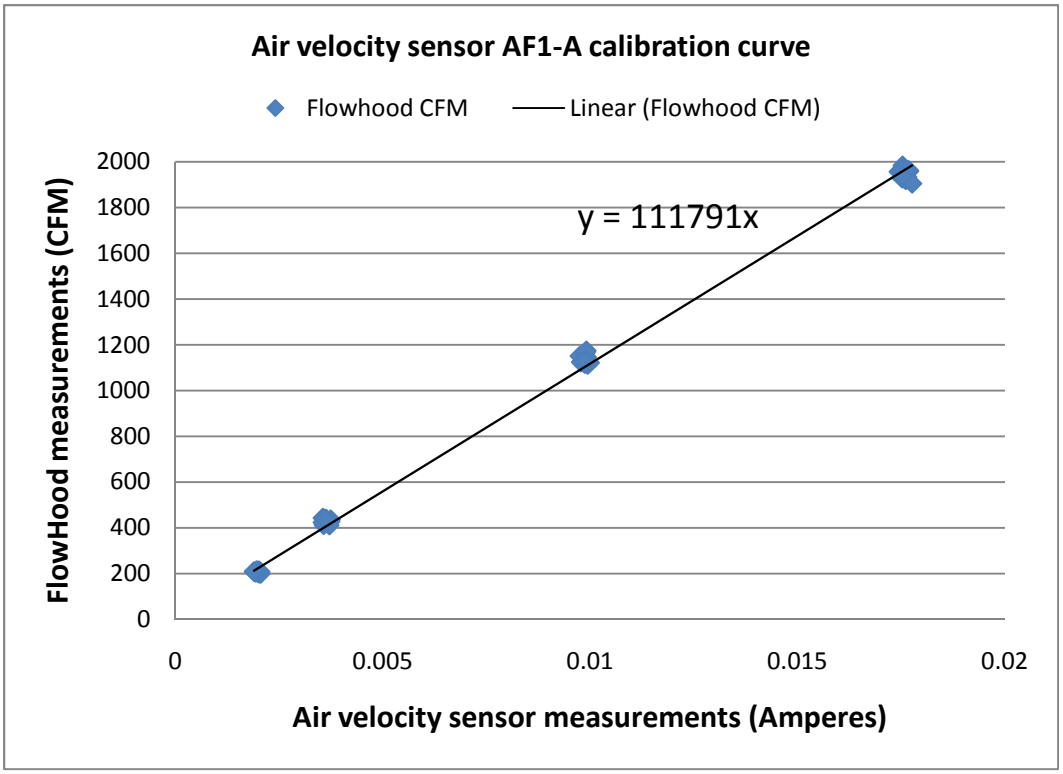

Fig. 4-10 (a) – Airflow – current relationship for air velocity sensor AF1-A

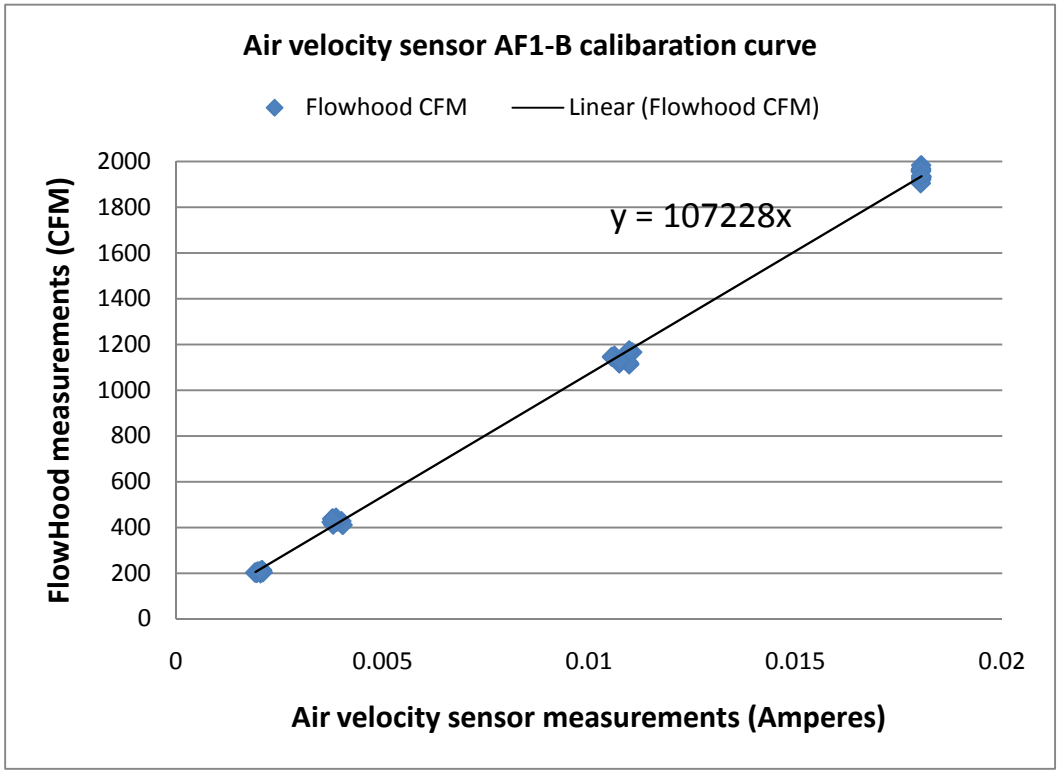

Fig. 4-10 (b) – Airflow – current relationship for air velocity sensor AF1-B

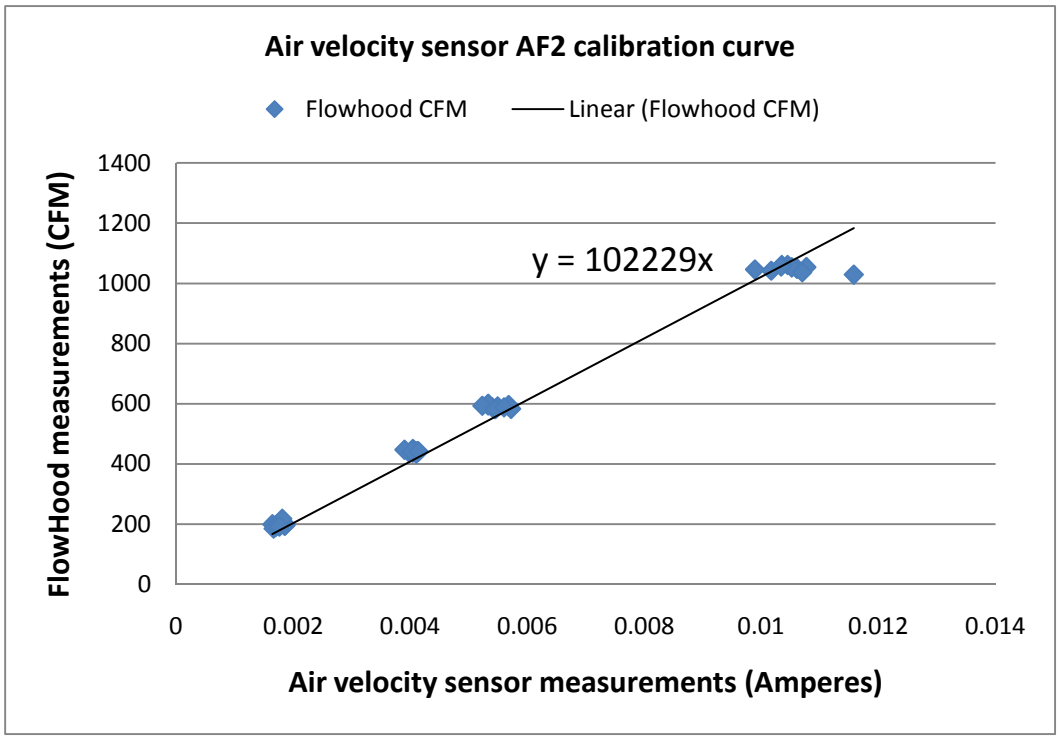

Fig. 4-10 (c) – Airflow – current relationship for air velocity sensor AF2

4.2.3 Relative Humidity Sensors Calibration

Although, the relative humidity sensors have not undergone any calibration due to the lack of precision sensors, the relative humidity measurements of these sensors have been compared to the relative humidity measurements of the HOBO data loggers (HDL). Similar to the thermocouples temperature measurements accuracy check, the relative humidity measurements have also been checked against the HOBO data loggers measurements. Three HOBO data loggers were installed at the same exact locations of the three installed relative humidity sensors: at the EAHE inlet (outdoor humidity sensor), the EAHE outlet (supply air humidity sensor), and between the EAHE supply duct and the solar collector connection duct (indoor humidity sensor). The relative humidity measurements have been recorded by the relative humidity sensors and the HOBO data loggers at the same time over a 15 minute interval during the 2009 testing period. One week of the relative humidity sensors measurements are compared against the equivalent HOBO data loggers' measurements. Figures 4-11 a, b; 4-12 a, and b show the relationship between the relative humidity sensors' measurements and the HOBO data loggers' measurements. The comparison shows a good agreement with an average error of about ±4.95%. It should be mentioned that the outdoor air relative humidity has not undergone any sort of comparison due to a connection problem between the relative humidity sensor and the National Instruments modules. Moreover, the only set of outdoor relative humidity data has been collected using the outdoor HOBO data logger.

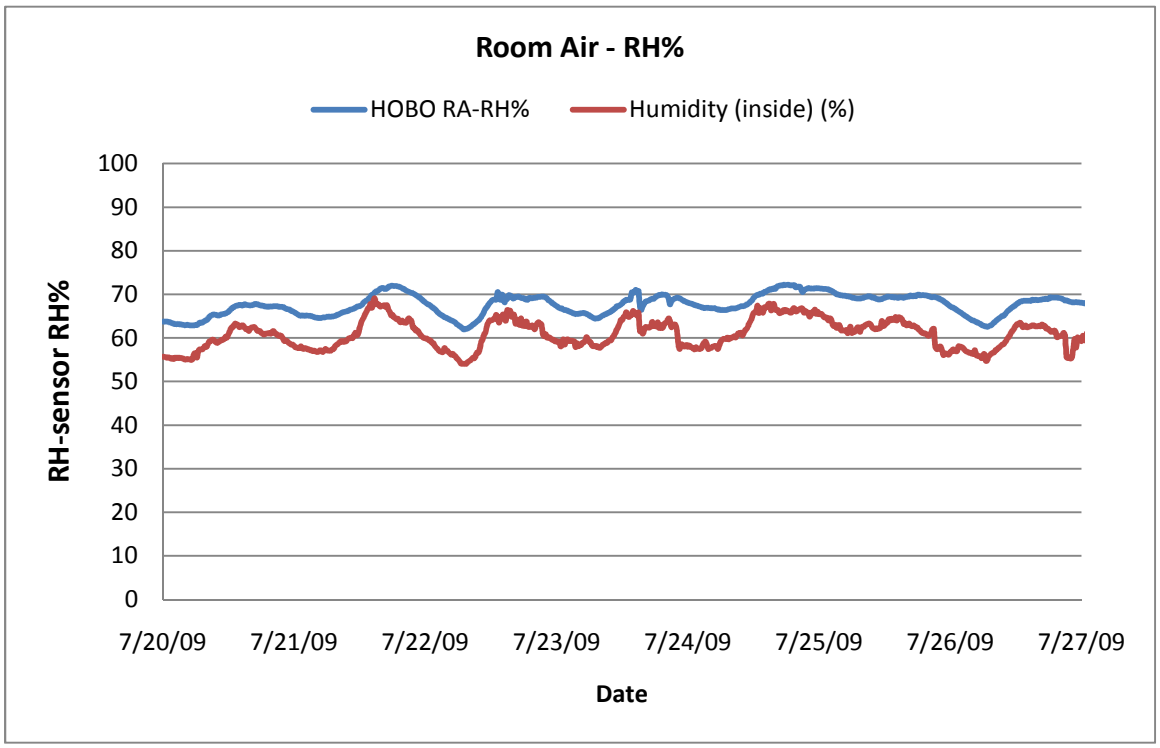

Fig. 4-11 (a) – Time series comparison between RA-RH% of RH-sensor & HDL

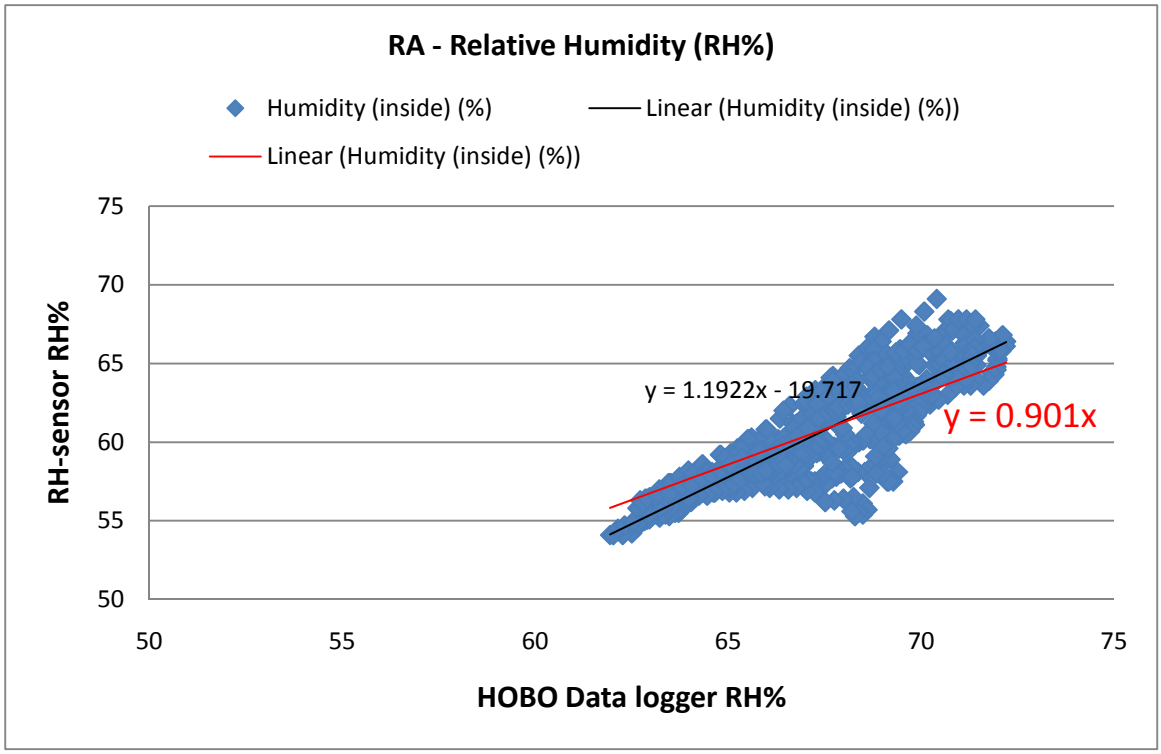

Fig. 4-11 (b) – Direct comparison between the RA-RH% of RH-sensor & HDL

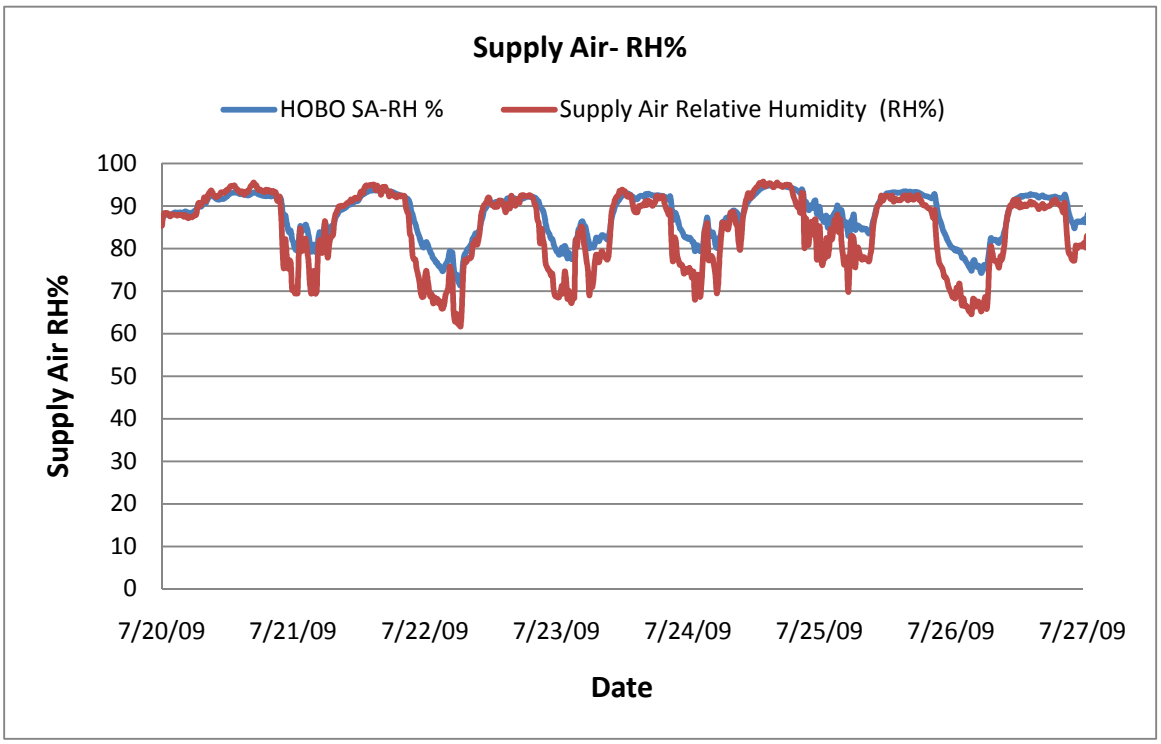

Fig. 4-12 (a) – Time series comparison between SA-RH% of RH-sensor &HDL

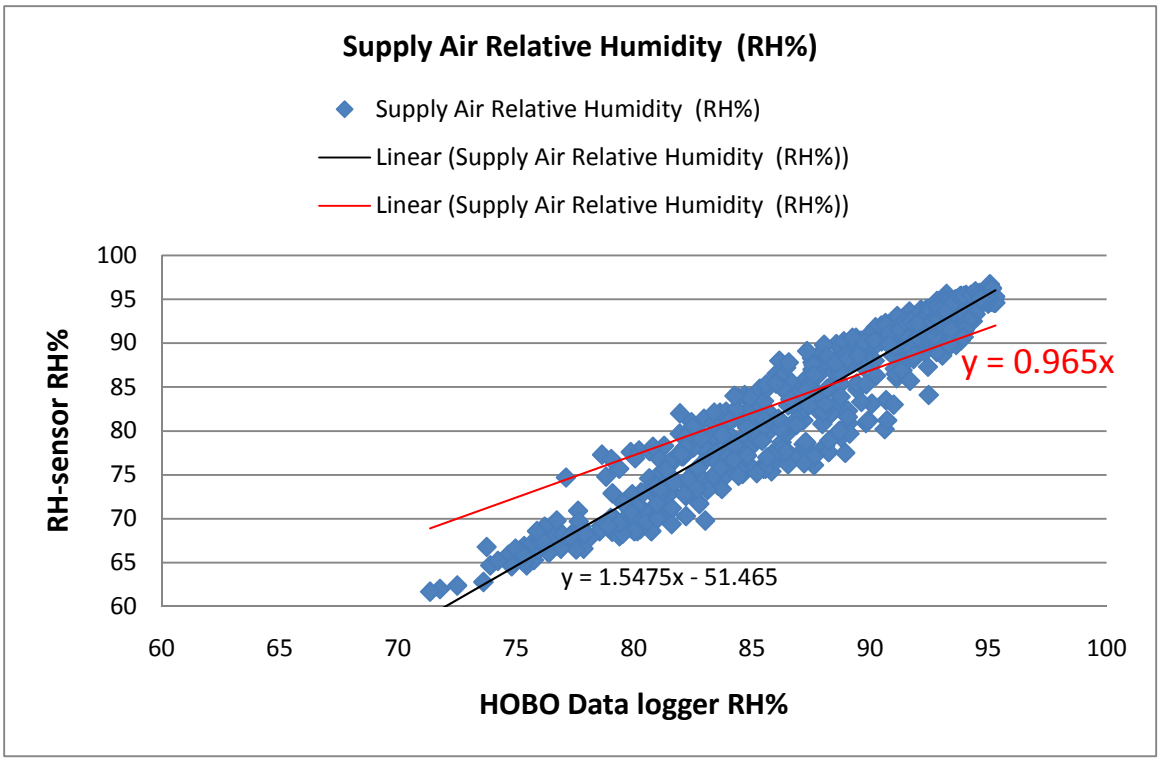

Fig. 4-12 (b) – Direct comparison between SA-RH% of RH-sensor and HDL

4.3 Data Acquisition and Logging

As mentioned earlier in chapters 3 and 4, all the weather measurement instruments (except the soil moisture sensors) are connected to the National Instruments modules which in turn are connected to a computer system. According to (Henkel, et al., 2004) a customized program has been programmed using the National Instruments LabVIEW software package to help calibrate, monitor and log the data measurements of the measurement instruments (e.g. thermocouples, humidity sensors, etc.). On the other hand, the soil moisture sensors are connected to the watermark data loggers which are specifically designed and programmed to log soil moisture measurements from the watermark soil moisture sensors. All the National Instruments modules and the Watermark data loggers are synchronized to log and store an average measurement over a 15 minute span, appendix A shows a sample of the measured data during the 2008 and 2009 testing periods. The measurements are then stored on a notepad file on the computer system, where a new notepad file is created everyday and named after that day's date. All the measurements are then copied to a one excel sheet, where time series were used for the graphical representation and data analysis of the system measurements. More information about the data analysis and the experimental results will be discussed on chapter 5 "Experimental Results" of the current study.

4.4 Experimental Uncertainty Analysis

The uncertainty analysis or error estimation of the measured data is one of the most important aspects of the current study as it gives an indication of the accuracy, precision and reliability of the measuring instruments. The uncertainty analysis has been carried out for the two main measuring instruments (i.e. the thermocouples and air velocity transmitters) as their precision is very important for the accurate estimation of the cooling capacity of the coupled system.

According to Elyyan (2001), there are two main types of uncertainty analysis; the uncertainty analysis of the measured data, and the uncertainty analysis of the calculated results. Where the calculated results uncertainty analysis can be written in terms of the measured data uncertainty analysis as follows:

$$e_R = \pm\sqrt{\left(\frac{\partial R}{\partial x_1}e_1\right)^2 + \left(\frac{\partial R}{\partial x_2}e_2\right)^2 + \cdots + \left(\frac{\partial R}{\partial x_n}e_n\right)^2} \qquad (4.2)$$

Where:

R = the calculated results, $R=R(x_1,x_2,\ldots,x_n)$

e_R = the uncertainty interval in the results

e_n = the uncertainty interval in the n^{th} variable

$\frac{\partial R}{\partial x_n}$ = the sensitivity of the results to a single variable, x_n

On the other hand, the measured data uncertainty analysis can be determined through the measurement technique. According to (Jiang, et al., 2006) the measured data uncertainty of a specific measuring instrument can be determined as follows:

$$e_{instrument} \approx \pm\sqrt{e_{ref}^2 + e_{stab}^2} \qquad (4.3)$$

Where:

$e_{instrument}$ = the uncertainty of a specific measuring instrument (e.g. thermocouple)

e_{ref} = the precision error of the reference measuring instrument

e_{stab} = the stable bias error between the reference and measuring instruments

In the following sections more focus will be given to the measured data uncertainty (i.e. temperature measurements and airflow measurements) as well as the uncertainty analysis of the calculated cooling capacity. The uncertainty analysis technique used for each measuring instrument (i.e. sensor) will be discussed. Moreover, the uncertainty results of each measuring instrument will be presented.

4.4.1 Temperature Measurement Uncertainty

The temperature measurement uncertainty analysis has been carried out using the type-T thermocouples along with the FLUKE thermometer model 51-54 series II (Appendix B includes the FLUKE thermometer data sheet). The uncertainty analysis has been conducted after the calibration of the thermocouple wires against the water boiling and freezing points as discussed earlier on the "Calibration of Experimental Devices" section of this chapter. The thermocouple uncertainty experiments have been carried out by wrapping the thermocouple wire around the FLUKE thermometer wire probe, so both sensors would read the temperature of almost the same exact point. Thereafter, the two sensors are immersed into a boiling water pot for few minutes till the boiling water temperature stabilizes. Afterwards, the temperature measurements of both the

thermocouple and FLUKE thermometer have been recorded at the same time every 15 seconds for 5 minutes. Subsequently, the two sensors are immersed in an ice water bath for few minutes till the ice water bath temperatures stabilize and temperature measurements have been recorded in the same manner as mentioned above. The FLUKE thermometer temperature readings are considered to be reference temperatures, and the difference between the FLUKE thermometer and thermocouple temperature readings are considered the thermocouple reading deviations (i.e. error scatter). These temperature reading differences are then used to estimate the scatter of the thermocouple readings and consequently, the thermocouple uncertainty. Figure 4-13 shows one of the thermocouple scatter readings, where the average thermocouple deviation (i.e. error) from the reference reading is about ± 0.048 °F.

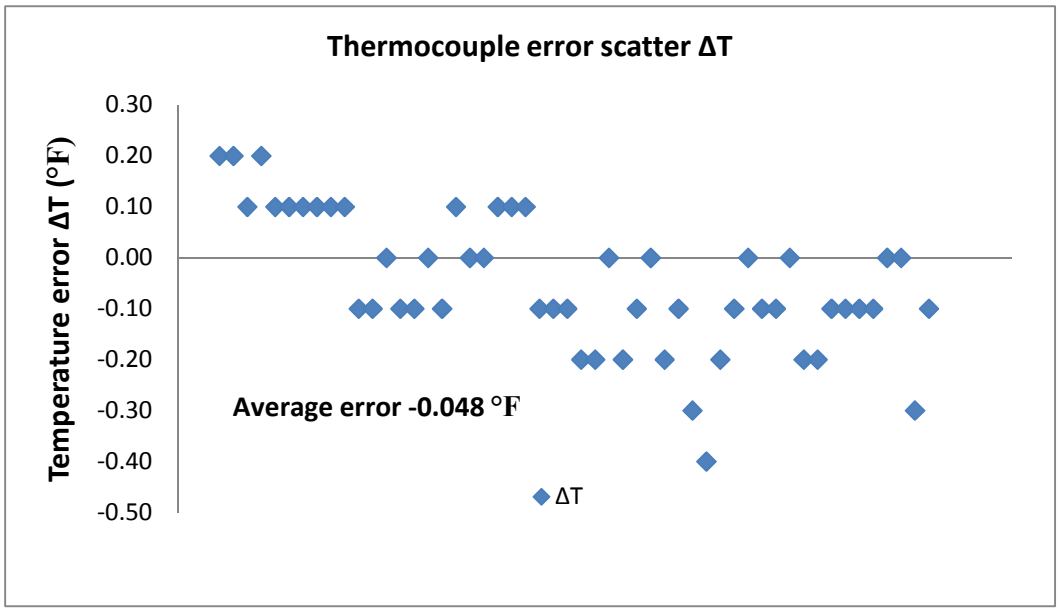

Fig. 4-13 – Thermocouple deviations from the FLUKE values

From the FLUKE thermometer data sheet, the FLUKE type-T probe thermometer accuracy is found to be [±0.05% + 0.5 °F (0.3°C)]. Knowing the FLUKE accuracy, the thermocouple uncertainty can be calculated according to equation (4.3) as follows:

$$e_{TC} \approx \pm\sqrt{e_{T-ref}^2 + e_{T-stab}^2}$$

$$= \pm\sqrt{(0.5)^2 + (0.048)^2}$$

$$e_{TC} = \pm 0.502\ °\text{F}$$

4.4.2 Flow Rate Measurement Uncertainty

The airflow measurements uncertainty analysis has been carried out using the Dwyer (Series 641RM) air velocity transmitters along with the Shortridge Instruments FlowHood (model CFM-88L). The airflow uncertainty analysis has been conducted after the calibration of the air velocity transmitters against the measurements of the precision airflow meter (i.e. FlowHood CFM-88L) discussed earlier on the "Calibration of Experimental Devices" section of this chapter. In the same manner as the air velocity transmitters' calibration, the uncertainty analysis has been carried out by adjusting the EAHE outlet damper to four different positions (i.e. 100% open, 75% open, 50% open, and 25% open). At each damper position, ten airflow measurements are recorded using the air FlowHood, while concurrently, the corresponding ten air velocity measurements are recorded using the air velocity transmitters. It should be mentioned that the air velocity measurements are recorded in the form of DC-current in mamps proportional to the air velocity readings.

By applying the relationships between the airflows and the DC-current signals (obtained earlier in the "Air velocity transmitters' calibration" section of this chapter) to the air velocity transmitters readings, the mamps signals of the air velocity transmitters are converted to airflow rate values in cubic feet per minute (CFM).

Considering the airflow measurements of the FlowHood as the reference measurements, then the difference between the FlowHood and air velocity transmitters, airflow measurements are considered the airflow deviations (i.e. ΔCFM). These airflow measurements differences are then used to estimate the error scatter of the airflow measurements and consequently, the airflow measurements' uncertainty. Figures 4-14 a, b, and c show the three airflows error scatter for the three air velocity transmitters used during the 2008 and 2009 testing periods. The average airflow error (i.e. deviation) from the FlowHood reference measurements for the three air velocity transmitters AF1-A, AF1-B and AF2 are; +4.5 CFM, -1.7 CFM, and +12.5 CFM respectively.

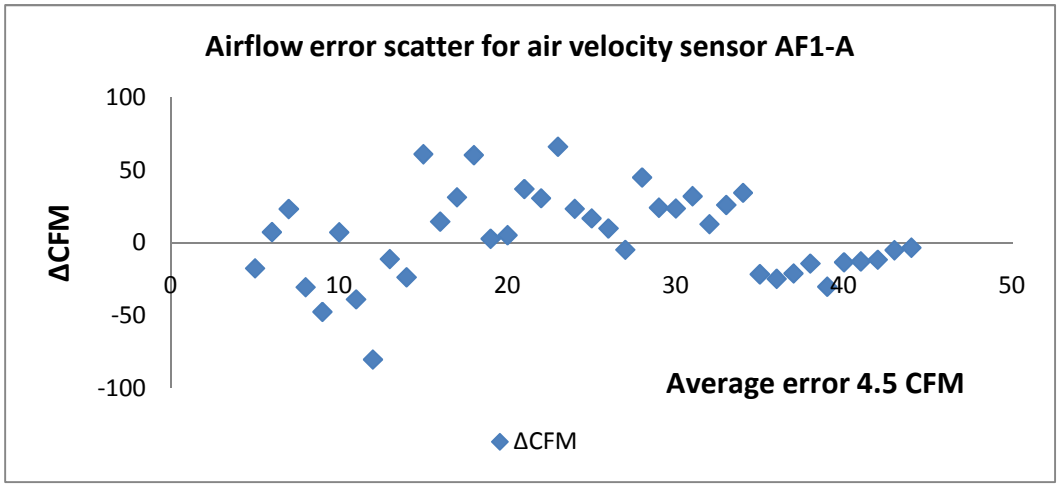

Fig. 4-14 (a) – Air velocity transmitter AF1-A readings deviations (scatter)

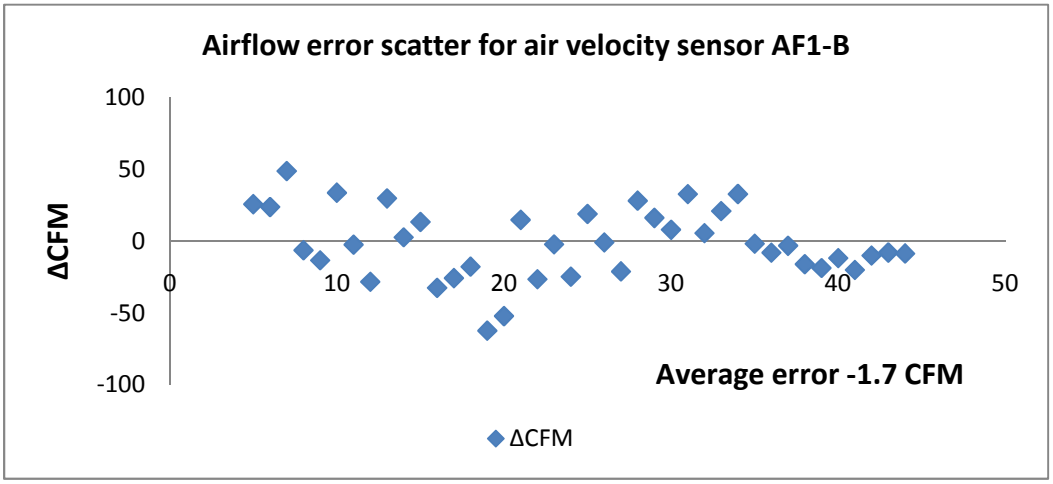

Fig. 4-14 (b) – Air velocity transmitter AF1-B readings deviations (scatter)

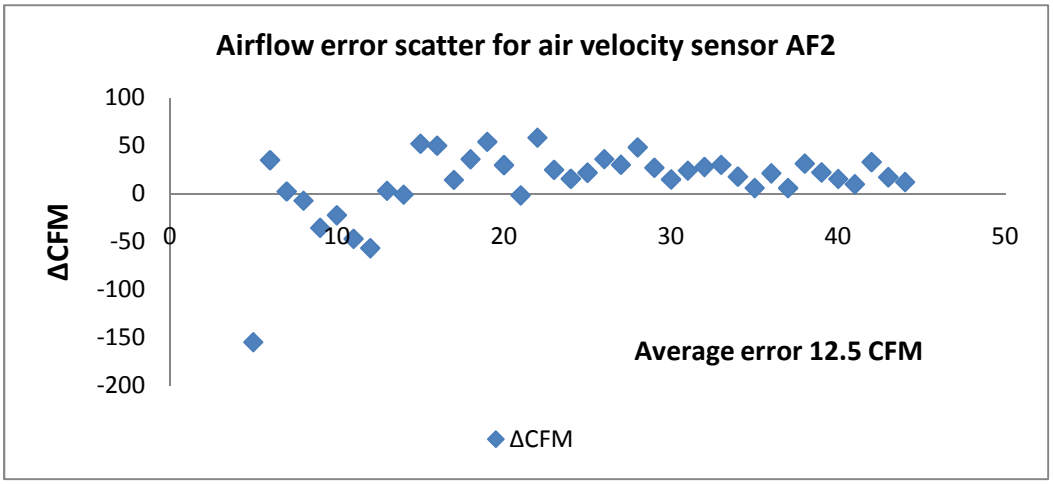

Fig. 4-14 (c) – Air velocity transmitter AF2 readings deviations (scatter)

The FlowHood airflow measurement accuracy is found to be [±3% of reading ± 7 CFM]. Knowing the FlowHood accuracy, the airflow measurements' uncertainty can be calculated according to equation (4.3) as follows:

$$e_{AF} \approx \pm\sqrt{e_{AF-ref}^2 + e_{AF-stab}^2}$$

The airflow measurement error for the air velocity transmitter AF1-A is estimated as follows:

$$= \pm\sqrt{(7)^2 + (4.5)^2}$$

$$e_{AF-AF1-A} = 8.32 \pm \text{CFM}$$

The airflow measurement error for the air velocity transmitter AF1-B is estimated as follows:

$$= \pm\sqrt{(7)^2 + (1.7)^2}$$

$$e_{AF-AF1-B} = \pm 7.2\text{CFM}$$

The airflow measurement error for the air velocity transmitter AF2 is estimated as follows:

$$= \pm\sqrt{(7)^2 + (12.5)^2}$$

$$e_{AF-AF2} = \pm 14.33 \text{ CFM}$$

4.4.3 Cooling Capacity Uncertainty

In this section the calculated sensible cooling capacity relative uncertainty analysis is estimated. Since the sensible cooling capacity calculations is based on the supply airflow and temperature measurements, the relative uncertainty of the calculated sensible cooling capacity can be estimated from the relative uncertainty of the airflow and temperature calibration instruments. As the airflow calibration instrument (i.e. FlowHood) relative uncertainty error is ±3% and the temperature calibration instrument (i.e. Fluke) relative uncertainty error is ±0.05%, then the calculated sensible cooling capacity relative uncertainty error is calculated according to equation (4.2) as follows:

$$e_{S,cooling} = \pm\sqrt{(e_{FlowHood})^2 + (e_{Fluke})^2}$$

$$e_{S,cooling} = \pm\sqrt{(3)^2 + (0.05)^2}$$

$$e_{S,cooling} = \pm 3.000417\%$$

4.5 Summary

In this chapter the various weather measuring instruments have been presented. Moreover, the calibration curve, data and techniques of the main measuring instruments (i.e. thermocouples and air velocity transmitters) were obtained. Furthermore, uncertainty analyses for the temperature as well as airflow velocity measurements have been conducted to verify the accuracy and the reliability of the measuring instruments used during the test periods. The results shows that the sensors used for data logging are precise enough for collecting data and that the measured data have slight deviations from the reference measurements which can be ignored.

Chapter, 5

EXPERIMENTAL RESULTS

5.1 Overview

As mentioned earlier on chapter 3, the main purpose of the current study is to answer two main important questions: first, can the all passive coupled system provide enough cooling capacity for the testing facility over the summer time; second, can the fan assisted coupled system maintain a maximum cooling rate without saturating the soil surrounding the EAHE. To answer these two questions, two sets of experiments have been carried out on the summers of 2008 and 2009 respectively.

The first testing period lasted for 18 days; from August 14th, 2008 till August 31st, 2008. The main goal of this test is to evaluate the thermal performance of the all passive, naturally driven, coupled system, through assessing the maximum cooling capacity, as well as the airflow rate, that it can provide for the testing facility building. In doing so the EAHE outlet damper has been set to the 100% fully open position, and the computer system has been programmed to record, average, and log the weather data over a 15 minute span during the whole testing period (i.e. day and night). As previously mentioned on chapter 3 various measurements have been recorded during this testing period. The main measurements that have been recorded for the purpose of analyzing the cooling capacity of the naturally driven coupled system are: time and date, the indoor relative humidity (%), outdoor relative humidity

(%), supply air relative humidity (%), supply air flow rate (CFM), solar collector airflow rate (CFM), the average indoor temperature (ºF), the supply air temperature (ºF), and the outdoor (i.e. ambient) air temperature (ºF). The system thermal performance during this testing period is presented on the "Performance Analysis of the Coupled System" section of this chapter.

The second testing period lasted for 43 days; from July 24th, 2009 till September 4th, 2009. This testing period has been divided into three smaller time portions, with three different tests. The first test lasted for 14 days; started on July 24th, 2009 and ended on August 6th, 2009. The main goal of the first test is to run the all passive, naturally driven, coupled system and compare its thermal performance with that similar test carried out on 2008. The second test lasted for 9 days; started on August 7th, 2009 and ended on August 15th, 2009.

The second test has two main goals: the first is to evaluate the thermal performance of the fan assisted coupled system, through assessing the maximum cooling capacity, as well as the airflow rate, that it can provide for the testing facility building. And the second goal is to study how long it will take the fan assisted coupled system to thermally saturate the soil surrounding the EAHE. For this test a constant speed fan has been mounted on the top of the EAHE outlet, and it has been set to run continuously during the whole 9 days of testing (i.e. day and night).

The third test lasted for 20 days; started on August 16th, 2009 and ended on September 4th, 2009. The main goal of the third test is to determine how long it will take the soil surrounding the EAHE to recover from the thermal saturation and return

back to its original (normal) temperature range. For this test the assisting fan has been disabled (turned OFF) and the system was allows to run naturally (passively).

Similar to the 2008 testing period, the EAHE outlet damper has been set to the 100% fully open position, and the computer system has been programmed to record, average, and log the weather data over a 15 minute span during the whole testing period (i.e. day and night). Moreover, the assisting fan has been turned ON during the second test and OFF during the first and third tests of the 2009 testing period. The main measurements that have been recorded during this testing period are: time and date, the indoor relative humidity (%), outdoor relative humidity (%), supply air relative humidity (%), supply air flow rate (CFM), solar collector air flow rate (CFM), the average indoor temperature (ºF), the supply air temperature (ºF), the outdoor (i.e. ambient) air temperature (ºF), the underground temperature at 21 different locations above and beside the EAHE (ºF), and the soil moisture content at 20 different locations above and beside the EAHE. It should be mentioned that for the 2009 testing period a new set of underground thermocouples and soil moisture sensors have been installed and calibrated before the testing. Chapter 3 includes the sensors map figures which in turn show the sensors types, names, and locations. The thermal performance of the system as well as the ground (i.e. soil) thermal during this testing period is presented on the "Performance Analysis of the Coupled System" section of this chapter.

5.2 Undisturbed Underground Soil Testing

Before starting any of the coupled system experiments, a major check test for the undisturbed underground soil (UUS) has been carried out. The test has been conducted through monitoring the underground soil temperature profile at three different depths. For this test the three previously installed underground temperature reference thermocouples have been used to record the UUS temperatures every 15 minute span. Similar to the other thermocouples, these three thermocouples were connected to the National Instruments modules which in turn are connected to the computer system for data monitoring and logging.

According to (Henkel, et al., 2004) the underground temperature reference thermocouples had been calibrated then installed at the south west side of the testing facility building at a distance of 9.84ft (3m) away from the building to the west. The three thermocouples are called "#Ground Ref. –T"[1], "#Ground Ref.-M"[2], and "#Ground Ref.-B"[3], and they are used to monitor the UUS temperatures profiles at the depths of 2ft (0.6m), 5ft (1.5m), and 9.5ft (2.9m) respectively. It should be mentioned that these three thermocouples had been located away from the EAHE so they would measure the UUS temperatures without being influenced by any underground soil disturbance occurring due to other ongoing experiments.

[1] (#Ground Ref.-T) – Under-Ground Temperature Reference Thermocouple; Top - 2ft (0.6m) depth.
[2] (#Ground Ref.-M) – Under-Ground Temperature Reference Thermocouple; Middle - 5ft (1.5m) depth.
[3] (#Ground Ref.-B) – Under-Ground Temperature Reference Thermocouple; Bottom – 9.5ft (2.9m) depth.

The UUS test lasted for a whole year (366 days); from January 1st, 2008 till December 31st, 2008. One goal for this test is to study the UUS temperature variations over the course of a whole year to verify its capability of being a heat sink. Another goal is to examine the influence of the coupled system on the underground soil surrounding the EAHE by comparing the thermal performance of the UUS with that of the underground soil surrounding the EAHE.

Figure 5-1 shows the UUS temperature profiles at the three different depths for the entire year of 2008. And Table 5-1 shows the statistics for the UUS temperatures.

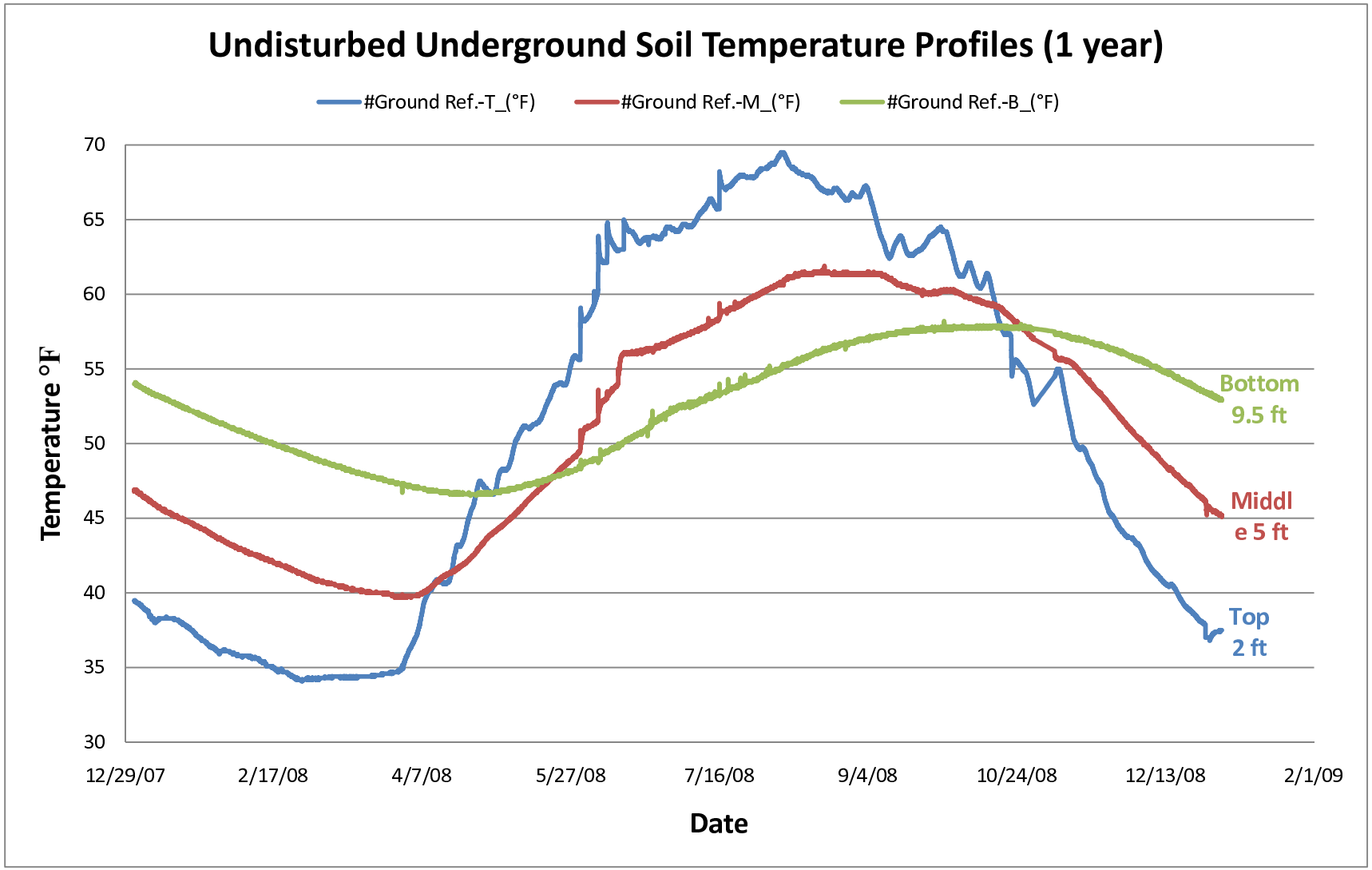

`Fig. 5-1 - The undisturbed underground soil (UUS) temperature profiles over the course of the year 2008

Table 5-1 – Undisturbed Underground Soil (UUS) Temperatures Statistics

Thermocouple Name	Thermocouple Depth	Max./Min.	Temperature Value	Date
Ground Ref. Top	2 ft	Max.	69.5 °F	8/5/08
		Min.	34.1 °F	2/26/08
Ground Ref. Middle	5 ft	Max.	61.9 °F	8/20/08
		Min.	39.7 °F	4/3/08
Ground Ref. Bottom	9.5 ft	Max.	58.2 °F	9/29/08
		Min.	46.5 °F	4/23/08

As shown in Figure 5-1, the deeper the depth of the thermocouple underground the less the temperature fluctuation. Moreover, by knowing that July and August are the peak hot summer months of Omaha Nebraska, it is clear that there is a phase shift between the ambient air temperatures and the underground temperature profile and this shift increases by the increase of the underground depth.

Table 5-1 shows that at a depth of 9.5ft (2.9m) the UUS temperature fluctuates between a maximum temperature of 58.2 ºF and a minimum of 46.5 ºF, which verifies its good ability to be a good heat sink for the EAHE heat dissipation. Furthermore, it is found that the maximum temperature at this depth during the period from July 1st, 2008 to August 31st, 2008 is 57 ºF while the minimum is 52.2 ºF.

These promising results of the UUS test motivated the current research to move forward to estimate the maximum cooling capacity that could be extracted by the coupled system during the natural (i.e. passive solar drive) and forced (i.e. fan assisted, mechanically driven) airflow modes. Accordingly, the following section of

this chapter is focusing on analyzing the coupled system thermal performance from different points of view as well as evaluating its cooling capacity.

5.3 Performance Analysis of the Coupled System and EAHE

The thermal performance analysis starts by comparing the indoor and outdoor air thermal environmental conditions, through plotting the indoor/outdoor temperature, relative humidity and humidity ratio profiles. The main goal of this comparison is to study the ability of the coupled system to comply with & maintain the indoor thermal environmental comfort conditions recommended by ASHRAE standard 55-2004.

Thereafter, the calculation method of the cooling capacities is explained. Afterwards, the design cooling load of the test facility building is calculated using TRACE 700 software to provide a baseline for the coupled system cooling capacities thermal analysis (refer to appendix C for more information about the design cooling load calculations and results). Then, the cooling capacities of the EAHE as well as the coupled system during the natural and forced airflow modes are calculated. Accordingly, the thermal performance data (e.g. supply airflow rate, outdoor air temperature (OAT), etc.) as well as the calculated cooling capacities data results of the EAHE and the coupled system, during the natural and forced airflow modes are plotted as time series on Excel sheets, to analyze thermal performance of the coupled system and EAHE, as well as to study the effect of the various environmental conditions on the different cooling capacities and vice versa.

Moreover, discussions on the comparison between the coupled system cooling capacities, during the natural and forced airflow modes, and the baseline design cooling load are presented. Lastly, conclusions are drawn after each analysis section.

5.3.1 Thermal Comfort Analysis of the Coupled System

The coupled system thermal comfort analysis starts with presenting the environmental thermal comfort conditions recommended by ASHRAE standard 55 of the year 2004 for thermal comfort. Thereafter, a comparison of the coupled system, testing facility building, indoor and outdoor environmental conditions is carried out. In this comparison the indoor and the outdoor temperatures, relative humidity, and humidity ratios of the natural and forced airflow modes of the coupled system are plotted as time series on Excel sheets. Consequently, the compliance of the indoor environmental conditions, of the testing facility building, with ASHRAE standard 55-2004 during the natural and forced airflow modes are discussed and conclusions are drawn after each comparison section.

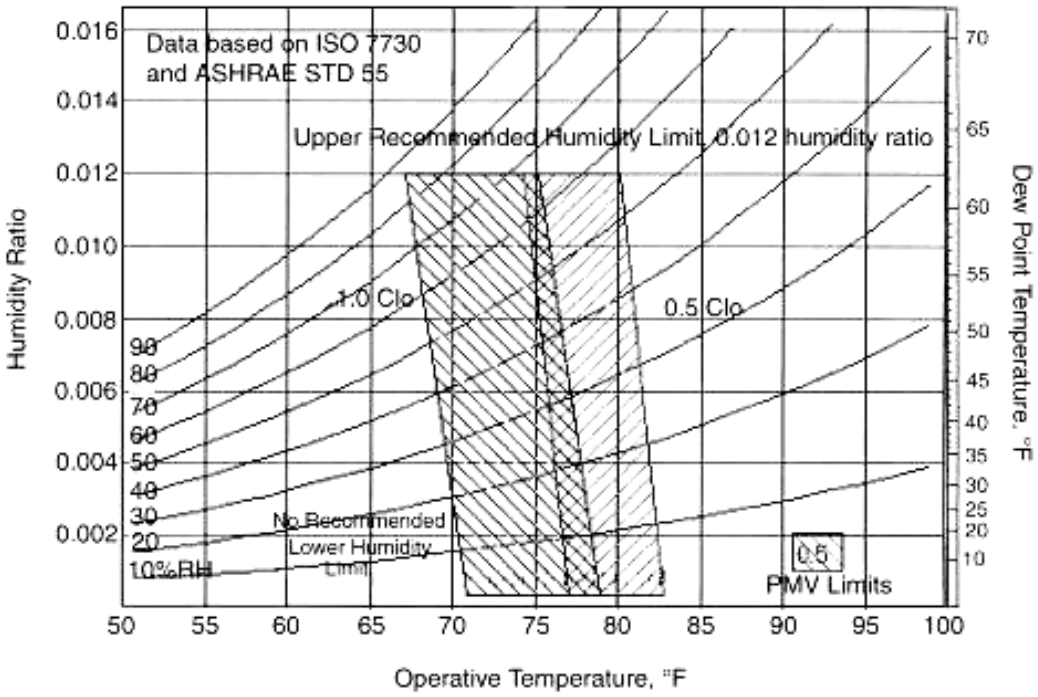

Fig. 5-2 – Acceptable Range of Indoor Thermal Environmental Conditions (ASHRAE standard 55-2004)

Figure 5-2 shows the acceptable range of indoor environmental conditions recommended by ASHRAE standard 55-2004. It is clear that the thermal comfort zone limits are almost between 71°F and 82.5°F. Moreover, it shows that the upper recommended humidity ration limit is 0.012, with no recommendation for the lower humidity limit. Based on ASHRAE recommended comfort zone limits, the indoor environmental conditions of the coupled system test facility building have been evaluated as shown in the following figures.

Figures 5-3 a, b and c, show comparisons between the indoor and outdoor thermal environmental conditions (i.e. temperatures, relative humidity, and Humidity ratios) for the natural airflow test carried out at the coupled system test facility building during summer 2008 (from August 14th, 2008 to August 31st, 2008). Furthermore, Table 5-2 presents the maximum and minimum values for the indoor (i.e. room) air thermal environmental conditions during this test.

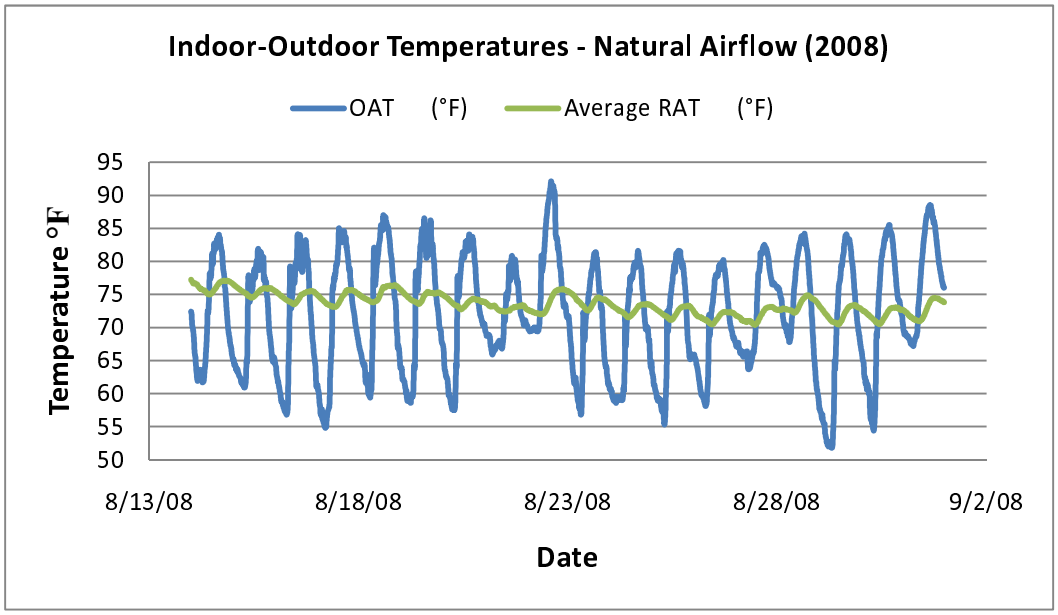

Fig. 5-3 (a) – Indoor-Outdoor Temperatures of 2008 Natural Airflow Test

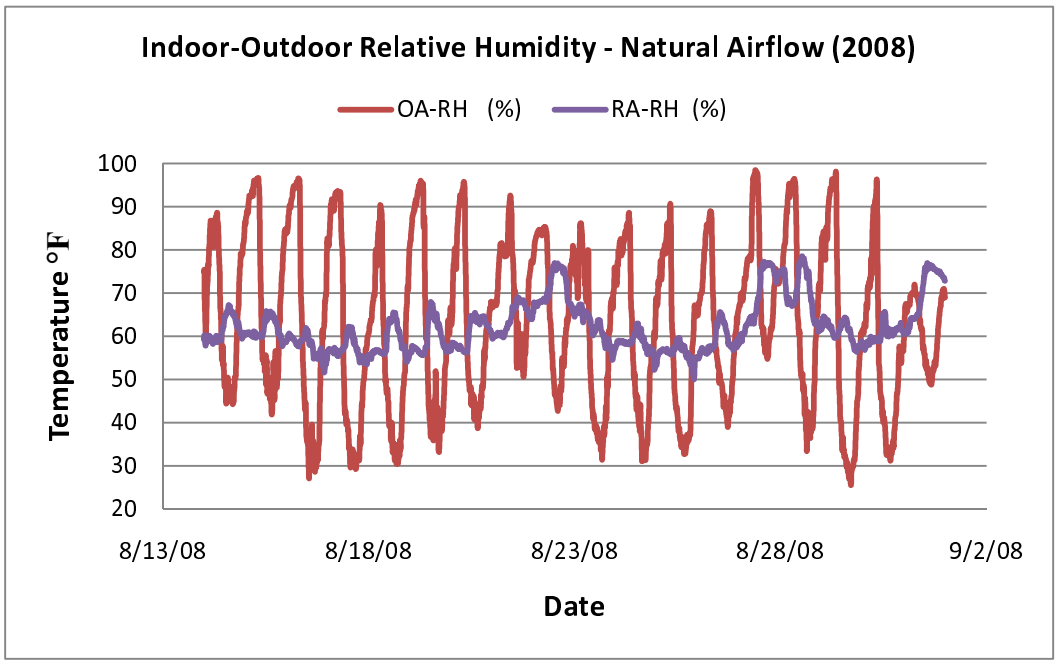

Fig. 5-3 (b) – Indoor-Outdoor Relative Humidity of 2008 Natural Airflow Test

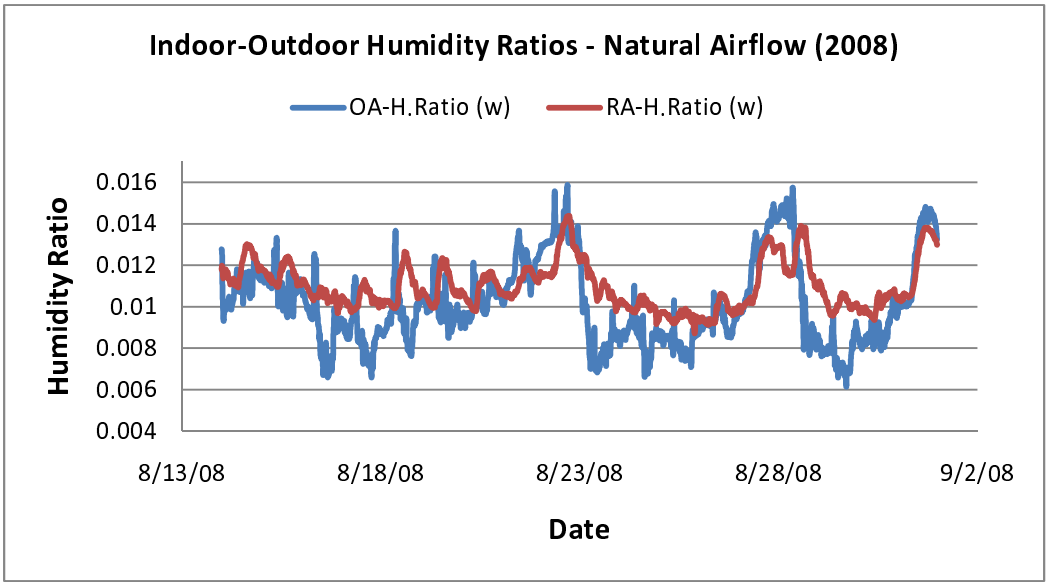

Fig. 5-3 (c) – Indoor-Outdoor Humidity Ratios of 2008 Natural Airflow Test

From Figures 5-3 a, b, and c it is clear that the coupled system has damped all the indoor environmental conditions (i.e. temperatures, relative humidity, and humidity ratios) to an acceptable level during most of the days of summer 2008

testing period. It is found through the analysis that the indoor thermal environmental conditions experienced an increase during the stormy and windy outdoor environmental conditions.

Table 5-2 – Indoor Environmental Conditions for 2008 Natural Airflow Test

Environmental Condition	Max./Min.	Value	Unit	Date	Time
RAT	Max.	77.2	°F	8/14/08	00:00
	Min.	70.4	°F	8/27/08	11:15
RA-RH%	Max.	78	%	8/28/08	12:30
	Min.	50	%	8/25/08	21:30
RA Hum. Ratio	Max.	0.01438	N/A	8/22/08	17:45
	Min.	0.008717	N/A	8/25/08	21:30

Moreover, the statistics of the indoor thermal environmental conditions of summer 2008 testing period, provided on Table 5-2, show that the coupled system maintained an acceptable indoor air temperature range of (70.4°F – 77.2°F) which complies with ASHRAE standard 55-2004. On the other hand, the humidity ratio has exceeded ASHRAEs' upper recommended humidity ratio limit 0.012 at few different days during the 2008 testing period when the outdoor air conditions were stormy and windy. Accordingly, it is concluded that the coupled system has the ability to provide an acceptable indoor thermal environmental conditions during the natural airflow test of summer 2008. Moreover, the windy and stormy outdoor air thermal environmental conditions could have a negative impact on the coupled system thermal performance.

Figures 5-4 a, b and c, show the coupled system indoor and outdoor thermal environmental conditions comparison during the natural airflow test carried out during the summer of 2009. Moreover, Table 5-3 presents the statistics of the indoor thermal environmental conditions during this test.

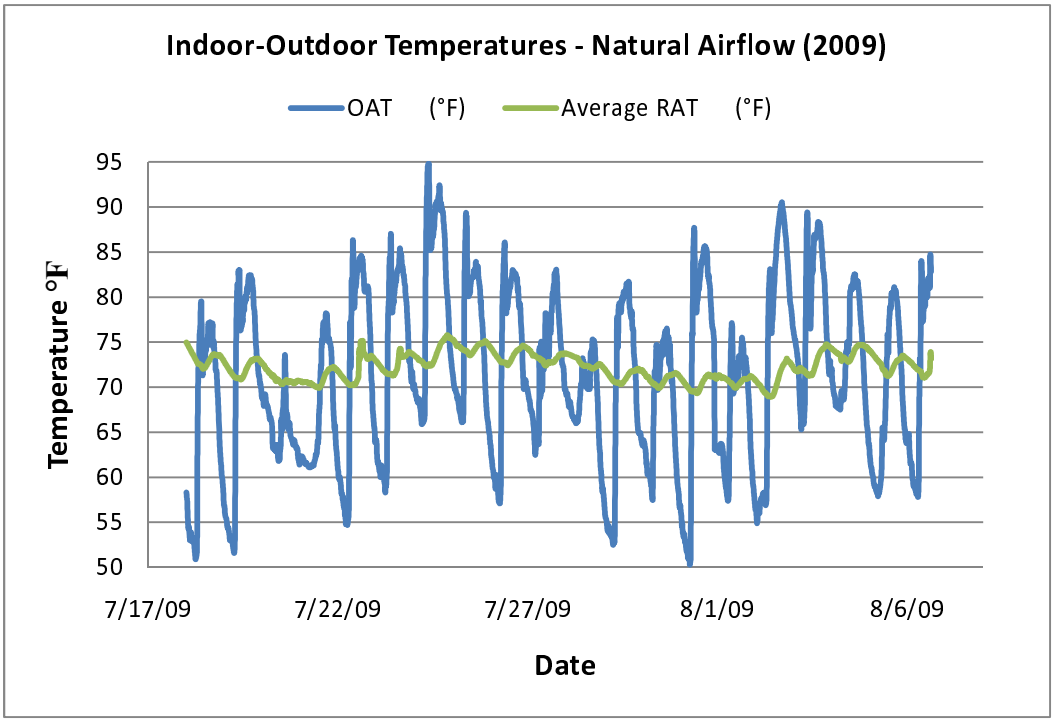

Fig. 5-4 (a) – Indoor-Outdoor Temperatures of 2009 Natural Airflow Test

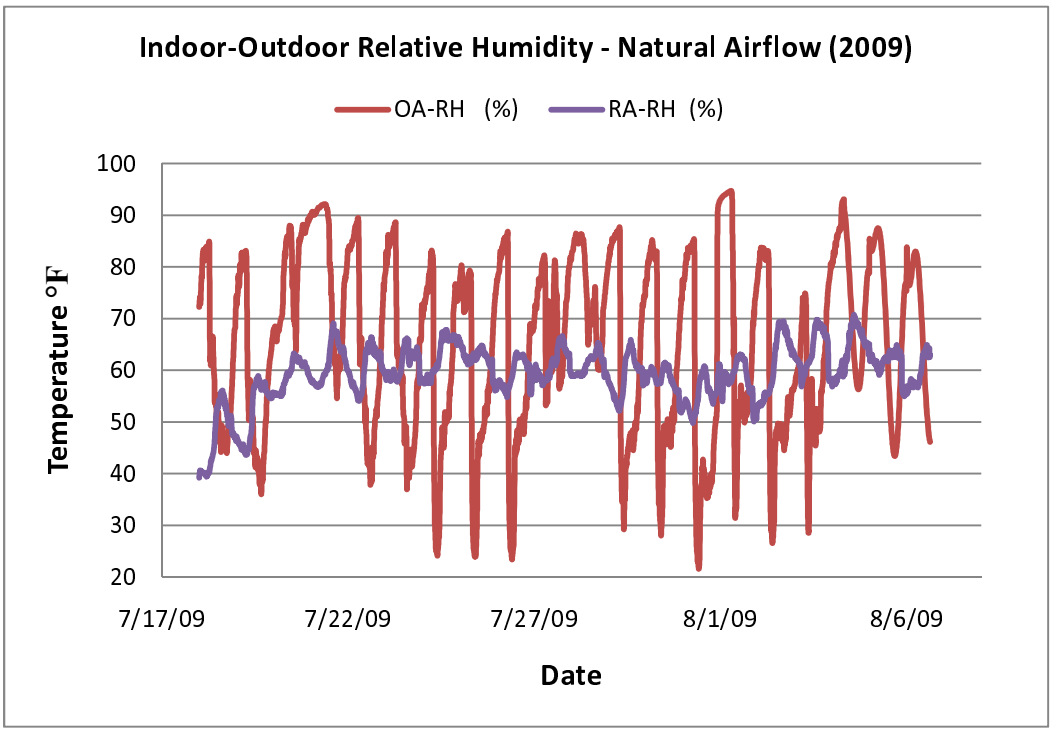

Fig. 5-4 (b) – Indoor-Outdoor Relative Humidity of 2009 Natural Airflow Test

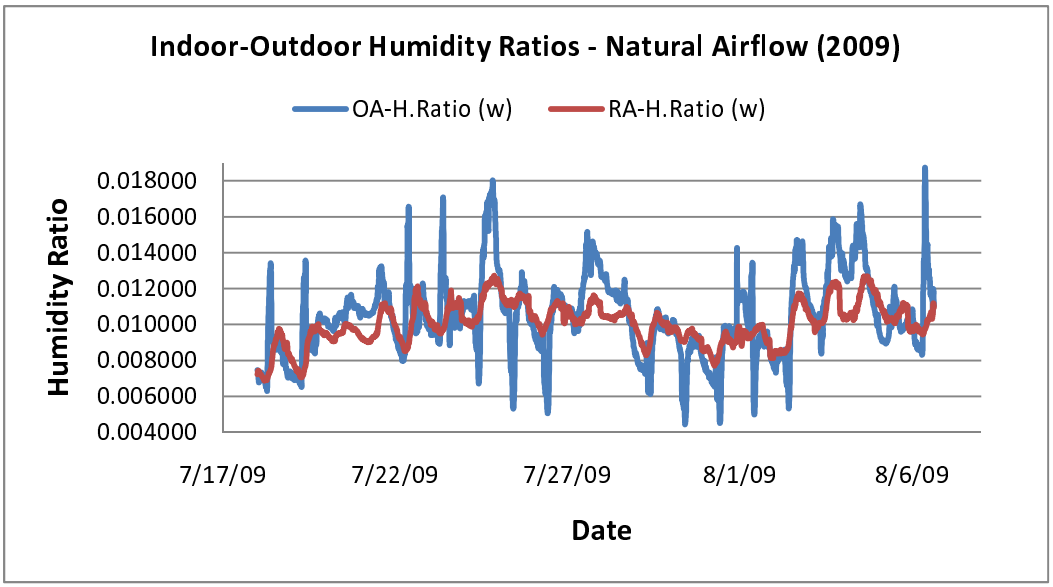

Fig. 5-4 (c) – Indoor-Outdoor Humidity Ratios of 2009 Natural Airflow Test

From Figures 5-4 a, b, and c it is concluded that the coupled system performance has improved during the summer 2009 testing period, which is related to the mild outdoor air conditions during summer 2009 testing period

compared to that of 2008 testing period. Similar to the 2008 testing period the coupled system proved its ability to dampen all the indoor environmental conditions (i.e. temperatures, relative humidity, and humidity ratios) during the natural airflow of summer 2009.

Table 5-3 – Indoor Environmental Conditions for 2009 Natural Airflow Test

Environmental Condition	Max./Min.	Value	Unit	Date	Time
RAT	Max.	75.8	°F	7/24/09	21:00
	Min.	69	°F	8/2/09	10:15
RA-RH%	Max.	70.8	%	8/4/09	14:00
	Min.	39.2	%	7/18/09	00:15
RA Hum. Ratio	Max.	0.012724	N/A	7/24/09	21:00
	Min.	0.006872	N/A	7/18/09	05:00

Furthermore, the indoor thermal environmental conditions statistics of summer 2009 testing period, provided on Table 5-3, show that the coupled system maintained more acceptable conditions than that of 2008. Where, both the indoor air temperature range (69°F – 75.8°F) and humidity ratio maximum value (0.012724) complied with the indoor thermal environmental comfort zone limits recommended by ASHRAE standard 55-2004. Thus, it can be concluded that the coupled system natural airflow mode is able to maintain an acceptable and comfortable indoor thermal environmental conditions.

Figures 5-5 a, b and c, show the indoor and outdoor thermal environmental conditions comparison during the forced airflow test carried out on summer 2009. Moreover, Table 5-4 gives the statistics of the indoor thermal environmental conditions of the forced airflow test.

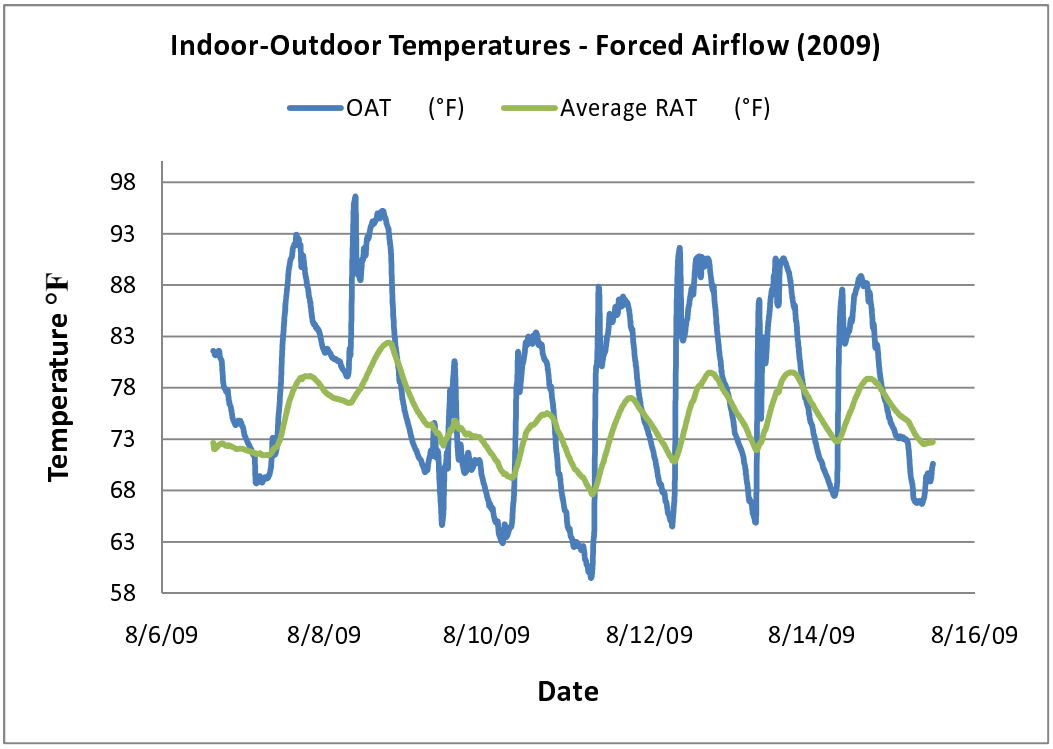

Fig. 5-5 (a) – Indoor-Outdoor Temperatures of 2009 Forced Airflow Test

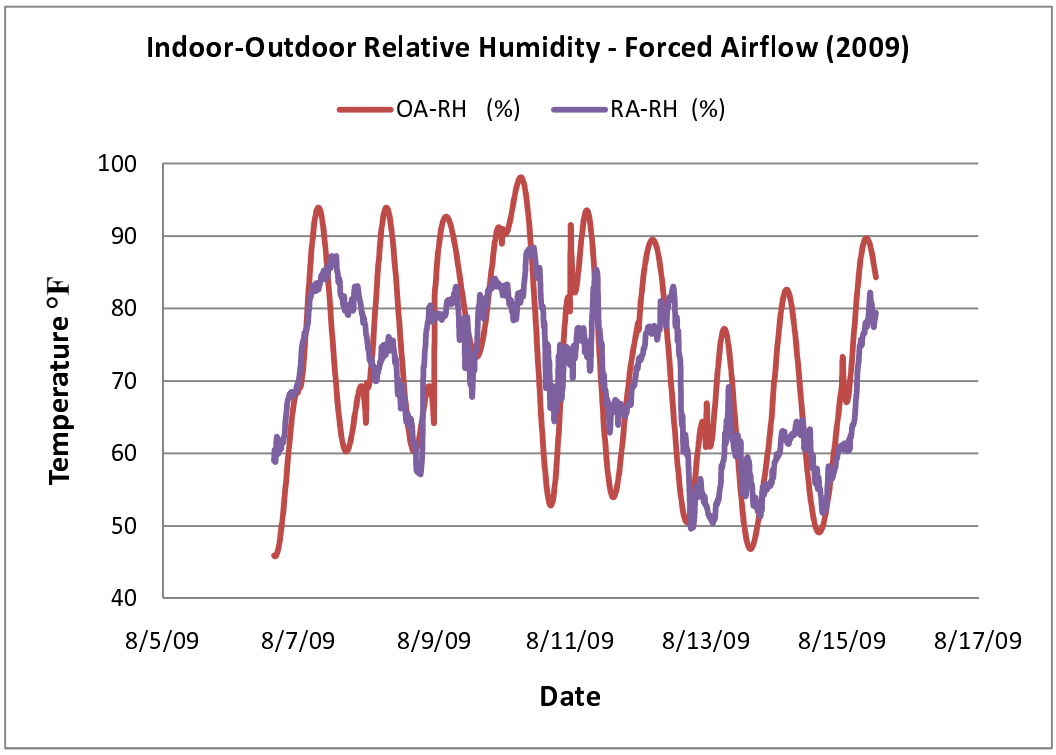

Fig. 5-5 (b) – Indoor-Outdoor Relative Humidity of 2009 Forced Airflow Test

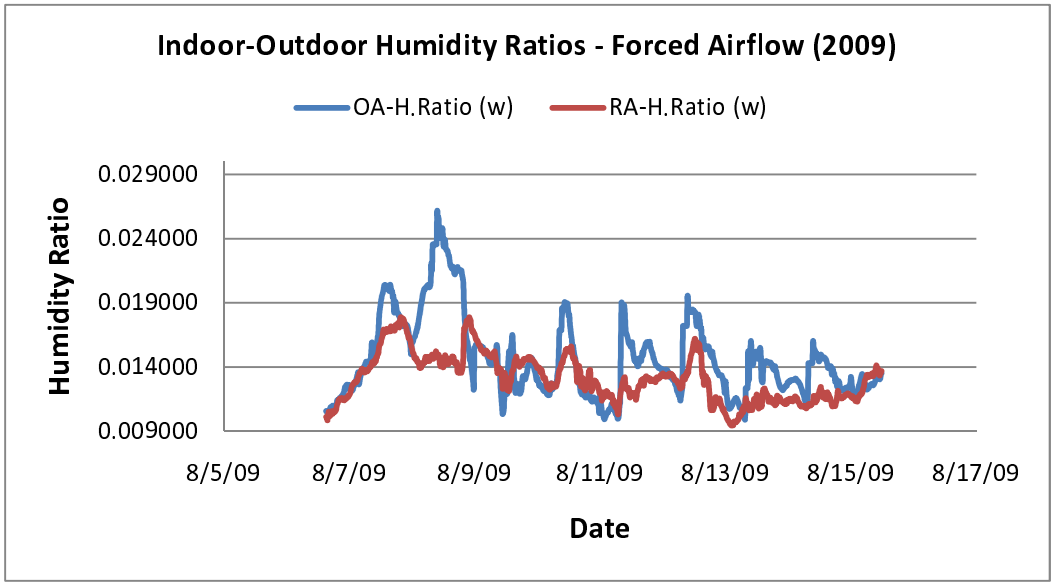

Fig. 5-5 (c) – Indoor-Outdoor Humidity Ratios of 2009 Forced Airflow Test

From Figures 5-5 a, b and c show that the coupled system has damped the indoor thermal environmental conditions during the forced airflow test of summer

2009 but not to the same extent as the natural airflow modes of 2008 and 2009. Through the analysis, it is found that the coupled system ability to dampen the indoor thermal environmental conditions is reduced during the forced airflow test, due to the fact that the amount of airflow extracted by the electric fan is more than the EAHE capacity for cooling and its surrounding underground soil for heat absorption. Consequently, it is concluded that the installed fan is oversized which allows too much air to bypass the EAHE without being cooled. This decreased the coupled system dampening ability/effect and increased the indoor thermal environmental conditions (i.e. temperatures, relative humidity, and humidity ratios) to an unfavorable level.

Table 5-4 – Indoor Environmental Conditions for 2009 Forced Airflow Test

Environmental Condition	Max./Min.	Value	Unit	Date	Time
RAT	Max.	82.4	°F	7/24/09	21:00
	Min.	67.6	°F	8/2/09	10:15
RA-RH%	Max.	88.4	%	8/4/09	14:00
	Min.	49.6	%	7/18/09	00:15
RA Hum. Ratio	Max.	0.017868	N/A	7/24/09	21:00
	Min.	0.009437	N/A	7/18/09	05:00

Moreover, the indoor thermal environmental conditions statistics of summer 2009 forced airflow test, provided on Table 5-4, show that the indoor air temperature was maintained at the range of (67.6°F – 82.4°F) which does not

comply with the thermal comfort zone limits recommended by ASHRAE standard 55-2004. It should be mentioned that the indoor air temperature dropped down to a level lower than the lower temperature limit of ASHRAE's comfort zone during few days of test, while it was maintained at the edge of the comfort zone upper limit during most of the days.

It also show that the relative humidity was higher than 70% most of the test time and that the humidity ratio exceeded the upper humidity ratio limit, recommended by ASHRAE, during most of 2009 forced airflow testing period. Accordingly, it is concluded that the coupled system forced airflow mode could not comply with ASHRAE standard 55-2004 recommendations for the indoor thermal environmental comfort conditions due to the oversized installed fan.

5.3.2 Cooling Capacity Calculation Method

According to (McQuiston, et al., 2004) there are two heat transfer modes involved in the cooling process: the sensible heat transfer mode, which is involved exclusively in reducing or maintaining the temperature of the air; and the latent heat transfer mode, which involves moisture removal from the air stream during the cooling process. Consequently, the total cooling capacity is divided into two portions: the sensible cooling capacity and the latent cooling capacity, this is represented mathematically as follows:

$$\dot{Q}_{total,cooling} = \dot{Q}_{s,cooling} + \dot{Q}_{l,cooling} \qquad (5.1)$$

Where:

$\dot{Q}_{total,cooling}$ = the rate of total cooling heat transfer, Btu/hr (W)

$\dot{Q}_{s,cooling} =$ the rate of sensible cooling heat transfer, Btu/hr (W)

$\dot{Q}_{l,cooling} =$ the rate of latent cooling heat transfer, Btu/hr (W)

The total cooling capacity of any system or subsystem (e.g. heat exchanger) that utilizes air as the heat transfer medium can be formulated as shown in equation (5.2):

$$\dot{Q}_{total,cooling} = \dot{m}_{air} \Delta h \qquad (5.2)$$

Where:

$\dot{m}_{air} =$ the mass flow rate of air flow, lbm/hr (kg/s)

$\Delta h =$ the difference between the system entering and exiting air enthalpies, Btu/lbm (kJ/kg)

As the mass flow rate of air can be formulated as follows:

$$\dot{m}_{air} = \frac{Q_{air}}{v_{air}} \qquad (5.3)$$

Where:

$Q_{air} =$ the volume flow rate of air flow, ft^3/hr (m^3/s)

$v_{air} =$ the specific volume of air, ft^3/lbm (m^3/kg)

And the specific volume of air can be formulated as the reciprocal of the specific density of air as shown in equation (5.4):

$$v_{air} = \frac{1}{\rho_{air}} \qquad (5.4)$$

Where:

$\rho_{air} =$ the specific density of air, lbm/ft^3 (kg/m^3)

Then, by substituting the specific volume of air in equation (5.3) by using equation (5.4), it can be simplified to be written as follows:

$$\dot{m}_{air} = 60\ \rho_{air}\ CFM \qquad (5.5)$$

Where:

60 = the constant for converting the volume flow rate of air flow from ft^3/min (CFM) to ft^3/hr

CFM = the volume flow rate of air flow, ft^3/min (CFM)

Accordingly, by substituting the mass flow rate of air in equation (5.2) by using equation (5.5), it can be formulated as follows:

$$\dot{Q}_{total,cooling} = 60\ \rho_{air}\ CFM\ \Delta h \qquad (5.6)$$

The sensible cooling capacity of any system or subsystem (e.g. heat exchanger) that utilizes air as the heat transfer medium is formulated as follows:

$$\dot{Q}_{s,cooling} = \dot{m}_{air} C_{P_{air}} \Delta T \qquad (5.7)$$

Where:

$\dot{Q}_{s,cooling}$ = the rate of sensible cooling heat transfer, Btu/hr (W)

$C_{P_{air}}$ = the constant-pressure specific heat of air, Btu/(lbm-°F) [J/(kg-K)]

ΔT = the difference between the system entering and exiting temperatures,°F (K)

In the same manner as the total cooling capacity, the mass flow rate of air of the sensible cooling capacity in equation (5.7) is substituted by using equation (5.5), to be formulated as follows:

$$\dot{Q}_{s,cooling} = 60\ \rho_{air}\ CFM\ C_{P_{air}} \Delta T \qquad (5.8)$$

On the other hand, the latent cooling capacity of any system or subsystem (e.g. heat exchanger) that utilizes air as the heat transfer medium is formulated as shown in equation (5.9).

$$\dot{Q}_{l,cooling} = h_{fg}\dot{m}_w \qquad (5.9)$$

Where:

$\dot{Q}_{l,cooling} =$ the rate of latent cooling heat transfer, Btu/hr (W)

$h_{fg} =$ the enthalpy of vaporization, Btu/lbm (J/kg)

$\dot{m}_w =$ the mass flow rate of water condensation/vaporization, lbm/hr (kg/s)

As the mass flow rate of water condensation/vaporization (i.e. moisture removal/addition) can be formulated as follows:

$$\dot{m}_w = \dot{m}_{air}\,\Delta\omega \qquad (5.10)$$

Where:

$\Delta\omega =$ the difference between the system entering and exiting air humidity ratios

By using equation (5.5) to substitute the mass flow rate of air flow in equation (5.10), the mass flow rate of water condensation/vaporization can be formulated as follows:

$$\dot{m}_w = 60\,\rho_{air}\,CFM\,\Delta\omega \qquad (5.11)$$

Accordingly, the mass flow rate of water condensation/vaporization in equation (5.9) is substituted by equation (5.11), to be formulated as follows:

$$\dot{Q}_{l,cooling} = 60\,\rho_{air}\,h_{fg}\,CFM\,\Delta\omega \qquad (5.12)$$

In order to determine the total, sensible and latent cooling capacities that the coupled system can provide for the testing facility building as well as the

EAHE cooling capacity, equations (5.6), (5.8), and (5.12) are applied to the different system components. Consequently, the coupled system and EAHE, total, sensible, and latent cooling capacities are formulated as follows:

a. The coupled system total cooling capacity is formulated as:

$$\dot{Q}_{system,t} = 60\ \rho_{air}\ CFM_{EAHE}\ (h_{RA} - h_{SA}) \qquad (5.13)$$

Where:

$CFM_{EAHE} =$ the EAHE supply air mass flow rate, ft^3/min

$h_{RA} =$ the room air enthalpy, Btu/lbm

$h_{SA} =$ the supply air enthalpy, Btu/lbm

b. The coupled system sensible cooling capacity is formulated as:

$$\dot{Q}_{system,s} = 60\ \rho_{air}\ CFM_{EAHE}\ C_{P_{air}}(T_{RAT} - T_{SAT}) \qquad (5.14)$$

Where:

$T_{RAT} =$ the average room air temperature, °F

$T_{SAT} =$ the EAHE supply air temperature, °F

c. The coupled system latent cooling capacity is formulated as:

$$\dot{Q}_{system,l} = 60\ \rho_{air}\ h_{fg}\ CFM_{EAHE}\ (\omega_{RA-HR} - \omega_{SA-HR}) \qquad (5.15)$$

Where:

$\omega_{RA-HR} =$ the room air humidity ratio

$\omega_{SA-HR} =$ the EAHE supply air humidity ratio

d. The EAHE total cooling capacity is formulated as:

$$\dot{Q}_{EAHE,t} = 60\ \rho_{air}\ CFM_{EAHE}\ (h_{OA} - h_{SA}) \qquad (5.16)$$

Where:

$h_{OA} =$ the outdoor air enthalpy, Btu/lbm

e. The EAHE sensible cooling capacity is formulated as:

$$\dot{Q}_{EAHE,s} = 60\, \rho_{air}\, CFM_{EAHE}\, C_{P_{air}}(T_{OAT} - T_{SAT}) \qquad (5.17)$$

Where:

$T_{OAT} =$ the outdoor air temperature, °F

f. The EAHE latent cooling capacity is formulated as:

$$\dot{Q}_{EAHE,l} = 60\, \rho_{air}\, h_{fg}\, CFM_{EAHE}\, (\omega_{OA-HR} - \omega_{SA-HR}) \qquad (5.18)$$

Where:

$\omega_{OA-HR} =$ the outdoor air humidity ratio

By applying the above 6 formulas, from equation (5.13) to equation (5.18), on the measured data of the 2008 and 2009 testing periods, the different cooling capacities of the coupled system and EAHE are calculated for both the natural and forced air flow modes. Furthermore, the calculated cooling capacities are plotted as time series with other measured data (e.g. room/indoor air temperature, underground soil temperature, etc.) to study the mutual effect the cooling capacities and the measured data (i.e. environmental conditions on one another. These plots are presented in the following sections to further understand the thermal performance of the coupled system as well as the EAHE.

Table 5-5 – The Atmospheric Air Condition Constants

Contents	Unit	Value
Air Enthalpy of Vaporization, h_{fg}	Btu/lbm	1061.2
Constant-pressure specific heat of air, $C_{P\,air}$	Btu/(lbm-°F)	0.24
Specific density of air, ρ_{air}	lbm/ft^3	0.0764

It should be mentioned that for the cooling capacities calculations the Engineering Equation Solver (EES) has been used to calculate the indoor, outdoor, and supply humidity ratios and enthalpies. Moreover, Excel spread sheets are used to calculate and plot the different cooling capacities. Table 5-5 shows the values of the constants that have been used during the calculations.

5.3.3 Thermal Performance Analysis of the Coupled System and EAHE

To evaluate the thermal performance of the coupled system, the test facility building design cooling load is calculated first to provide a baseline for the coupled system cooling capacities thermal analysis. Accordingly, the load calculation software program, TRACE 700, is used to obtain the design cooling load of the test facility building.

The design cooling load calculations started by determining the R-values of the test facility building envelope (i.e. walls, roof, and slab) as well as the U-values of the windows and the static pressure loss through the EAHE. Thereafter, the design indoor, outdoor, and supply air conditions are selected as well as the infiltration rate and the shading coefficient. Afterwards, a building load simulation is conducted using TRACE 700 software. A variable air volume

(VAV) system is chosen as the design system for the test facility building, working in a similar way to the coupled system. The similarities between the coupled system and the VAV system are: in the coupled system the amount of airflow rate changes with the change of the solar radiation (which is an indication for the building cooling load). Likewise, in the VAV system the amount of airflow rate changes with the building cooling load. Moreover, in the coupled system the supply air temperature is almost constant due to the steady underground soil temperature which acts as the cooling coil of the VAV system, providing a constant supply air temperature of 55°F.

Consequently, the design cooling load and airflow rate values are determined and recorded. Moreover, a fan is sized based on the calculated airflow rate and the total pressure losses of the air path (i.e. EAHE). Table 5-6 show the main design calculated values to be compared with the actual coupled system cooling capacities.

It should be mentioned that the test facility building is a one story building and the test room dimensions are 49.875ft (15.2m) length, 14.83ft (4.52m) width, and 7.75ft (2.36m) height with a floor area of 740ft^2 (68.75m^2). It should also be pointed out that it is an unoccupied space with no internal loads. Moreover, all the windows were covered with R-5 Styrofoam insulation during the 2008 and 2009 testing periods to minimize the solar gain. This explains why the calculated design cooling load and airflow rate are relatively small compared to the floor area. Furthermore, very few reasonable assumptions where made where the values were not provided or unknown (e.g. some of the roof construction materials).

Lastly, Appendix C includes a table of all the selected and calculated design values, in addition to, the detailed design cooling load calculation report created by TRACE 700 software.

Table 5-6 – Main Design Calculated Values

Design Component	Calculated Value	Unit
Total Cooling Load	0.8	Tons
Sensible Cooling Load	0.47	Tons
Latent Cooling Load	0.32	Tons
Fan size	225	CFM
	0.0414	in.H_2O

After estimating the baseline design cooling load, the thermal performance analysis of the EAHE and coupled system is evaluated through plotting their cooling capacities (i.e. total, sensible, and latent) during both the natural airflow mode (2008 testing period) and the forced airflow mode (2009 testing period) on Excel sheets, to be able to visualize the thermal performance of the system over time. Thereafter, discussions on the coupled system cooling capacities during the 2008 and 2009 tests and the test facility building design cooling load is provided.

Furthermore, comparisons between the coupled system and EAHE cooling capacities are conducted. Moreover, the analyses on the effect of the outdoor air temperature (OAT) on the sensible cooling capacity, the outdoor air relative humidity on the latent cooling capacity, and the airflow rate on the total cooling

capacity during the natural and forced airflow tests are presented. Consequently, conclusions are drawn after each analysis section.

It should be mentioned that the thermal performance of the coupled system and EAHE during the natural airflow modes of the 2008 and 2009 testing periods showed similar results, accordingly, only the results of the 2008 testing period are presented in the following section beside the results of the forced airflow mode test of the 2009 testing period.

5.3.3.1 Thermal Performance Analysis of 2008 Natural Airflow Test

Figures 5-6 a, b, and c show the total, sensible, and latent cooling capacities of the EAHE during the natural airflow test of 2008 with time, respectively.

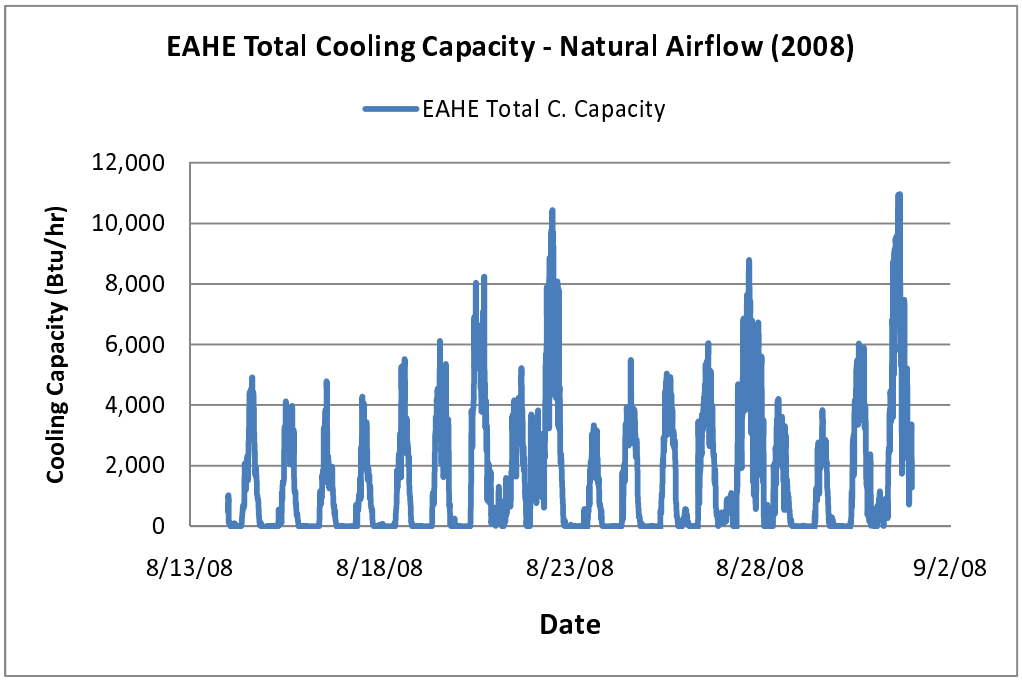

Fig. 5-6 (a) – EAHE Total Cooling Capacity (2008 Natural Airflow Test)

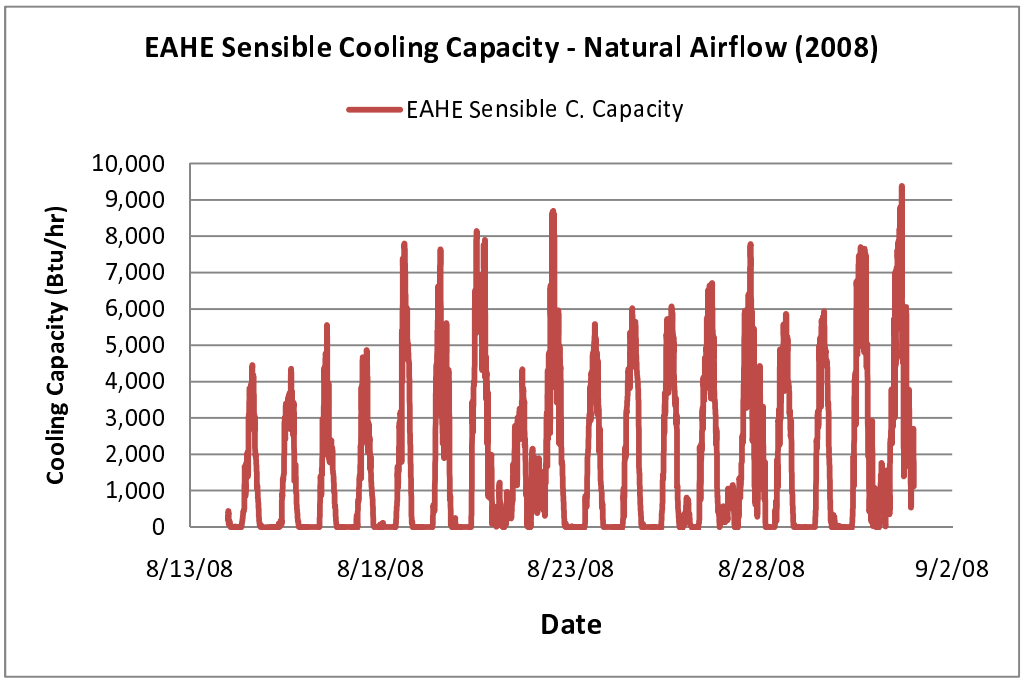

Fig. 5-6 (b) – EAHE Sensible Cooling Capacity (2008 Natural Airflow Test)

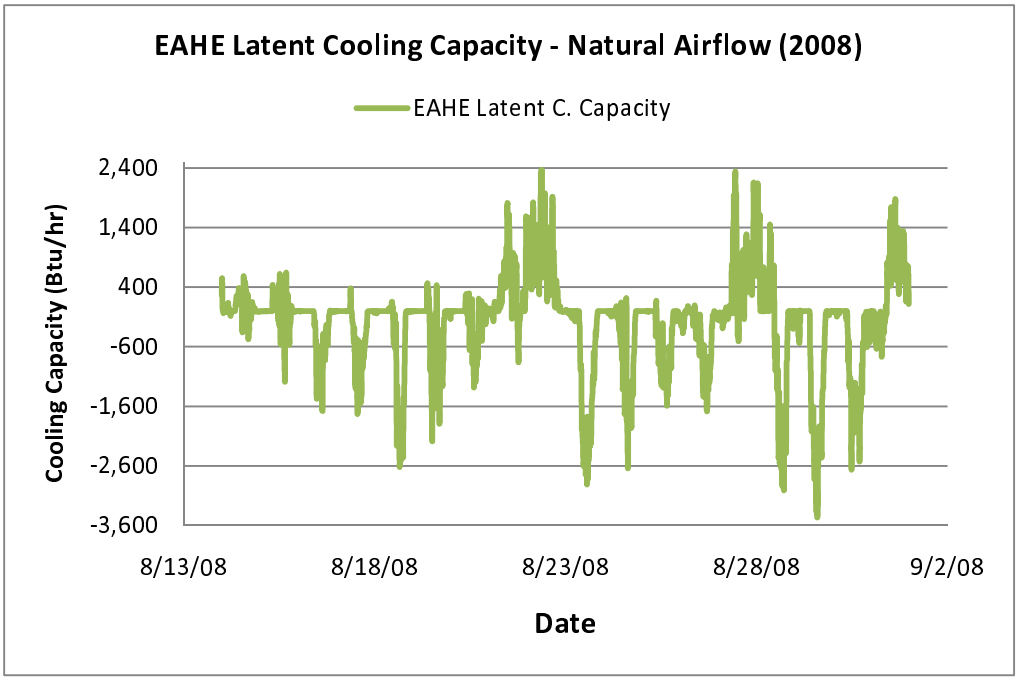

Fig. 5-6 (c) – EAHE Latent Cooling Capacity (2008 Natural Airflow Test)

Figure 5-6 a show that the EAHE reached a maximum cooling Capacity of about 10,950 Btu/hr (0.91 tons of cooling per hour), and a maximum sensible cooling capacity of about 9,270 Btu/hr (0.77 tons of cooling per hour). It is clear from both figures that the cooling capacities reach their maximum peak during the day time due to the increase in the solar radiation intensity.

Moreover, Figure 5-6 c, shows that the EAHE latent cooling capacity usually have negative values during the night time. This is explained as follows: since the solar radiation drops to zero when the sun goes down, the airflow rate through the EAHE drops to zero as well because the solar collector cannot collect any solar radiation during the night time. Accordingly, the supply relative humidity sensor reads the indoor/room air relative humidity instead of the actual supply air relative humidity. On the other hand, the outdoor air temperature and humidity ratio decreases during the night time. Thus, the difference between the outdoor air humidity ratio and the supply air humidity ratio (which in this case is the indoor humidity ratio reading) become negative and produce inaccurate negative values for the EAHE latent cooling capacity.

It is also clear from Figure 5-6 c, that the value of the EAHE latent cooling capacity was positive during the nights when the outdoor air conditions were stormy and windy. This phenomenon is due to the outside air wind producing a draft through the EAHE. This draft was humid because of the stormy outdoor air conditions, and consequently, condensation occurred inside the EAHE while this draft was migrating through it. This led to a reduction on the

supply air relative humidity ratio. On the other hand, the outdoor humidity ratio was relatively high due to the outdoor air stormy conditions. Accordingly, the difference between the outdoor and supply air humidity ratios was positive during those nights. This also proves the aforementioned explanation of the negative EAHE latent cooling capacities values during the night time.

Figures 5-7 a, b, and c show the total, sensible, and latent cooling capacities of the coupled system during the natural airflow test of 2008.

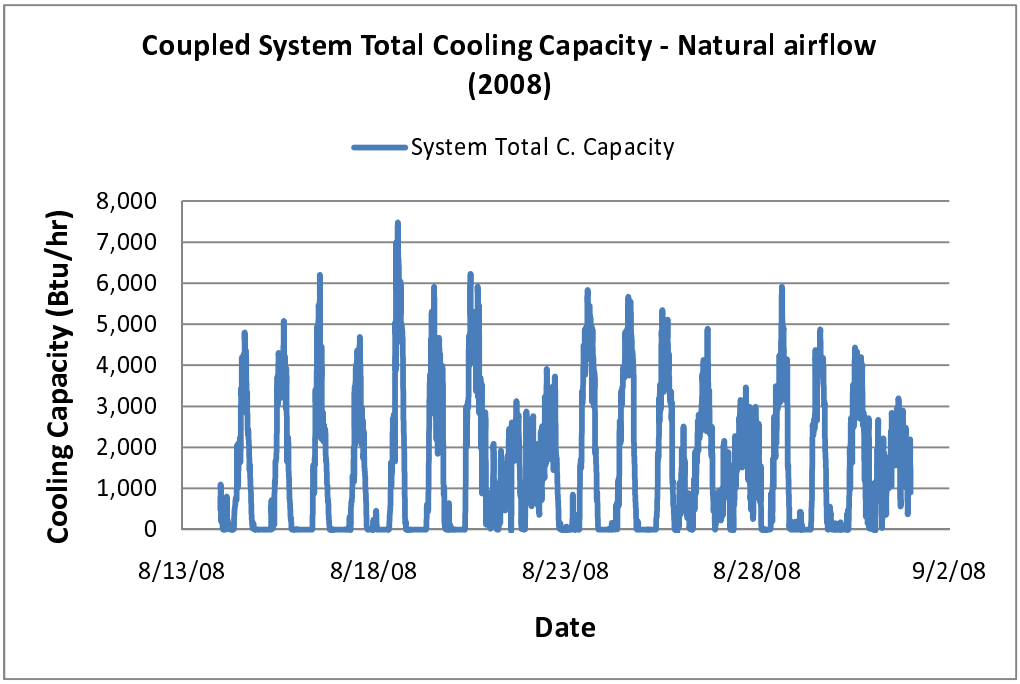

Fig. 5-7 (a) – Coupled System Total Cooling Capacity

(2008 Natural Airflow Test)

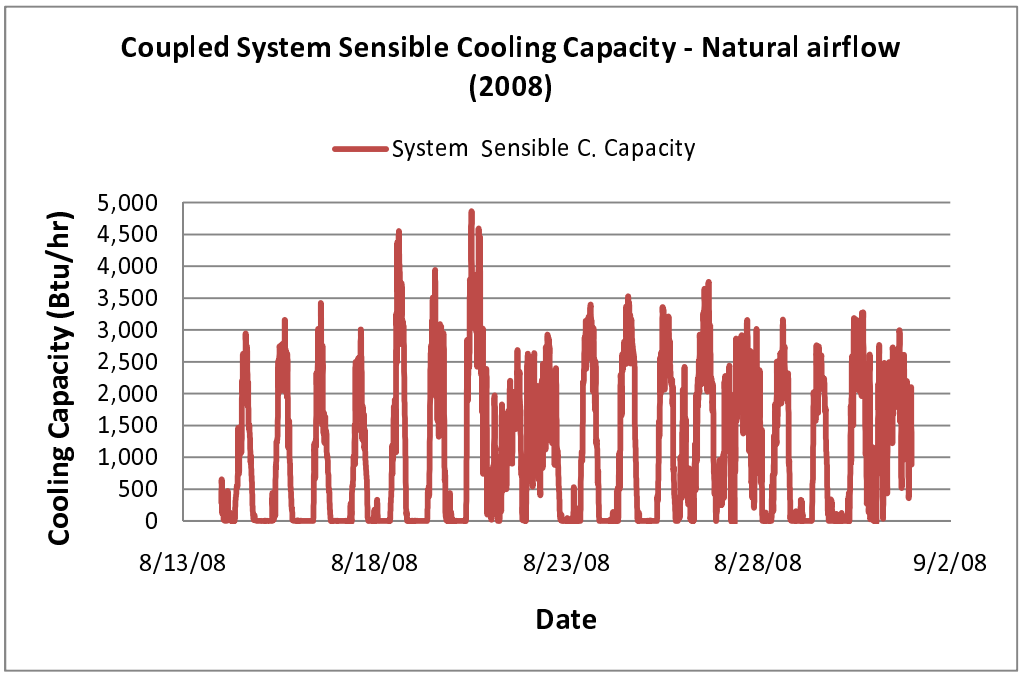

Fig. 5-7 (b) – Coupled System Sensible Cooling Capacity

(2008 Natural Airflow Test)

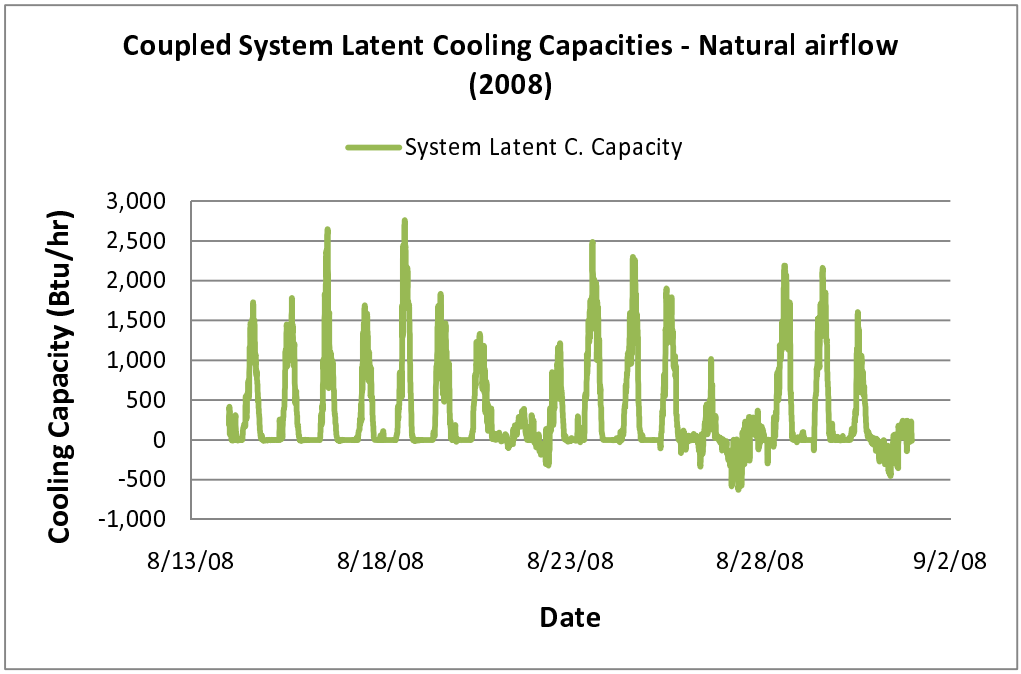

Fig. 5-7 (c) – Coupled System Latent Cooling Capacity

(2008 Natural Airflow Test)

From Figure 5-7 a and b it is clear that the coupled system reached a maximum total cooling capacity of about 7,450 Btu.hr (0.63 tons of cooling per hour), in the mean time it reached a maximum sensible cooling capacity of about 4,860 Btu/hr (0.41 tons of cooling per hour). Comparing these values with the design cooling load, it can be concluded that the coupled system almost satisfied the test facility building design cooling load which is an extreme condition that happens rarely. This implies the feasibility of the coupled system performance during the natural airflow mode and its ability to provide almost the same amount of cooling as the VAV system under the same operational conditions.

Figure 5-7 c shows that the latent cooling capacity has some negative values during a few nights of the 2008 natural airflow test. It is found that during these few nights the outdoor environmental conditions were stormy and windy. This leads to an increase in the outdoor air humidity ratio. Consequently, the difference between the outdoor air and supply humidity ratios is very small during the days while it is negative during the night time. This is explained as follows: since the solar radiation drops to zero when the sun goes down, the airflow rate through the EAHE drops to zero as well because the solar collector cannot collect any solar radiation during the night time. Accordingly, the supply relative humidity sensor reads the indoor/room air relative humidity instead of the actual supply air relative humidity.

From Figures 5-7 a, b, and c it is clear that the outdoor environmental conditions impacts the performance of the coupled system. Furthermore, when

the solar radiation increases the coupled system cooling capacity increases. This proves the natural controllability of the coupled system.

Moreover, Figure 5-8 show a comparison between the EAHE and coupled system total cooling capacities during the same test.

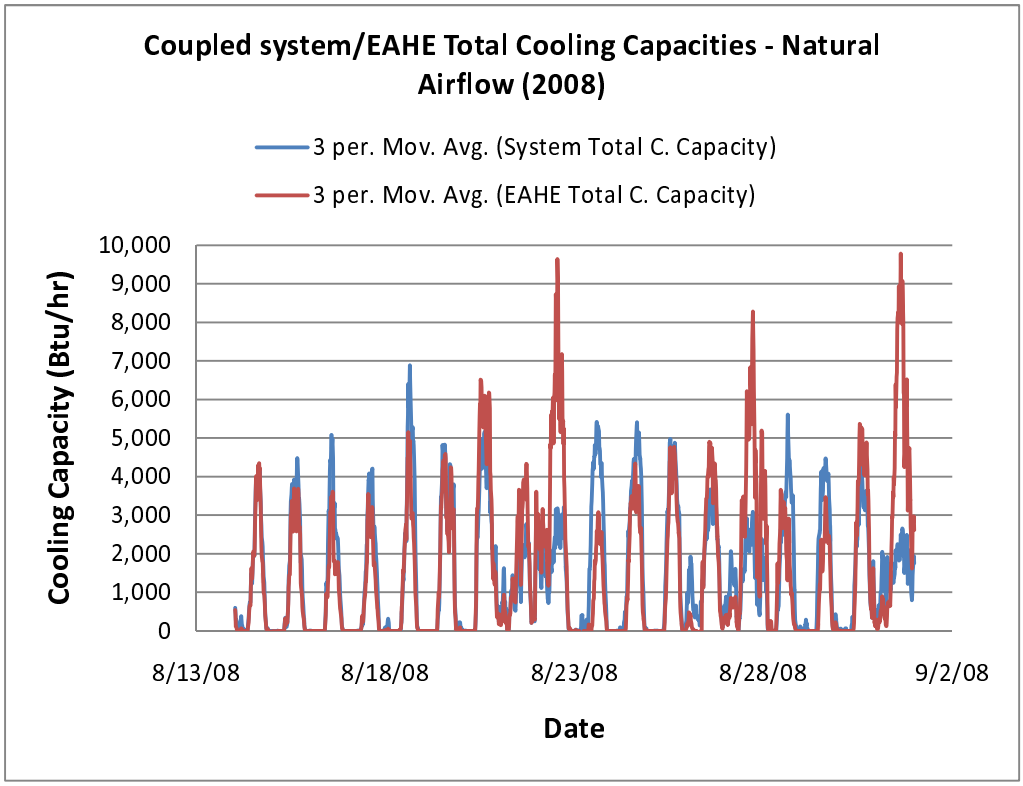

Fig. 5-8 – EAHE - Coupled System Total Cooling Capacity Comparison (2008 Natural Airflow Test)

Figures 5-9 show the effect of the supply airflow rate on the coupled system total cooling capacity. It is obvious that the total cooling capacity follows the same pattern as the supply natural airflow rate. Accordingly, it is concluded that as the natural airflow draft increases the cooling capacity increases, which agrees with the common sense.

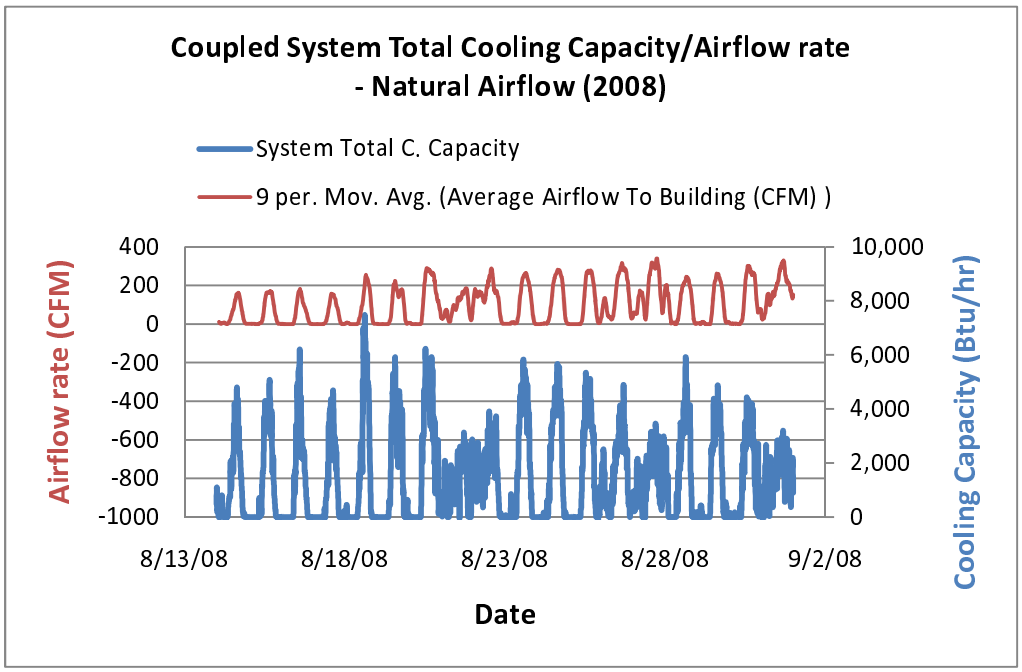

Fig. 5-9 – Coupled System Total Cooling Capacity – Natural Airflow Rate Comparison (2008 Natural Airflow Test)

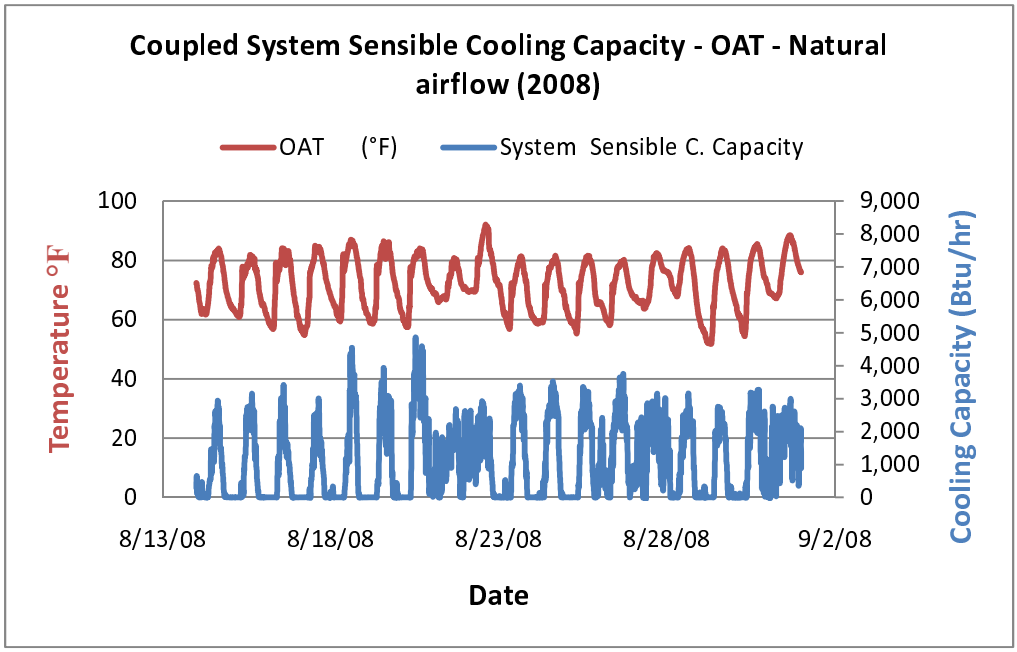

Fig. 5-10 – Coupled System Sensible Cooling Capacity – Outdoor Air Temperature Comparison (2008 Natural Airflow Test)

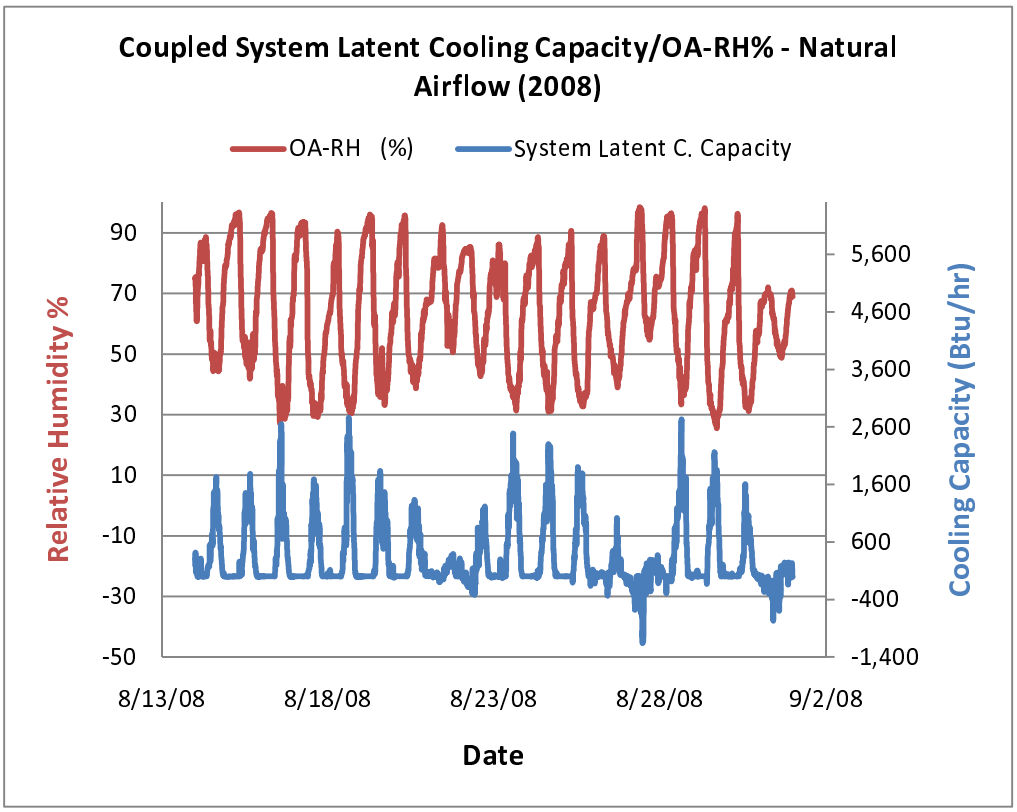

Fig. 5-11 – Coupled System Latent Cooling Capacity – Outdoor Air Relative Humidity Comparison (2008 Natural Airflow Test)

It is apparent from Figure 5-10 that the sensible cooling capacity follows the same pattern as the outdoor air temperature. In other words, as the outdoor air temperature increases the system sensible cooling capacity increases and vice versa. This proves the efficiency of the coupled system as it has a sort of natural control system as the cooling capacity increases when it is required (i.e. when the outdoor air temperature increases). On the other hand, Figure 5-11 show that the latent cooling capacity follows a reverse pattern of the outdoor air relative humidity. In other words, as the relative humidity decrease the latent cooling capacity increase and vice versa.

5.3.3.2 Thermal Performance Analysis of 2009 Forced Airflow Test

Figures 5-12 a, b, and c show the total, sensible, and latent cooling capacities of the EAHE during the forced airflow test of 2009 with time, respectively. In addition, Figures 5-13 a, b, and c show the total, sensible, and latent cooling capacities of the coupled system during the forced airflow test of 2009 as well. Moreover, Figure 5-14 show a comparison between the EAHE and coupled system total cooling capacities during the same test.

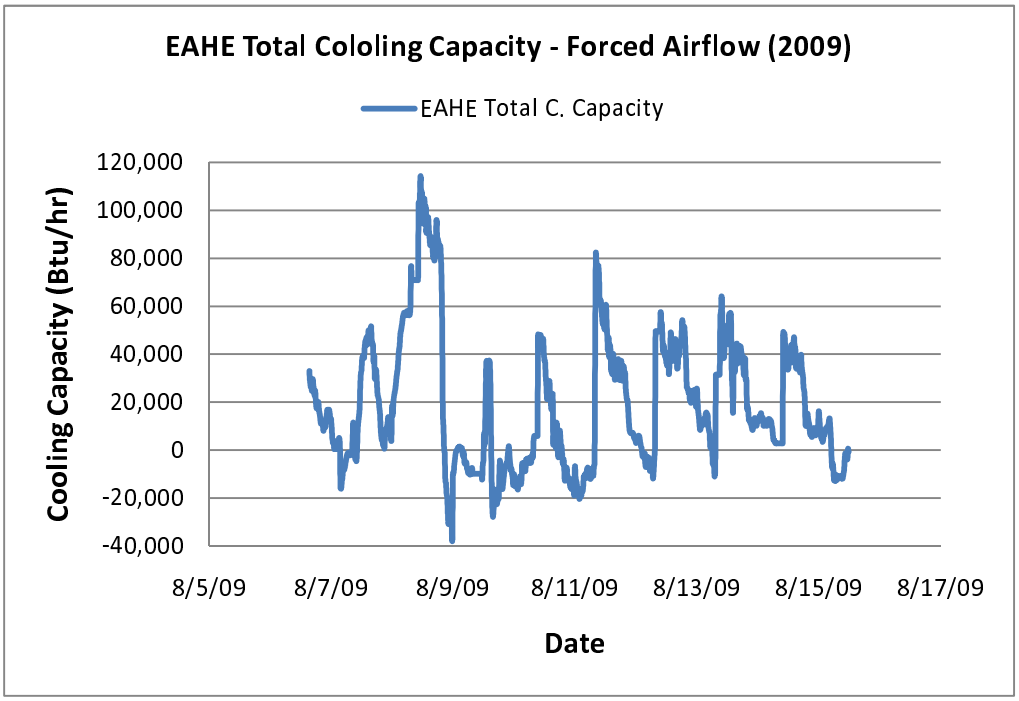

Fig. 5-12 (a) – EAHE Total Cooling Capacity (2009 Forced Airflow Test)

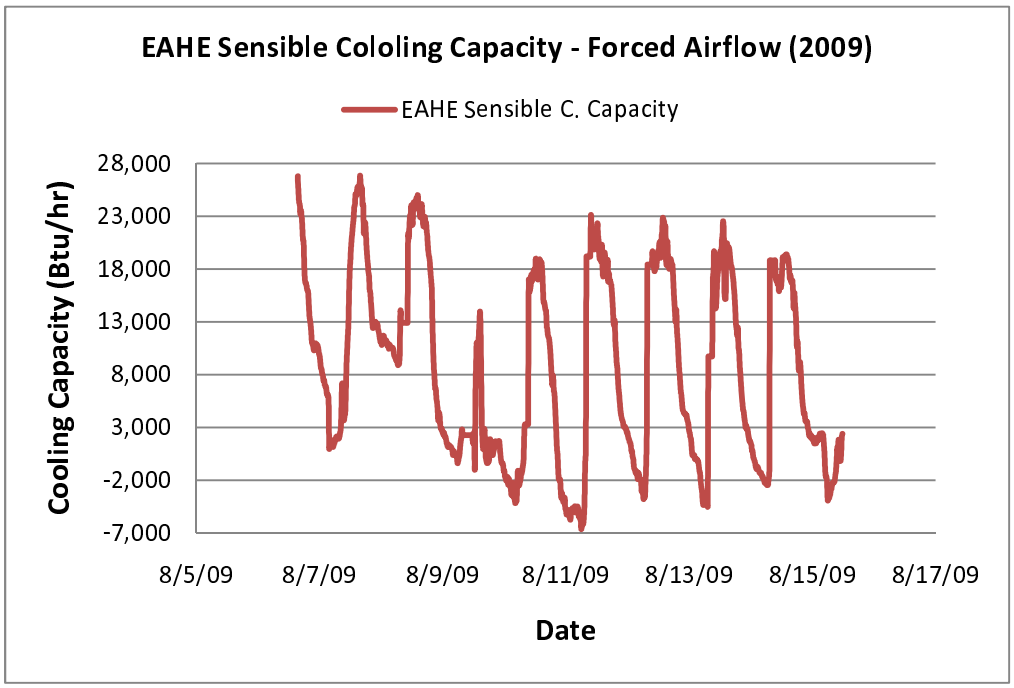

Fig. 5-12 (b) – EAHE Sensible Cooling Capacity

(2009 Forced Airflow Test)

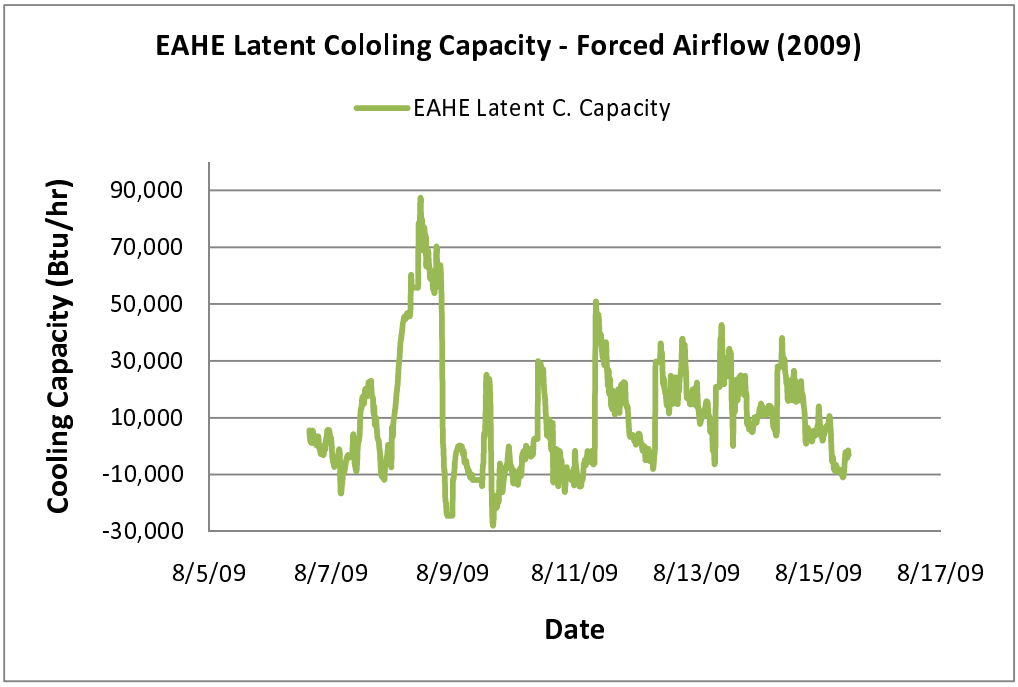

Fig. 5-12 (c) – EAHE Latent Cooling Capacity

(2009 Forced Airflow Test)

Figure 5-12 a show that the EAHE reached a maximum cooling Capacity of about 114,421 Btu/hr (9.54 tons of cooling per hour), and a maximum sensible cooling capacity of about 26,846 Btu/hr (2.24 tons of cooling per hour). Moreover, Figure 5-12 c, shows that the EAHE average latent cooling capacity is about 10,150 Btu/hr (0.85 tons per hour). It is clear from all the figures that all the capacities have negative values during the night time. This phenomenon is explained as follows: As the sun goes down the solar collector does not collect solar radiation and the solar chimney natural draft that exhausts the hot air inside the building decreases. In the same time, as explained earlier the oversized fan extracts a huge amount of ambient air that bypasses the EAHE without enough time to cool down. Accordingly, all the supply air conditions increases during the night time which leads to negative values in all the forms of cooling capacities. This can be clearly seen on Figures 5-5 a, b, and c where there is a shit between the indoor and outdoor air conditions peaks.

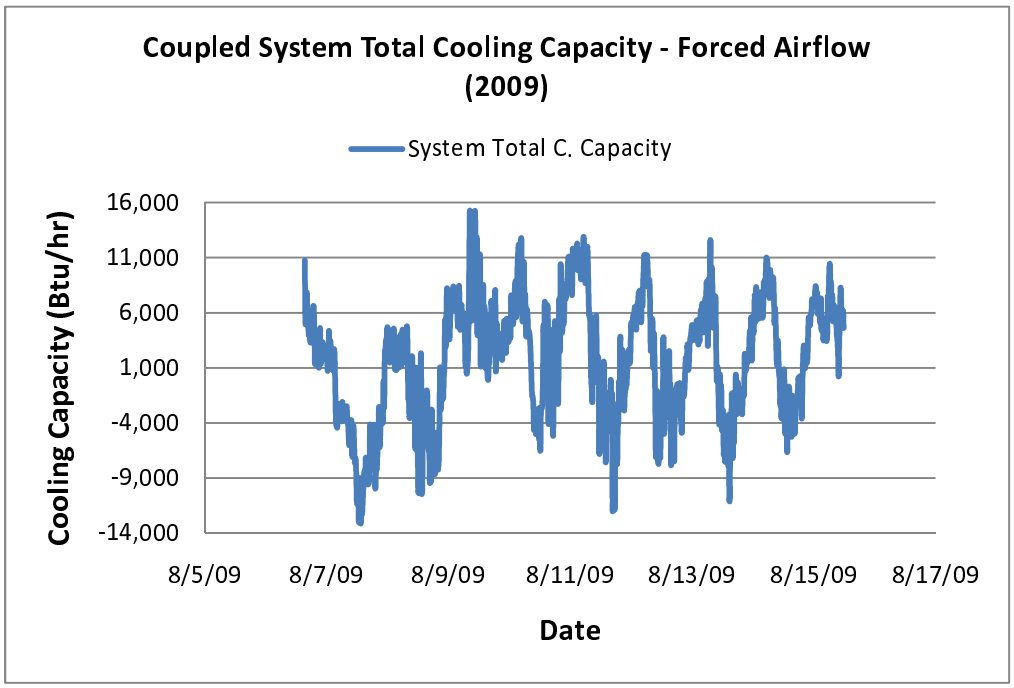

Fig. 5-13 (a) – Coupled System Total Cooling Capacity

(2009 Forced Airflow Test)

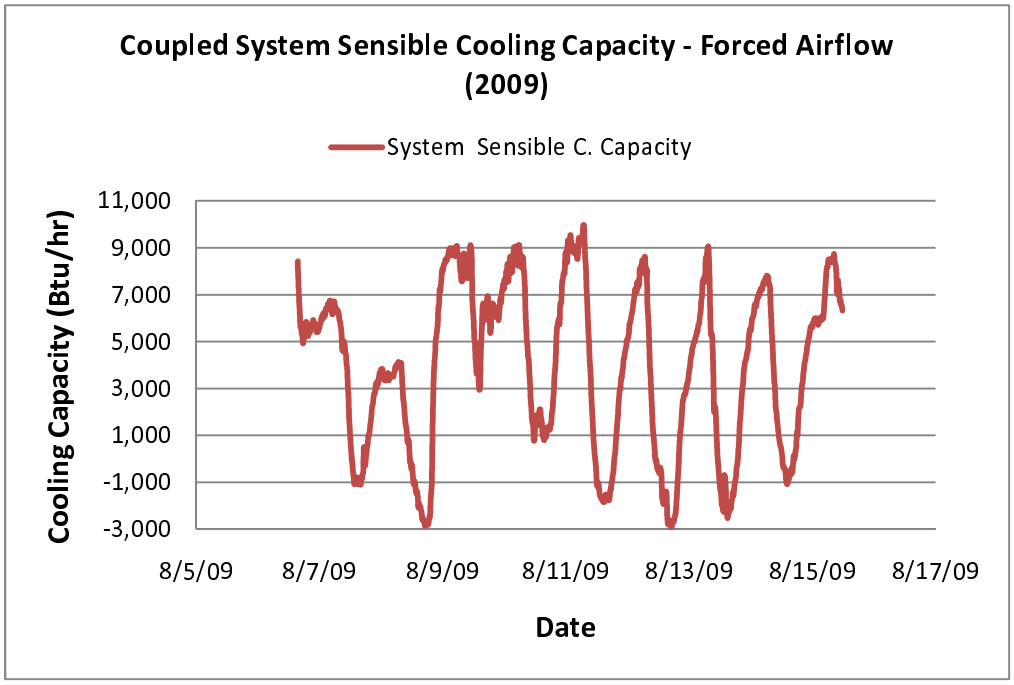

Fig. 5-13(b) – Coupled System Sensible Cooling Capacity

(2009 Forced Airflow Test)

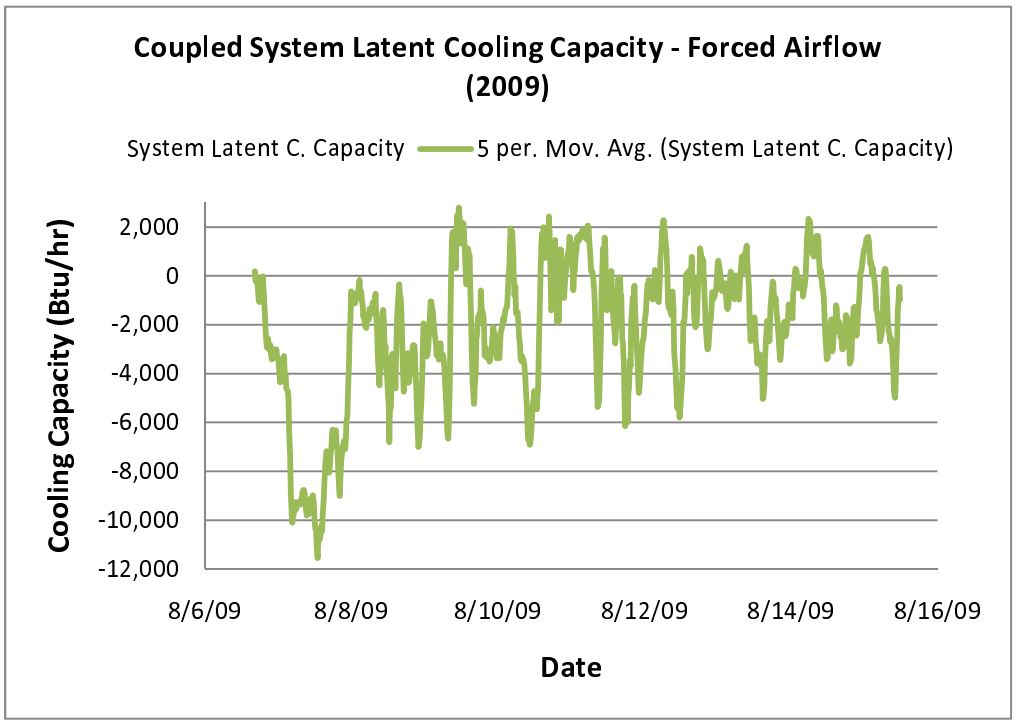

Fig. 5-13 (c) – Coupled System Latent Cooling Capacity

(2009 Forced Airflow Test)

From Figure 5-13 a, b and c it is clear that the coupled system reached a maximum total cooling capacity of about 15,275 Btu.hr (1.27 tons of cooling per hour), maximum sensible cooling capacity of about 9,965 Btu/hr (0.83 tons of cooling per hour) and maximum latent cooling of about 6,330 Btu/hr (0.53 tons of cooling per hour). It is also apparent that all the cooling capacities have negative values during the night time. Again this phenomenon happened because the natural chimney draft that exhausts the hot humid air out of the building does not work during the night time. Accordingly, all the hot air that bypassed the EAHE without being cooled down is trapped inside the building which increases all the indoor environmental conditions

extensively. This leads to a warm up of the building during the night time, consequently negative cooling occurs.

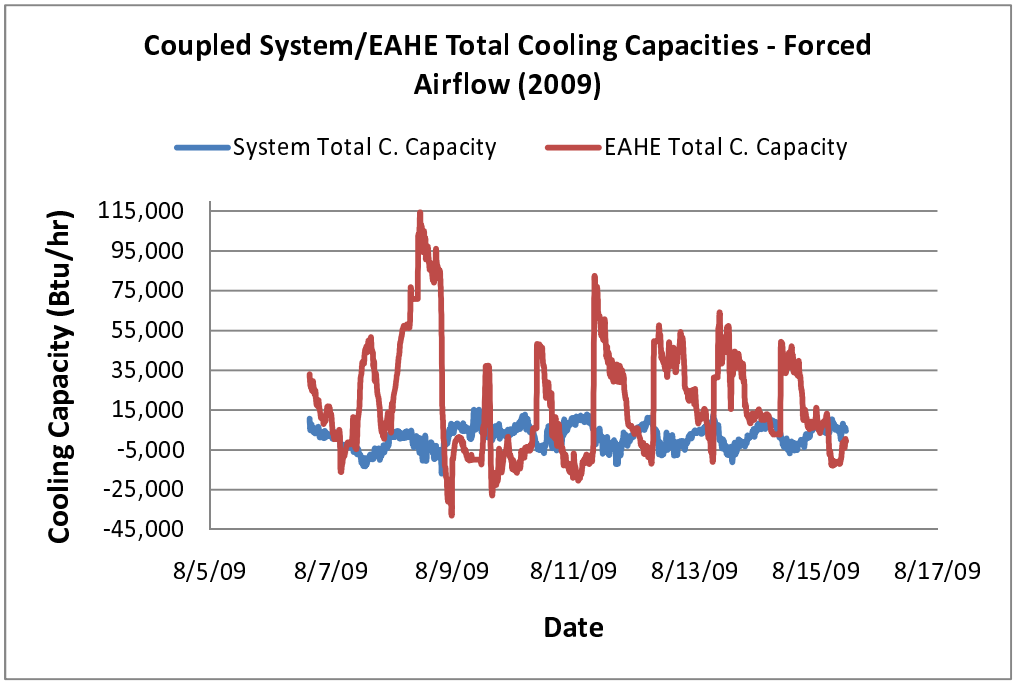

Fig. 5-14 – EAHE - Coupled System Total Cooling Capacity Comparison (2009 Forced Airflow Test)

It is clear from Figure 5-14 that the EAHE cooling capacity is much higher than that of the coupled system during the day time while the system cooling capacity is higher than that of the EAHE during the night time. This implies that EAHE performance during the day time is much better than the night time because of the effect of the solar chimney and collector natural air draft.

Figures 5-15 show the effect of the supply airflow rate on the coupled system total cooling capacity during 2009 forced airflow test. It is obvious that the total cooling capacity does not follow the forced air flow pattern. This is due to the small capacity of the EAHE compared to the fan airflow rate. And also because of the day and night changes which affects the solar chimney natural air draft.

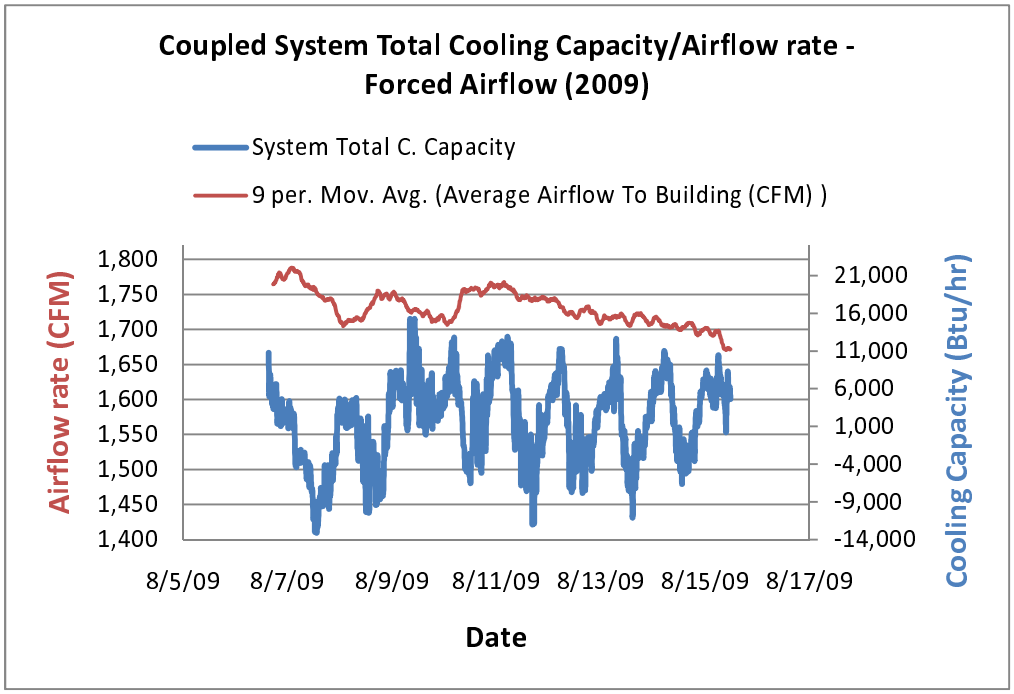

Fig. 5-15 – Coupled System Total Cooling Capacity – Forced Airflow Rate Comparison (2009 Forced Airflow Test)

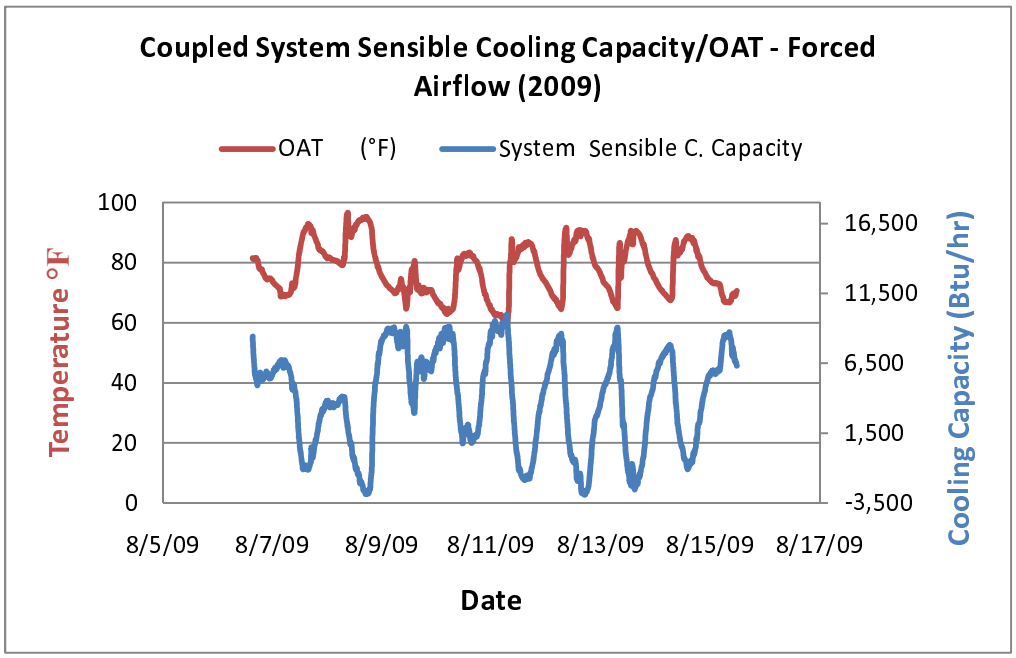

Fig. 5-16 – Coupled System Sensible Cooling Capacity – Outdoor Air Temperature Comparison (2009 Forced Airflow Test)

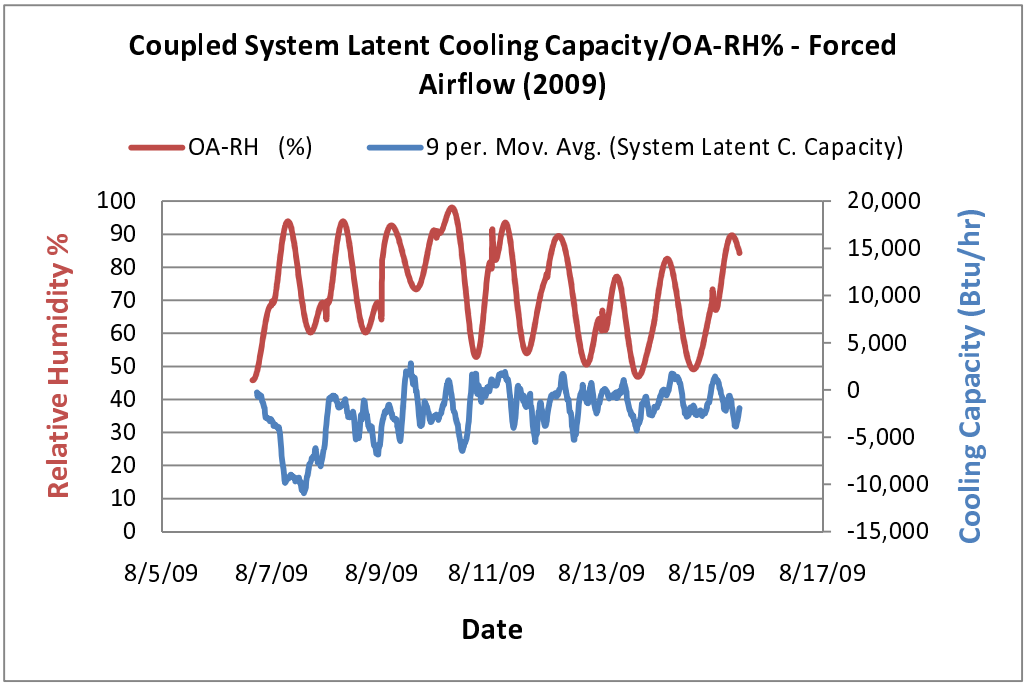

Fig. 5-17 – Coupled System Latent Cooling Capacity – Outdoor Air Relative Humidity Comparison (2009 Forced Airflow Test)

It is apparent from Figure 5-16 that the sensible cooling capacity follows an opposite pattern of the outdoor air temperature. In other words, as the outdoor air temperature increases the system sensible cooling capacity decreases and vice versa. On the other hand, Figure 5-17 show that the latent cooling capacity follows almost the same pattern of the outdoor air relative humidity. In other words, as the relative humidity increase the latent cooling capacity increase and vice versa.

5.4 Earth-to-Air Heat Exchanger and the Effect on Air and Soil

In this section the analysis of the effect of the heat transfer of air along the length of the EAHE during the natural airflow test of 2008 and the forced airflow test of 2009 are presented. Moreover, the analysis of the effect of the heat transfer from the EAHE to the surrounding underground soil during the 2009 forced air flow test is provided. And the effect of the EAHE and coupled system total cooling capacities on the underground soil is discussed. This analysis aims to study how the heat transfer of the EAHE affects the air migrating through it and the underground soil surrounding it, to develop a better understanding of its thermal performance and provide recommendations for future enhanced performance.

5.4.1 Earth-to-Air Heat Exchanger and the Effect on Air

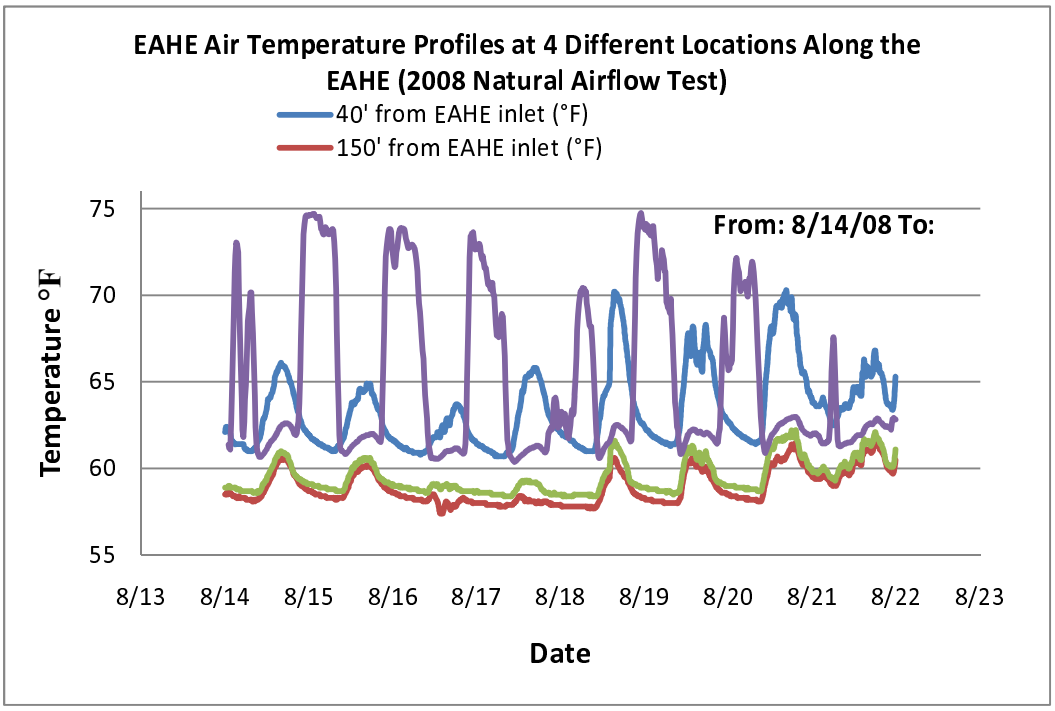

Fig. 5-18 – EAHE Air Temperature Profiles at 4 Different Locations (2008 Natural Airflow Test)

Figure 5-18 show the EAHE air temperature profiles of 4 different points along the EAHE during the natural airflow test of 2008. It is clear from the figure that air temperature decreases extensively while it is migrating through the 188ft long EAHE. This proves the effectiveness it effectiveness and ability for heat dissipation. Moreover, the peaks on the supply air temperature during the night time are related to the false reading of the supply air temperature sensor during the night time as there is no supply airflow during the night time so it reads the room air temperature instead which is high during the nights.

It should be mentioned that for the EAHE air temperature profiles analysis during the 2008 natural airflow test, only one week worth of data is presented (from August 14, 2008 to August 21, 2008) as the rest of the data show a similar pattern.

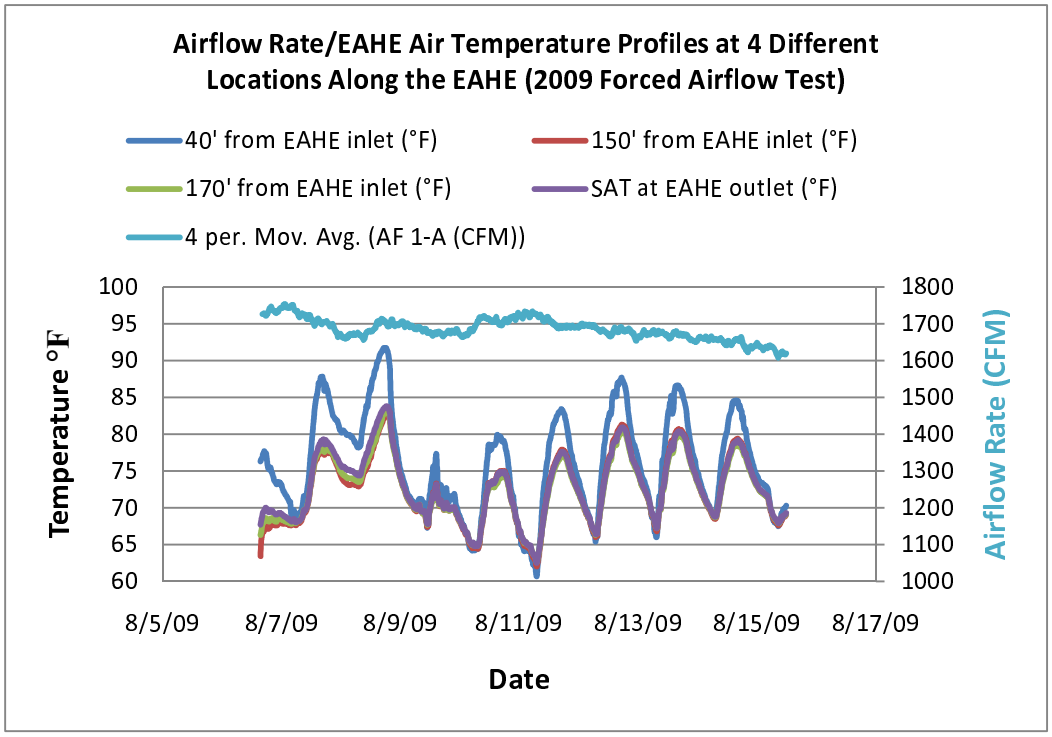

Fig. 5-19 – Airflow Rate – Air Temperature Profiles at 4 Different Locations (2009 Forced Airflow Test)

Figure 5-19 show the EAHE air temperature profiles of 4 different points along the EAHE during the natural airflow test of 2009 as well as the airflow rate profile. It is clear that the air temperature profiles followed the same pattern as the natural airflow test of 2008 which proves the effect of the test facility building thermal mass on the underground soil surrounding the building vicinity and the outlet of the EAHE. It is also apparent from the above figure that the EAHE air

temperature profile follows the same pattern as the airflow rate. In other words as the airflow rate increases the temperature of air inside the EAHE increases and vice versa, which follows the common sense. It should be mentioned that the natural airflow test of 2008 showed a similar results for the airflow rate and EAHE air temperature profiles.

5.4.2 Earth-to-Air Heat Exchanger and the Effect on Soil

This sub-section starts studying the effect of the ambient air on the UUS temperature profiles during the 2009 natural airflow test. Thereafter, the analysis on the effect of the forced air flow rate on the underground soil above and next the EAHE is conducted. Furthermore, the effect of the EAHE and coupled system total cooling capacities on the underground soil surrounding the EAHE is studied.

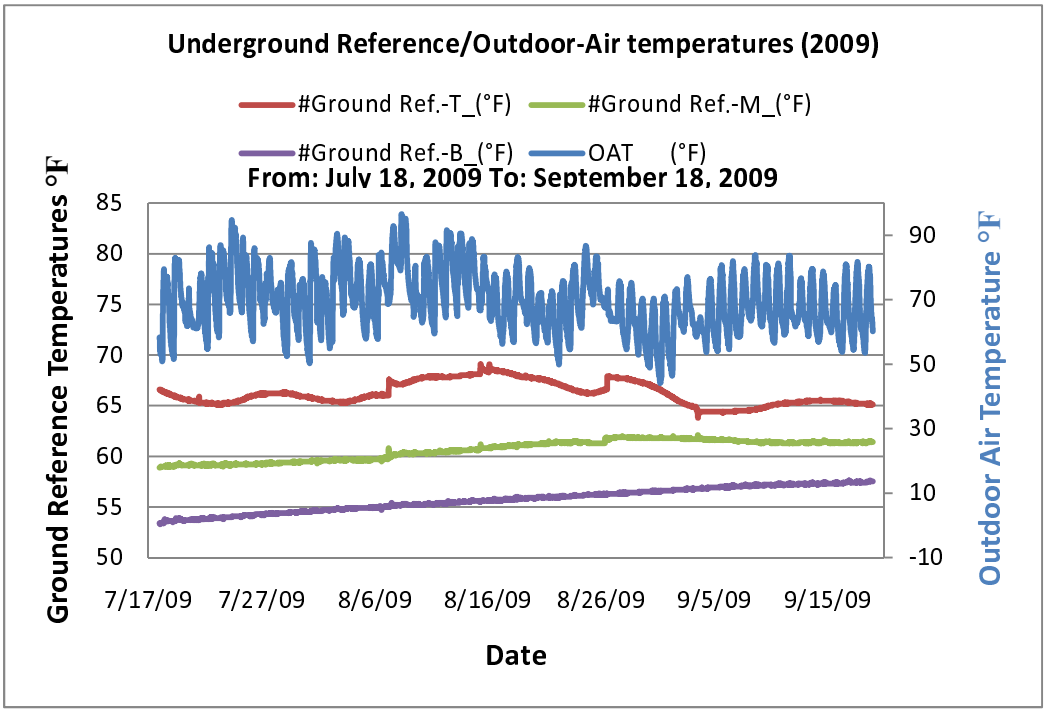

Fig. 5-20 – 2009 Underground Reference – Outdoor Air Temperatures

As shown in Figure 5-20 the UUS temperature profile at 9.5ft depth stayed at a range of 53.3°F-57.6°F which is considered as a good temperature range for a heat sink as discussed earlier. Moreover, the UUS temperature profile at 2ft depth almost followed the main changes in the outdoor air temperature (i.e. the weekly temperature rage changes not the daily temperature changes).

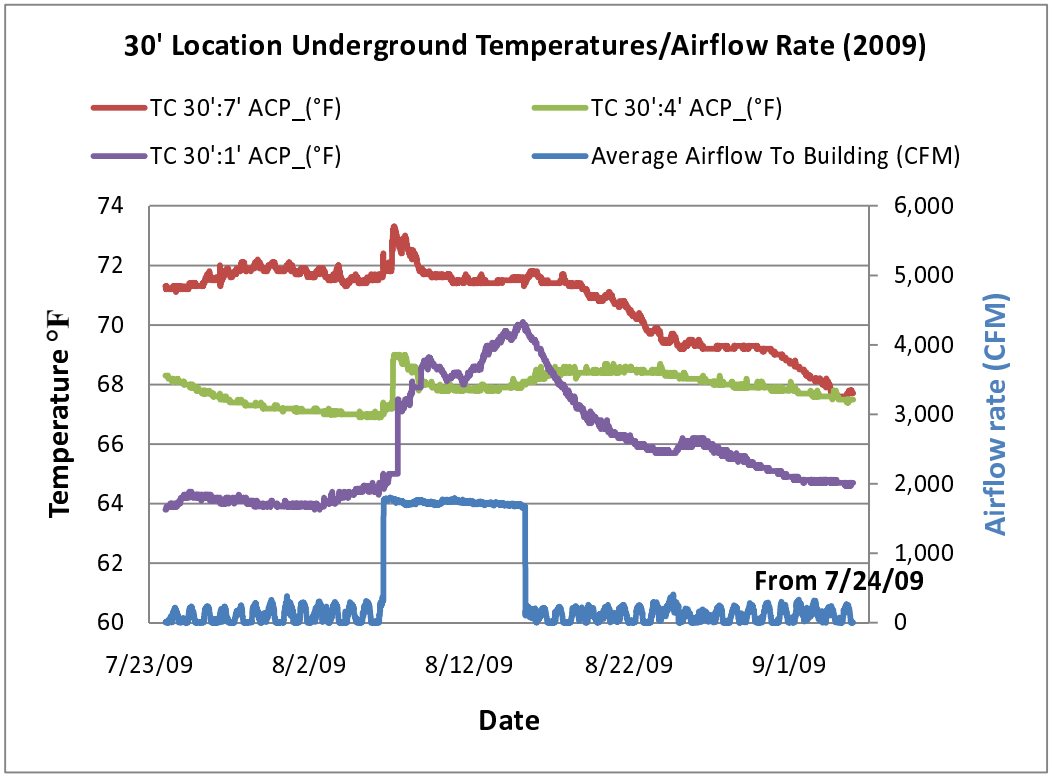

Fig. 5-21 – Airflow Rate – Underground Temperature profile at 30 ft from the Test Facility Building (2009 Entire Testing Period)

Figure 5-21 shows the underground soil temperature profiles at 30ft away from the test facility building at 3 different heights 1ft, 4ft, and 7ft above the EAHE along with the airflow rate profile during the entire 2009 testing period. It is clear from the above figure that the underground soil temperatures at the

different depths increased drastically during the forced airflow testing period, with higher values closer to the EAHE tube and less values away from it. For example, the underground soil temperature at 1ft above the EAHE preserved at a temperature of about 64°F then it rose up to 70°F during the forced airflow test, afterwards it settled down again at a temperature of about 64.5°F. This phenomenon is called the ground thermal saturation, where the underground temperatures rise above their normal temperatures during the time of the year. It should be mentioned that it took the forced airflow test few hours to thermally saturate the ground, while it took the ground over two weeks to recover from it thermal saturation. This answers one of the main questions on which this current research is based on "how long will it take the underground soil to recover from its thermal saturation?"

The underground thermal saturation negatively affects the EAHE and coupled system cooling performance. As it decreases the underground ability to be a heat sink, accordingly it reduced the cooling capacity that could be extracted by both the EAHE and the coupled system. This explains why during the forced airflow test, the system could not maintain the indoor environmental conditions within the thermal comfort zone limits recommended by ASHRAE. Moreover, it explains the negative values that appeared for all the cooling capacities forms during the night time of the forced airflow test.

Figure 5-22 show the underground temperature profile at 30 ft away from the test facility building at 6 inches above the EAHE and 6 inches next to the

EAHE. The results of this figure show that the underground heat dissipation in the vertical level is higher than that on the horizontal level. And that both the vertical and the horizontal levels experienced thermal saturation with different degrees during the forced airflow test conducted during the 2009 testing period. Moreover, it shows that the underground temperatures followed the outdoor air temperature pattern especially during the forced airflow test and with a less damping degree than the period before and after the forced airflow test.

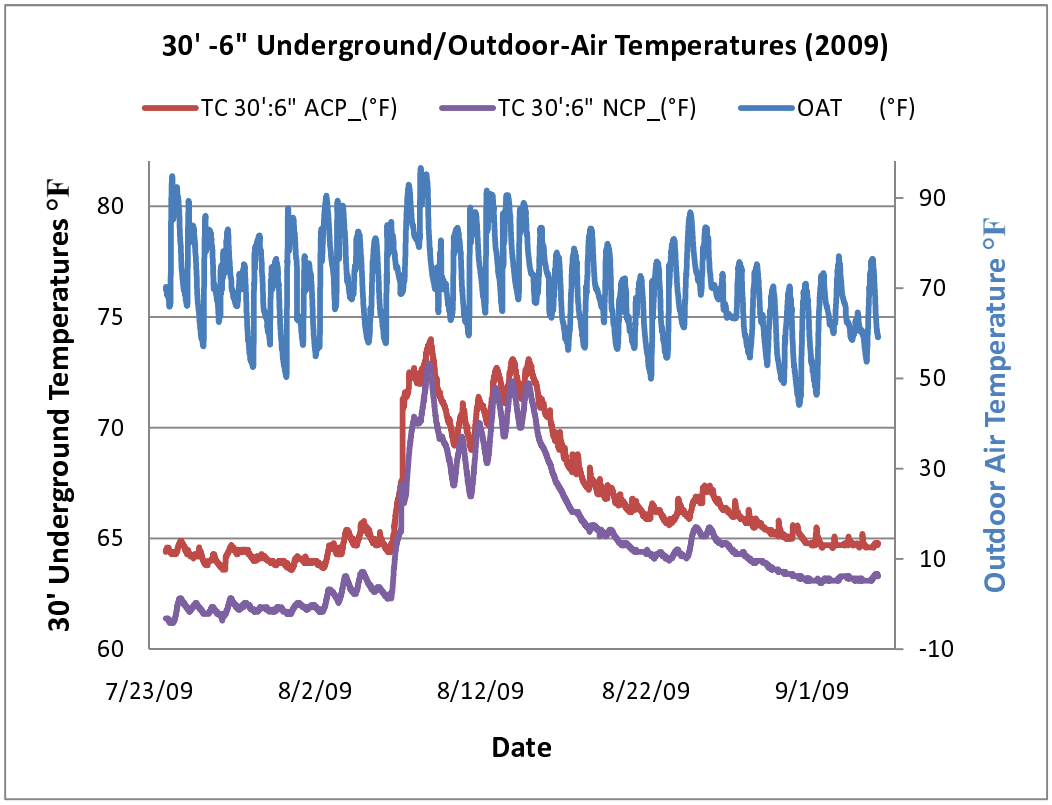

Fig. 5-22 – Outdoor Air Temperature and Underground Temperature Profiles at 6 Inches above and next to the EAHE (2009 Entire Testing Period)

Figure 5-23 show the underground temperature profile at 30ft away from the test facility building and 1ft above the EAHE along with the EAHE and

coupled system total cooling capacities. It is clear from this figure that although the underground soil experienced thermal saturation during the forced airflow test, both the EAHE and the coupled system cooling capacities increased during the same period. This is because of the great amount of airflow rate that traveled along the EAHE, not because temperature difference between either the outdoor air and supply air or the indoor air and the supply air. The increase in the cooling capacities during the 2009 forced airflow test is considered as a good indication for the underground capacity for heat dissipation.

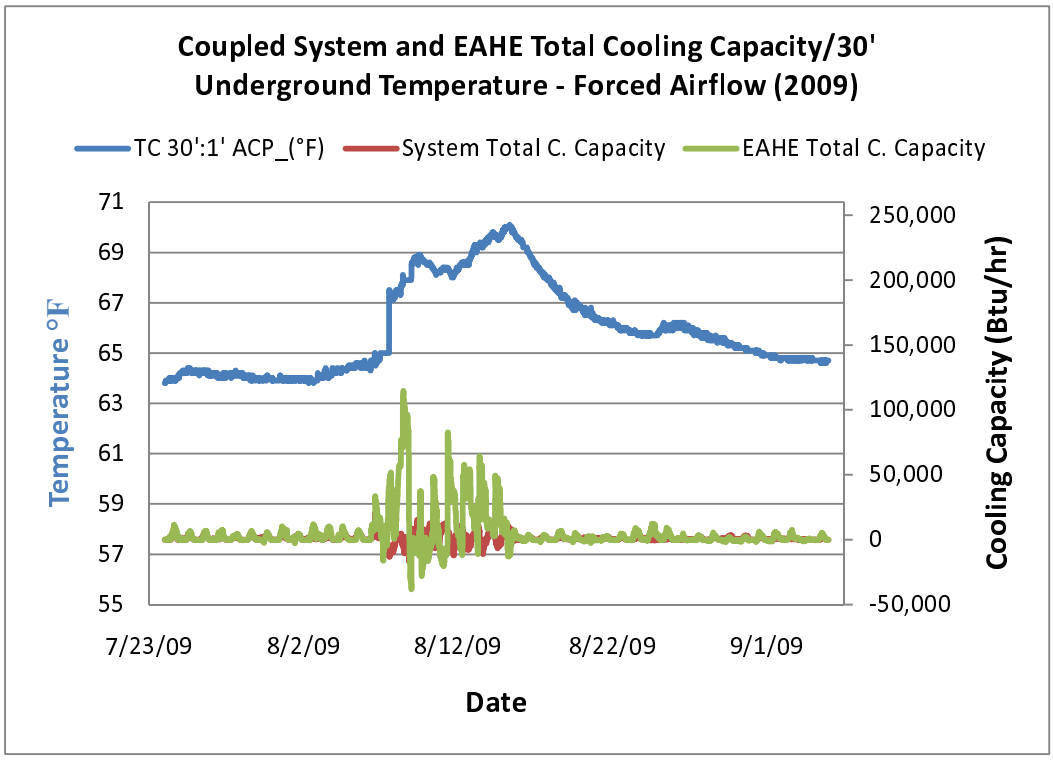

Fig. 5-23 – Coupled System and EAHE Total Cooling Capacities – Underground Temperature profile at 30ft away from the Test Facility Building during the 2009 Forced Airflow Test

5.5 Solar Chimney Driving Force

In this section an analysis of the solar chimney driving force during the 2008 natural airflow test is conducted. The analyses begin with studying the effect of the outdoor air temperature on the EAHE airflow rate which is a result/part of the solar chimney natural draft. Thereafter, the effect of the outdoor air temperature on the solar chimney air temperatures which controls its natural draft driving force is presented. Moreover, a comparison between the solar chimney temperature and the airflow rates is carried out. Furthermore, the effect of the solar chimney air temperatures on the coupled system total cooling capacity is introduced.

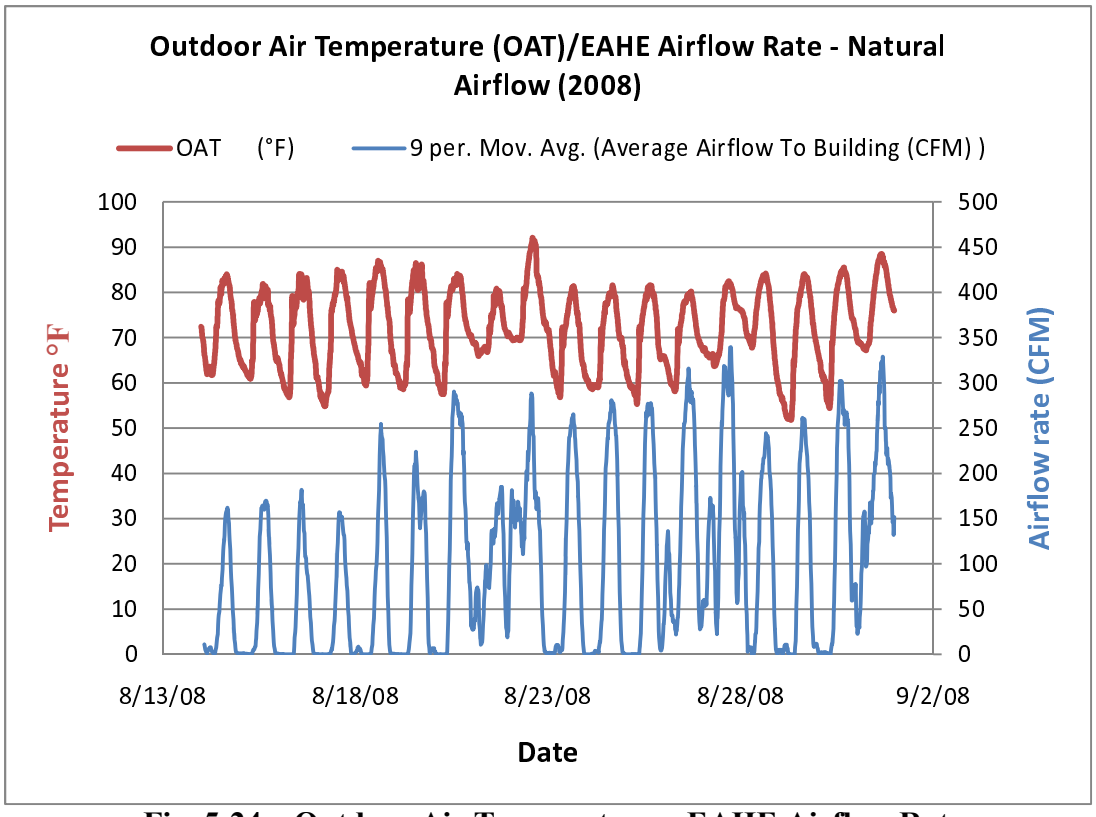

Fig. 5-24 – Outdoor Air Temperature – EAHE Airflow Rate

(2008 Natural Airflow Test)

It is clear from Figure 5-24 that the EAHE airflow rate followed the same exact pattern of the outdoor air temperature. In other words, as the outdoor air temperature increases the EAHE airflow rate, which is derived by the solar chimney natural draft, increases. This proves the effectiveness of coupling the EAHE with the solar chimney technology and shows the effect of the solar radiation and the outdoor air temperature on the solar chimney natural draft and consequently the supply airflow to the building.

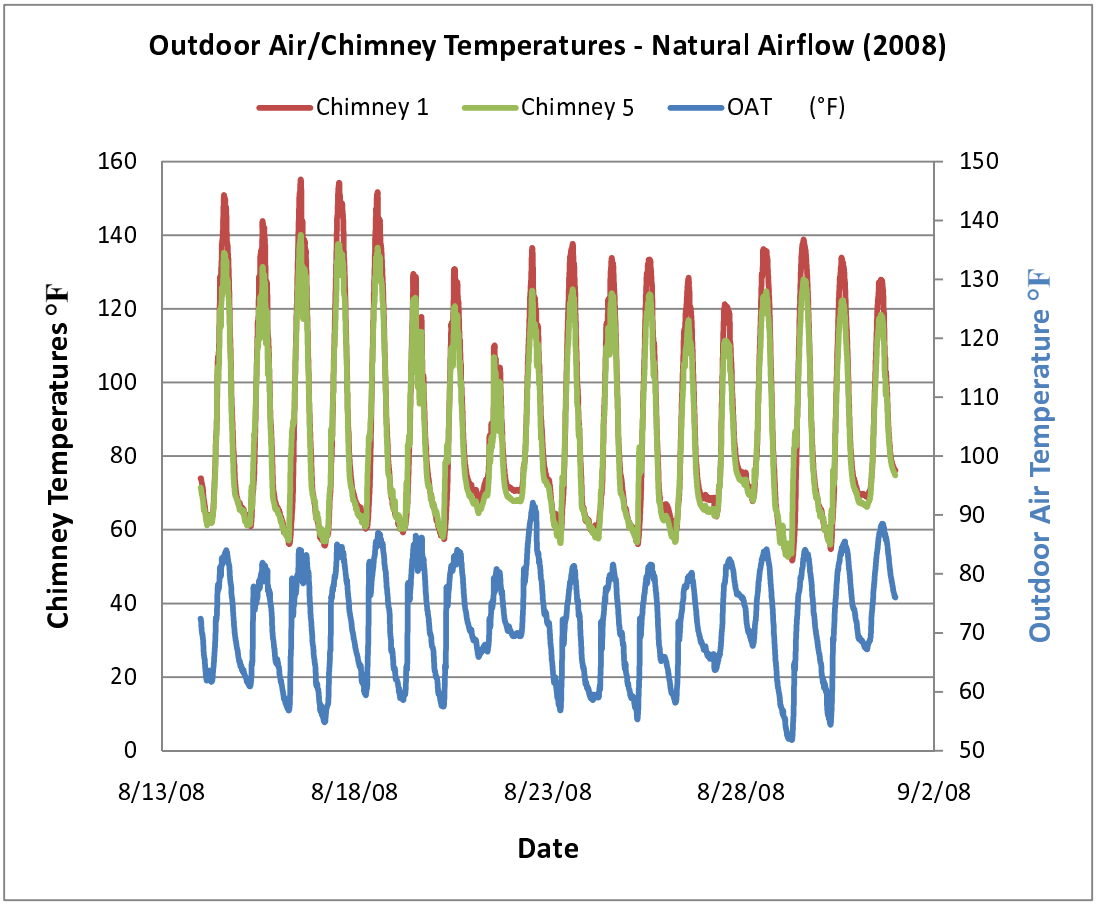

Fig. 5-25 – Comparison between the Outdoor Air and Chimney air Temperatures

Figure 5-25 shows how using the solar collector and solar chimney techniques amplifies the amount of the ambient air temperature to create a natural draft. It is clear from the figure that the solar chimney temperatures follows the same pattern as the outdoor air temperature, which implies that increasing the outdoor air temperature increase the solar chimney driving force. The same fact is also proved through Figure 5-26 that show the effect of the chimney air temperatures on the EAHE and the solar collector airflow rates. As the chimney air temperatures increase, the airflow rates increases. It is worth mentioning that from Figure 5-26 it is concluded that the airflow rate through the solar collector is higher than that through the EAHE. This means that there is an undesired amount of air infiltration through the building which affects the coupled system cooling capacity as it increased the test facility building cooling loads. Recommendations on how to reduce the amount of air infiltration to the building are provided on chapter 6 of this thesis.

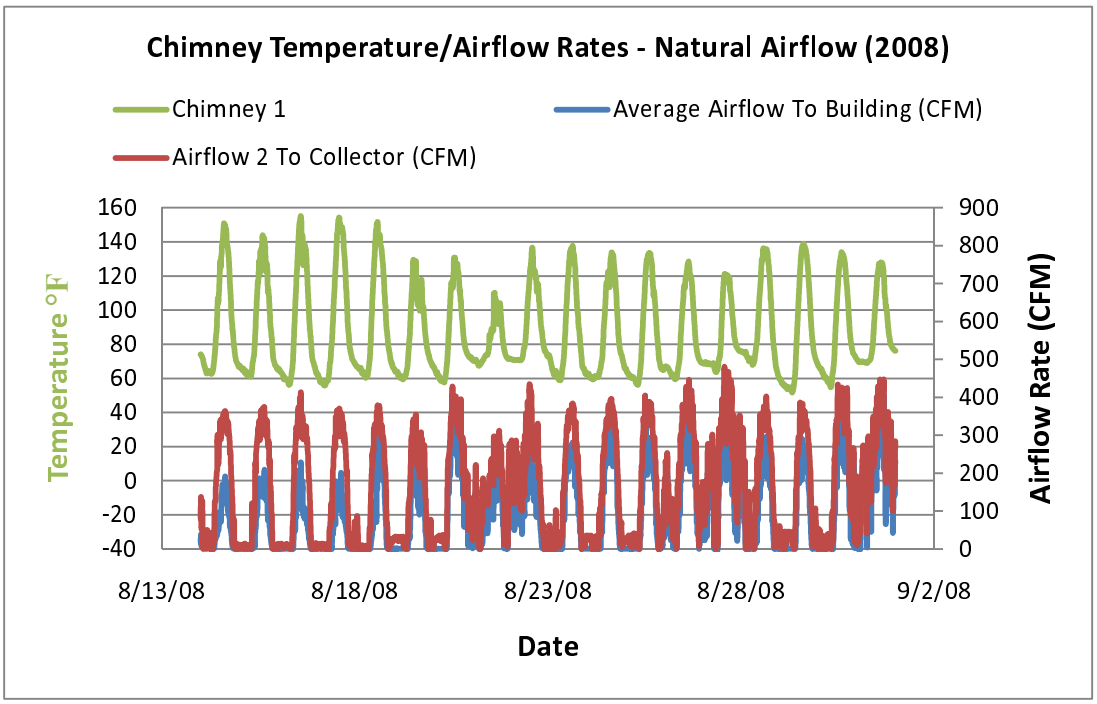

Fig. 5-26 – Chimney Temperature and the Airflow Rates Comparison

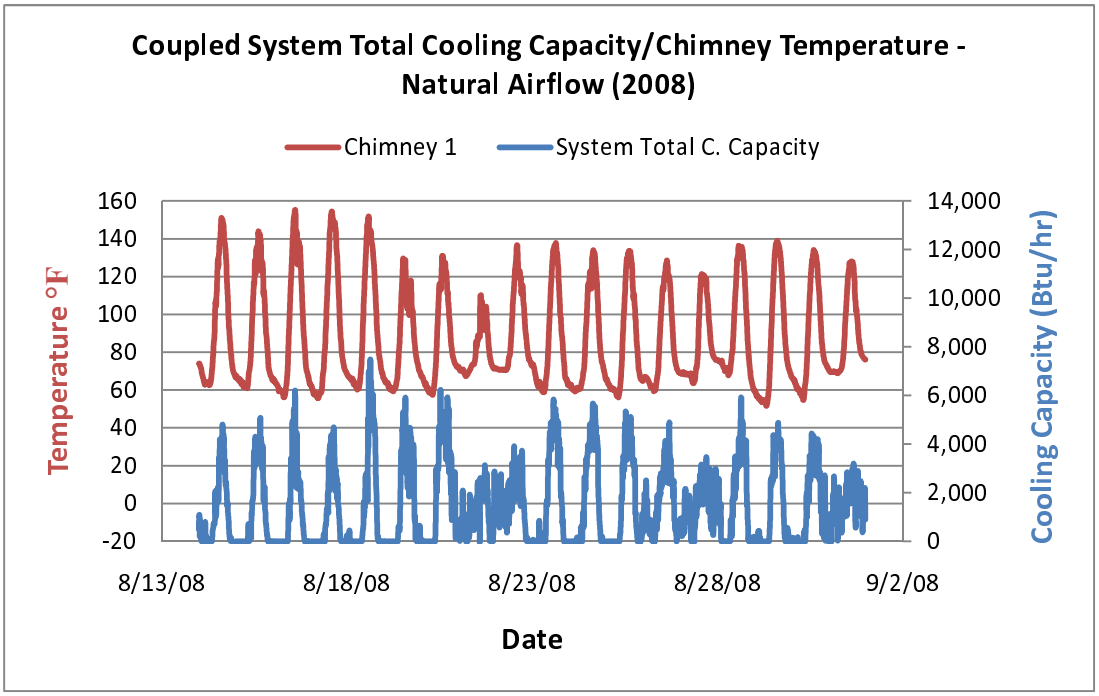

Fig. 5-27 – Chimney Temperature – Coupled System Total Cooling Capacity Comparison

As shown in Figure 5-27 the total cooling capacity of the coupled system is largely affected by the solar chimney air temperatures (i.e. driving force), where the coupled system total cooling capacity increases with the increase of the solar chimney air temperatures and vice versa. This follows the common sense. It can be clearly seen that a maximum chimney air temperature of about 155°F can create a total cooling capacity of more than 6,000 Btu/hr (0.5 tons of cooling per hour) which is very good compared to the amount of energy required by conventional air conditioning system to provide the same amount of cooling. The above analysis proves the feasibility of the coupled system through some design improvements which are presented on chapter 6 of this thesis.

5.6 Summary

In this chapter a study on the undisturbed underground soil temperatures has been conducted, where the results of the study motivated the further analysis of the coupled system. Thereafter, the thermal performance analysis of the coupled system and the EAHE is evaluated from different points of view to answer few the important questions about the feasibility of the coupled system. The first question is "could the coupled system provide comfort indoor environmental conditions that complies with ASHRAE standard 55?" the answer to this question is found to be yes with few improvements on the design side of the system. Another question is "how much cooling capacity could the coupled system provide for the test facility building during the hot summer months on both the natural airflow mode and the forced airflow mode?" to answer this question the cooling capacities calculation method has been presented, moreover, cooling capacity analysis has been conducted. Furthermore, the analysis of the effect of the EAHE heat transfer on the air flowing through it and the underground soil surrounding it is provided. Finally, the solar chimney driving force has been discussed from various points and its effect on the coupled system total cooling capacity has been evaluated.

Chapter, 6

CONCLUSIONS AND RECOMMENDATIONS

6.1 Conclusions

Since in the United States the HVAC systems is one of the main energy consuming components in the building sector which in turn consumes about 70% of the annual electrical energy consumption, especially during the summer due to the summer cooling loads. It is necessary to investigate the renewable energy alternatives for cooling residential and commercial buildings. Accordingly, a literature review on utilizing the geothermal energy through the use of the EAHE system, and the solar energy, by the use of a solar chimney, has been conducted. The results of the review showed that most of the previous researches have been conducted on each system separately and a few experiments have been done on the coupled system.

Consequently, the present research has been conducted on the coupled system at the Solar Energy Research Test Facility (SERTF) in Omaha, Nebraska to further investigate the thermal performance of the coupled system. The dimensions of the test room at the SERTF are: 49.875ft in length, 14.83ft in width, and 7.75ft in height with a total floor area of 740ft^2. Two tests have been conducted in order to investigate the cooling capacity that the coupled system can provide to the test room and to determine if the underground soil would experience thermal saturation when the airflow is extracted through the EAHE by means of an electrical fan.

In the first test, a “Natural Airflow” test, the coupled system was allowed to be naturally driven by means of the passive solar energy and the stack effect. While in the second test, a “Forced Airflow” test, a fan was installed to the coupled system to enhance the airflow rate. Sufficient measuring instruments (e.g. thermocouples, air velocity transmitters, and relative humidity sensor) were installed at various locations of the test facility building to allow the calculation of the EAHE and coupled system cooling capacities as well as to study the various effects of the system components on the different environmental parameters and vice versa. Moreover, the measured data was logged and collected using an *in situ* computer system.

Furthermore, calibration for the measuring instruments was done *in situ* to minimize the measuring and calculation errors. In addition, an uncertainty analysis for the measured and calculated data was performed. The resulting data was analyzed and cooling capacities were determined to study the thermal performance of the implemented system during the two tests. Consequently, several conclusions were drawn from the results of the two tests as follows:

- The uncertainty error of the measured and calculated data is found to be in an acceptable range, where the thermocouple uncertainty is ±0.502°F. While the airflow measuring instruments uncertainty is in the range from ±7.2CFM to ±14.33CFM and the calculated sensible cooling capacity relative uncertainty error is ±3.0%.
- The undisturbed underground soil at a depth of 9.5ft proved to be a good heat sink as its temperature fluctuates in the range of 46.5°F – 58.2°F over the

course of a whole year. Furthermore, its temperature range during the hot summer months (i.e. July and August) is 52.2°F - 57°F, which validates its ability as a good heat sink during the hot summer season. In addition, it is found that the deeper the depth of the thermocouple in the ground the cooler the underground temperature is, and the more stable the temperature fluctuation are around the whole year.

- During 2008 and 2009 natural airflow modes/test, the coupled system was able to maintain the indoor thermal environmental comfort conditions at a favorable range that complied with ASHRAE standard 55-2004 for thermal comfort. The indoor air temperature was maintained at a range of 69°F - 77.2°F, while the indoor humidity ratio was maintained at a range of 0.006872 - 0.01438.
- During 2009 forced airflow mode/test, the coupled system was not able to maintain comfortable indoor thermal environmental conditions, as the indoor air temperature was maintained at the high range of 67.6°F - 82.4°F, while the indoor humidity ratio was maintained at the high range of 0.009437 - 0.017868 which does not comply with the recommended upper humidity ratio level (i.e. 0.012) by ASHRAE. The reason for this non-compliance is that the fan is oversized, causing the amount airflow rate to be much higher than the EAHE capacity for heat dissipation. Thus, there is not enough time and area for the heat exchange.

- The coupled system provided an acceptable amount of cooling capacity during the natural airflow test of 2008. The EAHE maximum cooling capacity during that test was 0.91 tons of cooling per hour, while the coupled system maximum cooling capacity was 0.63 tons of cooling which almost covered the building design cooling load (i.e. 0.8 tons, maximum extreme condition).
- It was found during the forced airflow test of 2009, that although the system can not entirely provide favorable thermal comfort, it can provide a very good amount of cooling capacity, where the EAHE maximum cooling capacity was 9.54 tons of cooling per hour, while the coupled system maximum cooling capacity was 1.27 tons of cooling, which is even more than the building design cooling load amount.
- During the forced airflow test of 2009, the underground soil surrounding the EAHE experienced thermal saturation in the first few hours of operation. The underground soil temperature at 1ft above the EAHE rose up from 64°F to 70°F. After the forced airflow test, the underground temperature at the same location recovered over a period of more than two weeks, where the underground soil temperatures drop down to 64.5°F. This phenomenon happened due to the oversized installed fan.
- It is found that the air temperature is reduced by about 40°F while it migrates through the 188ft long EAHE.
- During the natural airflow mode, it is found that the increase in the outdoor air temperature and solar radiation increases the solar chimney natural draft (i.e.

driving force) and the amount of airflow to the building which in turn, increases the amount of cooling capacity provided to the building.

- In addition, there is a great amount of infiltration to the test facility building which increases the building cooling load and consequently reduces the ability of the system to provide enough cooling for the test facility building.
- By comparing the coupled system during the natural airflow more with a VAV system, it is found that the coupled system was able to provide a similar amount of airflow to the building as the VAV system, which almost covered the building design cooling load, an extreme condition. This implies that the coupled system is feasible as it provided the same amount of airflow and cooling capacity as the VAV system under the same operational conditions.

6.2 Recommendations

The coupled system thermal performance and resulting cooling capacities can be further improved over the systems two operational modes. The author suggests the following to improve the performance of the implemented coupled system.

- Increase the size of the solar collector, design and size the EAHE based on the required airflow and use a multiple pipe EAHE to increase the amount of airflow and cooling capacities that could be provided to the building.
- Re-size the fan based on the required airflow amount and the total pressure losses through the EAHE. (The recommended fan size is 244 CFM at 0.414 in.H_2O).

- Study the possibility of delaying the onset of the underground thermal saturation by adding moisture to the underground soil and adjust the perforation position of the EAHE to optimize the humidity ratio of supply air.
- Insulate the very last portion of the EAHE that penetrates the test facility building through the concrete slab to prevent warming up the supply air.
- Develop a complete mathematical model for the whole system (i.e. EAHE, test facility building, solar collector, and solar chimney) to further understand the performance of the coupled system.
- Implement the system with a conventional HAVC system to pre-cool/pre-heat the outdoor air temperature to help reduce the electrical energy consumption.

REFERENCES

Al-Ajmi, F., D.L. Loveday, and V.I. Hanby. 2006. The cooling potential of earth-air heat exchangers for domestic buildings in a desert climate. *Building and Environment* 41 (2006) 235-244.

ASHRAE, 1999. *ASHRAE handbook, HVAC Applications*. American Society of Heating, Refrigeration and Air-conditioning Engineers, Inc., Atlanta, GA.

ASHRAE, 2001. *ASHRAE handbook, fundamentals*. American Society of Heating, Refrigeration and Air-conditioning Engineers, Inc., Atlanta, GA.

Athienitis, A.K., M. Roy, and M. Zhao. 2005. Design and simulation of a hybrid ventilation system with earth-air heat exchanger. Ninth International IBPSA conference. Montreal, Canada, August 15-18.

Bacharoudis, E., M. Gr. Vrachopoulos, M.K. Koukou, D. Margaris, A.E. Filios, and S.A. Mavrommatis. 2007. Study of the natural convection phenomena inside a wall solar chimney with one wall adiabatic and one wall under a heat flux. *Applied Thermal Engineering* 27 (2007) 2266-2275.

Bansal, N.K., and Shail. 1999. Characteristic parameters of a hypocaust construction. *Building and Environment* 34 (1999) 305-318.

Bansal, V., R. Misra, G.D. Agrawal, and J. Mathur. 2009a. Performance analysis of earth-pipe-air heat exchanger for winter heating. *Energy and Buildings* 41 (2009) 1151-1154.

Bansal, V., R. Misra, G.D. Agrawal, J. Mathur. 2009b. Performance analysis of earth-pipe-air heat exchanger for summer cooling. *Energy and buildings*

Bojic, M., N. Trifunovic, G. Papadakis, and S. Kyritsis. 1997. Numerical simulation, technical and economical evaluation of air-to-earth heat exchanger coupled to a building. *Energy* Vol.22, No. 12, pp. 1151-1158.

Bouchair, A. 1994. Solar chimney for promoting cooling ventilation in southern Algeria. *Building Service Engineering, Research and Technology* 15(2) 81-93.

Bureau of Ocean Energy Management, Regulation, and Enforcement (BOEMRE). 2004. *The Need Project.* Secondary Energy Infobook. http://www.boemre.gov/omm/pacific/kids/Watts/Appendix/7.%20Geothermal%20.pdf

Chel, A., and G.N. Tiwari. 2009. Performance evaluation and life cycle cost analysis of earth to air heat exchanger integrated with adobe building for New Delhi composite climate. *Energy and Buildings* 41 (2009) 56-66.

Chel, A., and G.N. Tiwari. 2010. Stand-alone photovoltaic (PV) integrated with earth to air heat exchanger (EAHE) for space heating/cooling of adobe house in New Delhi (India). *Energy Conversion and Management* 51 (2010) 393-409.

Chen, B., T.C. Wang, J. Maloney, J. Ennenga, and M. Newman. 1983a. Measured cooling performance of earth contact cooling tubes. Proceeding of the American Solar Energy Society, Minneapolis, MN.

Chen, B., T.C. Wang, J. Maloney, and M. Newman. 1983b. Measured and predicted cooling performance of earth contact cooling tubes. Proceeding of the American Solar Energy Society, Minneapolis, MN.

Chen, Z.D., P. Bandopadhayay, J. Halldorsson, C. Byrjalsen, P. Heiselberg, and Y. Li. 2003. An experimental investigation of a solar chimney model with uniform wall heat flux. *Building and Environment* 38 (2003) 893-906.

Correia-da-Silva, J.J. 2004. Performance evaluation of two passive cooling systems. The 21st Conference on Passive and Low Energy Architecture. Eindhoven, The Netherlands, 19-22.

Correia-da-Silva, J. 2006. Improvement of precooling supply air by way of coupled earth to air heat exchanger and solar chimney. The 23rd Conference on Passive and Low Energy Architecture, Geneva, Switzerland, 6-8 September.

Correia-da-Silva, J. 2007. Preheating of supply air through an earth to air heat exchanger coupled with a solar chimney. Proceedings: *Building Simulation.*

Deb, K., S. Agrawal, A. Pratap, and T. Meyarivan. 2000. A fast elitist non-dominated sorting genetic algorithm for multi-objective optimization: NSGA-II.

De Paepe, M., and A. Janssens. 2003. Thermo-hydraulic design of earth-air heat exchangers. *Energy and Buildings* 35 (2003) 389-397.

Elyyan, M., D. Fisher, F. Chambers, D. Lilley, and A.G. Emslie. 2001. Design of an experimental facility for building airflow and heat transfer measurements. A master thesis, The State University of Oklahoma.

Energy Star. 2010. http://www.energystar.gov

Environmental Protection Agency (EPA). 2010. http://www.epa.gov/

Fluent. 2010. http://www.fluent.com/solutions/whatcfd.htm

Gan, G., and S.B. Riffat. 1998. A numerical study of solar chimney for natural ventilation of buildings with heat recovery. *Applied Thermal Engineering* 18 (1998) 1171-1187.

Ghosal, M.K., G.N. Tiwari, and N.S.L. Srivastava. 2004. Thermal modeling of a greenhouse with an integrated earth to air heat exchanger: an experimental validation. *Energy and Buildings* 36 (2004) 219-227.

Ghosal, M.K., G.N. Tiwari, D.K. Das, and K.P. Pandey. 2005. Modeling and comparative thermal performance of ground air collector and earth air heat exchanger for heating of greenhouse. *Energy and Buildings* 37 (2005) 613-621.

Ghosal, M.K., and G.N. Tiwari. 2006. Modeling and parametric studies for thermal performance of an earth to air heat exchanger integrated with a greenhouse. *Energy Conversion and Management* 47 (2006) 1779-1798.

Henkel, J., B. Chen, M. Liu, and G. Wang. 2004. Analysis, design and testing of an earth contact cooling tube for fresh air conditioning. Proceedings of Solar: A Solar Harvest: Growing Opportunities. Portland, Oregon. July 11-14.

Hollmuller, P., and B. Lachal. 2001. Cooling and preheating with buried pipe systems: monitoring, simulation and economic aspects. *Energy and Buildings* 33 (2001) 509-518.

Hollmuller, P. 2003. Analytical characterization of amplitude-dampening and phase-shifting in air/soil heat-exchangers. *International Journal of Heat and Mass Transfer* 46 (2003) 4303-4317.

Hollmuller, P., and B. Lachal. 2005. Buried pipe systems with sensible and latent heat exchange: validation of numerical simulation against analytical solution and long-term monitoring. The 9th Conference of International Building Performance Simulation Association, pp. 411-418. Ecole polytechnique de Montreal. August 15-18.

Irmak, S., J. Payero, D.E. Eisenhauer, W.L. Kranz, D.L. Martin, G.L. Zoukbek, J.M. Ress, B. VanDeWalle, A.P. Christiansen, and D. Leininger. 2006. Watermark granular matrix sensor to measure soil matric potential for irrigation management. *Institute of Agriculture and Natural Resources.* The University of Nebraska.

Jiang, H., Y. Jiang, Y. Wang, Z. Ma, and Y. Yao. 2006. An experimental study on a modified air conditioner with a domestic hot water supply (ACDHWS). *Energy* 31 (2006) 1453-1467.

Kumar, R., S. Ramesh, and S.C. Kaushik. 2003. Performance evaluation and energy conservation potential of earth-air-tunnel system coupled with non-air-conditioned building. *Building and Environment* 38 (2003) 807-813.

Kumar, R., S.C. Kaushik, and S.N. Garg. 2006. Heating and cooling potential of earth-to-air heat exchanger using artificial neural network. *Renewable Energy* 31 (2006) 1139-1155.

Kumar, R., A.R. Sinha, B.K. Singh, and U. Modhukalya. 2008. A design optimization tool of earth-to-air heat exchanger using a genetic algorithm. *Renewable Energy* 33 (2008) 2282-2288.

Lee, K. H., and R.K. Strand. 2006. Implementation of an earth tube system into ENERGYPLUS program. *Proceedings of SimBuild.* MIT, Cambridge, Massachusetts. August 2-4.

Lenchener, N. 2001. *Heating, Cooling, Lighting: Design Methods for Architects.* 2nd Edition. John Wiley & Sons, Inc., Canada.

McQuiston, F., J.D. Parker, and J.D. Spitler. 2005. *Heating, ventilating, And Air Conditioning: Analysis and Design.* 6th Edition. John Wiley & Sons, Inc., Danvers, MA.

Mihalakakou, G., M. Santamouris, D. Asimakopoulos, and I. Tselepidaki. 1995. Parametric prediction of the buried pipes cooling potential for passive cooling applications. *Solar Energy,* Vol. 55, No. 3, pp. 163-173.

Mihalakakou, G., J.O. Lewis, and M. Santamouris. 1996a. The influence of different ground covers on the heating potential of earth-to-air heat exchangers. *Renewable Energy,* Vol. 7, No. 1, pp. 33-46.

Mihalakakou, G., J.O. Lewis, and M. Santamouris. 1996b. On the heating potential of buried pipes techniques – application in Ireland. *Energy and Buildings* 24 (1996) 19-15.

Mihalakakou, G. 2003. On the heating potential of a single buried pipe using deterministic and intelligent techniques. *Renewable Energy* 28 (2003) 917-927.

Ming, T., W. Liu, Y. Pan, and G. Xu. 2008. Numerical analysis of flow and heat transfer characteristics in solar chimney power plants with energy storage layer. *Energy Conversion and Management* 49 (2008) 2872-2879.

Newman, M.A., B. Chen, T.C. Wang, and J. Maloney. 1983. Analysis of the performance of earth contact cooling tubes. A senior project, The University of Nebraska.

Nouanégué, H.F., and E. Bilgen. 2009. Heat transfer by convection, conduction and radiation in solar chimney systems for ventilation of dwellings. *International Journal of Heat and Fluid Flow* 30 (2009) 150-157.

Nugroho, A.M., M.H. Ahmad, and J. Hiung. 2006. Evaluation of parametrics for the development of vertical solar chimney ventilation in hot and humid climate. The 2nd International Network for Tropical Architecture Conference. Christian Wacana University, Jogjakarta. April 3-5. pp. 160-170.

Pfafferott, J. 2003. Evaluation of earth-to-air heat exchangers with as standardized method to calculate energy efficiency. *Energy and Buildings* 35 (2003) 971-983.

Sakonidou, E.P., T.D. Karapantsios, A.I. Balouktsis, and D. Chassapis. 2008. Modeling of the optimum tilt of solar chimney for maximum air flow. *Solar Energy* 82 (2008) 80-94.

Santamouris, M., G. Mihalakakou, C.A. Balaras, J.O. Lewis, M. Vallindras, and A. Argirious. 1996. Energy conservation in greenhouses with buried pipes. *Energy,* Vol. 21, No. 5, pp. 353-360.

Science Education Resource Center (SERC). 2010. Carleton College. http://serc.carleton.edu/introgeo/mathstatmodels/Numerical.html

Shukla, A., G.N. Tiwari, and M.S. Sodha. 2006. Parametric and experimental study on thermal performance of an earth-air heat exchanger. *International Journal of Energy Research* 30:365-379.

Thevenard, D. 2007. Bibliographic search on the potential of earth tubes. *Numerical Logics Inc.* September 6. (website: www.numlog.ca).

Tittelein, P., G. Achard, and E. Wurtz. 2009. Modeling earth-to-air heat exchanger behaviour with the convolutive response factors method. *Applied Energy* 86 (2009) 1683-1691.

Tiwari, G.N., M.A. Akhtar, A. Shukla, and M. Emran Khan. 2006. Annual thermal performance of greenhouse with an earth-air heat exchanger: An experimental validation. *Renewable Energy* 31 (2006) 2432-2446.

Toro, E.F. 2009. *Riemann solvers and numerical methods for fluid dynamics*: *a practical introduction*. Dordretch Heidelberg London New York: Springer.

U.S. Energy Information Administration (EIA). 2008. http://www.eia.doe.gov/overview_hd.html

Wang, G., B. Chen, M. Liu, J. Henkel, and S. Raulin. 2004. Analysis, design and preliminary testing of solar chimney for residential air-conditioning applications. Solar. A Solar Harvest: Growing Opportunities. Portland, Oregon. July 11-14.

Wordnetweb, Princeton. 2010. Princeton University. http://wordnetweb.princeton.edu/perl/webwn

Zhang, J., and F. Haghighat. 2009. Convective heat transfer prediction in large rectangular cross-sectional area Earth-to-Air Heat Exchangers. *Building and Environment* 44 (2009) 1892-1898.

Appendix, A

CALCULATED AND MEASURED DATA

2008 NATURAL AIRFLOW TEST (SAMPLE DATA)

		Outdoor Air Conditions				Indoor Air Conditions				Supply Air Conditions				System Capacities			EAHE Capacities		
Date - Time	Airflow (CFM)	OAT (°F)	OA-RH (%)	OA-H.Ratio (w)	OA-Enthalpy (Btu/lbm)	Average RAT (°F)	RA-RH (%)	RA-H.Ratio (w)	RA-Enthalpy (Btu/lbm)	SAT (°F)	SA-RH (%)	SA-H.Ratio (w)	SA-Enthalpy (Btu/lbm)	System Total C. Capacity	System Sensible C. Capacity	System Latent C. Capacity	EAHE Total C. Capacity	EAHE Sensible C. Capacity	EAHE Latent C. Capacity
8/14/08 0:00	17	72.4	75	0.0127	31.36	77.2	59.2	0.0118	31.49	62	80.2	0.0094	25.22	488.61	285.00	192.35	478.48	194.51	271.74
8/14/08 0:15	38	72.1	75.4	0.0127	31.21	77.1	60.2	0.0119	31.65	61.5	83.8	0.0097	25.38	1092.1	652.17	414.07	1015.54	443.14	547.16
8/14/08 0:30	7	70.9	67.8	0.0109	28.99	77.0	59.8	0.0118	31.49	61.2	84.9	0.0097	25.33	197.66	121.80	71.03	117.44	74.70	40.04
8/14/08 0:45	9	70.1	64.6	0.0101	27.91	76.9	58.5	0.0115	31.13	61.1	86.2	0.0098	25.43	235.16	156.75	73.11	102.31	89.11	10.95
8/14/08 1:00	16	69.9	61	0.0094	27.16	76.8	57.8	0.0113	30.91	61	86.9	0.0099	25.46	399.72	277.31	112.39	124.68	156.66	-34.01
8/14/08 1:15	9	69.4	60.9	0.0093	26.84	76.7	58.3	0.0114	30.96	61	86.6	0.0098	25.42	228.56	155.15	67.82	58.58	83.17	-25.39
8/14/08 1:30	1	68.7	64.9	0.0096	27.09	76.6	58.5	0.0114	30.93	61.2	86.1	0.0099	25.48	24.98	16.98	7.47	7.38	8.25	-1.03
8/14/08 1:45	1	67.6	69.3	0.0099	27.12	76.7	59.6	0.0117	31.24	69.1	86.1	0.0131	30.91	1.51	8.38	-6.86	-17.37	-1.65	-15.27
8/14/08 2:00	1	66.3	71.9	0.0098	26.72	76.7	59.6	0.0117	31.24	68.3	78.4	0.0115	29.06	9.99	9.25	0.58	-10.73	-2.20	-8.23
8/14/08 2:15	1	65.9	73.1	0.0099	26.65	76.7	60.1	0.0118	31.35	72.6	76	0.0130	31.69	-1.56	4.49	-5.98	-23.10	-7.37	-15.15
8/14/08 2:30	1	65.3	76.7	0.0101	26.8	76.7	59.9	0.0117	31.31	72.4	74.4	0.0126	31.24	0.32	4.69	-4.38	-20.35	-7.81	-12.02
8/14/08 2:45	1	64.5	76.3	0.0098	26.24	76.6	60.1	0.0117	31.28	74.2	70.9	0.0128	31.86	-2.66	2.67	-5.16	-25.76	-10.67	-14.42
8/14/08 3:00	1	63.6	80.2	0.0100	26.22	76.6	59.9	0.0117	31.24	74	68.7	0.0123	31.27	-0.14	2.84	-2.97	-23.15	-11.44	-11.14

		Outdoor Air Conditions				Indoor Air Conditions				Supply Air Conditions				System Capacities			EAHE Capacities		
Date - Time	Airflow (CFM)	OAT (°F)	OA-RH (%)	OA-H.Ratio (w)	OA-Enthalpy (Btu/lbm)	Average RAT (°F)	RA-RH (%)	RA-H.Ratio (w)	RA-Enthalpy (Btu/lbm)	SAT (°F)	SA-RH (%)	SA-H.Ratio (w)	SA-Enthalpy (Btu/lbm)	System Total C. Capacity	System Sensible C. Capacity	System Latent C. Capacity	EAHE Total C. Capacity	EAHE Sensible C. Capacity	EAHE Latent C. Capacity
8/14/08 3:15	1	62.9	81.2	0.0099	25.91	76.5	60	0.0117	31.19	72	67.5	0.0113	29.66	7.01	5.00	1.90	-17.19	-10.01	-6.77
8/14/08 3:30	1	62.3	84	0.0100	25.91	76.5	59.9	0.0116	31.17	71.7	66.6	0.0110	29.3	8.57	5.25	3.11	-15.54	-10.34	-4.82
8/14/08 3:45	1	61.9	85.6	0.0101	25.86	76.4	59.9	0.0116	31.1	70.5	69.5	0.0110	29.03	9.49	6.52	2.82	-14.53	-9.46	-4.67
8/14/08 4:00	33	62.1	86.8	0.0103	26.15	76.3	58.8	0.0113	30.8	63.3	76.3	0.0094	25.5	801.74	471.13	310.63	98.33	-43.57	138.86
8/14/08 4:15	4	62.9	84.8	0.0103	26.4	76.2	59.1	0.0114	30.8	62.6	80	0.0096	25.57	95.90	59.65	33.76	15.22	1.32	13.72
8/14/08 4:30	9	63.3	84.5	0.0104	26.62	76.1	58.8	0.0113	30.66	61.4	81.9	0.0094	25.07	230.62	145.40	79.64	63.95	18.81	43.74
8/14/08 4:45	6	63.4	81.9	0.0101	26.33	76.0	59	0.0113	30.64	62.4	82	0.0098	25.71	135.59	89.87	42.61	17.05	6.60	10.22
8/14/08 5:00	2	63.4	81.2	0.0101	26.23	75.9	58.7	0.0112	30.51	61.4	81.8	0.0094	25.06	49.97	31.99	16.93	10.73	4.40	6.13
8/14/08 5:15	1	63.6	80.9	0.0101	26.32	75.8	58.2	0.0110	30.34	61.3	85	0.0098	25.41	22.60	16.00	6.12	4.17	2.53	1.55
8/14/08 5:30	13	63.4	80.8	0.0100	26.18	75.9	58.8	0.0112	30.53	67	80.4	0.0113	28.49	121.57	127.07	-8.22	-137.66	-51.49	-82.84
8/14/08 5:45	1	62.9	80.7	0.0098	25.85	75.8	58.9	0.0112	30.49	67.8	77.5	0.0112	28.57	8.80	8.83	-0.19	-12.47	-5.39	-6.78
8/14/08 6:00	1	62.6	81.9	0.0098	25.82	75.8	59	0.0112	30.51	66.6	69.2	0.0096	26.49	18.43	10.13	7.87	-3.07	-4.40	1.39
8/14/08 6:15	0	62.1	85.5	0.0101	25.98	75.8	58.6	0.0111	30.42	69.8	72.7	0.0113	29.12	0.00	0.00	0.00	0.00	0.00	0.00
8/14/08 6:30	0	61.7	86.5	0.0101	25.85	75.8	58.8	0.0111	30.47	71.4	72.4	0.0119	30.16	0.00	0.00	0.00	0.00	0.00	0.00
8/14/08 6:45	1	61.7	87.3	0.0102	25.96	75.7	58.8	0.0111	30.4	68.7	68.2	0.0101	27.64	12.65	7.70	4.67	-7.70	-7.70	0.19
8/14/08 7:00	0	61.8	87.6	0.0103	26.06	75.7	59.8	0.0113	30.61	70	67.2	0.0105	28.3	0.00	0.00	0.00	0.00	0.00	0.00
8/14/08 7:15	0	61.9	87.6	0.0103	26.12	75.6	60.1	0.0113	30.61	70.8	68.4	0.011	29.03	0.00	0.00	0.00	0.00	0.00	0.00
8/14/08 7:30	1	62.7	88.3	0.0107	26.74	75.6	59.6	0.0112	30.5	69.9	67.1	0.0104	28.21	10.50	6.30	3.99	-6.74	-7.92	1.31
8/14/08 7:45	0	63.6	88.6	0.0111	27.39	75.6	59	0.0111	30.38	65.7	70.4	0.0094	26.12	0.00	0.00	0.00	0.00	0.00	0.00
8/14/08 8:00	1	64.1	86.2	0.011	27.39	75.5	58.6	0.0110	30.23	62.7	78.3	0.0094	25.4	22.14	14.12	7.54	9.12	1.54	7.34
8/14/08 8:15	0	64.9	86.1	0.0113	27.92	75.4	58.7	0.0110	30.18	61.2	81	0.0093	24.84	0.00	0.00	0.00	0.00	0.00	0.00
8/14/08 8:30	2	66.1	83.1	0.0113	28.29	75.4	59.9	0.0112	30.43	61.5	81.5	0.0094	25.08	49.05	30.55	17.34	29.43	10.12	18.60
8/14/08 8:45	16	67.1	79.3	0.0112	28.38	75.3	59.6	0.0111	30.3	60.8	84.7	0.0096	25.06	384.32	255.37	120.56	243.50	110.90	127.57

		Outdoor Air Conditions				Indoor Air Conditions				Supply Air Conditions				System Capacities			EAHE Capacities		
Date - Time	Airflow (CFM)	OAT (°F)	OA-RH (%)	OA-H.Ratio (w)	OA-Enthalpy (Btu/lbm)	Average RAT (°F)	RA-RH (%)	RA-H.Ratio (w)	RA-Enthalpy (Btu/lbm)	SAT (°F)	SA-RH (%)	SA-H.Ratio (w)	SA-Enthalpy (Btu/lbm)	System Total C. Capacity	System Sensible C. Capacity	System Latent C. Capacity	EAHE Total C. Capacity	EAHE Sensible C. Capacity	EAHE Latent C. Capacity
8/14/08 9:00	22	68.3	76.8	0.0113	28.79	75.2	59.6	0.0111	30.24	60.7	85.9	0.0097	25.14	514.32	351.32	151.54	368.10	183.95	175.08
8/14/08 9:15	25	70.2	74.9	0.0118	29.77	75.1	59.3	0.0110	30.11	60.6	86.5	0.0097	25.16	567.27	399.65	155.91	528.31	264.04	251.98
8/14/08 9:30	32	72.5	66.9	0.0114	29.89	75.1	59.4	0.0110	30.13	60.6	87	0.0097	25.22	720.24	509.39	193.80	685.03	418.94	249.84
8/14/08 9:45	35	72.2	65.9	0.0111	29.5	75.1	59.3	0.0110	30.11	60.7	87.6	0.0098	25.36	762.09	552.70	190.86	664.22	442.81	206.18
8/14/08 10:00	34	72.6	63.6	0.0108	29.33	75.0	59	0.0109	29.98	60.7	87.8	0.0099	25.38	716.94	536.05	166.72	615.63	445.12	156.79
8/14/08 10:15	36	74.6	58.8	0.0107	29.68	75.0	59.3	0.0109	30.04	60.7	88.4	0.0099	25.46	755.81	566.36	173.20	696.40	550.52	131.17
8/14/08 10:30	93	77	54.6	0.0108	30.34	75.0	61	0.0113	30.4	60.8	89	0.0101	25.59	2050.5	1453.66	542.88	2024.98	1657.50	321.21
8/14/08 10:45	65	78.2	55.6	0.0114	31.35	75.0	61.2	0.0113	30.44	61	89.6	0.0102	25.8	1382.5	1000.05	347.81	1653.68	1229.98	385.76
8/14/08 11:00	48	77.4	57.7	0.0115	31.29	75.0	61.5	0.0114	30.5	61	89.9	0.0102	25.84	1025.3	739.31	263.85	1199.17	866.05	308.22
8/14/08 11:15	58	77.5	53.3	0.0107	30.37	75.0	62.2	0.0115	30.64	61	90	0.0102	25.85	1273.5	895.78	349.86	1201.74	1052.85	121.32
8/14/08 11:30	95	77.9	53.8	0.0109	30.74	75.1	62.2	0.0115	30.71	61.1	90	0.0103	25.91	2090.3	1462.41	577.66	2103.37	1755.86	300.39
8/14/08 11:45	81	79.2	50.7	0.0107	30.86	75.1	63.4	0.0118	30.96	61.2	90.1	0.0103	25.99	1845.3	1242.78	563.46	1808.25	1604.03	165.49
8/14/08 12:00	85	81	48.6	0.0109	31.5	75.2	64	0.0119	31.15	61.4	90.8	0.0105	26.21	1924.8	1291.21	587.15	2061.20	1832.87	181.93
8/14/08 12:15	94	81.2	48.2	0.0109	31.53	75.3	64.7	0.0121	31.37	61.5	90.3	0.0105	26.21	2223.4	1429.51	740.77	2292.37	2037.28	201.20
8/14/08 12:30	70	79.6	50.4	0.0108	31.05	75.4	64.7	0.0121	31.44	61.5	91.2	0.0106	26.33	1639.7	1071.64	531.21	1514.55	1393.90	88.53
8/14/08 12:45	88	81	48.5	0.0109	31.48	75.5	64.7	0.0122	31.51	61.6	91.2	0.0106	26.4	2061.3	1347.21	667.80	2049.23	1878.19	128.42
8/14/08 13:00	14	81.3	44.5	0.0101	30.65	75.6	65.1	0.0123	31.66	61.6	91.2	0.0106	26.4	3423.8	2185.92	1160.4	2766.44	3077.59	-359.20
8/14/08 13:15	13	82.7	45.8	0.0109	31.87	75.7	65.5	0.0124	31.82	61.7	90.5	0.0106	26.37	3272.7	2014.37	1172.5	3302.77	3026.54	197.55
8/14/08 13:30	16	82.2	47	0.0110	31.87	75.8	65.4	0.0124	31.87	61.7	91.2	0.0106	26.46	4191.1	2612.99	1463.3	4191.11	3811.50	279.52
8/14/08 13:45	17	81.8	49.8	0.0115	32.33	75.8	65.9	0.0125	31.97	61.8	92.2	0.0108	26.66	4137.9	2624.14	1422.3	4418.52	3740.54	578.88
8/14/08 14:00	12	81.9	50.4	0.0117	32.56	75.9	66.2	0.0126	32.11	61.9	92.6	0.0109	26.78	3151.8	1990.16	1085.6	3417.92	2838.41	495.75
8/14/08 14:15	14	82.6	48.4	0.0115	32.5	76.0	66.9	0.0128	32.33	62	92.6	0.0109	26.85	3692.6	2262.89	1337.2	3807.24	3331.50	386.15
8/14/08 14:30	13	82.8	45	0.0107	31.72	76.1	67.2	0.0129	32.47	62.1	92.6	0.0110	26.91	3415.2	2068.44	1258.0	2954.57	3051.62	-162.96

		Outdoor Air Conditions				Indoor Air Conditions				Supply Air Conditions				System Capacities			EAHE Capacities		
Date - Time	Airflow (CFM)	OAT (°F)	OA-RH (%)	OA-H.Ratio (w)	OA-Enthalpy (Btu/lbm)	Average RAT (°F)	RA-RH (%)	RA-H.Ratio (w)	RA-Enthalpy (Btu/lbm)	SAT (°F)	SA-RH (%)	SA-H.Ratio (w)	SA-Enthalpy (Btu/lbm)	System Total C. Capacity	System Sensible C. Capacity	System Latent C. Capacity	EAHE Total C. Capacity	EAHE Sensible C. Capacity	EAHE Latent C. Capacity
8/14/08 14:45	17	83.2	48	0.0116	32.79	76.2	66.7	0.0129	32.43	62.2	92.7	0.0110	26.99	4264.2	2633.78	1522.2	4546.41	3950.67	482.47
8/14/08 15:00	15	83.2	45.1	0.0109	32	76.3	66.4	0.0128	32.44	62.3	92.5	0.0110	27.04	3737.7	2332.13	1322.1	3433.23	3471.99	-110.18
8/14/08 15:15	19	83.6	46.9	0.0115	32.75	76.4	66.9	0.0130	32.62	62.4	92.8	0.0111	27.14	4797.9	2945.06	1728.1	4911.80	4454.77	343.78
8/14/08 15:30	15	83.3	47.7	0.0116	32.77	76.5	65.8	0.0128	32.46	62.5	92.7	0.0111	27.2	3665.0	2343.71	1227.4	3881.00	3478.27	310.55
8/14/08 15:45	17	83.7	46	0.0113	32.57	76.6	65.9	0.0129	32.55	62.5	93.1	0.0112	27.25	4227.3	2703.55	1413.5	4243.32	4058.27	84.64
8/14/08 16:00	17	84	45.7	0.0113	32.68	76.7	65.9	0.0129	32.62	62.5	92.9	0.0112	27.22	4356.6	2743.56	1498.2	4405.04	4163.01	145.55
8/14/08 16:15	16	82.9	48.2	0.0115	32.64	76.7	65.4	0.0128	32.51	62.6	92.7	0.0112	27.27	3891.2	2521.21	1284.5	3987.80	3617.99	275.82
8/14/08 16:30	11	83.5	47.7	0.0116	32.91	76.8	65.6	0.0129	32.63	62.6	92.9	0.0112	27.29	2839.5	1818.07	953.64	2988.40	2667.23	248.29
8/14/08 16:45	13	82.7	44.3	0.0105	31.47	76.9	65	0.0128	32.57	62.6	93	0.0112	27.31	3327.4	2167.55	1074.0	2631.58	3051.62	-469.91
8/14/08 17:00	10	82.5	46.5	0.0110	31.93	76.9	65.5	0.0129	32.68	62.6	91.7	0.0111	27.13	2544.1	1577.46	904.80	2200.32	2189.32	-38.92
8/14/08 17:15	92	82	44.7	0.0104	31.14	77.0	65.1	0.0129	32.66	62.6	91.8	0.0111	27.15	2323.7	1452.82	810.04	1682.69	1963.57	-317.75
8/14/08 17:30	95	81.7	47.1	0.0108	31.57	77.0	65	0.0129	32.64	62.6	91.2	0.0110	27.07	2425.6	1505.02	864.19	1959.66	1996.24	-73.94
8/14/08 17:45	86	81.4	47.6	0.0108	31.51	77.0	64.5	0.0128	32.53	62.6	91.4	0.0110	27.09	2144.5	1364.62	727.93	1742.47	1778.74	-79.49
8/14/08 18:00	79	80.5	50.2	0.0111	31.58	77.0	64.5	0.0128	32.53	62.5	91.4	0.0110	27.02	1995.3	1262.91	684.05	1651.34	1564.43	46.12
8/14/08 18:15	58	79.5	50.7	0.0109	31.05	77.1	64.1	0.0127	32.51	62.5	91.4	0.0110	27.02	1459.6	929.65	490.93	1071.46	1084.76	-36.68
8/14/08 18:30	63	78.7	50.4	0.0105	30.47	77.1	63.6	0.0126	32.4	62.4	91.5	0.011	26.97	1568.1	1017.26	511.80	1010.77	1129.75	-137.91
8/14/08 18:45	48	78.3	53.5	0.0110	30.93	77.1	63	0.0125	32.27	62.3	91.4	0.0109	26.89	1183.7	780.74	371.26	888.93	844.92	25.68
8/14/08 19:00	41	77.8	57.5	0.0117	31.52	77.1	62.7	0.0124	32.2	62.2	91.7	0.0109	26.86	1003.6	671.05	305.15	875.82	703.66	149.58
8/14/08 19:15	31	76.3	60.4	0.0117	31.14	77.0	62.2	0.0123	32.02	62.1	91.2	0.0108	26.73	751.73	509.48	224.69	626.68	484.29	128.18
8/14/08 19:30	15	76	63	0.0120	31.5	77.0	62.5	0.0124	32.09	61.9	90.4	0.0106	26.49	385.06	249.95	126.23	344.49	232.68	103.61
8/14/08 19:45	8	75.3	65.5	0.0122	31.54	77.1	62.8	0.0125	32.22	61.8	88.8	0.0104	26.22	220.03	134.25	80.17	195.10	118.82	71.61
8/14/08 20:00	3	74.3	66.1	0.0119	30.96	77.0	63.2	0.0125	32.24	61.8	87.8	0.0103	26.09	84.57	50.19	32.40	66.97	41.26	24.23
8/14/08 20:15	1	73.1	67.2	0.0116	30.35	77.1	63	0.0125	32.27	62	86.1	0.0101	25.99	28.79	16.57	11.43	19.99	12.21	7.30

		Outdoor Air Conditions				Indoor Air Conditions				Supply Air Conditions				System Capacities			EAHE Capacities		
Date - Time	Airflow (CFM)	OAT (°F)	OA-RH (%)	OA-H.Ratio (w)	OA-Enthalpy (Btu/lbm)	Average RAT (°F)	RA-RH (%)	RA-H.Ratio (w)	RA-Enthalpy (Btu/lbm)	SAT (°F)	SA-RH (%)	SA-H.Ratio (w)	SA-Enthalpy (Btu/lbm)	System Total C. Capacity	System Sensible C. Capacity	System Latent C. Capacity	EAHE Total C. Capacity	EAHE Sensible C. Capacity	EAHE Latent C. Capacity
8/14/08 20:30	1	72.4	71.7	0.0121	30.73	77.1	62.1	0.0123	32.07	62.7	84.9	0.0103	26.29	26.50	15.82	10.02	20.35	10.67	9.19
8/14/08 20:45	6	71.4	73.6	0.0121	30.38	77.1	61.4	0.0122	31.91	63.5	83.2	0.0103	26.57	146.87	89.67	53.41	104.79	52.15	49.91
8/14/08 21:00	1	70.5	75.9	0.0121	30.16	77.0	61.2	0.0121	31.8	63.4	84.2	0.0104	26.64	23.65	14.99	8.08	16.14	7.81	7.88
8/14/08 21:15	1	69.8	76.6	0.0119	29.79	77.0	60.8	0.0120	31.71	67.2	80.9	0.0115	28.7	13.80	10.83	2.68	5.00	2.86	1.99
8/14/08 21:30	1	69.3	79.2	0.0121	29.89	77.0	60.9	0.0120	31.73	71.5	82	0.0135	32	-1.24	6.08	-7.20	-9.67	-2.42	-7.00
8/14/08 21:45	1	68.8	79.1	0.0119	29.52	77.0	60.4	0.0119	31.62	72.6	78.5	0.0134	32.17	-2.52	4.84	-7.25	-12.15	-4.18	-7.64
8/14/08 22:00	1	68.5	78.7	0.0117	29.24	77.0	59.8	0.0118	31.49	74.4	76.3	0.0139	33.11	-7.43	2.84	-10.07	-17.74	-6.49	-10.75
8/14/08 22:15	1	67.9	78.9	0.0115	28.86	76.9	59.4	0.0117	31.33	74.7	75.2	0.0138	33.11	-8.16	2.46	-10.31	-19.48	-7.48	-11.43
8/14/08 22:30	1	67.5	79.2	0.0113	28.64	76.9	59.7	0.0117	31.4	74.4	74.6	0.0136	32.76	-6.23	2.73	-8.80	-18.89	-7.59	-10.80
8/14/08 22:45	1	67.2	81.1	0.0115	28.73	76.8	59.8	0.0117	31.35	74.4	73	0.0133	32.43	-4.95	2.68	-7.44	-16.96	-7.92	-8.56
8/14/08 23:00	1	66.9	81.4	0.0114	28.57	76.8	60.3	0.0118	31.46	74.7	72.6	0.0133	32.57	-5.09	2.29	-7.20	-18.34	-8.58	-9.24
8/14/08 23:15	1	66.3	82.1	0.0113	28.27	76.7	60.2	0.0118	31.37	74.9	71.9	0.0133	32.58	-5.55	2.02	-7.30	-19.76	-9.46	-9.73
8/14/08 23:30	1	65.8	83.2	0.0112	28.1	76.7	60.2	0.0118	31.37	74.7	72	0.0132	32.45	-4.95	2.19	-6.96	-19.94	-9.79	-9.63
8/14/08 23:45	1	65.5	85.3	0.0114	28.21	76.7	60.8	0.0119	31.5	74.4	71.9	0.0131	32.21	-3.25	2.48	-5.64	-18.34	-9.79	-8.08
8/15/08 0:00	1	65.1	86.6	0.0114	28.13	76.6	60.6	0.0118	31.39	74.2	72.5	0.0131	32.18	-3.62	2.64	-6.13	-18.57	-10.01	-8.12
8/15/08 0:15	0	65	86	0.0113	27.97	76.5	60.3	0.0117	31.26	75	69.6	0.0129	32.18	0.00	0.00	0.00	0.00	0.00	0.00
8/15/08 0:30	1	65.1	87.4	0.0115	28.24	76.4	60.5	0.0117	31.23	74.9	67.6	0.0125	31.69	-2.11	1.70	-3.65	-15.81	-10.78	-4.62
8/15/08 0:45	1	64.3	87.7	0.0112	27.74	76.4	60.5	0.0117	31.23	74.7	67.5	0.0124	31.53	-1.38	1.88	-3.16	-17.37	-11.44	-5.50
8/15/08 1:00	1	64.5	88.8	0.0115	28.03	76.3	60.7	0.0117	31.21	74.6	67.3	0.0123	31.42	-0.96	1.91	-2.77	-15.54	-11.11	-4.04
8/15/08 1:15	1	64.3	89.1	0.0114	27.94	76.3	60.8	0.0117	31.23	74.2	67.6	0.0122	31.19	0.18	2.32	-2.14	-14.90	-10.89	-3.65
8/15/08 1:30	0	64.2	88.5	0.0113	27.78	76.2	60.9	0.0117	31.18	75	66.7	0.0123	31.57	0.00	0.00	0.00	0.00	0.00	0.00
8/15/08 1:45	1	63.7	88.7	0.0111	27.47	76.2	60.9	0.0117	31.18	74.4	66.6	0.0121	31.13	0.23	1.97	-1.75	-16.78	-11.77	-4.62
8/15/08 2:00	1	63.8	90.6	0.0114	27.8	76.1	60.9	0.0117	31.12	74.3	66.4	0.0120	31.02	0.46	2.01	-1.51	-14.76	-11.55	-2.82

2009 FORCED AIRFLOW TEST (SAMPLE DATA)

		Outdoor Air Conditions				Indoor Air Conditions				Supply Air Conditions				System Capacities			EAHE Capacities		
Date - Time	Airflow (CFM)	OAT (°F)	OA-RH (%)	OA-H.Ratio (w)	OA-Enthalpy (Btu/lbm)	Average RAT (°F)	RA-RH (%)	RA-H.Ratio (w)	RA-Enthalpy (Btu/lbm)	SAT (°F)	SA-RH (%)	SA-H.Ratio (w)	SA-Enthalpy (Btu/lbm)	System Total C. Capacity	System Sensible C. Capacity	System Latent C. Capacity	EAHE Total C. Capacity	EAHE Sensible C. Capacity	EAHE Latent C. Capacity
8/6/09 15:30	1765.5	81.5	45.8	0.010	31.11	72.0	60.5	0.01	28.3	67.7	68.3	0.009	27.03	10763.7	8416.7	2226.46	33019.65	26804.1	5549.69
8/6/09 15:45	1762.5	81.2	45.8	0.010	30.92	72.0	58.8	0.00	28.0	68.2	68.8	0.010	27.42	5089.96	7432.9	-2384.31	28277.55	25207.4	2494.65
8/6/09 16:00	1753.5	81.2	45.9	0.010	30.95	72.1	60.9	0.01	28.5	68.6	68.8	0.010	27.67	6671.58	6735.8	-242.11	26364.78	24307.0	1452.46
8/6/09 16:15	1784.5	81.3	46.1	0.010	31.06	72.2	62.3	0.01	28.8	69	68.4	0.010	27.86	7852.94	6249.6	1424.04	26176.47	24147.7	1453.70
8/6/09 16:30	1759.0	81.4	46.4	0.010	31.20	72.3	61.9	0.01	28.8	69.4	68.4	0.010	28.12	5563.65	5644.2	-115.07	24834.83	23222.1	1079.70
8/6/09 16:45	1769.0	81.6	46.8	0.010	31.42	72.4	60	0.01	28.5	69.5	66	0.010	27.77	6081.82	5579.0	287.51	29598.20	23548.8	5396.73
8/6/09 17:00	1754.5	81.6	47.3	0.010	31.55	72.5	60.4	0.01	28.6	69.7	67.5	0.010	28.16	4021.31	5356.3	-1442.84	27264.51	22969.7	3711.01
8/6/09 17:15	1783.5	81	47.8	0.010	31.31	72.5	60.9	0.01	28.7	69.8	67.4	0.010	28.2	4496.56	5281.4	-894.67	25426.00	21975.9	2889.85
8/6/09 17:30	1749.5	80.8	48.5	0.010	31.35	72.6	61.8	0.01	28.9	70	68.3	0.010	28.49	4009.85	4924.1	-1083.16	22936.36	20787.0	1676.20
8/6/09 17:45	1771.0	80.6	49.2	0.010	31.41	72.6	60.6	0.01	28.7	70	67.5	0.010	28.35	3328.49	5049.5	-1795.24	24841.89	20652.8	3622.42
8/6/09 18:00	1759.5	79.4	50.1	0.010	30.84	72.6	61.5	0.01	28.9	69.9	67.5	0.010	28.28	5242.61	5226.4	-133.28	20647.80	18389.4	1756.93
8/6/09 18:15	1775.5	78.4	50.9	0.010	30.41	72.5	61.7	0.01	28.9	69.7	68	0.010	28.24	5371.67	5534.4	-197.17	17661.40	16994.0	281.72
8/6/09 18:30	1785.0	78	51.9	0.010	30.37	72.5	61.5	0.01	28.8	69.5	68.8	0.010	28.25	4991.29	5793.1	-951.54	17346.77	16692.1	309.11
8/6/09 18:45	1779.0	77.9	52.9	0.010	30.53	72.4	62.2	0.01	28.9	69.4	68.4	0.010	28.12	6605.50	5838.9	643.01	19653.40	16636.0	2637.58
8/6/09 19:00	1776.5	77.7	53.9	0.010	30.64	72.4	62.5	0.01	28.9	69.4	68.8	0.010	28.18	6596.22	5781.8	550.95	20032.95	16221.8	3315.10
8/6/09 19:15	1793.5	77.6	55.0	0.011	30.82	72.3	64.2	0.01	29.2	69.5	71.8	0.011	28.76	4028.49	5607.0	-1624.90	16936.09	15982.4	528.74
8/6/09 19:30	1783.0	77.8	56.1	0.011	31.19	72.4	65.2	0.01	29.5	69.7	74.3	0.011	29.33	1389.46	5230.8	-3882.79	15202.29	15888.8	-951.48
8/6/09 19:45	1786.5	77.1	57.2	0.011	30.98	72.4	66	0.01	29.6	69.6	75	0.011	29.38	2211.12	5535.9	-3298.28	13102.91	14740.7	-1921.07
8/6/09 20:00	1772.5	76.5	58.3	0.011	30.82	72.4	67.1	0.01	29.8	69.5	75.9	0.011	29.46	3250.06	5557.6	-2502.24	11050.19	13650.2	-2835.24
8/6/09 20:15	1782.0	76.3	59.4	0.011	30.93	72.4	67.5	0.01	29.9	69.6	76	0.011	29.55	3104.10	5391.3	-2405.79	11272.79	13135.2	-2109.09

		Outdoor Air Conditions				Indoor Air Conditions				Supply Air Conditions				System Capacities			EAHE Capacities		
Date - Time	Airflow (CFM)	OAT (°F)	OA-RH (%)	OA-H.Ratio (w)	OA-Enthalpy (Btu/lbm)	Average RAT (°F)	RA-RH (%)	RA-H.Ratio (w)	RA-Enthalpy (Btu/lbm)	SAT (°F)	SA-RH (%)	SA-H.Ratio (w)	SA-Enthalpy (Btu/lbm)	System Total C. Capacity	System Sensible C. Capacity	System Latent C. Capacity	EAHE Total C. Capacity	EAHE Sensible C. Capacity	EAHE Latent C. Capacity
8/6/09 20:30	1772.5	76	60.5	0.011	30.96	72.3	67.7	0.01	29.9	69.5	76.4	0.011	29.55	2843.80	5525.1	-2624.25	11456.45	12675.2	-1449.14
8/6/09 20:45	1778.0	75.5	61.6	0.011	30.85	72.3	68.2	0.01	30	69.4	76.7	0.011	29.53	3830.67	5623.7	-1938.40	10758.46	11932.1	-1420.04
8/6/09 21:00	1760.0	75	62.6	0.011	30.73	72.2	67.8	0.01	29.8	69.3	78.3	0.011	29.73	1048.82	5679.7	-4631.78	8067.84	11036.8	-3199.71
8/6/09 21:15	1763.5	74.8	63.6	0.011	30.79	72.2	68.3	0.01	29.9	69.2	78.2	0.011	29.65	2425.17	5788.0	-3412.62	9215.63	10864.7	-1809.71
8/6/09 21:30	1763.5	74.6	64.5	0.011	30.84	72.2	68.5	0.01	29.9	69.1	77.3	0.011	29.42	4607.81	5917.4	-1566.13	11479.12	10670.7	534.15
8/6/09 21:45	1767.5	74.4	65.4	0.011	30.88	72.1	68.3	0.01	29.8	69.1	79	0.012	29.71	1377.38	5833.6	-4469.13	9479.60	10306.0	-1059.25
8/6/09 22:00	1782.0	74.4	66.1	0.012	31.04	72.0	68.2	0.01	29.7	69.1	77.5	0.011	29.46	2695.67	5767.0	-2982.66	12906.53	10390.5	2185.78
8/6/09 22:15	1775.5	74.5	66.8	0.012	31.24	72.0	68	0.01	29.7	69.1	77.7	0.011	29.49	2197.50	5746.0	-3533.97	14243.06	10548.0	3358.20
8/6/09 22:30	1777.5	74.8	67.4	0.012	31.57	72.1	68.5	0.01	29.9	69.2	77.4	0.011	29.51	3340.70	5605.8	-2411.36	16785.00	10950.9	5434.14
8/6/09 22:45	1785.0	74.8	67.9	0.012	31.67	72.1	68.4	0.01	29.9	69.3	77.7	0.011	29.63	2209.26	5433.1	-3334.36	16692.18	10800.8	5455.87
8/6/09 23:00	1778.0	74.8	68.2	0.012	31.74	72.1	68.5	0.01	29.9	69.3	77.9	0.011	29.67	2037.59	5395.5	-3442.84	16871.23	10758.4	5724.65
8/6/09 23:15	1779.5	74.8	68.4	0.012	31.79	72.1	69.2	0.01	30.0	69.3	78.3	0.011	29.73	2610.31	5449.0	-2947.56	16803.89	10767.5	5538.18
8/6/09 23:30	1783.5	74.6	68.5	0.012	31.66	72.1	69.5	0.01	30.1	69.3	78.6	0.012	29.78	2697.94	5444.9	-2914.09	15370.06	10399.3	4520.06
8/6/09 23:45	1777.0	74.3	68.4	0.012	31.43	72.1	69.4	0.01	30.0	69.2	79.4	0.012	29.85	1954.98	5604.2	-3764.55	12870.31	9970.42	2568.29
8/7/09 0:00	1784.5	74.2	69.7	0.012	31.61	72.1	70.2	0.01	30.2	69.2	80.4	0.012	30.02	1799.63	5627.9	-3940.11	13006.44	9816.17	2886.53
8/7/09 0:15	1784.0	73.8	69.2	0.012	31.23	72.0	70.7	0.01	30.2	69.1	80.9	0.012	30.03	1880.91	5773.5	-3851.89	9813.43	9224.62	332.31
8/7/09 0:30	1780.5	73.4	69.1	0.012	30.93	72.0	71.4	0.01	30.3	69	82.9	0.012	30.3	734.56	5843.8	-5114.07	5141.94	8618.87	-3595.18
8/7/09 0:45	1803.0	73.2	69.3	0.012	30.83	71.9	72.7	0.01	30.5	68.9	84.3	0.012	30.46	826.50	6033.4	-5105.31	3058.03	8529.43	-5528.97
8/7/09 1:00	1787.5	73	69.8	0.012	30.79	71.9	74.2	0.01	30.8	68.9	83.4	0.012	30.31	4342.77	5948.7	-1630.47	3933.07	8062.79	-4212.37
8/7/09 1:15	1802.5	72.8	70.6	0.012	30.79	71.9	75	0.01	30.9	68.8	86.3	0.013	30.73	2148.29	6163.9	-3969.42	495.76	7932.15	-7340.40
8/7/09 1:30	1782.5	72.6	71.5	0.012	30.84	71.9	75.5	0.01	31.0	68.8	86	0.012	30.67	3431.81	6013.8	-2785.19	1389.07	7451.93	-6137.77
8/7/09 1:45	1786.0	72.5	72.6	0.012	30.98	71.9	75.6	0.01	31.1	68.7	87	0.013	30.77	2783.59	6222.1	-3580.48	1719.28	7466.56	-5758.38
8/7/09 2:00	1782.0	72.3	73.9	0.012	31.07	71.8	76.6	0.01	31.2	68.7	88.5	0.013	31.02	1633.74	6077.5	-4469.39	408.43	7057.74	-6597.55

		Outdoor Air Conditions				Indoor Air Conditions				Supply Air Conditions				System Capacities			EAHE Capacities		
Date - Time	Airflow (CFM)	OAT (°F)	OA-RH (%)	OA-H.Ratio (w)	OA-Enthalpy (Btu/lbm)	Average RAT (°F)	RA-RH (%)	RA-H.Ratio (w)	RA-Enthalpy (Btu/lbm)	SAT (°F)	SA-RH (%)	SA-H.Ratio (w)	SA-Enthalpy (Btu/lbm)	System Total C. Capacity	System Sensible C. Capacity	System Latent C. Capacity	EAHE Total C. Capacity	EAHE Sensible C. Capacity	EAHE Latent C. Capacity
8/7/09 2:15	1783.0	72.1	75.3	0.012	31.19	71.8	76.5	0.01	31.2	68.6	89.3	0.013	31.08	980.79	6260.7	-5277.06	899.06	6865.54	-5987.48
8/7/09 2:30	1781.5	72	76.7	0.012	31.38	71.8	77	0.01	31.2	68.5	89.3	0.013	31	2368.25	6418.7	-4129.32	3103.23	6859.77	-3837.47
8/7/09 2:45	1783.0	71.7	78.1	0.012	31.43	71.7	77	0.01	31.2	68.5	90.1	0.013	31.13	735.59	6342.4	-5574.77	2451.98	6277.07	-3884.79
8/7/09 3:00	1775.0	71.5	79.6	0.013	31.56	71.7	77.8	0.01	31.3	68.4	90	0.013	31.04	2685.08	6395.3	-3839.71	4231.03	6053.63	-1930.64
8/7/09 3:15	1785.0	71.4	81.1	0.013	31.76	71.7	77.9	0.01	31.3	68.3	91.1	0.013	31.15	1963.79	6611.4	-4752.74	4991.29	6087.73	-1197.77
8/7/09 3:30	1785.0	71.3	82.6	0.013	31.96	71.7	79.3	0.01	31.6	68.4	94.2	0.014	31.74	-736.42	6415.0	-7194.30	1800.14	5694.97	-3965.68
8/7/09 3:45	1780.5	68.8	84.0	0.012	30.34	71.6	80.5	0.01	31.8	68.3	98	0.014	32.29	-3999.29	6464.1	10380.49	15915.53	979.417	16420.0
8/7/09 4:00	1794.0	68.7	85.4	0.012	30.50	71.5	81.7	0.01	31.9	68.1	100	0.014	32.46	-4276.32	6743.4	10705.42	16118.44	1184.21	16707.2
8/7/09 4:15	1784.0	69	86.7	0.013	30.94	71.6	81.6	0.01	32	68.2	100	0.014	32.54	-4416.04	6575.0	10837.15	13084.57	1570.14	14139.4
8/7/09 4:30	1786.5	69	87.9	0.013	31.15	71.6	82.1	0.01	32.0	68.2	100	0.014	32.54	-3685.19	6649.7	10115.76	11383.15	1572.34	12516.1
8/7/09 4:45	1770.0	69.3	89.1	0.013	31.57	71.6	83	0.01	32.2	68.4	99	0.014	32.54	-2271.83	6263.7	-8424.99	-7870.27	1752.55	-9385.46
8/7/09 5:00	1777.5	69.4	90.1	0.013	31.82	71.7	83.2	0.01	32.3	68.5	100	0.014	32.79	-3422.19	6159.9	-9394.08	-7903.62	1759.98	-9258.84
8/7/09 5:15	1773.0	68.9	91.0	0.013	31.59	71.6	82.6	0.01	32.1	68.3	99.8	0.014	32.59	-3332.25	6436.9	-9626.55	-8127.43	1170.35	-9058.29
8/7/09 5:30	1786.0	68.8	91.8	0.013	31.65	71.5	82.6	0.01	32.1	68.1	100	0.014	32.46	-2865.46	6713.3	-9336.68	-6631.49	1375.42	-7704.81
8/7/09 5:45	1769.0	68.8	92.5	0.013	31.76	71.4	82.4	0.01	31.9	68	100	0.014	32.38	-3162.55	6681.9	-9498.44	-5027.64	1556.94	-6291.17
8/7/09 6:00	1772.0	69	93.0	0.014	32.01	71.4	82.4	0.01	31.9	68.1	100	0.014	32.46	-3817.74	6498.2	-9961.03	-3655.28	1754.53	-5167.01
8/7/09 6:15	1759.5	69.1	93.4	0.014	32.16	71.4	83.5	0.01	32.2	68.1	100	0.014	32.46	-2097.04	6436.3	-8305.12	-2419.66	1935.73	-4143.88
8/7/09 6:30	1755.5	69.3	93.7	0.014	32.37	71.4	82.8	0.01	32.0	68.2	100	0.014	32.54	-3782.19	6244.6	-9736.83	-1368.03	2124.46	-3331.05
8/7/09 6:45	1763.0	69.3	93.9	0.014	32.40	71.5	83	0.01	32.1	68.2	100	0.014	32.54	-2909.37	6303.6	-9082.32	-1131.42	2133.54	-3124.25
8/7/09 7:00	1768.5	69.2	93.9	0.014	32.32	71.5	82.6	0.01	32.1	68.2	100	0.014	32.54	-3485.93	6339.5	-9692.21	-1783.50	1945.63	-3520.55
8/7/09 7:15	1760.5	69.2	93.8	0.014	32.31	71.4	83.1	0.01	32.1	68.2	100	0.014	32.54	-3389.46	6246.2	-9331.87	-1856.13	1936.83	-3626.66
8/7/09 7:30	1769.5	69.3	93.6	0.014	32.35	71.5	83.4	0.01	32.2	68.3	100	0.014	32.62	-2920.10	6132.2	-8982.49	-2190.07	1946.73	-3951.04
8/7/09 7:45	1761.0	69.5	93.3	0.014	32.45	71.5	84	0.01	32.3	68.4	100	0.014	32.7	-2663.90	5925.1	-8518.24	-2018.11	2131.11	-3967.60

		Outdoor Air Conditions				Indoor Air Conditions				Supply Air Conditions				System Capacities			EAHE Capacities		
Date - Time	Airflow (CFM)	OAT (°F)	OA-RH (%)	OA-H.Ratio (w)	OA-Enthalpy (Btu/lbm)	Average RAT (°F)	RA-RH (%)	RA-H.Ratio (w)	RA-Enthalpy (Btu/lbm)	SAT (°F)	SA-RH (%)	SA-H.Ratio (w)	SA-Enthalpy (Btu/lbm)	System Total C. Capacity	System Sensible C. Capacity	System Latent C. Capacity	EAHE Total C. Capacity	EAHE Sensible C. Capacity	EAHE Latent C. Capacity
8/7/09 8:00	1761.5	69.8	92.8	0.014	32.61	71.5	84.6	0.01	32.4	68.5	100	0.014	32.79	-2503.16	5829.9	-8100.59	-1453.45	2519.31	-3732.71
8/7/09 8:15	1758.5	70.2	92.3	0.014	32.84	71.6	84.3	0.01	32.5	68.7	100	0.015	32.95	-3627.43	5642.6	-9008.50	-886.71	2901.94	-3659.59
8/7/09 8:30	1758.5	71.3	91.6	0.015	33.61	71.7	84.5	0.01	32.6	68.9	99.9	0.015	33.1	-3949.87	5416.9	-9209.13	4111.09	4643.11	-644.14
8/7/09 8:45	1758.0	73.1	90.8	0.015	34.96	71.9	85.2	0.01	32.9	69.4	100	0.015	33.53	-5076.96	4738.5	-9636.07	11523.90	7156.10	4184.54
8/7/09 9:00	1781.0	72.6	90.0	0.015	34.38	72.1	85.1	0.01	33.0	69.7	100	0.015	33.78	-6041.44	4604.5	10463.44	4898.46	5682.21	-844.15
8/7/09 9:15	1766.5	71.5	89.0	0.014	33.30	72.1	84.3	0.01	32.8	69.5	99.2	0.015	33.48	-4777.61	5020.5	-9676.38	-1457.57	3886.86	-5297.10
8/7/09 9:30	1754.0	71.5	88.0	0.014	33.11	72.2	84	0.01	32.9	69.6	99.2	0.015	33.56	-5226.22	4936.7	10090.85	-3618.15	3666.39	-7193.53
8/7/09 9:45	1775.5	71.8	86.9	0.014	33.15	72.2	85.5	0.01	33.2	69.7	99.3	0.015	33.66	-3743.89	4899.6	-8573.03	-4150.83	4102.00	-8182.49
8/7/09 10:00	1725.5	72.2	85.8	0.014	33.25	72.3	85.3	0.01	33.2	69.9	99.3	0.015	33.83	-4666.72	4524.3	-9115.65	-4587.62	4366.14	-8838.57
8/7/09 10:15	1757.0	73.5	84.6	0.014	34.06	72.4	84.5	0.01	33.1	70.1	99.5	0.015	34.04	-7087.60	4445.8	11259.93	161.08	6572.13	-6377.43
8/7/09 10:30	1750.5	75.2	83.3	0.015	35.20	72.6	85.9	0.01	33.5	70.5	98.1	0.015	34.12	-4252.87	4028.1	-8195.39	8666.24	9051.40	-657.33
8/7/09 10:45	1764.5	76.1	82.0	0.015	35.68	72.8	85.4	0.01	33.6	70.8	97.3	0.015	34.23	-4610.43	3850.1	-8422.86	11728.28	10288.5	1061.22
8/7/09 11:00	1769.5	77.4	80.7	0.016	36.49	73.0	86.1	0.01	33.9	71.4	97.3	0.016	34.75	-6489.11	3082.3	-9355.47	14113.82	11680.3	2034.89
8/7/09 11:15	1757.0	78.6	79.4	0.016	37.22	73.3	85.6	0.01	34.1	71.9	96.6	0.016	35.05	-7651.38	2657.8	10105.27	17477.37	12950.9	3969.56
8/7/09 11:30	1760.5	80.9	78.1	0.017	38.92	73.6	87.2	0.01	34.6	72.7	95.7	0.016	35.57	-7263.12	1775.4	-8833.46	27034.94	15882.0	10265.9
8/7/09 11:45	1757.0	82.5	76.7	0.018	40.02	74.0	87.2	0.01	35	73.3	95.5	0.016	36.06	-8537.33	1320.8	-9634.12	31894.19	17783.4	13087.7
8/7/09 12:00	1763.5	83.6	75.4	0.018	40.67	74.4	86.3	0.01	35.1	73.9	95.3	0.017	36.55	11317.4	889.23	11959.57	33305.60	18819.2	13370.0
8/7/09 12:15	1769.5	84.8	74.1	0.019	41.42	74.7	86.1	0.01	35.3	74.5	93.6	0.017	36.74	11193.7	405.57	11241.19	37961.30	20051.3	16602.5
8/7/09 12:30	1748.0	85.8	72.8	0.019	41.98	75.1	86.5	0.01	35.7	75	93	0.017	37.07	10256.4	128.21	10139.13	39343.01	20769.2	17265.4
8/7/09 12:45	1740.0	86.7	71.5	0.019	42.45	75.4	86.3	0.01	36	75.5	93.5	0.017	37.63	13001.1	-159.52	12382.12	38445.09	21439.9	15704.3
8/7/09 13:00	1754.0	87.5	70.3	0.019	42.83	75.8	86.8	0.01	36.4	76	93.3	0.018	38.05	12784.1	-450.26	12004.84	38432.81	22191.3	14949.2
8/7/09 13:15	1738.5	88.4	69.1	0.020	43.31	76.1	87.2	0.01	36.8	76.5	90.7	0.017	37.93	-9005.29	-749.11	-7952.67	42874.75	22760.2	18640.1
8/7/09 13:30	1748.5	89.4	68.0	0.020	43.91	76.4	85.1	0.01	36.6	77	90	0.018	38.24	13064.6	1074.0	11497.30	45445.75	23853.0	20027.4

		Outdoor Air Conditions				Indoor Air Conditions				Supply Air Conditions				System Capacities			EAHE Capacities		
Date - Time	Airflow (CFM)	OAT (°F)	OA-RH (%)	OA-H.Ratio (w)	OA-Enthalpy (Btu/lbm)	Average RAT (°F)	RA-RH (%)	RA-H.Ratio (w)	RA-Enthalpy (Btu/lbm)	SAT (°F)	SA-RH (%)	SA-H.Ratio (w)	SA-Enthalpy (Btu/lbm)	System Total C. Capacity	System Sensible C. Capacity	System Latent C. Capacity	EAHE Total C. Capacity	EAHE Sensible C. Capacity	EAHE Latent C. Capacity
8/7/09 13:45	1740.0	89.9	66.9	0.020	44.03	76.7	85	0.01	36.8	77.3	89.1	0.018	38.31	11645.1	1068.8	10145.10	45623.64	24119.9	19919.5
8/7/09 14:00	1755.0	90.4	65.9	0.020	44.17	77.0	83.6	0.01	36.8	77.4	88.8	0.018	38.33	12308.7	-836.67	-1201.49	46982.33	25100.1	20194.6
8/7/09 14:15	1746.0	90.6	64.9	0.020	44.03	77.2	84.1	0.01	37.0	77.6	88.8	0.018	38.52	11525.2	-800.37	-0343.09	44100.19	24971.4	17616.8
8/7/09 14:30	1763.0	90.8	64.1	0.020	43.92	77.4	83.7	0.01	37.1	77.8	87.6	0.018	38.42	-0101.99	-792.00	-9051.58	44448.76	25214.5	17643.3
8/7/09 14:45	1747.5	91.6	63.3	0.020	44.41	77.7	81.9	0.01	37.0	78.2	85	0.017	38.18	-9292.23	-041.37	-8067.94	49905.66	25761.8	22384.1
8/7/09 15:00	1746.0	91.8	62.6	0.020	44.35	77.9	81.8	0.01	37.1	78.4	84.4	0.017	38.22	-8403.85	-056.48	-7196.37	49062.46	25739.7	21583.2
8/7/09 15:15	1741.5	92	62.0	0.020	44.32	78.0	81.4	0.01	37.1	78.6	84.1	0.017	38.33	-9340.15	-085.69	-7878.77	47818.39	25673.4	20431.4
8/7/09 15:30	1733.0	91.9	61.5	0.019	44.03	78.2	81.4	0.01	37.3	78.6	83.7	0.017	38.24	-7149.66	-826.18	-6145.88	45996.18	25357.4	19049.7
8/7/09 15:45	1743.0	92.9	61.0	0.020	44.83	78.3	80.4	0.01	37.1	78.9	83.1	0.017	38.36	-9348.20	-086.63	-7922.76	51694.73	26846.1	22990.8
8/7/09 16:00	1745.0	92.7	60.7	0.020	44.51	78.5	81.7	0.01	37.6	79.1	83.7	0.017	38.69	-8159.06	-103.87	-6727.46	46554.65	26108.9	18787.3
8/7/09 16:15	1739.0	92.4	60.5	0.019	44.13	78.7	79.7	0.01	37.3	79.1	83.2	0.017	38.57	-9565.89	-860.93	-8461.01	44321.96	25445.2	17323.1
8/7/09 16:30	1755.5	92.5	60.3	0.019	44.17	78.8	79.8	0.01	37.4	79.2	83.3	0.017	38.68	-9576.18	-853.00	-8573.18	44179.19	25686.7	16886.2
8/7/09 16:45	1738.0	91.8	60.3	0.019	43.48	78.9	80.2	0.01	37.6	79.2	84	0.018	38.85	-9401.05	-653.29	-8575.24	36887.17	24092.1	11502.4
8/7/09 17:00	1740.0	91.9	60.3	0.019	43.59	79.0	80.1	0.01	37.7	79.3	82.8	0.017	38.65	-7338.07	-574.28	-6543.18	39402.23	24119.9	13868.8
8/7/09 17:15	1736.5	89.8	60.4	0.018	41.70	78.9	79.2	0.01	37.4	78.6	82.5	0.017	37.95	-4139.26	477.61	-4600.35	29850.44	21396.7	7447.08
8/7/09 17:30	1738.5	90.2	60.6	0.018	42.13	78.9	79.1	0.01	37.4	78.8	83.1	0.017	38.27	-6933.28	111.57	-6895.89	30761.44	21803.9	7896.16
8/7/09 17:45	1741.0	90.9	60.9	0.019	42.87	79.1	80.5	0.01	37.9	79.2	83.3	0.017	38.68	-6065.37	-287.31	-5738.86	33439.32	22409.9	9857.21
8/7/09 18:00	1749.5	90.3	61.2	0.018	42.45	79.1	80.2	0.01	37.8	79.1	84.3	0.018	38.84	-8019.71	-32.08	-7693.20	28951.15	21556.9	6386.02
8/7/09 18:15	1745.5	89.5	61.7	0.018	41.86	79.1	80.4	0.01	37.8	79	84.7	0.018	38.84	-7601.30	208.04	-7531.09	24164.14	20163.4	3168.46
8/7/09 18:30	1748.5	88.9	62.1	0.018	41.48	79.2	80.4	0.01	37.9	78.9	84.5	0.018	38.7	-5770.89	496.94	-6155.97	22282.04	19236.2	2286.07
8/7/09 18:45	1743.0	88.5	62.7	0.018	41.30	79.1	81.3	0.01	38.1	78.8	84.6	0.017	38.63	-4154.75	639.19	-4619.16	21333.07	18600.5	1975.76
8/7/09 19:00	1735.5	87.9	63.3	0.018	40.95	79.1	81.2	0.01	38.0	78.6	85.6	0.018	38.69	-4773.32	1002.4	-5595.21	17979.50	17756.7	-371.95

Appendix, B

INSTRUMENTATION DATA SHEETS

FLUKE THERMOMETER 51-54 SERIES II

51, 52, 53, 54 Series II
Service Manual

Specifications

General Specifications

Weight	280 g (10 oz)
Dimensions (without holster)	2.8 cm × 7.8 cm × 16.2 cm (1.1 in × 3 in × 6.4 in)
Battery	3 AA batteries
Certification	CE, GS, (TÜV pending)
Safety	CSA C22.2 No. 1010.1 1992 EN 61010 Amendments 1, 2
CAT I	OVERVOLTAGE (Installation) CATEGORY I, Pollution Degree 2 per IEC1010-1*
* Refers to the level of Impulse Withstand Voltage protection provided. Equipment of OVERVOLTAGE CATEGORY I is equipment for connection to circuits in which measures are taken to limit the transient over voltages to an appropriate low level.	

Environmental

Operating Temperature	–10 °C to +50 °C (+14 °F to +122 °F)
Storage Temperature	–40 °C to +60 °C (–40 °F to +140 °F)
Humidity	Non Condensing (< 10 °C) (< 50 °F) 95% RH (+10 °C to +30 °C) (+50 °F to +86 °F) 75% RH (+30 °C to +40 °C) (+86 °F to +104 °F) 45% RH (+40 °C to +50 °C) (+104 °F to +122 °F) (Without Condensation)

Electrical

Measurement Range	J-type: –210 °C to +1200 °C (–346 °F to +2192 °F) K-type: –200 °C to +1372 °C (–328 °F to +2501 °F) T-type: –250 °C to +400 °C (–418 °F to +752 °F) E-type: –150 °C to +1000 °C (–238 °F to +1832 °F) N-type: –200 °C to +1300 °C (–328 °F to +2372 °F) R- and S-type: 0 °C to +1707 °C (+32 °F to +3212 °F)
Display Resolution	0.1 °C / °F / K < 1000° 1.0 °C / °F / K ≥ 1000°
Measurement Accuracy	J-, K-, T-, E-, and N-type: ±[0.05 % of reading + 0.3 °C (0.5 °F)] [below –100 °C (–148 °F): add 0.15 % of reading for J, K, E, and N; and 0.45 % of reading for T] R- and S-type: ±[0.05 % of reading + 0.4 °C (+0.7 °F)]
Temperature Coefficient	0.01 % of reading + 0.03 °C per °C (0.05 °F per °F) outside the specified +18 °C to +28 °C (+64 °F to +82 °F) range [below –100 °C (–148 °F): add 0.04 % of reading for J-, K-, E-, and N-type; and 0.08 % of reading for T-type]
Electromagnetic Compatibility	Susceptibility ± 2 °C (± 3.6 °F) for 80 MHz to 200 MHz in 1.5 V/m field, for 200 MHz to 1000 MHz in 3 V/m field. Emissions: Commercial limits per EN50081-1
Maximum Differential Common Mode Voltage	1 V (Maximum voltage difference between T1 and T2)
Temperature Scale	ITS-90
Applicable Standards	NIST-175
Accuracy is specified for ambient temperatures between +18 °C (+64 °F) and +28 °C (+82 °F) for a period of 1 year. The above specifications do not include thermocouple error.	

Performance Test and Calibration Required Test Equipment

Refer to Table 2 for a list of test equipment used in the performance test and calibration procedures.

Table 2. Recommended Test Equipment

Equipment	Required Characteristics	Recommended Model
DC Voltage Calibrator	Output Voltage: 0-1V Accuracy: 0.0125 % Resolution: 0.1 µV	Fluke 5700A or equivalent
Thermocouple connector	For K-type thermocouple	Fluke 80CK-M Fluke P/N 779942
Thermocouple connector	Copper	Fluke P/N 601747
K-type Thermocouple wire	Standard	Omega
Dewar Flask/Cap	1- pint, or larger capacity	Thermos
Mercury Thermometer (either °C or °F)	0.02 °C Resolution 0.05 °F Resolution	Princo Model ASTM50C Princo Model ASTM56F
DB9 Adapter Connector		Fluke P/N 804549
IR Adapter		Fluke P/N 690513
PC with Microsoft Windows® installed		

Performance Tests

Performance tests are recommended for incoming inspection, periodic maintenance, and for checking the thermometer's specifications. If the thermometer fails any part of the performance tests, calibration and/or repair is indicated.

Before performing these tests:

1. Allow the thermometer to stabilize to room temperature, +23 °C ± 5 °C (+73 °F ± 9 °F).
2. Check the batteries and replace them if necessary.

Display Test

Turn the thermometer on while pressing the HOLD button. All display segments are displayed until the HOLD button is released. Confirm that all the display segments are showing as in Figure 1.

DWYER SERIES 641RM AIR VELOCITY TRANSMITTER

Bulletin E-66-RM

Series 641RM Air Velocity Transmitter

Specifications - Installation and Operating Instructions

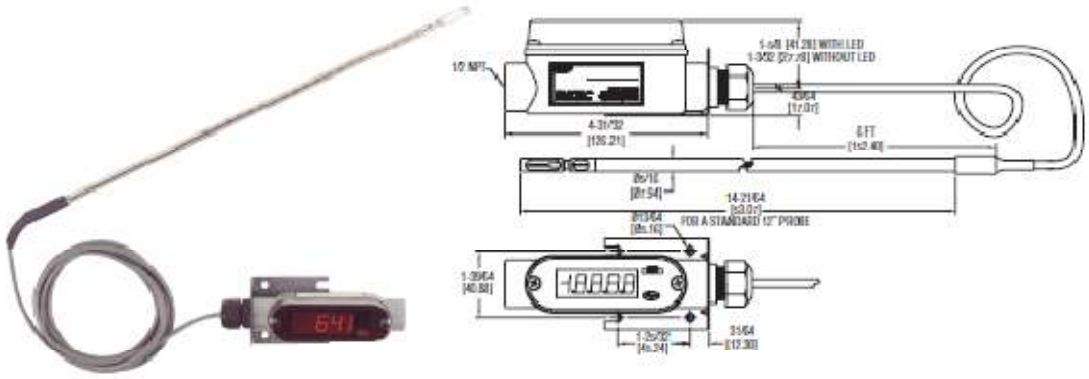

The Series 641RM Air Velocity Transmitter uses a heated mass flow sensor technology. It has 8 user selectable ranges from 250 FPM to 15000 FPM with corresponding metric ranges of 1.25 MPS to 75 MPS. The Series 641RM Air Velocity Transmitter provides an isolated 4-20 mA output proportional to the velocity. With the optional 1/2" 4-1/2 digit LED display, the Series 641RM Air Velocity Transmitter will provide a highly visible local readout of the velocity.

INSTALLATION

Location: Select a location where the temperature will be within 32 to 140°F (0 to 60°C) to mount the enclosure. The transmitter may be located any distance from the receiver provided that the total loop resistance does not exceed 600 ohms. The probe should be located where conditions are representative of the overall environment being monitored. Avoid locations where turbulence, stagnation, or rapidly fluctuating velocities or temperatures are present as these conditions may affect the readings. The filter setting may be used to average velocity readings in turbulent conditions.

Position: The transmitter is not position sensitive and may be mounted in any orientation.

Probe Orientation: Dots on the probe indicate the direction of the calibrated airflow. Align these dots toward the source of the process air.

Airflow: The Series 641RM Air Velocity Transmitter is intended for use with clean dry air. Particulates in the air may cause sensor damage. Dust accumulation may impair the velocity measurement and will require probe cleaning.

TO READ DISPLAY UNIT MUST BE MOUNTED HORIZONTALLY AS SHOWN ABOVE. DISPLAY CAN BE TURNED 180° SO CONDUIT OPENING CAN BE POSITIONED TO THE RIGHT OR LEFT.

SPECIFICATIONS

Service: Air and compatible, non-combustible gases.
Accuracy:
3% FS Process gas: 32 to 122°F (0 to 50°C).
4% FS Process gas: -40 to 32°F & 122 to 212°F (-40 to 0°C & 50 to 100°C).
Response Time: Flow: 1.5 seconds to 95% of final value (output filter set to minimum).
Temperature Limits: Process: -40 to 212°F (-40 to 100°C). Ambient: 32 to 140°F (0 to 60°C).
Pressure Limit: 100 psi (6.89 bar) maximum.
Humidity Limit: Non-Condensing.
Power Requirements: 12–35 VDC, 10–16 VAC.
Output Signal: 4-20 mA, isolated 24V source, 3 or 4-wire connection.
Output Filter: Selectable 0.5 –15 (seconds).
Loop Resistance: 600 ohms max.
Current Consumption: 300 mA max.
Electrical Connections: Screw terminal.
Mounting Orientation: Unit not position sensitive. Probe must be aligned with airflow.
Weight: 13.2 oz (374.26 g).
Cable Length: 6 ft (1.82 m).
Probe Length: 12" (30.48 cm) standard.
Probe Diameter: 5/16" (0.79 cm).

OPTIONAL DISPLAY VERSION:

Display: 4-1/2 digit 1/2" Red LED.
Resolution: 1 FPM, 0.01 MPS (10 FPM @ 10,000 and 15,000 FPM ranges).
Weight: 13.9 oz (394.16 g).

Agency Approvals: CE
The following standards were used for CE approval:
IEC 61000-4-2: 2001
IEC 61000-4-3: 2002
IEC 61000-4-4: 1995
IEC 61000-4-5: 2001
IEC 61000-4-6: 2003
IEC 55011: 1998
IEC 61326: 2002
89/336/EEC EMC Directive

DWYER INSTRUMENTS, INC.
P.O. BOX 373 • MICHIGAN CITY, INDIANA 46361, U.S.A.
Phone: 219/879-8000
Fax: 219/872-9057
www.dwyer-inst.com
e-mail: info@dwyer-inst.com

NOTE: Where conduit connections are not made, a 1/2" NPT cable seal should be used to prevent contaminants from entering the case. Where conduit connections are made, make sure that any possible condensation within the conduit will not flow into the transmitter housing.

ELECTRICAL CONNECTION

The Series 641RM Air Velocity Transmitter has been designed for easy and flexible connection to power and loop receivers. Electrical connection is made inside the body of the device with a "Euro" style terminal block. The device features a current loop that is fully isolated from the power source. The current loop has an internal 24V isolated supply so no external loop power is required. With full isolation, loop grounding is not a concern. The input power requirements are also very flexible. The device may be powered from either an AC or DC power source.

3 or 4-Wire Connection

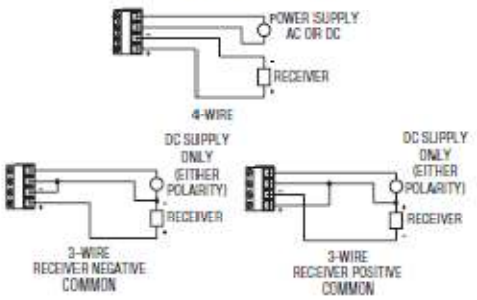

CAUTION: Do not exceed the specified supply voltage rating. Permanent damage not covered by the warranty may result. Do not use an external power source on the current loop connection.

Receiver-Transmitter Connection — The Series 641RM Air Velocity Transmitter is designed as a three or four wire 4-20 mA device. The current loop output is isolated from the power supply input and provides an internal 24-volt loop supply. With a DC power supply, a three or four-wire connection may be used. Do not use a three-wire connection with an AC power source. In a three-wire connection either power supply wire may be used as the common. The total loop resistance should not exceed 600 ohms.

CAUTION: Do not use a receiver with an internal power supply or use an external supply in the current loop. The current loop is powered from within the Series 641RM Air Velocity Transmitter. Connecting an external supply to the current loop may destroy the transmitter. Using an external supply voids the warranty.

Power Supply Connection — The power supply may be either AC or DC. The DC power may be from 12 to 35 volts. The power connection is not polarity sensitive so the positive and negative connections may be made to either power terminal. The AC connection may be from 10 to 16 VAC RMS. Do not exceed 20 VAC. When selecting a transformer please note that the specified output for transformers is at some specified current. With a load current less than the specified current transformer output may be significantly higher than the specified voltage. Transformers with secondary voltages of 10 to 16 VAC are recommended.

CAUTION: Do not use transformers with a secondary voltage rating greater than 16 VAC RMS.

Wire Type and Length — The wire selection for an installation is often overlooked or neglected and may contribute to improper or even intermittent operation. In all cases ensure that the connection meets all applicable national and local electrical codes. Although the 4-20 mA current loop systems are relatively immune to wire or wiring related problems, selection of the wire for some installations will be an important factor in ensuring satisfactory system operation. Twisted conductors will usually be immune to most stray electric and magnetic fields and to some extent electromagnetic fields, such as interference from RF transmitters. With twisted pair wiring the current loop and the power connections should be separate pairs. Avoid using flat or ribbon cable that has no regular conductor twist. Where interference is possible, it is recommended that shielded wire be used. The shield must not be used as one of the conductors and should be connected to ground at only one end, generally at the power supply. Similarly, if the installation uses conduit, the conduit should be connected to protective ground as specified by the applicable code and the signal wiring must not be connected to the conduit at more than one point or as specified by the code.

The maximum length of wire connecting the transmitter and receiver is a function of the wire resistance and receiver resistance. The total loop resistance must not exceed 600 ohms, including the receiver resistance and wire resistance. The power supply connection must be designed so that the worst case voltage drop due to wire resistance will not cause the power supply voltage at the transmitter to drop below the specified value. Provided the power supply voltage is maintained within the specified voltage range, the Series 641RM Air Velocity Transmitter is not affected by variations in power supply voltage.

TRANSMITTER SETUP

The Series 641RM Air Velocity Transmitter has been designed for easy setup. It has five configuration parameters that may be adjusted by the user. These parameters are Output Filter, Range (in English or Metric), span, 4 mA set-point and 20 mA set-point. All of these may be adjusted at any time in the field. These adjustments may also be easily returned to factory default.

Interior Label Diagram

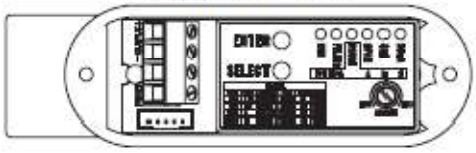

A set of controls and indicators are provided within the unit consisting of the select button, enter button, adjustment control, and six LED indicators. When operating normally, only the RUN LED indicator will be illuminated. During the setup operation the LED indicators will indicate the parameter selected, when it is being adjusted, and status of the adjustment process. If the unit is left in the setup mode for several minutes without any activity it will return to the normal operating mode.

Two buttons and a potentiometer control the setup process.
The SELECT button is used to scroll between the setup parameters.
The ENTER button allows access to each parameter for adjustment.
The ADJUST potentiometer is used to change the value of the parameters.
Holding the ENTER button for 2.5 seconds saves the new parameter value.

Making Adjustments
The adjustment process has three steps: select the parameter, adjust the parameter, save the new value. These are described in the following steps.

1. Select the parameter: Each time the SELECT button is pressed the LED indicator will advance to the next parameter. When the last parameter, SPAN, is selected, the next time the SELECT is pressed the unit will return to RUN mode. Press the SELECT button until the LED indicator illuminates the desired parameter. Press ENTER. The selected indicator will begin to blink, showing the parameter may now be adjusted. If the unit is left in the setup mode, after several minutes it will reset to the operate mode.

2. Adjust the parameter: Turn the ADJUST potentiometer until the desired setting is made. This may be adjusted using a small screwdriver or similar tool. Be careful not to force the control past its stops or damage will result.

3. Save the parameter: To save the new parameter press and hold the ENTER button. The LED indicator will begin to flash at a faster rate. After about 2.5 seconds all of the LED indicators will flash when the parameter is saved. If you do not want to save the parameter press the SELECT button without entering the parameter. The adjusted value will be discarded and next LED indicator will be illuminated.

Adjusting the Output Filter
The output filter may be adjusted to smooth the readings when measuring turbulent flow. The time constant may be adjusted from 0.5 seconds to 15 seconds. To adjust the filter time constant, select the FILTER indicator. Press ENTER to enable adjustment. Turn the ADJUST until the desired amount of damping is achieved. To save the value press and hold the ENTER button until the LED indicators all flash, indicating the value was saved. To discard the adjustment press SELECT before pressing the ENTER button.

OUTPUT FILTER RESPONSE (values in seconds)

% of Full Velocity	Filter Setting on Adjust Dial		
	Min.	Mid.	Max.
63%	0.5	7.5	15
90%	1.1	17.3	34.5
95%	1.5	22.5	44.9
99%	2.3	34.5	69.0

Range Selection
The range selection allows you to select one of eight ranges in either feet per minute (FPM) or meters per second (MPS).

Ranges:
FPM: 250, 500, 1000, 2000, 3000, 5000, 10000, 15000
MPS: 1.25, 2.5, 5, 10, 15, 25, 50, 75

Select the RANGE indicator by pressing ENTER when the RANGE LED indicator is illuminated. The A,B,C LED indicators will display which range setting is currently active. Press ENTER to enable adjustment. Turn the ADJUST until the desired range indication is achieved. If you want to discard the adjustment press SELECT. If you want to save the range press and hold ENTER. The RANGE LED will blink at a faster rate for about 2.5 seconds then all of the LEDs will flash indicating the value was saved.

The range setting is displayed with the LED indicators. The function of these indicators is summarized on the control label inside the unit. The following table summarizes the indicator status for each range setting

Range/Units	Run	Filter	Range	Span A	4 mA B	20 mA C
250 FPM	1	0	1	0	0	0
500 FPM	1	0	1	0	0	1
1000 FPM	1	0	1	0	1	0
2000 FPM	1	0	1	0	1	1
3000 FPM	1	0	1	1	0	0
5000 FPM	1	0	1	1	0	1
10000 FPM	1	0	1	1	1	0
15000 FPM	1	0	1	1	1	1
1.25 MPS	0	1	1	0	0	0
2.5 MPS	0	1	1	0	0	1
5 MPS	0	1	1	0	1	0
10 MPS	0	1	1	0	1	1
15 MPS	0	1	1	1	0	0
25 MPS	0	1	1	1	0	1
50 MPS	0	1	1	1	1	0
75 MPS	0	1	1	1	1	1

1: Indicator on
0: Indicator off

Span Setting

The Series 641RM Air Velocity Transmitter has been calibrated for standard sea level conditions. As a mass flow device it will always read the air velocity for standard conditions. Density changes due to barometric or absolute pressure are not corrected automatically. The span setting allows correction for altitude or other static pressure conditions that affect the density of the process air. This parameter allows for a ±50% adjustment in the span value.

To make the span adjustment you will need to know either the absolute static pressure or the corrected velocity of the process air. Set the air velocity to a known value, ideally about 3/4 of the full-scale range value. Press SELECT until the SPAN LED indicator is illuminated then press ENTER. The SPAN LED will begin to blink. Adjust the control for the desired velocity then press and hold the ENTER button until all of the LED's flash, indicating the new value was saved. If you know the absolute static pressure you can compute the corrected velocity using the following equation:

$$V_{cor} = \frac{P_o}{P_A} V_{rdg}$$

Where:
P0 is the standard pressure of 29.9 in. Hg. or 760 mm Hg
PA is the absolute pressure reading
Vrdg is the indicated velocity
Vcor is the corrected velocity

4 mA Setting

To make this setting you will need a milliammeter connected in the current loop. It is not required to use a known air flow velocity to make this calibration setting. The calibration settings of the velocity and mA outputs are independent of each other. Press SELECT until the 4 mA LED indicator is illuminated then press ENTER. The milliammeter will now read approximately 4.0 mA. Adjust the control for a 4.0 mA reading on the milliammeter. Press and hold ENTER to save the new setting. Pressing SELECT before pressing ENTER will restore the previous calibration value.

20 mA Setting

It is not required to use a known air flow velocity to make this calibration setting. The calibration settings of the velocity and mA outputs are independent of each other. With the milliammeter connected in the current loop, press SELECT until the 20 mA LED indicator is illuminated. Press ENTER to begin adjustment of the 20 mA set point. The 20 mA LED will now be blinking. Adjust the control until the milliammeter reads 20.0 mA. Press and hold ENTER to save the new setting. Pressing SELECT before pressing ENTER will restore the previous calibration value.

Restoring Factory Default Settings

The 4 mA, 20 mA, and Range settings override factory default values. To restore these to the factory default settings, start with the unit in the RUN mode. Press and hold the ENTER button. The RUN LED indicator will begin to blink. After about 2.5 seconds all LED indicators will flash indicating the factory settings have been restored. Range and Filter settings are not affected by this operation. If you are unsure whether any have been altered, press the SELECT button six times to sequence through all settings. When you return to the RUN mode, the RUN LED indicator will blink several times if either the 4 mA, 20 mA, or span settings have been changed. The RUN LED will otherwise remain on.

MAINTENANCE

In general the Series 641RM Air Velocity Transmitter should require very little maintenance. In some installations dust may accumulate on the sensor over time. This can be removed by carefully brushing the probe with a small camel hairbrush. If too much force is applied during cleaning, the sensor of the Series 641RM Air Velocity Transmitter may be damaged. Therefore, a trained technician should perform the cleaning operation. A jet of air may also dislodge the accumulated buildup. However, the sensor is delicate and this operation should be done carefully with clean regulated air. Using a shop air supply may exert enough force to damage the sensor. Most air supplies of this sort will also contain water or oil that could damage the sensor. Technical grade denatured or isopropyl alcohol may be used where the dust accumulation does not respond to brushing. Do not use water. Always disconnect the power when performing a cleaning operation.

Aside from field calibrations for span, 4 mA and 20 mA setting as described above, the Series 641RM Air Velocity Transmitter cannot be fully factory calibrated in the field. Because of specialized computer instrumentation required, these units must be returned to Dwyer Instruments for factory calibration. Contact customer service to receive a return goods authorization number before shipping.

Printed in U.S.A. 1/05

FR# 443309-00 Rev. 1

DWYER INSTRUMENTS, INC.
P.O. BOX 373 • MICHIGAN CITY, INDIANA 46361, U.S.A.
Phone: 219/879-8000
Fax: 219/872-9057
www.dwyer-inst.com
e-mail: info@dwyer-inst.com

HOBO DATA LOGGER TEMP/RH/2 EXT CHANNELS

HOBO U12 Temp/RH/
2 External Data Logger
(Part # U12-013)

Thank you for purchasing a HOBO data logger. With proper care, it will give you years of accurate and reliable measurements.
The HOBO U12 Temperature/Relative Humidity/2 External Data Logger is a four-channel logger with 12-bit resolution and can record up to 43,000 measurements or events. The two external channels accept a variety of sensors, including temperature and split-core AC current sensors as well as 4-20 mA and voltage input cables (sold separately). The logger uses a direct USB interface for launching and data readout by a computer.

An Onset software starter kit is required for logger operation. Visit www.onsetcomp.com for compatible software.

Inside this package:

- HOBO U12 Temp/RH/2 External Data Logger
- Mounting kit with magnet, hook and loop tape, tie-wrap mount, tie wrap, and two screws.

Doc # 13129-A, MAN-U12013
Onset Computer Corporation

Specifications

Measurement range	Temperature: -20° to 70°C (-4° to 158°F) RH: 5% to 95% RH External input channels (see sensor manual): 0 to 2.5 DC Volts
Accuracy	Temperature: ± 0.35°C from 0° to 50°C (± 0.63°F from 32° to 122°F), see Plot A RH: +/- 2.5% from 10% to 90% RH (typical), to a maximum of +/- 3.5%. See Plot B. External input channels (see sensor manual): ± 2 mV ± 2.5% of absolute reading
Resolution	Temperature: 0.03°C at 25°C (0.05°F at 77°F), see Plot A RH: 0.03% RH External Input Channels: 0.6 mV
Drift	Temperature: 0.1°C/year (0.2°F/year) RH: <1% per year typical; RH hysteresis 1%
Response time in airflow of 1 m/s (2.2 mph)	Temperature: 6 minutes, typical to 90% RH: 1 minute, typical to 90%
Time accuracy	± 1 minute per month at 25°C (77°F), see Plot C
Operating temperature	Logging: -20° to 70°C (-4° to 158°F) Launch/readout: 0° to 50°C (32° to 122°F), per USB specification
Battery life	1 year typical use
Memory	64K bytes (43,000 12-bit measurements)
Weight	46 g (1.6 oz)
Dimensions	58 x 74 x 22 mm (2.3 x 2.9 x 0.9 inches)
CE	The CE Marking identifies this product as complying with all relevant directives in the European Union (EU).

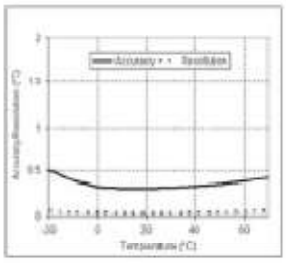

Plot A

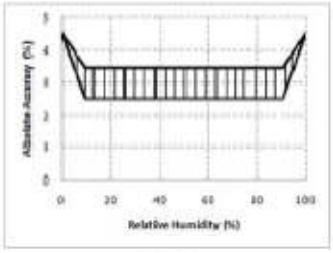

Plot B

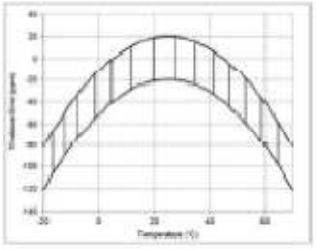

Plot C

Connecting the Logger

The U-Family logger requires an Onset-supplied USB interface cable to connect to the computer. If possible, avoid connecting at temperatures below 0°C (32°F) or above 50°C (122°F).

1. Plug the large end of the USB interface cable into a USB port on the computer.
2. Plug the small end of the USB interface cable into the bottom of the logger as shown in the following diagram.

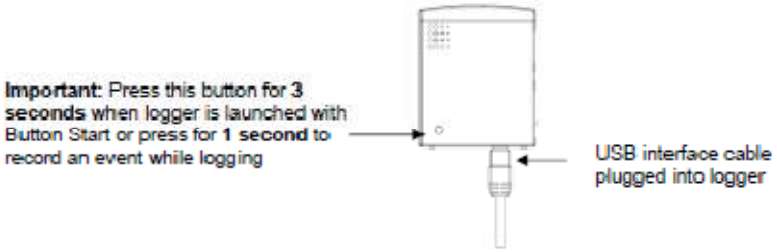

If the logger has never been connected to the computer before, it may take a few seconds for the new hardware to be detected. Use the logger software to launch and read out the logger.

Important: If you configure the logger to start with a button start, be sure to press and hold down the button on the front of the logger for at least three seconds when you want to begin logging data.

Be sure to plug any external sensors (if applicable) into the side of the logger before logging begins. Also select the correct sensors and activate the external channels in the logger software when configuring the launch. **Important: If you select an external channel, but do not plug the probe in, false data will be recorded for that channel.**

You can read out the logger while it continues to log, stop it manually with the software, or let it record data until the memory is full. Refer to the software user's guide for complete details on launching, reading out, and viewing data from the logger.

Sample and Event Logging

The logger can record two types of data: samples and events. Samples are the sensor measurements recorded at each logging interval (for example, the temperature every minute). Events are independent occurrences triggered by a logger activity. Examples of events recorded asynchronously during deployment include when the logger is connected to the host, when the battery is low, the end of a data file once the logger is stopped, and button pushes.

Press the button on the front of the logger for one second to record an event. Both a button up and down event will be recorded. This is useful if you want to mark the datafile at a particular point. For example, if the logger is located in an incubator, you might press the button each time the door is opened. The logger stores 64K of data, and can record up to 43,000 samples and events combined.

Using the RH Sensor

In order to take humidity measurements, the temperature sensor must be used in conjunction with the RH sensor.

Conditions outside the recommended range may offset the RH signal. Vapors may also affect the RH sensor. The diffusion of chemicals into the sensor may cause a shift in both offset and sensitivity. High levels of pollutants may cause permanent damage to the sensor.

Upon returning to normal conditions, the RH sensor will slowly return towards calibration state by itself. However, prolonged exposure to extreme conditions may accelerate aging and eventually lead to a permanent shift. To recondition the sensor, do the following:

1. Remove the battery
2. Warm 24 hours 80–90°C (176–194°F) at < 5% RH
3. Re-hydrate 48 hours 20–30°C (70–90°F) at 75–95% RH

Mounting

There are four ways to mount the logger using the materials in the mounting kit included with the logger:

- Use the hook and loop tape to affix the logger to a surface.
- Attach the magnet, then place the logger on a magnetic surface.
- Use the tie wrap and tie wrap mount to tie the logger to an object.
- Fasten the logger to a surface with the two Phillips-head screws. The back of the logger has two inserts for the screws, 32 mm (1¼ inches) apart.

Battery

The logger requires one 3-Volt CR-2032 lithium battery. Expected battery life varies based on the temperature and the frequency at which the logger is recording data (the logging interval). A new battery will typically last one year with logging intervals greater than one minute. Deployments in extremely cold or hot temperatures or logging intervals faster than one minute may significantly reduce battery life.

To replace the battery:

1. Disconnect the logger from the computer.
2. Unscrew the logger case.
3. Lift the circuit board and carefully push the battery out with a small blunt instrument, or pull it out with your fingernail.
4. Insert a new battery, positive side facing up.
5. Carefully realign the logger case and re-fasten the screws.

⚠ **WARNING:** Do not cut open, incinerate, heat above 85°C (185°F), or recharge the lithium battery. The battery may explode if the logger is exposed to extreme heat or conditions that could damage or destroy the battery case. Do not dispose of the logger or battery in fire. Do not expose the contents of the battery to water. Dispose of the battery according to local regulations for lithium batteries.

TYPE-T THERMOCOUPLE

T Duplex Insulated Copper-Constantan Duplex ANSI Type T

ANSI Color Code: Positive Wire, Blue; Negative Wire, Red; Overall, Brown
OMEGA Engineering does not use reprocessed PFA or PVC in manufacturing thermocouple wire.

MOST POPULAR MODELS HIGHLIGHTED!

Insulation	AWG No.	Model Number	Price/ 1000'	SLE/ 1000'**	Type Wire	Insulation: Conductor	Insulation: Overall	Max Temp °C	Max Temp °F	Nominal Size mm (Inches)	Wt. kg/300 m (lb/1000')
Glass	20	GG-T-20	$365	$430	Solid	Glass Braid	Glass Braid	260	500	1.5 x 2.4 (0.060 x 0.095)	4 (9)
	20	GG-T-20S	460	550	7 x 28	Glass Braid		260	500	1.5 x 2.5 (0.060 x 0.100)	4 (9)
	24	GG-T-24	265	305	Solid	Glass Braid		200	400	1.3 x 2.0 (0.050 x 0.080)	3 (5)
	24	GG-T-24S	420	500	7 x 32	Glass Braid		200	400	1.3 x 2.2 (0.050 x 0.085)	3 (5)
	26	GG-T-26	230	280	Solid	Glass Braid		200	400	1.1 x 1.9 (0.045 x 0.075)	2 (4)
	28	GG-T-28	220	255	Solid	Glass Wrap		200	400	1.0 x 1.4 (0.040 x 0.055)	2 (3)
	30	GG-T-30	225	270	Solid	Glass Wrap		150	300	0.9 x 1.3 (0.037 x 0.050)	2 (3)
Glass with Stainless Steel Overbraid	20	GG-T-20-SB	710	850	Solid	Glass	SS Braid Over Glass	482	900	2.2 x 3.0 (0.090 x 0.120)	6 (14)
	24	GG-T-24-SB	495	595	Solid			482	900	2.2 x 3.0 (0.085 x 0.117)	5 (11)
Kapton Polymide Tape	20	KK-T-20	870	990	Solid	Fused Polymide Tape	Fused Polymide Tape	316	600	1.5 x 2.5 (0.060 x 0.100)	5 (11)
	24	KK-T-24	660	755	Solid			316	600	1.2 x 1.9 (0.050 x 0.075)	2 (6)
	30	KK-T-30	650	750	Solid			316	600	1.0 x 1.4 (0.040 x 0.055)	3 (5)
PFA Glass	30	TG-T-30	490	-	Solid	PFA	Glass Braid	150	300	0.9 x 1.2 (0.034 x 0.047)	1 (2)
	36	TG-T-36	550	-	Solid			150	300	0.7 x 1.0 (0.028 x 0.038)	1 (2)
	40	TG-T-40	620	-	Solid			150	300	0.7 x 0.9 (0.026 x 0.035)	1 (2)
Neoflon PFA (High Performance)	20	TT-T-20	455	515	Solid	PFA	PFA	260	500	1.7 x 3.0 (0.068 x 0.116)	5 (11)
	20	TT-T-20S	595	715	7 x 28			260	500	1.9 x 3.2 (0.073 x 0.126)	5 (11)
	22	TT-T-22S	580	695	7 x 30			260	500	1.7 x 3.4 (0.065 x 0.133)	4 (9)
	24	TT-T-24	370	415	Solid			200	400	1.4 x 2.4 (0.056 x 0.092)	3 (7)
	24	TT-T-24S	400	485	7 x 32			200	400	1.6 x 2.6 (0.063 x 0.102)	3 (7)
	30	TT-T-30**	390	430	Solid			150	300	0.6 x 1.0 (0.024 x 0.040)	1 (2)
	36	TT-T-36**	450	495	Solid			150	300	0.5 x 0.8 (0.019 x 0.030)	1 (2)
	40	TT-T-40**	500	650	Solid			150	300	0.4 x 0.7 (0.017 x 0.026)	1 (2)
PFA Polymer w/ Twisted and Shielded Conductors	20	TT-T20-TWSH	975	1125	Solid	PFA Polymer	PFA Polymer and Shielding	260	500	3.7 (0.15)	9 (20)
	20S	TT-T20S-TWSH	1170	1405	7 x 28			260	500	3.8 (0.15)	9 (20)
	24	TT-T24-TWSH	560	645	Solid			260	500	2.7 (0.11)	4 (9)
	24S	TT-T24S-TWSH	670	805	7 x 32			200	500	2.9 (0.12)	4 (9)
Neoflon FEP	20	FF-T-20	430	540	Solid	FEP	FEP	200	392	1.7 x 3.0 (0.068 x 0.116)	5 (11)
	24	FF-T-24	335	345	Solid			200	392	1.4 x 2.4 (0.056 x 0.092)	3 (7)
FEP Polymer w/ Twisted and Shielded Conductors	20	FF-T20-TWSH	735	845	Solid	FEP Polymer	FEP Polymer and Shielding	200	392	3.7 (0.15)	9 (20)
	20S	FF-T20S-TWSH	885	1060	7 x 28			200	392	3.8 (0.15)	9 (20)
	24	FF-T24-TWSH	425	490	Solid			200	392	2.7 (0.11)	4 (9)
	24S	FF-T24S-TWSH	505	610	7 x 32			200	392	2.9 (0.12)	4 (9)
TFE Tape Polymer	20	TFE-T-20	450	510	Solid	TFE Tape Polymer	Fused TFE Tape Polymer	260	500	1.5 x 2.5 (0.060 x 0.100)	5 (11)
	20S	TFE-T-20S	570	650	7 x 28			260	500	1.5 x 2.7 (0.060 x 0.105)	5 (11)
	24	TFE-T-24	315	350	Solid			260	500	1.3 x 1.9 (0.050 x 0.075)	3 (6)
	24S	TFE-T-24S	370	415	7 x 32			260	500	1.3 x 2.2 (0.050 x 0.085)	3 (6)
Polyvinyl	24	PP-T-24	265	305	Solid	Polyvinyl	Polyvinyl Polyvinyl (Rip Cord)**	105	221	1.9 x 3 (0.075 x 0.120)	5 (10)
	24	PP-T-24S	335	400	7 x 32			105	221	1.9 x 3.1 (0.080 x 0.130)	5 (10)
	24	PR-T-24	155	175	Solid			105	221	1.3 x 2.2 (0.050 x 0.086)	3 (5)

See Fused Tape Insulated TFE-T Series.
*** Two insulated leads bonded together, but with no overjacket.*
' Weight of spool and wire rounded to the next highest lb. (does not include packing material).
" Overall color clear. '" To order special limits of error wire, add "-SLE" to model number before spool length.
***Ordering Example:** TT-T-24-SLE-1000, 1000' (300 m) of Type T duplex insulated special limits of error thermocouple wire, SLE.*

ANSI color code shown | To order IEC color code see page A-8

Discount Schedule *(1000 ft spools only)*

3 to 4 spools	10%
5 to 9 spools	15%
10 to 19 spools	20%

SPOOL PRICING

STANDARD SPOOL LENGTHS

7.5 m (25')	60 m (200')
15 m (50')	150 m (500')
30 m (100')	300 m (1000')

FOR LONGER LENGTHS CONSULT SALES FOR PRICE AND DELIVERY!

To order standard length spools, multiply the 300 m or 1000' spool price by the multipiler and round to the nearest dollar.

Example: GG-K-20-50, 50' (15 m) spool of GG-K-20 wire = $410 x 0.1 = **$41**

Spool Pricing Guidelines

Multiply 300 m or 1000' spool price by multiplier and round to the nearest dollar. Consult Sales for price quote.

7.5 m or 25' = Price from Chart x	0.0025
15 m or 50' = Price from Chart x	0.1
30 m or 100' = Price from Chart x	0.175
60 m or 200' = Price from Chart x	0.3
150 m or 500' = Price from Chart x	0.5
300 m or 1000' = Price from Chart x	1.0

Note: Published prices are based on market value at time of printing and are subject to change due to Nickel surcharges. Chromium and precious-metal market fluctuations.

Appendix, C

TEST FACILITY BUILDING COOLING LOAD DESIGN

Selected and Calculated Cooling Load Design Parameters

Parameter	Value	Unit	Comment
Test Facility Building Floor Area	740	ft^2	Length 49.875 ft x Width 14.83 ft With a Height of 7.75ft
Wall R-Value	15.625	ft^2.hr.°F/Btu	Outdoor/Indoor Air Films, 4"Frame Wood, Batt Insulation R-5, 0.5" Gypsum Board, ¾" Air Gap
Roof R-Value	19.445	ft^2.hr.°F/Btu	Outdoor/Indoor air films, 4"frame wood, 4" Insulation, 0.5", ¾" air gap, 4"Water pond, 4"Aspestos Coating
Slab R-Value	11.37	ft^2.hr.°F/Btu	This values is assumed using TRACE 700 input (12"LW Concrete)
Windows U-Value	0.478	Btu/ft^2.hr.°F	6mm Double Glazed, Clear Glass with 13mm Air Gap All windows are covered with R-5 insulation from the outside during the testing periods to reduce the solar gain, which reduced the total window U-Value to be 0.181 Btu/ft^2.hr.°F
Shading Coefficient	0.81	N/A	Assumed: TRACE 700 default

Selected and Calculated Cooling Load Design Parameters

Parameter	Value	Unit	Comment
EAHE 45° Elbow Fitting Loss Coefficients (EAHE 18" Diameter)	0.09	N/A	This value is determined from ASHARE fundamentals handbook -2001. For the fitting CD3-14 Elbow, 45 degree
EAHE 90° Elbow Fitting Loss Coefficients (EAHE 18" Diameter)	0.15	N/A	This value is determined from ASHARE fundamentals handbook -2001. For the fitting CD3-9 Elbow, 90 degree
EAHE Total Dynamic Pressure Losses	0.038304	in. H_2O	Hand Calculations
EAHE Total Static Pressure Friction Losses	0.376	in. H_2O	Hand Calculations
Design Fan Head (i.e. Total Pressure Losses)	0.414	in. H_2O	Hand Calculations Summation of dynamic and static pressure losses
Designed System	N/A	N/A	A Variable Air Volume (VAV) system is selected as its control performance mirrors that of the coupled system as discuss in chapter 5.
Internal Loads	0	Btu/hr	The test facility building is an unoccupied space. Moreover, the testing room is empty from any equipment that could dissipate heat
Infiltration Rate	0.6	Air Changes/hr	The building tightness is chosen as neutral

Selected and Calculated Cooling Load Design Parameters

Parameter	Value	Unit	Comment
		(ACH)	for an average construction
Indoor Air Temperature Set Point	75	°F	Selected based on the ASHRAE standard 55-2004 for thermal comfort
Indoor Air Relative Humidity Set Point	50%	%	Selected based on the ASHRAE standard 55-2004 for thermal comfort
Design Cooling Supply Air Temperature	55	°F	Selected to reduce indoor humidity issues
Airflow Recommendations	N/A	N/A	The airflow rate is chosen to comply with ASHRAE standard 62.1-2004/2007 for minimum ventilation requirements ($0.06 CFM/ft^2$)
Calculated Design Airflow Rate	244	CFM	Simulated using TRACE 700 software
Calculated Design Total Cooling Load	0.8	tons	Simulated using TRACE 700 software
	9,389	Btu/hr	Simulated using TRACE 700 software
Calculated Design Sensible Cooling Load	0.465	tons	Simulated using TRACE 700 software
	5,583	Btu/hr	Simulated using TRACE 700 software
Calculated Design Latent Cooling Load	0.317	tons	Simulated using TRACE 700 software
	3,805	Btu/hr	Simulated using TRACE 700 software
Fan Size	244	CFM	The fan airflow is designed based on the design airflow requirements, while, its head is designed to overcome the total pressure losses through the EAHE
	0.414	in. H_2O	

TRACE 700 DESIGN COOLING LOAD SIMULATION REPORT

Solar Driven Underground Cooling System

Location		
Building owner		
Program user	Michel Emil Shafik	
Company		
Comments	The design cooling load and airflow	
By	University of Nebraska	
Dataset name	C:\DOCUMENTS AND SETTINGS\MSHAFIK\DESKTOP\SOLAR SITE BUILDING SIMULATION\SOLAR SITE SIMULATION.TRC	
Calculation time	02:23 PM on 07/27/2010	
TRACE® 700 version	6.2.5	
Location	Omaha, Nebraska	
Latitude	41.0	deg
Longitude	95.0	deg
Time Zone	6	
Elevation	978	ft
Barometric pressure	28.8	in. Hg
Air density	0.0732	lb/cu ft
Air specific heat	0.2444	Btu/lb·°F
Density-specific heat product	1.0738	Btu/h·cfm·°F
Latent heat factor	4,726.8	Btu·min/h·cu ft
Enthalpy factor	4.3930	lb·min/hr·cu ft
Summer design dry bulb	91	°F
Summer design wet bulb	77	°F
Winter design dry bulb	-3	°F
Summer clearness number	0.95	
Winter clearness number	0.95	
Summer ground reflectance	0.20	
Winter ground reflectance	0.20	
Carbon Dioxide Level	400	ppm
Design simulation period	January - December	
Cooling load methodology	CLTD-CLF (ASHRAE TFM)	
Heating load methodology	UATD	

TRANE

TRACE 700

Design Cooling Load Summary

By University of Nebraska
Solar Driven Underground Cooling System

System - VAV System

Type - Bypass VAV with Reheat (30% Min Flow Default)

Coil Location - System

Coil Peak Calculation Time: July hour 15
Ambient DB/WB/HR: 91 / 77 / 123

COOLING COIL LOAD INFORMATION

Load Component	Sensible Btu/h	Latent Btu/h	Total Btu/h	Percent of Total
Solar Gain	0		0	0.0%
Glass Transmission	327		327	3.5%
Wall Transmission	2,483		2,483	26.4%
Roof Transmission	849		849	9.0%
Floor Transmission	0		0	0.0%
Adj Floor Transmission	0		0.00	0.0%
Partition Transmission	0		0	0.0%
Net Ceiling Load	0		0	0.0%
Lighting	0		0	0.0%
People	0	0	0	0.0%
Misc. Equipment Loads	0	0	0	0.0%
Cooling Infiltration	1,112	2,257	3,369	35.9%
Sub Total --->	4,771	2,257	7,028	74.9%
Ventilation Load	762	1,548	2,310	24.6%
Exhaust Heat	0	0	0	0.0%
Supply Fan Load	50		50	0.5%
Return Fan Load	0		0	0.0%
Net Duct Heat Pickup	0		0	0.0%
Wall Load to Plenum	0		0	0.0%
Roof Load to Plenum	0		0	0.0%
Adj Floor to Plenum	0		0	0.0%
Lighting Load to Plenum	0		0	0.0%
Misc. Equip. Load to Plenum	0	0	0	0.0%
Glass Transmission to Plenum	0		0	0.0%
Glass Solar to Plenum	0		0	0.0%
Over/Under Sizing	0		0	0.0%
Reheat at Design	0	0	0	0.0%
Underfloor Sup Heat Pickup	0		0	0.0%
Supply Air Leakage	0	0	0	0.0%
Total Cooling Loads	5,583	3,805	9,389	100.0 %

COOLING COIL SELECTION

Coil Selection Parameters		
Coil Entering Air (DB / WB)	70.2 / 67.0	°F
Coil Entering Humidity Ratio	85.08	gr/lb
Coil Leaving Air (DB / WB)	54.3 / 53.3	°F
Coil Leaving Humidity Ratio	60.63	gr/lb
Coil Sensible Load	5.58	MBh
Coil Total Load	9.39	MBh
Cooling Supply Air Temperature	55.00	°F
Total Cooling Airflow	224.42	cfm
Resulting Room Relative Humidity	55.01	%

General Engineering Checks

Total Cooling Load	0.8	ton
Area / Load	945.38	ft²/ton
Total Floor Area	740	ft²
Cooling Airflow	0.30	cfm/ft²
Airflow / Load	288.84	cfm/ton
Percent Outdoor Air	19.8	%
Cooling Load Methodology	CLTD-CLF (ASHRAE TFM)	

System Checksums

By University of Nebraska

VAV System — **Bypass VAV with Reheat (30% Min Flow Default)**

COOLING COIL PEAK

Peaked at Time: Mo/Hr. 7 / 15
Outside Air: OADB/WDB/R: 91 / 77 / 123

	Space Sens. + Lat. Btu/h	Plenum Sens. + Lat Btu/h	Net Total Btu/h	Percent Of Total (%)
Envelope Loads				
Skylite Solar	0	0	0	0
Skylite Cond	0	0	0	0
Roof Cond	849	0	849	9
Glass Solar	0	0	0	0
Glass/Door Cond	327	0	327	3
Wall Cond	2,483	0	2,483	26
Partition/Door	0		0	0
Floor	0		0	0
Adjacent Floor	0	0	0	0
Infiltration	3,369		3,369	36
Sub Total ==>	7,028	0	7,028	75
Internal Loads				
Lights	0	0	0	0
People	0	0	0	0
Misc	0	0	0	0
Sub Total ==>	0	0	0	0
Ceiling Load	0	0	0	0
Ventilation Load	0	0	2,310	25
Adj Air Trans Heat	0		0	0
Dehumid. Ov Sizing			0	0
Ov/Undr Sizing	0		0	0
Exhaust Heat		0	0	0
Sup. Fan Heat			50	1
Ret. Fan Heat		0	0	0
Duct Heat Pkup		0	0	0
Underflr Sup Ht Pkup			0	0
Supply Air Leakage		0	0	0
Grand Total ==>	7,028	0	9,389	100.00

CLG SPACE PEAK

Mo/Hr. 7 / 10
OADB: 90

	Space Sensible Btu/h	Percent Of Total (%)
Envelope Loads		
Skylite Solar	0	0
Skylite Cond	0	0
Roof Cond	930	19
Glass Solar	0	0
Glass/Door Cond	325	7
Wall Cond	2,485	52
Partition/Door	0	0
Floor	0	0
Adjacent Floor	0	0
Infiltration	1,070	22
Sub Total ==>	4,820	100
Internal Loads		
Lights	0	0
People	0	0
Misc	0	0
Sub Total ==>	0	0
Ceiling Load	0	0
Ventilation Load	0	0
Adj Air Trans Heat	0	0
Ov/Undr Sizing	14,242	14,242
Exhaust Heat		1,086
OA Preheat Diff.		0
RA Preheat Diff.		0
Additional Reheat		0
Underflr Sup Ht Pkup		0
Supply Air Leakage		0
Grand Total ==>	-723	-3,202

HEATING COIL PEAK

Mo/Hr. Heating Design
OADB: -3

	Space Peak Space Sens Btu/h	Coil Peak Tot Sens Btu/h	Percent Of Total (%)
Envelope Loads			
Skylite Solar	0	0	0.00
Skylite Cond	0	0	0.00
Roof Cond	-2,853	-2,853	89.10
Glass Solar	0	0	0.00
Glass/Door Cond	-1,859	-1,859	58.06
Wall Cond	-5,041	-5,041	157.43
Partition/Door	0	0	0.00
Floor	0	0	0.00
Adjacent Floor	0	0	0
Infiltration	-5,212	-5,212	162.79
Sub Total ==>	-14,965	-14,965	467.38
Internal Loads			
Lights	0	0	0.00
People	0	0	0.00
Misc	0	0	0.00
Sub Total ==>	0	0	0.00
Ceiling Load	0	0	0.00
Ventilation Load	0	-3,574	111.63
Adj Air Trans Heat	0	0	0
Ov/Undr Sizing	14,242	14,242	-444.80
Exhaust Heat		1,086	-34.21
OA Preheat Diff.		0	0.00
RA Preheat Diff.		0	0.00
Additional Reheat		0	0.00
Underflr Sup Ht Pkup		0	0.00
Supply Air Leakage		0	0.00
Grand Total ==>	-723	-3,202	100.00

TEMPERATURES

	Cooling	Heating
SADB	55.0	62.0
Ra Plenum	75.0	72.0
Return	75.0	62.7
Ret/OA	78.2	49.7
Fn MtrTD	0.0	0.0
Fn BltTD	0.1	0.0
Fn Frict	0.1	0.0

AIRFLOWS

	Cooling	Heating
Diffuser	224	67
Terminal	224	67
Main Fan	224	67
Sec Fan	0	0
Nom Vent	44	44
AHU Vent	44	44
Infil	65	65
MinStop/Rh	67	67
Return	289	289
Exhaust	109	109
Rm Exh	0	0
Auxiliary	0	0
Leakage Dwn	0	0
Leakage Ups	0	0

ENGINEERING CKS

	Cooling	Heating
% OA	19.8	19.8
cfm/ft²	0.30	0.30
cfm/ton	286.84	
ft²/ton	945.38	
Btu/hr-ft²	12.69	-4.33
No. People	0	

COOLING COIL SELECTION

	Total Capacity ton	Total Capacity MBh	Sens Cap MBh	Coil Airflow cfm	Enter DB °F	Enter WB °F	Enter HR gr/lb	Leave DB °F	Leave WB °F	Leave HR gr/lb
Main Clg	0.0	9.4	5.6	224	70.2	67.0	65.1	54.0	53.3	60.6
Aux Clg	0.0	0.0	0.0	0	0.0	0.0	0.0	0.0	0.0	0.0
Opt Vent	0.0	0.0	0.0	0	0.0	0.0	0.0	0.0	0.0	0.0
Total	0.8	9.4								

AREAS

	Gross Total ft²	Glass ft²	Glass (%)
Floor	740		
Part	0		
Int Door	0		
ExFlr	0		
Roof	740	0	0
Wall	888	175	20
Ext Door	0	0	0

HEATING COIL SELECTION

	Capacity MBh	Coil Airflow cfm	Ent °F	Lvg °F
Main Htg	-2.0	67	54.0	62.0
Aux Htg	0.0	0	0.0	0.0
Preheat	-1.2	224	49.7	54.8
Humidif	0.0	0	0.0	0.0
Opt Vent	0.0	0	0.0	0.0
Total	-3.2			